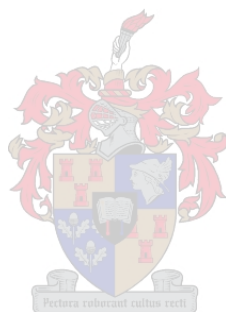


Structural Analysis of Transition Metal Complexes of Imidazole-Derived Ligands

by

Storm Victoria Potts

*Thesis presented in partial fulfilment of the requirements for the
degree of Master of Science*



At Stellenbosch University
Department of Chemistry and Polymer Science
Faculty of Science

Supervisor: Prof. Leonard. J. Barbour
December 2009

Declaration

By submitting this dissertation electronically, I declare that the entirety of the work contained therein is my own, original work, that I am the owner of the copyright thereof (unless to the extent explicitly otherwise stated) and that I have not previously in its entirety or in part submitted it for obtaining any qualification.

December 2009

Copyright © 2009 Stellenbosch University

All rights reserved

Abstract

The primary objective of this work was to investigate the architectures formed by the complexation of flexible imidazole-derived ligands; containing thioether linkages, with a range of metal salts and to analyse the resulting coordination networks by single-crystal X-ray diffraction (SCD).

To this end, the following six flexible ligands were prepared:

- 1,3,5-tris(1-imidazolyl-2-thione)-2,4,6-trimethylbenzene
- 1,4-bis(1-imidazolyl-2-thione)-2,3,5,6-tetramethylbenzene
- 1,4-bis(1-imidazolyl-2-thione)-2,5-dimethylbenzene
- 3,5-bis(1-imidazolyl-2-thione)toluene
- 1,3-bis(1-imidazolyl-2-thione)-2,4,6-trimethylbenzene
- 4,4'-bis(1-imidazolyl-2-thione)-1,1'-biphenyl

The rationale behind this work was to establish the effect of the added flexibility of the ligand on the resulting coordination networks and to determine if we could synthesise new porous materials based on a “donut-shaped” dinuclear metallocycle template. SCD was employed as the primary analytical tool, owing to the unique information it can provide regarding intermolecular interactions in the solid-state.

A total of 28 novel coordination complexes were analysed and a novel, cage-like hemicarcerand was obtained that was shown to have individual cavities sufficiently large to accommodate guest molecules. Preliminary gravimetric gas sorption isotherms were recorded and show that this compound is *transiently* porous and capable of absorbing H₂ and CO₂.

Opsomming

Die primêre doel van hierdie studie is om die argitekture te ondersoek wat ontstaan wanneer buigbare imidasool-ligande (wat tioëter skakels bevat) gekomplekseer word met 'n reeks metaalsoute. Die gevormde koördinasienetwerke is dan met behulp van enkel-kristal X-straal diffraksie geanaliseer.

Vir hierdie doeleindes is die volgende ses buigbare ligande voorberei:

- 1,3,5-tris(1-imidasooliel-2-tioon)-2,4,6-trimetielbenseen
- 1,4-bis(1-imidasooliel-2-tioon)-2,3,5,6-tetrametielbenseen
- 1,4-bis(1-imidasooliel-2-tioon)-2,5-dimetielbenseen
- 3,5-bis(1-imidasooliel-2-tioon)tolueen
- 1,3-bis(1-imidasooliel-2-tioon)-2,4,6-trimetielbenseen
- 4,4'-bis(1-imidasooliel-2-tioon)-1,1'-bifeniel

Die redenasie hieragter is om die effek van die bygevoegde buigbaarheid van die ligand op die resulterende koördinasienetwerke te bepaal, asook om te bepaal of nuwe poreuse materiale gesintetiseer kan word gebaseer op 'n binukleêre metallosikliese templaar. Enkel-kristal diffraksie word benut as die primêre analitiese tegniek as gevolg van die unieke inligting wat verkry kan word met betrekking tot die intermolekulêre interaksies.

'n Totaal van 28 nuutgevonde koördinasiekomplekse is geanaliseer, insluitend 'n hokvormige *hemicarcerand*. Die laasgenoemde verbinding toon individuele holtes wat groot genoeg is om gasmolekules te akkommodeer. Aanvanklike gravimetriese gassorpsie isoterme is verkry, en toon dat die *hemicarcerand* tydelik poreus is en dus daartoe in staat om H₂ en CO₂ te absorbeer.

Acknowledgements

Many people need to be thanked for making this difficult process a great deal easier.

Firstly, I would sincerely like to thank my supervisor Prof Len Barbour for his infinite supply of patience and enthusiasm, as well as for the amazing opportunities he has offered me in the past few years. I truly look forward to continuing my studies under your guidance. I would also like to thank Dr Liliana Dobrańska for all of her help during the initial stages of this project.

Then to my friends and colleagues in the Supramolecular Materials Group, Tia Jacobs, Leigh Loots, Martin Bredenkamp, Jan Gertenbach, Bettinah Chipimpi, Dinubanduh Das, Subhadip Neogi, Tanya le Roex, Delia Haynes, Eustina Batisai, Charl Marias, Catharine Esterhuysen and Marlene Milani, thank you so much for creating such a wonderful working environment. Special thanks need to go out to Catharine, Jan and Delia for all of your helpful conversations and extra reading. I would not have been able to get through this process without your valuable input and encouraging smiles.

To my housemates (past and present) Charl, Aimee and Elsa, thank you for all of the meals that were cooked, the dishes that were washed and the ranting sessions that were had. To my friends (who can no longer be labelled “chemistry” friends) Leigh, Haydn, Sassie, Ros and Dewald, know the support and endless flow of entertainment you have provided did not go unnoticed.

Lastly I would like to thank my family and Jean for all of the love and encouragement. I promise there will come a day when I’m no longer a student...just not yet!

Publications

1. S.V. Potts, D. Das and M.W. Bredenkamp, *Acta Crystallogr., Sect. E*, **2008**, E64, o966
2. S.V. Potts, M.W. Bredenkamp and J.A. Gertenbach, *Acta Crystallogr., Sect. E*, **2008**, E63, o2887

Conferences

1. **ECM '07 – 24 European Crystallographic Meeting**

Marrakech Morocco, 22-27 August 2007

Poster presentation – *CRYSTAL STRUCTURE PREDICTION-PACKING POLYMORPHISM, the use of supramolecular trends to deduce molecular packing.*

2. **ICMR 2008 – International Centre for Materials Research Summer School on Periodic Structures and Crystal Chemistry**

University of California Santa Barbara, July 27 – August 9 2008

Poster presentation – *CRYSTAL STRUCTURE PREDICTION-PACKING POLYMORPHISM, the use of supramolecular trends to deduce molecular packing.*

3. **SACI 2008 – 39th National Convention of the South African Chemical Institute**

Stellenbosch, South Africa, 30 November – 5 December 2008

Poster Presentation – *Flexible ligands in the construction of Ag(I) complexes.*

Abbreviations

0D	Zero Dimensional
1D	One Dimensional
2D	Two Dimensional
3D	Three Dimensional
ASU	Asymmetric Unit
CIF	Crystallographic Information File
CSD	Cambridge Structural Database
DSC	Differential Scanning Calorimetry
IR	Infrared Spectroscopy
LC ESI-MS	Liquid Chromatography Electrospray Ionisation Mass Spectrometry
M	Metal
MOF	Metal-organic Framework
NMR	Nuclear Magnetic Resonance
OFF	Offset face-to-face
SBU	Secondary Building Units
SCD	Single-Crystal X-ray Diffraction
TGA	Thermogravimetric Analysis
XRPD	X-ray Powder Diffraction

Atomic Colour Key



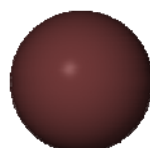
Carbon



Chlorine



Hydrogen



Bromine



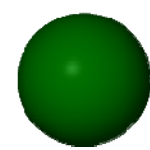
Nitrogen



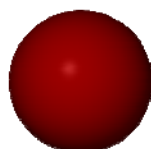
Iodine



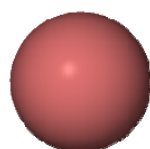
Sulphur



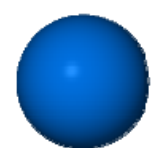
Phosphorus



Oxygen



Antimony



Fluorine



Metal

Table of Contents

Title.....	i
Declaration.....	ii
Abstract.....	iii
Opsomming.....	iv
Acknowledgements.....	v
Publications.....	vi
Conferences.....	vi
Abbreviations.....	viii
Atomic Colour Key.....	viii
Table of Contents.....	xi

CHAPTER 1 **1**

INTRODUCTION

1.1. Supramolecular Chemistry.....	1
1.2. Crystal Engineering.....	3
1.3. Intermolecular Interactions.....	6
1.4. Self-Assembly.....	13
1.5. Porosity.....	14
1.6. Coordination networks containing imidazole functionalised ligands.....	16
1.7. Aspects of this study.....	32
REFERENCES.....	34

CHAPTER 2 **38**

SYNTHETIC METHODS AND EXPERIMENTAL TECHNIQUES

2.1 Synthesis and Characterisation of Ligands L1 – L2.....	38
--	----

2.1.1	Preparation of	
	1,3,5-tris(1-imidazolyl-2-thione)-2,4,6-trimethylbenzene (L1)	38
2.1.2	Preparation of	
	1,4-bis(1-imidazolyl-2-thione)-2,3,5,6-tetramethylbenzene (L2)	42
2.1.3	Preparation of 1,4-bis(1-imidazolyl-2-thione)-2,5-dimethylbenzene (L3)	44
2.1.4	Preparation of 3,5-bis(1-imidazolyl-2-thione)toluene (L4)	47
2.1.5	Preparation of	
	1,3-bis(1-imidazolyl-2-thione)-2,4,6-trimethylbenzene (L5)	49
2.1.6	Preparation of 4,4'-bis(1-imidazolyl-2-thione)-1,1'-biphenyl (L6)	53
2.2	Experimental Techniques	56
2.2.1	Single-Crystal X-Ray Diffraction Analysis (SCD)	56
2.2.2	X-Ray Powder Diffraction (XPRD)	57
2.2.3	Thermogravimetric Analysis (TGA)	57
2.2.4	Differential Scanning Calorimetry (DSC)	57
2.2.5	Gravimetric gas Sorption	58
2.2.6	Infrared Spectroscopy (IR)	58
2.2.7	Nuclear Magnetic Resonance Spectroscopy (NMR)	58
2.2.8	Liquid Chromatography Electrospray Ionisation Mass Spectrometry (LC ESI-MS)	59
2.3	Computer programs	59
2.3.1	X-Seed	59
2.3.2	CrystalExplorer	60
	REFERENCES	62

CHAPTER 3**64****STRUCTURAL ANALYSIS OF A VARIETY OF TRANSITION METAL COMPLEXES OF IMIDAZOLE-DERIVED LIGANDS**

3.1	Introduction	64
3.2	Results and Discussions - Structure Determinations from Single-Crystal X-ray Diffraction.....	75
3.2.1	Single-crystal structures obtained with ligand L1	75
3.2.1.1	[AgL1]NO ₃ •CH ₃ OH (1).....	75
3.2.1.2	[CdL1(μ-NO ₃)] [CdL1(H ₂ O)(NO ₃)](NO ₃) ₃ •2H ₂ O (2).....	78
3.2.2	Single-crystal structures obtained with ligand L2.....	81
3.2.2.1	[AgL2]NO ₃ (3).....	82
3.2.2.2	([AgL2]NO ₃) _n (4).....	83
3.2.2.3	[CdL2I ₂] _n (5).....	91
3.2.3	Single-crystal structures obtained with ligand L3.....	95
3.2.3.1	[Ag ₄ (L2) ₂ (H ₂ O) ₂ (NO ₃) ₂]2nNO ₃ •2nH ₂ O•nCH ₃ CN (6).....	95
3.2.3.2	[CdL3I ₂] _n (7).....	98
3.2.3.3	[CdL3I ₂] _n (8).....	100
3.2.3.4	[Cd ₂ L3I ₄] _n (9).....	102
3.2.3.5	([CuL3Cl ₂] _n •nCH ₃ OH (10).....	105
3.2.3.6	[CoL3Cl ₂] _n (11).....	107
3.2.3.7	[CdL3Cl ₂] _n (12) and [ZnL3Br ₂] _n (13).....	108
3.2.4	Single-crystal structures obtained with ligand L4.....	109
3.2.5	Single-crystal structures obtained with ligand L5.....	110
3.2.5.1	[Ag ₃ (L5) ₂ (NO ₃) ₂]NO ₃ •3H ₂ O (14).....	110
3.2.5.2	[Ag ₂ (L5) ₂](NO ₃) ₂ (15).....	112
3.2.5.3	[AgL5](NO ₃) (16).....	116
3.2.5.4	[AgL5] ₂ (SO ₃ CF ₃) ₂ •CH ₃ OH (17).....	117
3.2.5.5	[Ag ₂ (L5) ₂](SbF ₆) ₂ (18).....	119
3.2.5.6	[Ag ₂ (L5) ₂](PF ₆) ₂ (19).....	122

3.2.5.7 [Ag ₂ (L5) ₂](BF ₄) ₂ (20)	123
3.2.5.8 [CdL5I ₂] _n •nH ₂ O (21)	128
3.2.5.9 [CdL5I ₂] _n •nCH ₃ OH (22)	129
3.2.5.10 [CdL5I ₂] _n •2nCH ₃ CN (23)	131
3.2.5.11 [CdL5I ₂] _n •2nCH ₃ OH (24)	132
3.2.6 Single-crystal structures obtained with ligand L6	135
3.2.6.1 [CuL6Br ₂] _n (25)	135
3.2.6.2 [ZnL6Cl ₃] _n (26)	139
3.2.6.3 [ZnL6Cl ₂] _n •nCH ₃ OH (27)	139
3.3 General Conclusions	142
REFERENCES	144

CHAPTER 4 **147**
**PRELIMINARY INVESTIGATION OF THE GAS SORPTION PROPERTIES
OF A NOVEL HEMICARCERAND**

4.1 Introduction	147
4.2 Single crystal structure of [Ni ₂ (L5) ₄](NO ₃) ₄ •H ₂ O (28)	149
4.3 Thermal analysis of 28	153
4.4 Preliminary gas sorption Studies	154
4.5 conclusions and future studies	157
REFERENCES	159

CHAPTER 5 **161**
SUMMARY AND CONCLUDING REMARKS

REFERENCES	167
------------	-----

CHAPTER 1

Introduction

1.1. SUPRAMOLECULAR CHEMISTRY

“...supermolecules are to molecules and the intermolecular bond what molecules are to atoms and the covalent bond”. *Jean-Marie Lehn^{1,2}*

Supramolecular chemistry, defined in 1987 by the Nobel laureate Jean-Marie Lehn as the ‘*chemistry beyond the molecule*’,¹ is a young and rapidly expanding branch of chemistry concerned with the intermolecular interactions which govern the assembly of molecules into higher order supramolecular assemblies.

The history of this field can be traced back to the discovery of chlorine hydrate by Davy^{3,4} in 1810 and the subsequent assignment of its chemical formula in 1823 by Faraday.^{3,5} From these initial discoveries the field grew, and the foundations of supramolecular chemistry are said to lie in three core concepts: fixation, recognition and coordination. In 1910 Ehrlich recognised that molecules will not act if they are not bound to one another,^{2,6} and with his statement of “*Corpora non agunt nisi fixata*” he introduced the concept of *receptor*. The notion that this binding must be selective was brought about by Fischer in 1894 and most expressively portrayed in his “lock and key” concept of steric fit. This model proposed that, in order for molecules to interact or ‘bind’, they must possess a degree of geometrical complementarity, thus establishing the concept of *molecular recognition*.^{2,7} The third concept of *coordination* is associated with the pioneering work of Werner (1893),^{2,8} who showed that selective fixation requires interaction; essentially an affinity must exist between the partners, and in this respect supramolecular chemistry may be viewed as a generalisation of coordination chemistry. But, it wasn’t until 1937 when Wolf⁹ used the term “*Übermoleküle*” or “*supermolecule*” to describe the ordered structural entities resulting from the association of many coordinatively saturated chemical species, that the roots of the word supramolecular chemistry were firmly planted.

Further advancements in this field include the work of Cram for his contribution to research regarding cyclophanes, spherands and carcerands, Lehn for the synthesis

of the first cryptands and Pederson for developments in the design of macrocyclic ligands for metal cations.³ These outstanding contributions to the field of supramolecular chemistry earned Pedersen, Cram and Lehn the Nobel Prize in Chemistry in 1987.

Much of the recent work in this area of supramolecular chemistry has focused on crystal engineering (Section 1.2). As the process of crystal formation involves the self-assembly of molecules from solution or the vapour, and fundamentally relies on molecular recognition in order to accomplish this, it is not unreasonable to view a crystal as the perfect supermolecule, “*a supermolecule par excellence*” in the words of Dunitz.¹⁰ Crystallography has thus proven to be an indispensable tool in supramolecular chemistry as it can provide information, specifically regarding intermolecular interactions, which is not readily obtainable by other, more conventional, analytical techniques. As an adjunct to this powerful technique, the Cambridge Structural Database (CSD) provides a user friendly storehouse of crystallographic information which can be used to search for patterns of intermolecular interactions.^{11,12}

For a more complete review on the subject of supramolecular chemistry the reader is referred to the following texts: the eleven volume series *Comprehensive Supramolecular Chemistry* published in 1996,¹³ and the two volumed *Encyclopedia of Supramolecular Chemistry* published in 2004.¹⁴

1.2. CRYSTAL ENGINEERING

Supramolecular chemists have recognised the need to formulate a systematic approach to the combination of molecules into targeted supermolecules.¹⁵ In order to achieve this, a strategy of this kind needs to take cognisance of both the energetic and geometric properties of different types of intermolecular interactions.¹⁶ When this methodology is applied to the systematic architecture of crystal structures it is called Crystal Engineering. A more formal definition has been proposed by Desiraju which encompasses all previously mentioned features “...*the understanding of intermolecular interactions in the context of crystal packing and in the utilisation of such understanding in the design of new solids with desired physical and chemical properties*”.¹⁷ In this regard Desiraju aptly draws a parallel between crystal engineering and organic synthesis.

The term crystal engineering had its inception in 1955 when Pepinsky presented a paper concerning the employment of complex ions in the application of direct methods for structure determination of optically active ions, entitled “Crystal Engineering: a new concept in crystallography”.¹⁸ However, the contribution in 1971 by Schmidt¹⁹ “...*we shall, in the present context of synthetic and mechanistic photochemistry, be able to ‘engineer’ crystal structures having intermolecular contact geometries appropriate for chemical reaction...*” is more commonly recognised as the point at which the field of crystal engineering first commenced.

Different strategies have been developed for the systematic design of molecular crystals, of which Desiraju’s concept of ‘supramolecular synthons’ is the most recognised.¹⁷ This methodology is based on a process in which designed combinations of intermolecular interactions are used to derive synthons, which incorporate chemical as well as geometrical recognition features of molecular fragments. The crystal becomes the retrosynthetic goal in a supramolecular retrosynthesis, a process which is analogous to the established concept of covalent retrosynthesis. Figure 1 features the relationship between a molecule, a functional group and the derived supramolecular synthon and shows how the intermolecular interaction forms an integral part of the synthon. There are two types of supramolecular synthons- the homosynthon formed between self-complementary donor and acceptor groups *e.g.* the carboxylic acid dimer, and the heterosynthon

formed between different, yet complementary donor and acceptor groups *e.g.* between hydroxyl and pyridine moieties.²⁰

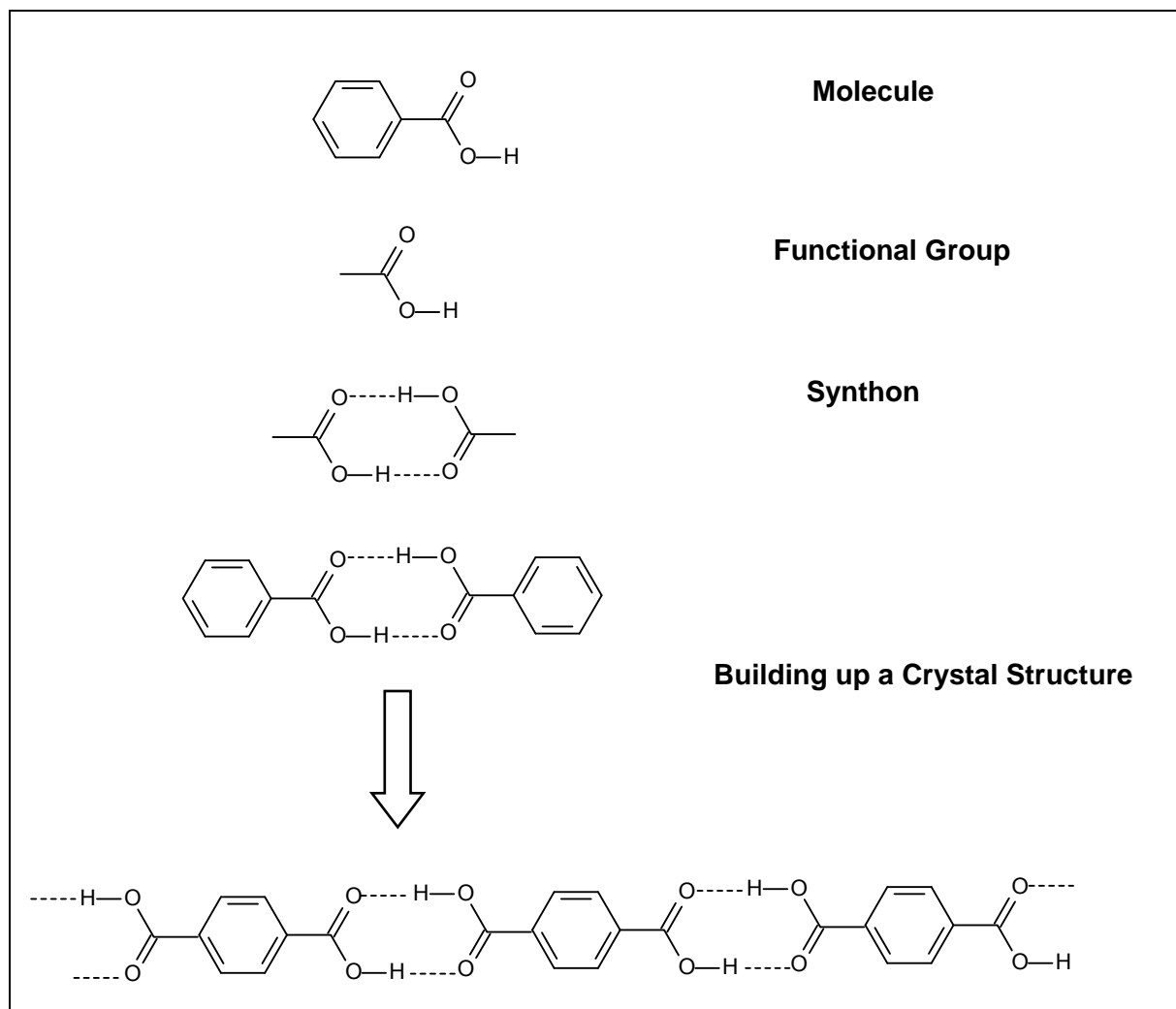


Figure 1. From molecules to crystal structures *via* supramolecular synthons.²¹

The recent expanse in the literature regarding the synthesis and analysis of coordination polymers (or metal-organic frameworks, MOFs)²² exemplifies how crystal engineering has become a paradigm for the design of new supramolecular architectures. Arguably the most noteworthy example of this is the sub-class of crystal engineering proposed by Yaghi *et al.*, *i.e.* reticular chemistry.²³

Reticular chemistry is informally defined as the construction of predetermined structures from molecular building blocks, which are linked together *via* strong bonds.²³ The methodology as employed by Yaghi borrows the concept of SBUs (secondary building units) from zeolite analysis to construct rigid networks with

permanent porosity. Owing to their ability to aggregate metal ions into M-O-C clusters (or SBUs), carboxylate linkers have been used most extensively in the construction of these porous materials (Figure 2). The frameworks thus created are neutral, which circumvents the problem of counter-ion clathration encountered with zeolites.²⁴

Although reticular synthesis of coordination networks may be distinguished from retrosynthesis of molecular crystals by examination of the bonds that link the building blocks together (strong bonds in the former, and weaker hydrogen bonds in the latter), the two concepts are remarkably similar.

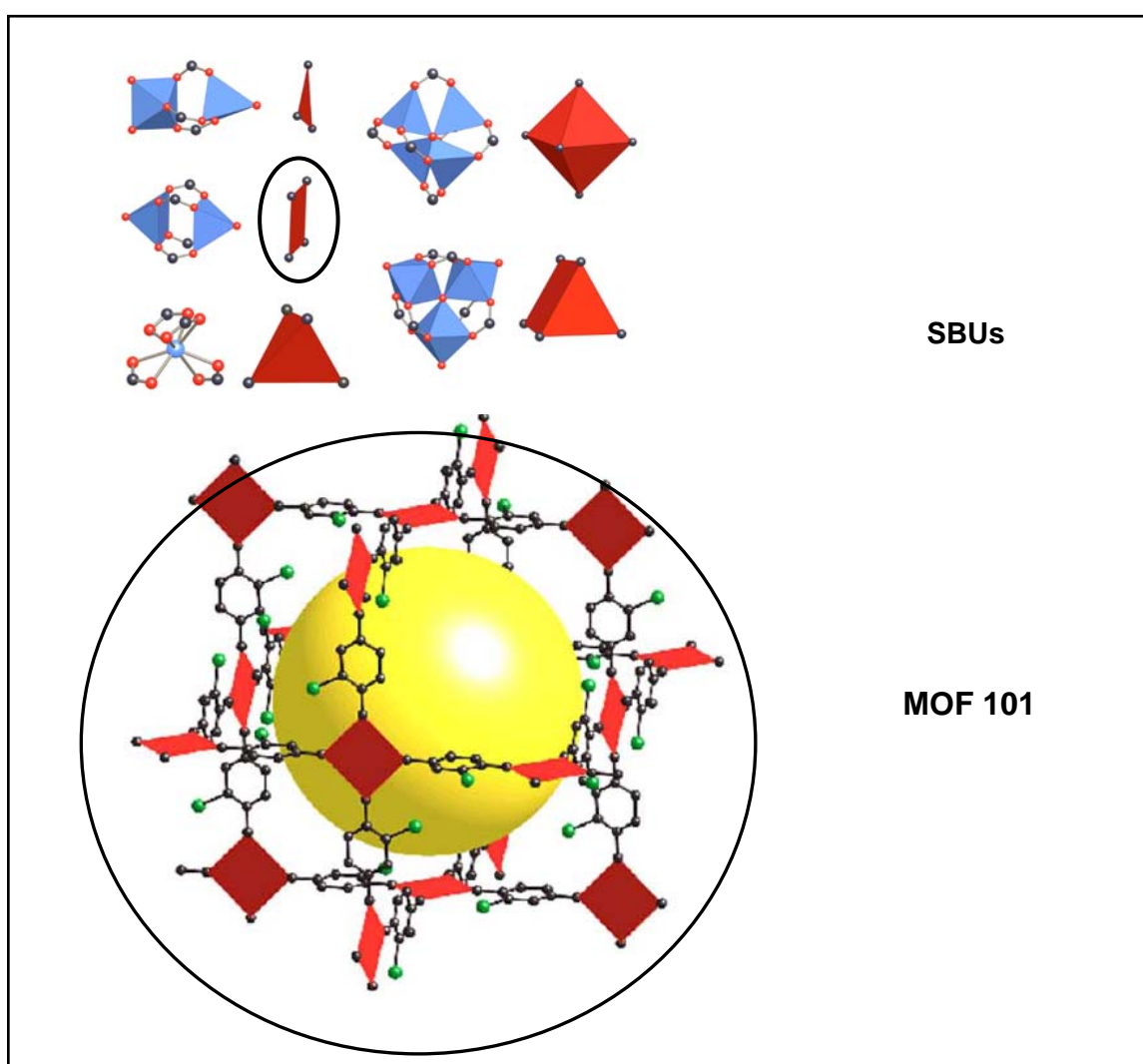


Figure 2. Examples of SBUs from carboxylate MOFs. Oxygen atoms are represented as red spheres and carbon atoms as black spheres. Metal-oxygen polyhedra are coloured blue, and the polyhedra defined by carboxylate carbon atoms (SBUs) are red (top).²³ An example of a MOF constructed from a set of SBUs (bottom).²⁵

1.3. INTERMOLECULAR INTERACTIONS

“Crystal packing results as the sum of many different contributions of directional and non-directional intermolecular interactions, so it is important that different types of interactions be considered jointly in structural analysis....”

Gautam R. Desiraju²⁶

A thorough understanding of the intermolecular forces that govern the aggregation of molecular components is at the heart of the field of crystal engineering. Once these interactions are fully understood, the ultimate aim would be to employ this information in the purposeful design of materials with specific properties. Although we are far from realising this, many advances have been made.

It is globally understood that intermolecular interactions can be divided into directional and non-directional (isotropic) terms.

THE HYDROGEN BOND

Of the directional forces, the hydrogen bond is the most understood and, arguably, the most important intermolecular interaction in the field of crystal engineering, as it combines strength with directionality.²⁷ Its earliest reference in the literature dates back to 1902 and 1910, when Werner²⁸ and Hantzsch²⁹ used the term *Nebenvaleanz* (secondary valence) to describe a binding interaction in ammonia salts. But, it was only in 1935 when Pauling³⁰ used the term ‘hydrogen bond’ to account for the residual entropy of ice and the subsequent chapter on hydrogen bonding in ‘The nature of the chemical bond’,³¹ that the subject of hydrogen bonding was thrust into the chemical mainstream.

The definition of a hydrogen bond in the modern context is, however, not as clear-cut as one would expect. Many attempts have been made to define a hydrogen bond and only the very general and most flexible definitions that include the broad range of accepted hydrogen bonds have stood the test of time. To date the most accepted definition of a hydrogen bond has been proposed by Steiner,³² which is an augmentation of the Pimentel and McClellan definition.³³ It states:

“A D-H...A interaction is called a ‘hydrogen bond’, if (1) it constitutes a local bond, and (2) D-H acts as proton donor to A.”

Despite the difficulty in finding an all-encompassing chemical definition for a hydrogen bond, the general geometrical characterisation of a hydrogen bond is relatively simple. The hydrogen bond $D-H\cdots A$ is comprised of a donor $D-H$ and an acceptor A (it is pertinent to note at this point that this is counter to the convention used in chemical literature, where a donor is an electron-rich species and an acceptor is an electron-deficient species). If the acceptor is extended, then the hydrogen bond may be represented by the notation $D-H\cdots A-X$, and the following parameters are valid: the $D-H$ distance or r , the $H\cdots A$ distance or d , the $D\cdots A$ distance or Y , the donor $\angle DHA$ or θ and the acceptor $\angle HAX$ or ϕ (Figure 3).²⁰

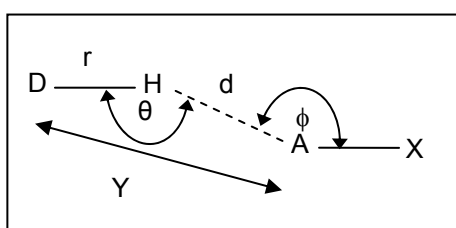


Figure 3. Definition of the geometrical parameters r , d , Y , θ and ϕ for a hydrogen bond.²⁶

Owing to the long-range nature of the hydrogen bond, the $D-H$ group may at one time be bonded to more than one acceptor A . In the case of there being two acceptors, $A1$ and $A2$, the bond is called a bifurcated hydrogen bond. Accordingly, in the case of three acceptors, $A1$, $A2$ and $A3$, the bond is called a trifurcated hydrogen bond.³⁴ The $D-H$ group is referred to as a bifurcated and trifurcated donor in the former and latter cases, respectively. A situation may also arise in which an acceptor group is simultaneously bonded to two distinct donor groups, and in this case the $A-X$ group is called a bifurcated acceptor. All three of these situations have been represented in Figure 4.

Hydrogen bond energies span about two orders of magnitude and can be found in the range of 0.5–40 kcal/mol. It is useful in the context of crystal engineering to classify hydrogen bonds in terms of geometric, energetic and thermodynamic properties. In this study the system proposed by Desiraju²⁶ will be followed. This classification system divides hydrogen bonds into three categories: very strong, strong and weak hydrogen bonds.

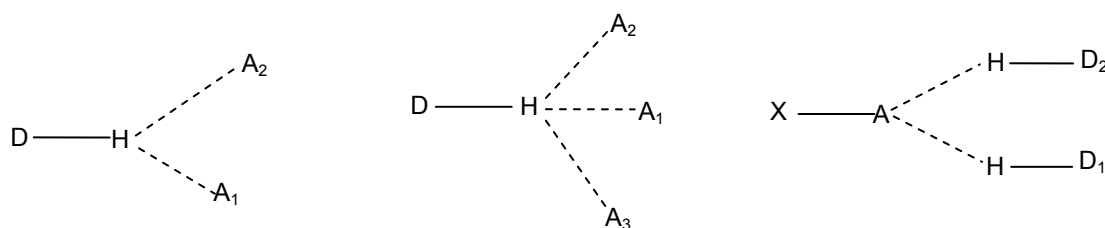
**Bifurcated Donor****Trifurcated Donor****Bifurcated Acceptor**

Figure 4. Definitions of a bifurcated donor (left), a trifurcated donor (middle) and a bifurcated acceptor (right).

Very strong hydrogen bonds (15–40 kcal/mol) are usually of the kind $D-H\cdots A^-$ or $D^+-H\cdots A$, *i.e.* between an acid and a conjugate base or *vice versa*. They are mostly intramolecular and are characterised by their near-covalent nature.

Strong hydrogen bonds (4–15 kcal/mol) are chiefly electrostatic in nature, and represent the largest category of hydrogen bonds. They are usually associated with oxygen and nitrogen donor acceptor pairs ($O-H\cdots O$, $O-H\cdots N$, $N-H\cdots O$). In the absence of steric effects, molecules with functional groups capable of forming these kinds of hydrogen bonds readily do so, and are thus associated with crystal engineering³⁴ and biological systems.³⁵

Weak hydrogen bonds (<4 kcal/mol) form the final category. They are electrostatic interactions, but this property is dependant on the nature of the donor and acceptor groups (*i.e.* their dispersive and charge-transfer components). Bonds that lie in the 2 – 4 kcal/mol energy range are mostly long-range electrostatic forces with an r^{-1} dependence on distance (as opposed to the inverse sixth power dependence of dispersion forces).³⁶ However, interactions falling at the bottom of the energy range for these hydrogen bonds are barely stronger than van der Waals interactions (approximately 0.5 kcal/mol).²⁶ Selected properties of these three classes of hydrogen bonding are shown in Table 1.

Table 1. Some properties of very strong, strong and weak hydrogen bonds.

	Very Strong	Strong	Weak
Bond energy (-kcal/mol)	15-40	4-15	<4
Examples	[F...H...F]- [N...H...N]+ P-OH...O=P	O-H...O=C N-H...O=C O-H...O-H	C-H...O O-H... π Os-H...O
Bond lengths	D-A \approx D-H	H...A > D-H	H...A \gg D-H
Lengthening of D-H (Å)	0.05-0.2	0.01-0.05	\leq 0.01
Y(D...A) range (Å)	2.2-2.5	2.5-3.2	3.0-4.0
d(H...A) range (Å)	1.2-1.5	1.5-2.2	2.0-3.0
Bonds shorter than vdW	100%	Almost 100%	30- 80%
θ (D-H...A) range (°)	175-180	130-180	90-180
Effect on crystal packing	Strong	Distinctive	Variable
Utility in crystal engineering	Unknown	Useful	Partly useful
Covalency	Pronounced	Weak	Vanishing
Electrostatics	Significant	Dominant	Moderate

Source: Adapted from Ref.²⁶NON DIRECTIONAL INTERACTIONS (π - π STACKING)

The isotropic terms may further be subdivided into exchange repulsion and dispersion (London) terms, the sum of which constitute “van der Waals interactions”. The exchange repulsion forces are responsible for keeping molecules apart from one another and follows an r^{-12} law, which implies that at short interatomic distances the repulsion between atoms is strong, thus providing a balancing effect of dispersion forces at short range.³ With increasing interatomic distances, however, the effects of these forces diminish rapidly. Exchange repulsion interactions are important as they define molecular shape and conformation.

The attractive or dispersion forces result from the interactions of fluctuating multipoles of neighbouring molecules. These forces are based on the premise that, at a given time, some adjacent molecules may have opposing poles and hence attractive charge distributions. The dispersion attraction decreases with r (interatomic separation) as $-r^{-6}$, and has an approximate dependence on the size of the molecules as each atom and polarisable bond contributes.¹⁶ Owing to the fact that all molecules are involved in this type of interaction, dispersive forces are the major contribution to the

overall lattice energy of a crystal, and as such can be viewed as “the universal glue that leads to the formation of condensed phases”.³⁷

C and H are the most prevalent atoms in organic systems, and for this reason most van der Waals interactions relevant to the field of crystal engineering involve C···C, C···H and H···H contacts. The latter case is found more commonly in aliphatic systems where the ratio of hydrogen to carbon is higher than in analogous aromatic systems. Closer inspection is required in order to understand why C···C and C···H interactions predominate in aromatic systems. An aromatic hydrocarbon molecule is usually flat and contains a cyclic carbon framework capable of sustaining π -delocalised electron density. It is the polarisable nature of this π -electron density which enhances the stabilising dispersion interactions between adjacent aromatic molecules. This stabilising effect is further improved by the addition of high-Z heteroatoms as they are more polarisable than molecules consisting exclusively of carbon atoms.³⁸ As aromatic molecules generally have high ratios of C:H, they tend to stack in an effort to maximise the number of C···C interactions. C···H interactions are also important in aromatic systems (see edge-to-face π -stacking below).

Although a wide variety of intermediate π -stacking geometries are known,³⁹ the two most commonly observed geometrical relationships between two adjacent aromatic rings molecules are:

(i) the offset face-to-face (OFF) motif, where rings are approximately parallel to one another, but offset to maximize intermolecular contact between oppositely charged regions;

(ii) the edge-to-face (EF) or ‘T-shaped’ motif, where the slightly electron deficient hydrogen atom of the one ring is directed towards the central negative π -electron density of the second aromatic ring (epitomised in the characteristic herringbone motif most commonly found in the crystal packing of small aromatic compounds).

A third geometrical relationship exists, termed face-to-face (FF) or eclipsed π -stacking. In this type of interaction, the adjacent faces of the aromatic molecules are parallel but not offset (Figure 5). For identical aromatic molecules this is a repulsive electrostatic interaction and is thus not common, but for different aromatic systems with complementary electron distributions (e.g. between C₆H₆ and C₆F₆) FF geometry serves to maximise electrostatic intermolecular stabilisation.³⁸

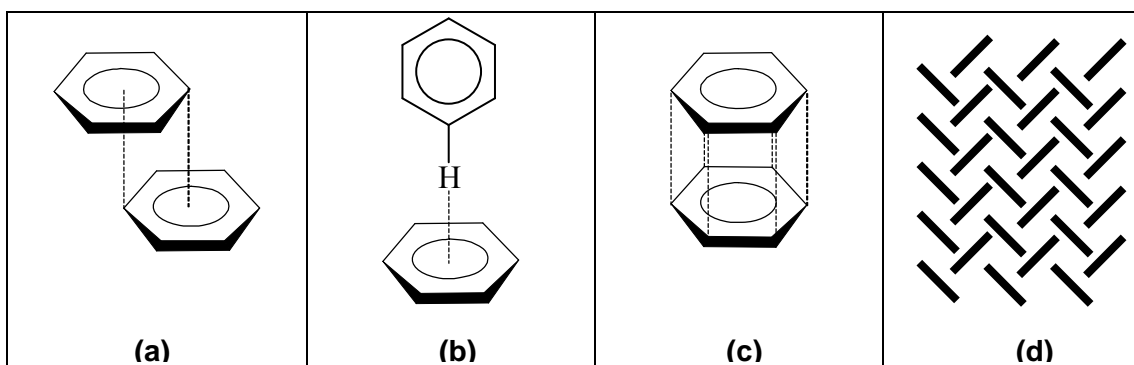


Figure 5. (a) OFF π - π stacking motif, where rings are off-set and parallel (b) EF or T-shaped motif, where the hydrogen atom of one ring is directed towards the centre of the second ring (c) FF or eclipsed stacking, where rings are parallel but not off-set (d) the well-known herringbone motif formed as a result of EF interactions.

Hunter and Sanders⁴⁰ proposed a model in which the range of geometries that exist in π - π -stacking interactions can be rationalised in terms of competing electrostatic and van der Waals influences. The authors postulated that π -stacking interactions occur when the attractive interactions between π -electrons and the sigma-framework prevail over unfavourable repulsive interactions. Finally, the model relates the strength and geometry of the π -interactions to the properties of the atoms in regions of intermolecular contact, rather than molecules as a whole.

It is useful to make a few general comments about these two kinds of intermolecular forces. It has been postulated that, in the absence of any other forces, non-directional forces will lead to a close-packed arrangement in the crystal structure. However, non-directional forces do not possess specific topological properties when other forces come into play, as it is not possible to predict their performance in different structural environments. Weak hydrogen bonds, such as C-H \cdots O and C-H \cdots N, are considered more important than dispersion interactions as they can have orienting effects on molecules prior to nucleation and crystallisation. In systems where these interactions are abundant, their effect on crystal packing is most pronounced.

It is also important to consider that there are cases where these weak hydrogen bonds display more isotropic character, and are thus poorly directing. It is this variable nature of these weak hydrogen bonds that make their effects difficult to predict. Strong hydrogen bonds, on the other hand, are exceptionally valuable in

crystal structure prediction. They combine the concepts of strength and directionality and, most importantly, reproducibility²⁷ - an area in which weak hydrogen bonds fall short. Indeed, as previously mentioned these interactions have been successfully applied in the construction of supramolecular synthons in crystal engineering.¹⁷

METALLOPHILIC INTERACTIONS

Some d^{10} metals have a propensity to aggregate at distances close to the sum of their van der Waals radii.⁴¹ This predominantly occurs in compounds containing Au(I), Ag(I) and Cu(I) cations and is attributed to aurophilic, argentophilic and cuprophilic interactions, respectively. The energy of these attractive supramolecular contacts is comparable in strength to strong hydrogen bonds and has been roughly estimated in the range of 5–7 kJ/mol.⁴²

METAL- π INTERACTIONS

This type of interaction occurs when transition metal cations accept π -electrons from unsaturated organic molecules and, in the process, a very stable organometallic molecule is formed. The paradigmatic interaction involving neutral arenes and Ag(I) cations is the most relevant to the present study. This interaction occurs within a distance range of 2.89-3.37 Å (Ag-centroid) via a η^6 mode of complexation.⁴³

THE COORDINATION BOND

A coordination bond is an ion-dipole interaction and predominantly forms through the donation of free electrons from a ligand (usually in the form of a lone pair of electrons) to an acceptor (typically a transition metal ion). This bond is superior to other intermolecular bonds because it is highly directional and it is relatively strong. Even though its energy range varies from being comparable to very strong hydrogen bonds to equalling those of strong covalent bonds (10-30 kcal/mol),⁴⁴ it is accepted that most coordination compounds are quite thermally stable, which has implications in the design of materials with prerequisites of stability. Owing to these characteristics, this type of interaction has been used extensively in the preparation of coordination networks as evidenced by the plethora of recent publications featuring exciting new topologies and crystal structures (the work of Yaghi²³ has already been

mentioned in this regard). Essentially, all coordination networks can be reduced to a set of nodes and linkers.⁴⁵ In this analogy the nodes may represent either a point *e.g.* a metal centre of certain geometry (tetrahedral, trigonal planar etc.) or a baricentre of a collection of atoms *e.g.* a metal cluster or a polyfunctional ligand. The linker may then be either an organic polydentate ligand or one of numerous linking interactions such as hydrogen bonds or π - π stacking interactions. In this simplified model the nodes are connected to one another by the linkers to form extended networks in 1D, 2D or 3D. Depending on the choice of node and linker, more than one rationalisation of the crystal packing may be possible. These alternative descriptions are not necessarily “wrong” and may merely reflect the crystal from a different perspective or correspond to the packing at various levels of structural organisation.⁴⁶

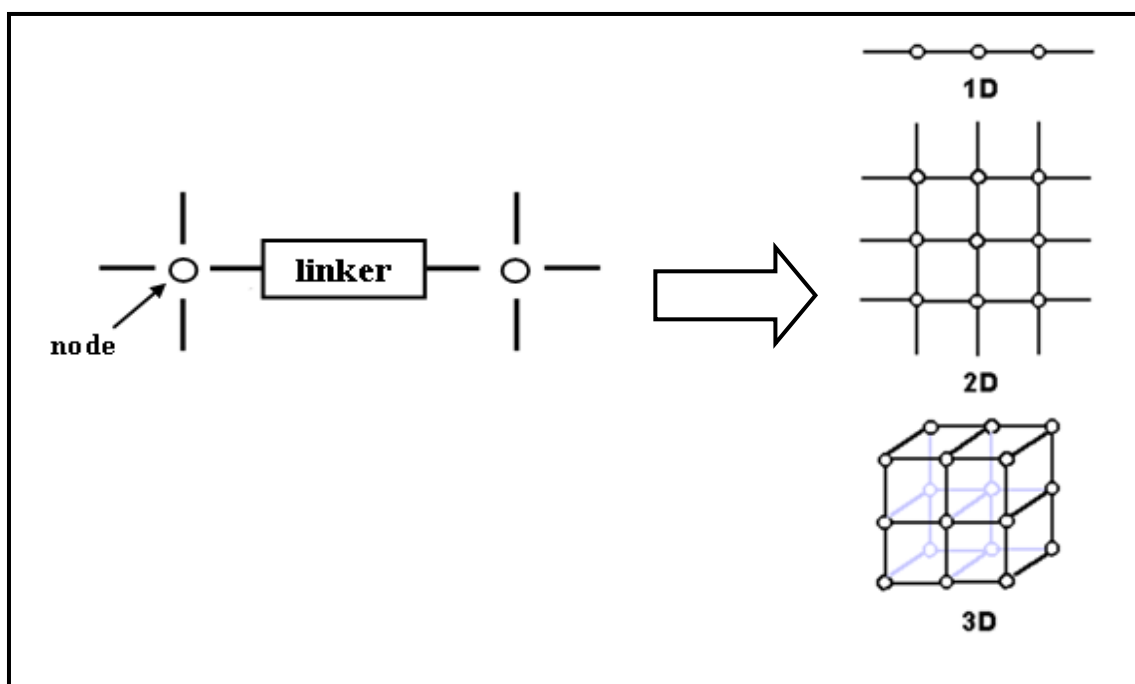


Figure 6. Schematic representation of 1D, 2D and 3D coordination polymers formed from a set of nodes connected to one another by linkers.

1.4. SELF-ASSEMBLY

Self-assembly is a valuable tool in the formation of supramolecular assemblies and has been studied most extensively in the context of biological systems *e.g.* the double-helical structure of DNA.³ This term is used to describe a process in which two or more complementary building blocks spontaneously associate, by way of non-

covalent forces, to form a new system of higher order; it therefore encompasses all of the intermolecular forces outlined in the previous section. The process is reversible and the resulting aggregate represents the most thermodynamically stable structure under prevailing conditions. In the context of this study we are interested in the process of self-assembly of molecules from solution or vapour, to form crystals.

1.5. POROSITY

A simple dictionary definition of a porous substance is one that is “full of or having pores; admitting the passage of gas or liquid through pores”. Furthermore, a pore is defined as “a small interstice admitting absorption or passage of a gas or liquid”.⁴⁷ It is therefore implied that a crystalline material possesses porosity in terms of interstitial volume in relation to its mass, and demonstrates porosity if it is permeable to gases or liquids moving in or out of the material.

Although porous crystalline materials have a large number of potential applications, our group is predominantly concerned with the gas sorption capabilities of these materials. Porosity, or sorption behaviour, is divided into two categories: *adsorption* and *absorption*. Adsorption is generally used to describe the condensation of gases onto the surface of a substance and it therefore a surface phenomenon.⁴⁸ Absorption occurs when gas molecules penetrate the mass of the absorbing phase and therefore involves the concept of incorporation of one substance within another. *Sorption* is a generic term used to describe either of the processes. Six different types of adsorption isotherms are recognised by IUPAC⁴⁹ (Figure 7). *Type I* isotherms refer to systems where the pore size of the adsorbent is similar to the dimensions of the sorbate molecule since a definite saturation limit exists due to the filling of adsorbent pores. These isotherms are reversible and have a characteristic concave shape.⁵⁰ The compounds mentioned in this study exhibit *Type I* sorption behaviour. *Type II – type VI* all refer to monolayer or multi-layer sorption processes and are not within the scope of this study.

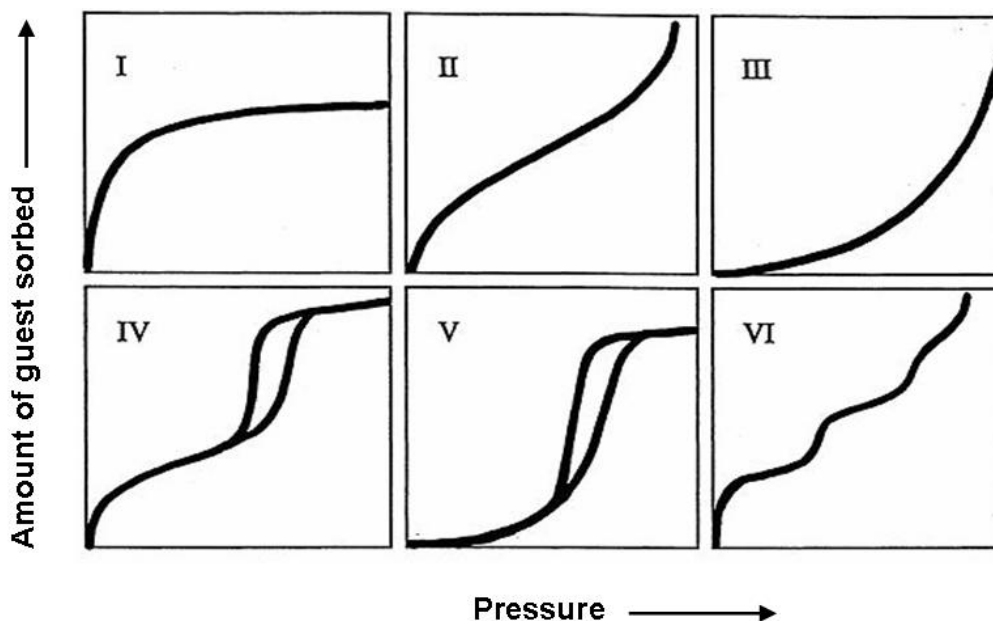


Figure 7. The six standard IUPAC adsorption isotherms.⁴⁹

Recent interest in the sorption capabilities of porous coordination networks has been accompanied by a vast increase in the volume of literature available on this topic. Although a simple dictionary definition has already been offered, an unambiguous answer to the question of what constitutes porosity in crystalline materials is not always found. This necessitates a short discussion on what constitutes porosity and what the different categories of porosity are. Recent reports by Barbour⁵¹ and Kitagawa⁵²⁻⁵⁴ state that claims of porosity need to be coupled with verifiable experimental results illustrating that guest uptake has taken place. The second component to this definition states that the term “porous” needs to be associated with a specific host phase and should not be considered a property of the bulk host material and, in principle, the host should be left unaffected by guest uptake/removal.

In the same report by Barbour⁵¹ three distinct categories of porosity are proposed:

1. Virtual porosity

In this category claims of porosity are usually created *in silico*. This is achieved by either a misrepresentation of the model by generating figures using the capped-stick or ball-and-stick metaphor instead of space filling diagrams, or by the deletion of judiciously selected atoms (such as counter-ions or solvent molecules). These claims are rarely supported by *in situ* demonstration of porosity.

2. Conventional porosity

In this form of porosity the host molecules play an integral role in creating channels in which guest molecules may be located. If the guest molecules can be removed or exchanged with another type of guest molecule without disrupting the topology of the host framework, that particular supramolecular phase may be termed *conventionally porous*. The most well-documented example of materials that adhere to the characteristics of this kind of porosity are zeolites.^{52, 54}

3. Porosity “without pores”

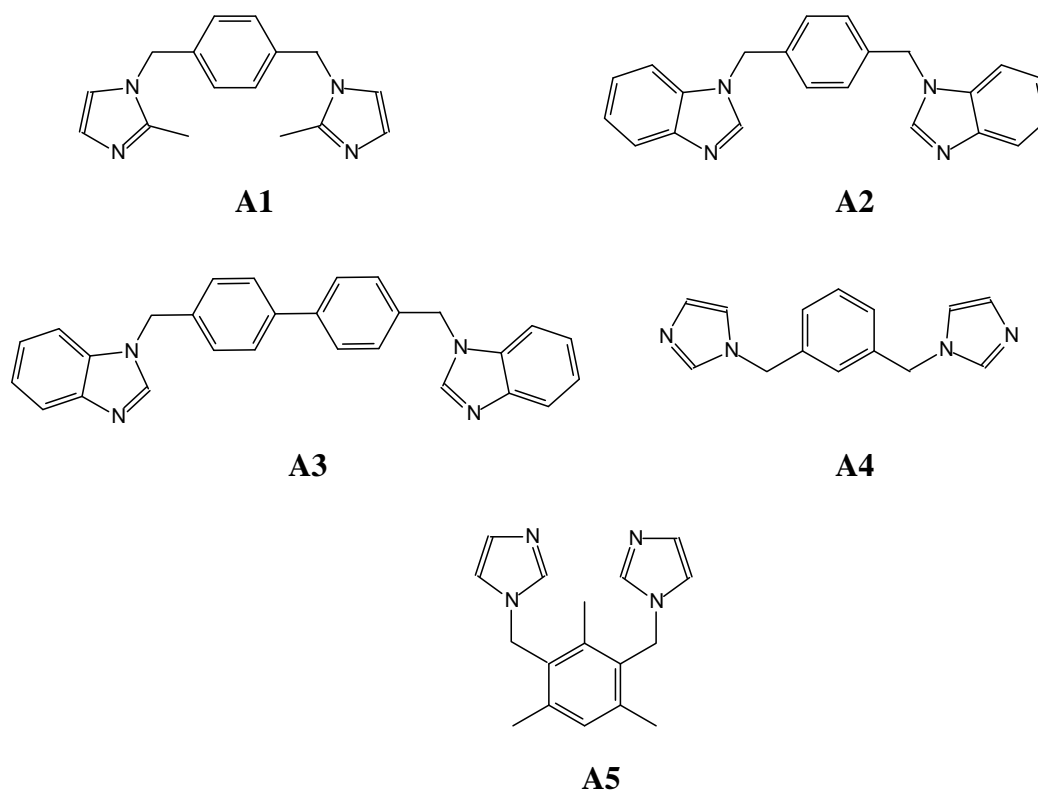
This form of porosity is also called *transient porosity* and arises when a crystal possesses discrete voids that are not interconnected to form a continuous channel through which a guest molecule may traverse. Many examples of porosity of this nature have been reported in the literature,⁵⁵⁻⁵⁸ and in most cases the exact mechanism of the absorption process is not known. It has been postulated however, that whilst the conventional classification of porosity is not valid (*i.e.* the materials are not permanently porous), a dynamic porosity exists in which thermal motion or guest-induced motion of the host molecules facilitates the movement of guest molecules through the crystal.

1.6. COORDINATION NETWORKS CONTAINING IMIDAZOLE FUNCTIONALISED LIGANDS

The use of ditopic or higher ordered ligands is required for the formation of coordination networks, and to date most groups have concentrated their efforts on utilising rigid ligands with pyridyl and carboxylate functional groups in this regard. Flexible ligands containing imidazole functional groups have received little attention in this regard. They have high affinities for metals and are easy to functionalise,⁵⁹ attributes which our group and others⁶⁰⁻⁶³ have exploited to successfully construct a range of complexes with interesting topologies.^{64, 65} We have also conducted systematic studies to probe the effects on the resulting structures when only one factor influences the process of crystallisation.^{66, 67} Finally, our group has shown that these flexible ligands can be used to construct functional devices capable of vapochromic responses⁶⁸ and the sorption of a variety of gases,^{69, 70} with retention of monocrystallinity. A short review of these results follows.

The first three ligands in Scheme 1 (**A1–A3**) are ditopic imidazole ligands used to construct eight novel coordination polymers.^{64, 65} It is convenient in the discussion

that follows to group these structures by dimensionality, therefore all 1D polymers will be discussed first, followed by the 2D polymers.



Scheme 1. The five structurally related ligands used in the construction of zero-, one- and two-dimensional coordination networks.

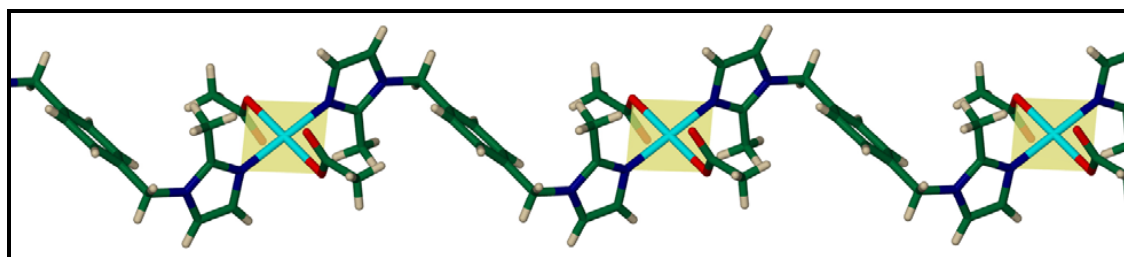


Figure 8. Capped-stick representation of the 1D strand formed in (a). Square planar copper ions have been highlighted yellow.

Exactly half of the coordination polymers formed are 1D, and surprisingly all featured Cu^{2+} in various coordination geometries. Of these structures, two contain **A1** as the bridging ligand between copper ions. In the first complex

$[\text{Cu}(\text{CH}_3\text{COO})_2(\mathbf{A1})_2]_n$ (**a**) simple 1D strands are formed, with the copper ion in a square planar coordination environment comprised of two coordinating ligands **A1** located *trans* to one another, and two monodentate acetate anions (Figure 8). The latter cooperate in the formation of hydrogen bonds with non-coordinated water molecules in the crystal lattice to link 1D strands into a 2D layer.

The second 1D structure containing **A1**, $[\text{Cu}(\text{NO}_3)_2(\text{H}_2\text{O})(\mathbf{A1})_{1.5}\cdot 4\text{H}_2\text{O}]_n$ (**b**), is slightly more complicated. The coordination environment about each copper ion is square pyramidal. The vertices of the pyramid consist of four ligands **A1** and the apex is occupied by a water molecule. As can be seen in Figure 9, the ligand assumes two distinctive roles in connecting the copper centres to one another. The red ligand contains an uncoordinated imidazole nitrogen atom that is free to accept a hydrogen bond from a lattice water molecule. The lattice water molecule in turn donates a hydrogen bond to the water molecule at the apex of the square pyramid, effectively forming a 34-membered ring through which the yellow ligand is threaded. This forms a *pseudo*-polyrotaxane arrangement.

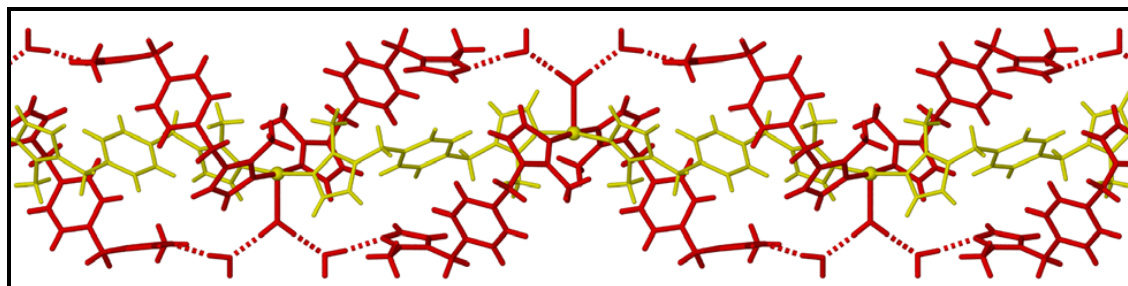


Figure 9. Capped-stick representation of the pseudo-polyrotaxane arrangement formed in (**b**). Two distinct ligands have been coloured red and yellow respectively.

$[\text{Cu}(\text{CH}_3\text{COO})_2(\text{H}_2\text{O})(\mathbf{A2})_2\cdot 3\text{H}_2\text{O}]_n$ (**c**) is the third 1D structure in this series, and it also features a copper ion in a square pyramidal environment. However, the vertices of the pyramid consist of only two ligands **A2** located *trans* to one another. The remaining vertical coordination sites are occupied by two monodentate acetate anions, and the apical position of the pyramid is occupied by a water molecule. The square pyramids are oriented in an up-down manner along the chain (**Figure 10**).

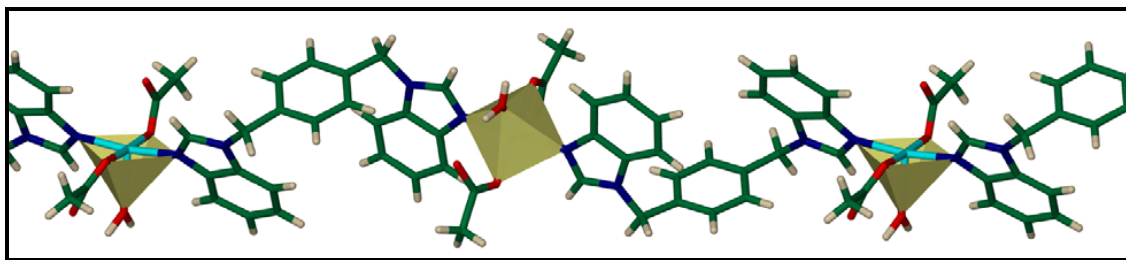


Figure 10. Capped-stick representation of the 1D strands formed in (c). The copper cations in the square pyramidal coordination environment have been highlighted in yellow.

The final 1D polymeric chain, $[\text{Cu}_2(\text{CH}_3\text{COO})_4(\text{A3})_{1.5}\cdot\text{CH}_3\text{CN}\cdot 2\text{CH}_3\text{OH}]_n$ (**d**), is the most interesting of the four structures since it features a 1D strand containing two different coordination geometries. At one node, the well-known paddle-wheel arrangement occurs, where two copper cations are bridged by four acetate anions. The apical positions of these two copper ions are occupied by benzimidazole groups of ligand **A3**. These copper cations are then connected to adjacent copper cations, which are in a distorted square planar environment, by means of a single bridging ligand. A second ligand is located *cis* to the first ligand of the square planar copper ion, and two monodentate acetate anions occupy the remaining *trans* and *cis* positions. The 1D chain resembles an approximate sine wave as seen in Figure 11.

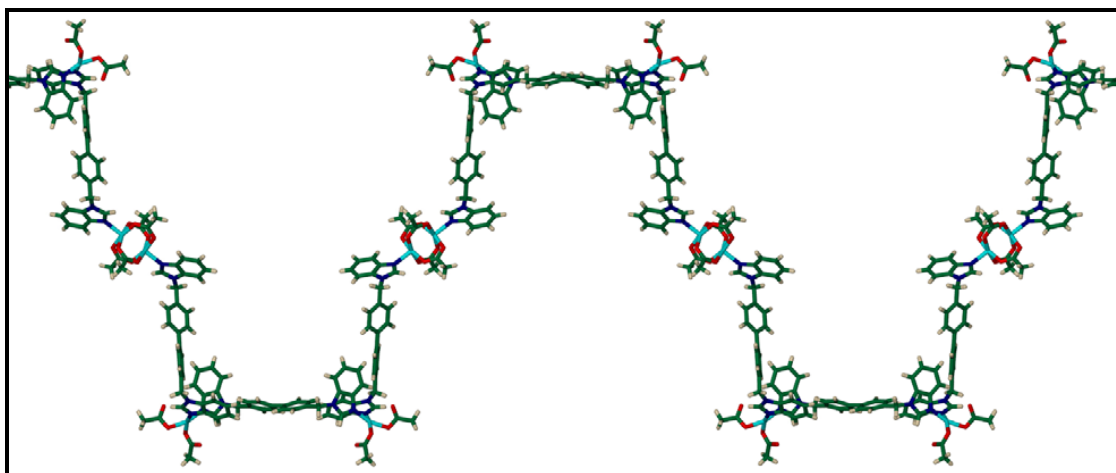
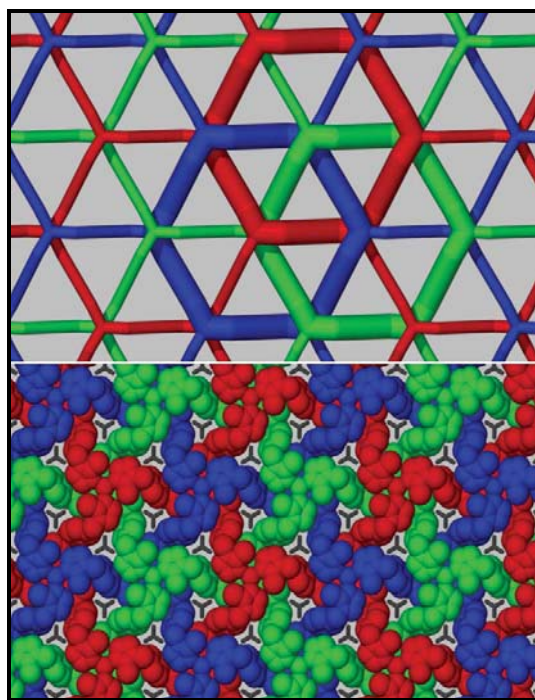


Figure 11. The sinusoidal 1D chain formed in (d). Molecules are shown in the capped-stick metaphor.



Two of the 2D structures, namely $[\text{Ag}(\mathbf{A1})(\text{BF}_4)]_n$ (**e**) and $[\text{Ag}(\mathbf{A1})(\text{CF}_3\text{SO}_3)]_n$ (**f**), are remarkably similar to one another in that they both contain silver ions in a trigonal planar coordination environment, with three imidazole rings (from three separate **A1** ligands) oriented in a propeller-like arrangement. Each ligand assumes an ‘S’ shape and bridges two silver ions which, in turn, each coordinate to three separate ligands, resulting in the formation of large hexagonal rings, which are connected in 2D to form a honeycomb lattice.

Figure 12. The topology of an infinite Borromean weave (top) and a space filling projection along [001]. BF_4^- anions are shown in capped-stick representation (bottom) showing the weave consisting of three separate honeycomb lattices (shown in red, green and blue).

Interestingly, three of the honeycomb lattices are entangled to form a Borromean weave (Figure 12), stabilised by ligand unsupported argentophilic ($\text{Ag}\cdots\text{Ag}$) interactions. In (**e**) the $\text{Ag}\cdots\text{Ag}$ separation is $3.0619(4)$ Å and the corresponding separation in (**f**) is $3.225(1)$ Å. No two layers are mutually interpenetrated in this motif and the entanglement cannot be unravelled without breaking covalent or coordination bonds. The counter-ion in each structure is situated in small gaps formed in the Borromean weave system. The two structures differ in the orientation of the three 2-methyl groups with respect to the plane defined by the coordinating nitrogen atoms. In (**e**), the methyl groups are oriented towards the outer surface of the Borromean layer (*i.e.* the same side of the plane), whereas in (**f**) they are oriented inwards. This orientation has an effect on the size of the triangular cavity in which the anions sit, *i.e.* the outward orientation in (**e**) gives rise to a smaller cavity and the inwards orientation in (**f**) gives rise to a larger cavity which can accommodate the larger anion (Figure 13).

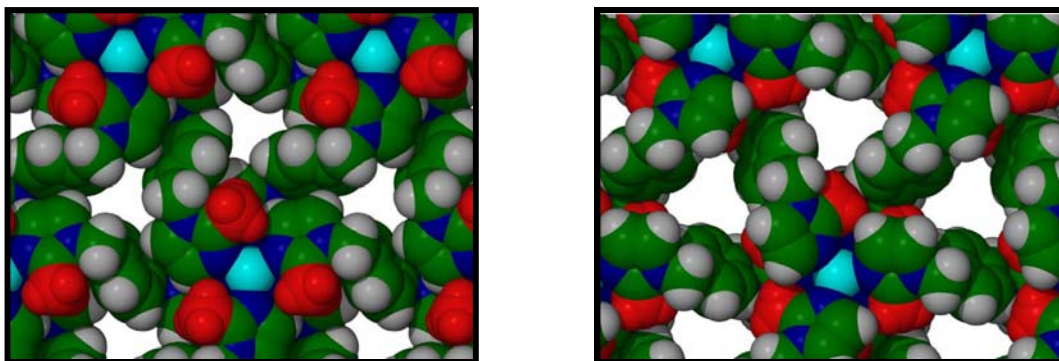


Figure 13. Space filled projection of (e) (left) and (f) (right) as viewed down [001]. Anions have been omitted in order to emphasise the difference in the size of the triangular cavities between the two structures and the methyl groups have been coloured red.

The third 2D structure in this series, $[\text{Co}(\text{NCS})_2(\text{CH}_3\text{OH})(\mathbf{A1})_{1.5}]_n$ (g), was obtained by slow evaporation of a methanolic solution of $\text{CoCl}_2 \cdot 6\text{H}_2\text{O}$, KSCN and **A1** in a 1:2:4 ratio. The cobalt ion is in an octahedral coordination environment in which the vertices of the square plane consist of two **A1** ligands (situated *trans* with respect to each other), a coordinated methanol molecule and an N-coordinated SCN^- ion. The apical positions of the octahedron are occupied by a third **A1** ligand and a second N-coordinated SCN^- ion. Owing to the arrangement of the three ditopic ligands, the metal centres act as three-connected nodes in the formation of a 2D distorted honeycomb coordination network. The large, corrugated nature of the honeycomb rings facilitates a threefold parallel interpenetration of the honeycomb layers (Figure 14), stabilised by O-H \cdots S hydrogen bonds formed by the donation of hydrogen bonds from coordinated MeOH molecules of one layer to the thiocyanate sulphur atoms of an adjacent layer ($\text{O}\cdots\text{S} = 3.225(1) \text{ \AA}$).

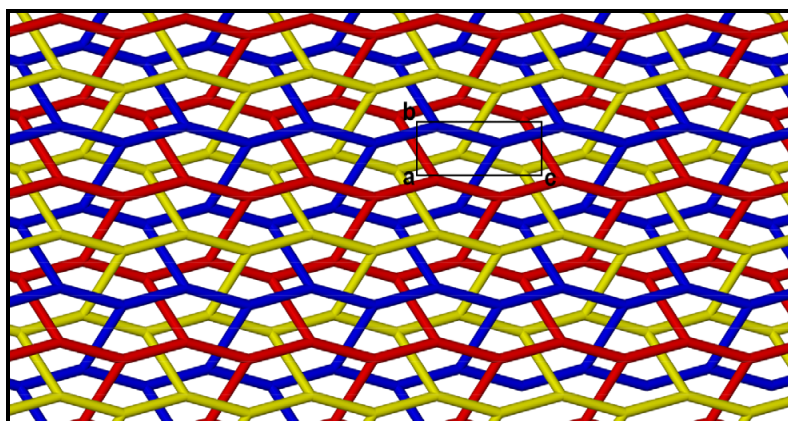


Figure 14. A representation of the threefold parallel interpenetration of the honeycomb layers formed in (g). Individual nets are coloured red, yellow and blue for clarity.

The final 2D structure, $[\text{CdCl}_2(\text{A}2)_2]_n$ (**h**), contains a cadmium ion in an octahedral coordination environment. The square plane is occupied by four imidazole groups from four different **A2** ligands, while the apical positions are occupied by two ligated chloride ions. Two adjacent benzimidazole groups are positioned with their benzo moieties on one side of the equatorial plane whilst the remaining two are positioned on the opposite side of the plane, to form a neutral 2D net (Figure 15). Adjacent layers are associated by means of van der Waals interactions.

As has been demonstrated thus far, imidazole functionalised ligands have a high propensity for metal coordination, and the resulting complexes can, in most cases, be studied by SCD with relative ease. This makes them ideal candidates for systematic studies that explore the structural diversity obtainable when the process of crystallisation is influenced by only one parameter.

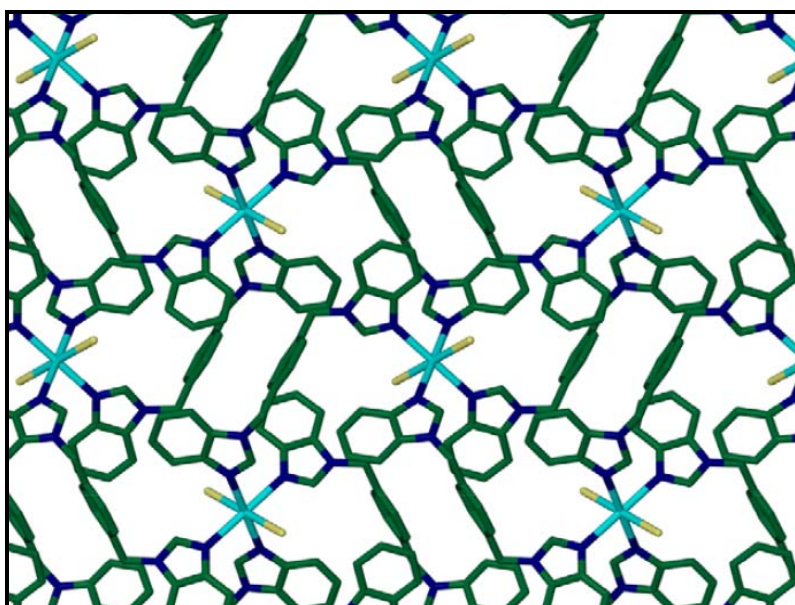


Figure 15. Capped-stick representation of the 2D nets formed in (**h**), as viewed down [101].

The conformationally flexible exo-bidentate ligand **A4** (Scheme 1) was used in combination with three copper(II) salts to study the influence of the metal-to-ligand molar ratio on the formation of the final product.⁶⁷ A second study was conducted on the metallocycle **M1** (formed from the combination of **A1** and $\text{CuCl}_2 \cdot 2\text{H}_2\text{O}$). This investigation was aimed at determining the effects of different solvents on the shapes and packing arrangements of **M1**.⁶⁶

It is not necessary in the context of the findings of these two investigations to provide a detailed structural analysis of all metal organic complexes obtained, and as such only a brief summary of the results follows.

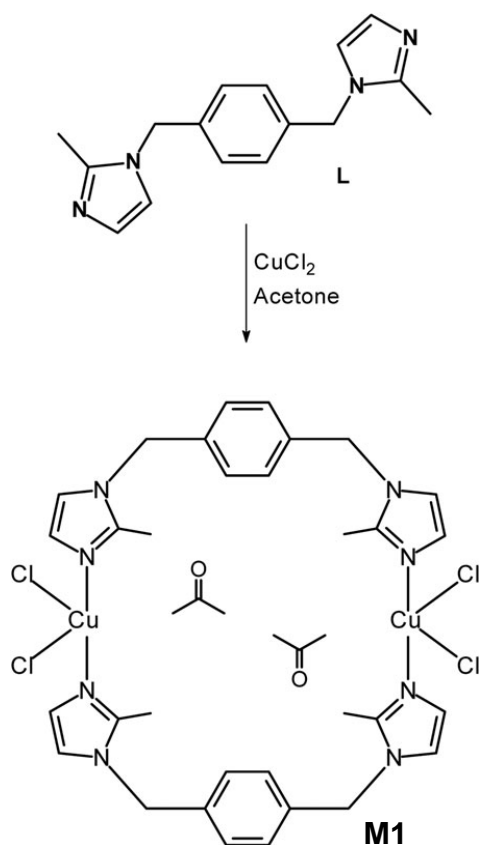
In the first study, *i.e.* the influence of metal-to-ligand ratio, a total of 8 unique complexes were obtained using ligand **A4** and three different copper (II) salts, namely $\text{CuCl}_2 \cdot 2\text{H}_2\text{O}$, CuBr_2 and $\text{Cu}(\text{NO}_3)_2 \cdot 4\text{H}_2\text{O}$. Single crystals of the metal complexes (**1**)-(**8**) were grown from methanolic solutions containing metal-to-ligand molar ratios of 1:4, 1:1 and 4:1, respectively. Table 2 contains a summary of the experimental conditions used to produce complexes (**1**)-(**8**) and a brief description of the resulting crystal structures. A typical entry consists of the formula of the complex, the morphology of the single crystal, the dimensionality of the structure, the coordination environment around the metal centre, notable features of the structure and the solid-state M:**A4** ratio.

A comparison of the complexes obtained for the reaction of **A4** with the metal salts $\text{CuCl}_2 \cdot 2\text{H}_2\text{O}$ and CuBr_2 yields the following generalised statements: when the solution M:**A4** ratio is high (*i.e.* 4:1) an overall 0D dinuclear complex with a solid-state M:**A4** ratio of 1:1 is obtained. However, when the solution ratio is low (*i.e.* 1:4) the corresponding solid state ratio is 1:2 and an infinite 1D strand is formed. It is not possible to make such generalised statements for the two complexes obtained from 1:1 solution ratios. In complex (**1**) the solution ratio is reflected in the solid-state ratio, but for the complex obtained with the CuBr_2 metal salt, complex (**3**), the solution ratio of 1:1 yields a solid-state ratio of 1:2. The authors account for this phenomenon by offering the simple suggestion that Cu^{2+} has a greater affinity for Cl^- than it does for water under conditions of crystallisation, but it will bind more readily to water when Br^- is present.

Four structures were obtained for the reaction of **A4** with $\text{Cu}(\text{NO}_3)_2 \cdot 4\text{H}_2\text{O}$. Complex (**8**), the only structure obtained for the 4:1 solution ratio, yields a M:**A4** ratio of 1:1 in the solid-state. Complex (**6**) forms from solutions in which the M:**A4** ratio is either 1:4 and 1:1 and is similar in structure to both complexes (**2**) and (**3**), indicating that this structure type is most probably preferred for this ligand when the M:**A4** ratio is less than or equal to unity. Complexes (**5**) and (**6**) crystallise concomitantly in the vial containing a 1:1 solution ratio, *ca.* 6 vol % of (**5**) and 94 vol% of (**6**). Complex (**7**) forms as a result of exposure of (**6**) to atmospheric water over a period of several weeks.

Table 2. A summary of the experimental conditions used to produce complexes (1)-(8). Each entry consists of the formula of the complex, the morphology of the single crystal, the dimensionality of the structure, the coordination environment around the metal centre, notable features of the structure and the solid state M:A4 ratio.

Solution ratio (M:A4)	Structures obtained with $\text{CuCl}_2 \cdot 2\text{H}_2\text{O}$	Structures obtained with CuBr_2	Structures obtained with $\text{Cu}(\text{NO}_3)_2 \cdot 4\text{H}_2\text{O}$
1:4	$([\text{CuA}_4\text{Cl}_2] \cdot 2\text{CH}_3\text{OH})_n$ (2) •Blue prism •1D strand •Octahedral <i>•Apical sites occupied by Cl</i> •1:2	$([\text{CuA}_4(\text{H}_2\text{O})_2]\text{Br}_2)_n$ (3) •Blue prism •1D strand •Octahedral <i>•Apical sites occupied by H₂O</i> •1:2	$[\text{CuA}_4(\text{NO}_3)_2]_n$ (6) •Violet block •1D strand •Octahedral <i>•Apical sites occupied by NO₃⁻</i> •1:2 $([\text{CuA}_4(\text{CH}_3\text{OH})_2][\text{CuA}_4(\text{H}_2\text{O})_2](\text{NO}_3)_4 \cdot 2\text{H}_2\text{O})_n$ (7) •Blue prism •1D strand •Octahedral <i>•Apical sites occupied by MeOH</i> •1:2
1:1	$[\text{Cu}_2\text{A}_4(\mu\text{-Cl})_2\text{Cl}_2]$ (1) •Green block •0D dinuclear complex •Distorted square-based pyramid <i>•Apex of the pyramid occupied by a bridging Cl ion.</i> •1:1	$([\text{CuA}_4(\text{H}_2\text{O})_2]\text{Br}_2)_n$ (3) •Blue prism •1D strand •Octahedral <i>•Apical sites occupied by H₂O</i> •1:2	$[\text{CuA}_4(\text{NO}_3)_2]_n$ (5) •Violet prism •2D layers •Octahedral <i>•Apical sites occupied by NO₃⁻</i> •1:2 $[\text{CuA}_4(\text{NO}_3)_2]_\infty$ (6) •1D strand •Octahedral <i>•Apical sites occupied by NO₃⁻</i> •1:2
4:1	$[\text{Cu}_2\text{A}_4(\mu\text{-Cl})_2\text{Cl}_2]$ (1) •Green block •0D dinuclear complex •Distorted square-based pyramid <i>•Apex of the pyramid occupied by a bridging Cl ion</i> •1:1	$[\text{Cu}_2\text{A}_4(\mu\text{-Br})_2\text{Br}_2]$ (4) •Green block •0D dinuclear complex •Distorted square-based pyramid <i>•Apex of the pyramid occupied by a bridging Br⁻ ion</i> •1:1	$[\text{CuA}_4(\text{H}_2\text{O})(\text{NO}_3)_2]_n$ (8) •Blue plate •1D strand •Square-based pyramid <i>•Apex of the pyramid occupied by a water molecule</i> •1:1



Scheme 2. Formation of $[\text{Cu}_2\text{Cl}_4\mathbf{A1}_2]\cdot 2(\text{acetone})$ (**M1**)

The $\text{Cu}_2\text{Cl}_4\mathbf{A1}_2$ complex was then dissolved in a variety of solvents and crystals suitable for SCD were grown by the method of slow evaporation over a period of several days.

If the resulting structure featured a metallocyclic complex, it was characterised by four specific parameters; conformation, stacking pitch, tilt angle and guest volume (Table 3). The conformation parameter refers to the orientation of the imidazole rings relative to the mean plane of the metallocycle, and according to the convention used, the imidazole rings can either be directed up (U) or down (D) with respect to this mean plane (Figure 16).

Structures **1–8** share many similarities in the conformation and stacking of their metallocycles *i.e.* the rings are canted either at an angle of 42° or 49° relative to their stacking axis which forms either channels or discrete pockets in which solvent molecules reside. The former was formed by those metallocycles with UDD conformations and the latter by those with UDDU conformations. The most important conclusion that was drawn from the analysis of these results was that the solvent,

The second study in this series involved the investigation of the effect of solvent templation on the shape and packing arrangement of the metallocycle $[\text{Cu}_2\text{Cl}_4\mathbf{A1}_2]$. This was achieved by the single crystal X-ray diffraction analysis of a series of eight recrystallisations of a $\text{CuCl}_2:\mathbf{A1}$ (1:1) mixture, from a selection of common solvents. The initial step involved the precipitation of the $[\text{Cu}_2\text{Cl}_4\mathbf{A1}_2]\cdot 2(\text{acetone})$ adduct (**M1** in

Scheme 2) from an equimolar solution of $\text{CuCl}_2\cdot 2\text{H}_2\text{O}$ and **A1** in acetone. The solvent was then removed *in vacuo* to yield a complex with an exact metal to ligand stoichiometry of 1:1.

trapped as guest molecules, had a direct affect on the conformation of the metallocycle, and that the resulting conformation was most likely solvent-templated. Unfortunately, a direct correlation could not be made between the choice of solvent and the resulting conformation, a finding which would have significant application in the field of crystal structure prediction. It was also noted that complexes **9** and **10** form 1D polymeric chains and that the structure of **9** is reminiscent of the metallocyclic structure with regard to its inclusion of guest molecules. The inclusion of complex **10** in this study served to illustrate the effect of a coordinating solvent on the resulting structural topology.

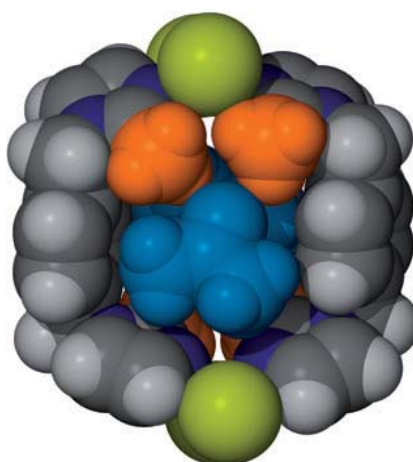


Figure 16. Space filling representation of metallocycle **M1**. Starting at the methyl group (orange) in the top left corner and proceeding clockwise, this structure may be assigned the conformation UUDD. Guest acetone molecules are shown as blue van der Waals surfaces.

Table 3. Guest identity, stoichiometry, topology, and conformation of compounds **1-10**.

Guest	Cu : G	Complex type ^a	Conformation	Stacking pitch ^b /Å	Tilt angle ^c /°	Guest volume/Å ³
1 Acetone	1 : 1	M	UDD	8.730(1)	49.1	60.6
2 Acetonitrile	1 : 1	M	UDDU	8.590(2)	42.5	43.7
3 DCM	1 : 1	M	UDD	8.589(3)	49.2	58.4
4 THF	1 : 1	M	UDD	8.826(3)	49.9	73.2
5 DMSO	1 : 1	M	UDD	8.882(1)	48.8	68.4
6 Ethyl acetate	2 : 1	M	UDDU	8.404(2)	42.6	85.8
7 Chloroform	2 : 3	M	UDDU	8.132(7)	55.3	74.5
8 1,4-Dioxane	4 : 3	M	UDD & UDDU	8.601(2)	48.2 & 42.3	81.2
9 1,2-Dichloroethane	1 : 1	1D polymer	-	-	-	74.2
10 DMF	1 : 2	1D polymer	-	-	-	70.7

^a M- metallocycle

^b The stacking pitch determines one of the unit cell axes and is therefore known to a relatively high level of accuracy.

^c The angle between the least-squares plane through the metallocyclic complex and the stacking direction.

The metallocycle **M1** (Scheme 2), also undergoes reversible transformations during the uptake and release of solvent vapours.⁶⁸ All transitions are accompanied by a conformational change[†] in the host framework (Figure 17), and the bulk integrity of each individual crystal is maintained in all cases *i.e.* it is possible to study all phases by single-crystal X-ray diffraction methods. SCD analysis revealed that, upon removal of the acetone solvent molecules, the crystals of **M1** changes from light brown to light green and the “imploded” **M2** conformation is formed.

M2 reversibly transforms back to **M1** upon exposure to acetone vapour for 2.5 hours. The red crystals of **M3** form by exposure of either **M1** or **M2** to acetonitrile vapours for just a few minutes. The exposure of **M3** to acetone vapour over a period of several hours reverses the former process, and light brown crystals characteristic of

[†] All conformations are classed according to the previously mentioned up (U), down (D) method.

M1 are obtained yet again. When the red crystals of **M3** are exposed to atmospheric conditions for *ca.* 15mins, light brown crystals of a fourth phase, **M4** appear.

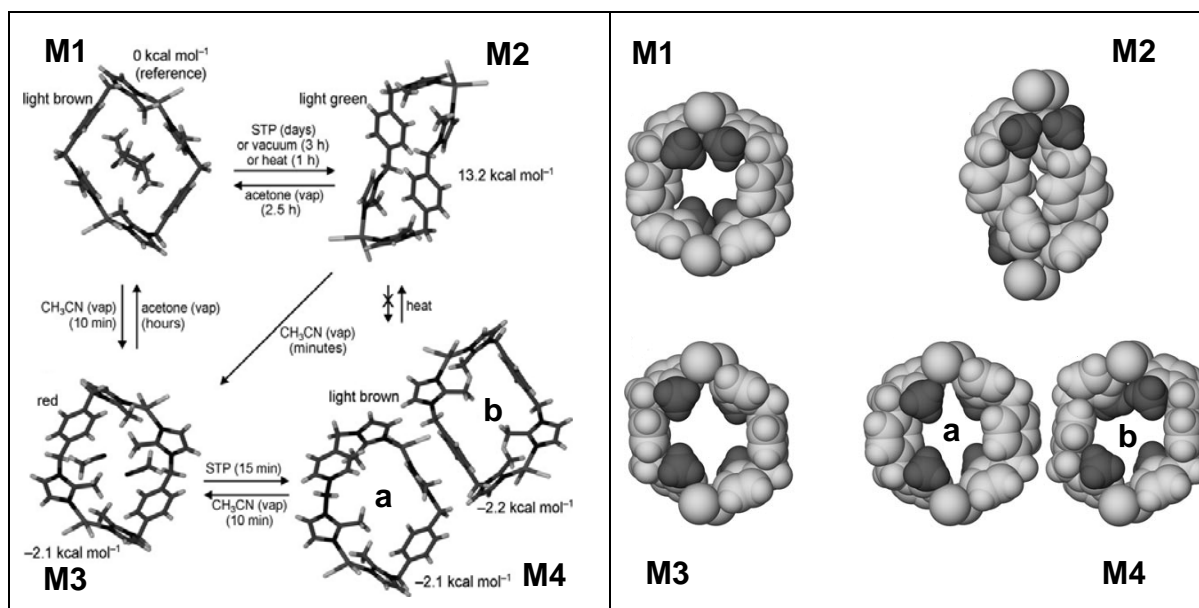


Figure 17. Capped-stick representation of the metallocycles in the four phases (**M1-M4**), conditions for the interconversion of the structures have been included, as well as the relative energies of the phases with respect to **M1** (left). Space-filling projections of the four phases. The methyl groups have been coloured dark to highlight the conformational differences in the phases (right).

As can be seen from Figure 17, this fourth phase contains two different conformations of the metallocyclic complex, **M4a** and **M4b**; and all four phases are conformationally distinct from one another by virtue of either the orientations of the methyl groups on the two imidazole moieties, or the angle of the phenylene spacer group. These drastic conformational changes are interesting in light of the fact that all phase transitions occurred with retention of monocrystallinity. This leads the authors to conclude that the molecules must cooperate in a concerted manner in order to accommodate these conformational changes. Finally, it was noted that the fully reversible phase transformations with retention of monocrystallinity, coupled with the change in colour seen in the crystals as a result of up-take or release of solvent vapour *i.e.* the vapochromic response, meets the requirements for the development of functional devices that have potential application as gas- or vapour sensing devices.

Following theme of the development of functional devices, our group has also devoted considerable attention to the development of porous crystals capable of

absorbing a variety of gases (the importance of this class of materials in the context of crystal engineering has been covered in more detail in Section 1.2).

Our group's approach to the synthesis of porous materials involves the use of discrete "donut-shaped" metal-organic complexes that entrap solvent molecules in their apertures.⁶⁸ The host molecules are necessarily shape-incompatible and accordingly preclude interdigitation and the formation of close-packed structures. Removal of the solvent molecules is achieved without a significant disruption to the host framework, thus yielding a porous lattice capable of absorbing gases. Using the method outlined here, our group has achieved success in the design of porous materials on two occasions.^{69, 70} The first case yielded a material which is porous in the conventional sense and the second case displayed transient porosity.

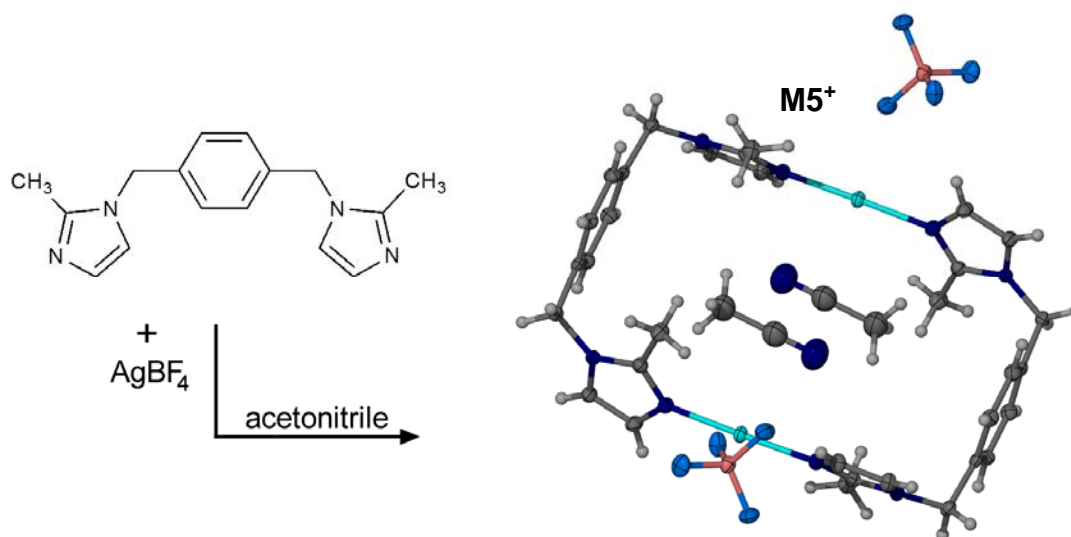


Figure 18. Formation of $[\text{Ag}_2\text{A1}_2](\text{BF}_4)_2 \cdot 2\text{CH}_3\text{CN}$.

Figure 18 shows the formation of the metallocycle M5^+ , which consists of a rectangular cationic complex composed of two linearly coordinated silver ions doubly bridged to one another by means of two ligands **A1**. The rings stack along the crystallographic c -axis to form 1D channels occupied by occluded acetonitrile molecules (two solvent molecules per metallocycle). The BF_4^- anions are situated between adjacent columns formed by the stacking of M5^+ units. Removal of the solvent molecules was effected by heating the crystals to $>80^\circ\text{C}$ to produce an empty porous host, with retention of monocrystallinity. Gas sorption isotherms were recorded for CO_2 , N_2 , CH_4 and H_2 at 30°C using a previously described device.⁷¹ It

was found that high pressure conditions (>48 bar) favoured the sorption of the smaller gases and at lower pressures (>10) the larger gases were absorbed more readily.

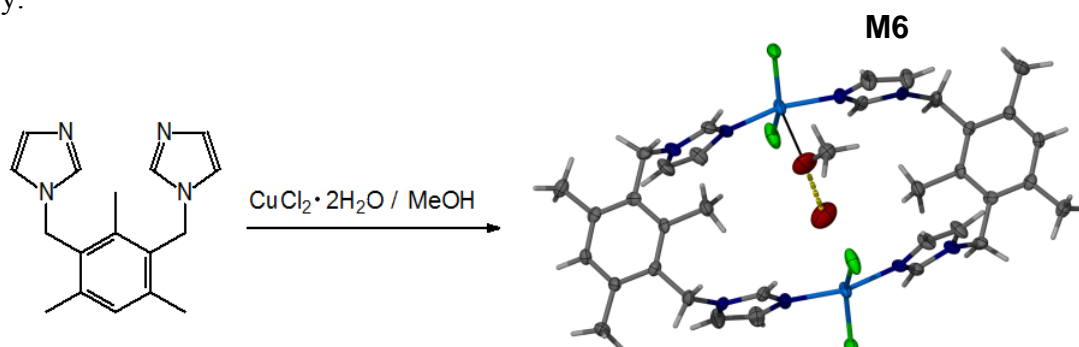


Figure 19. Formation of $[\text{Cu}_2(\mathbf{A5})_2\text{Cl}_4] \cdot \text{CH}_3\text{OH} \cdot \text{H}_2\text{O}$ (**M6**). The hydrogen bond between the methanol moiety and the water molecule is shown as a fragmented yellow cylinder.

The metallocycle shown in Figure 19 is similar in structure to $\mathbf{M5}^+$ but differs most notably in the coordination around the metal centre. In **M6** each copper ion is in a distorted square planar coordination environment and coordinates to two ligands **A5**, located *trans* to one another, as well as two chloride anions. These molecules also stack linearly, but form discrete voids; each containing one water molecule and one methanol molecule that can be removed by heating the crystals to 60 °C under vacuum for 1 hour. Single-crystal X-ray diffraction analysis revealed that the host lattice formed by the stacking of **M6** is not porous in the conventional sense. Instead, discrete pockets are formed that are accessible to gas molecules *via* the cooperative movement of the host molecules to create momentary “gaps” that would allow guest molecules to traverse the crystals. Gas sorption isotherms were recorded volumetrically⁷¹ for CO_2 , N_2 , CH_4 and H_2 at an initial pressure of 1.35 atm. The results showed that the material is indeed permeable to gases and that a certain degree of selectivity exists between the different gases tested.

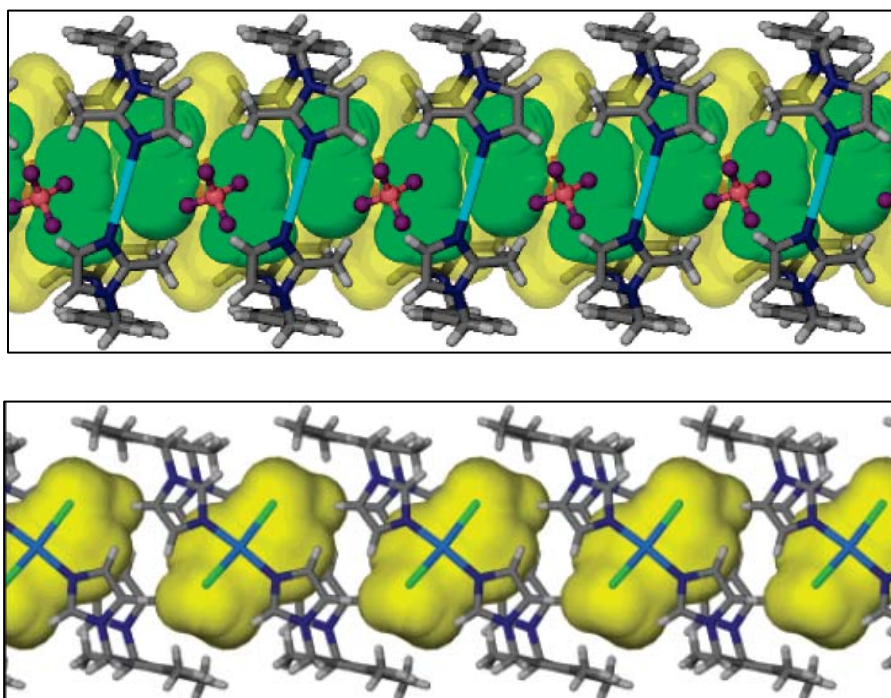


Figure 20. A comparison of conventional and transient porosity. A conventionally porous system: the metalocycles **M5⁺** stack such that a continuous channel is formed that allows guest molecules to traverse the material without disrupting the host framework (top). A transiently porous system: metalocycles **M6** stack such that discrete pockets are formed. The cooperative movement of the host framework creates momentary ‘gaps’ between the discrete voids to allow guest molecules to traverse the material (bottom).

1.7. ASPECTS OF THIS STUDY

Despite continuing efforts, we are far from the situation where we can definitively design and construct these targeted architectures at will,⁴⁵ necessitating further studies of the factors that influence the manner in which supramolecular architectures assemble. The first step in this process is the design and synthesis of coordination networks, with accompanying detailed structural analyses.

It was shown in the previous section that it is possible to incorporate imidazole functionalised ligands in the construction of coordination networks with a variety of interesting topologies, and to study these systems by means of single-crystal X-ray diffraction analysis. All of these ligands are based on the simple design strategy in which two imidazole moieties are separated by a variable aromatic spacer in such a manner that the imino nitrogens may coordinate to metals in the formation of infinite polymeric networks, or discrete 0D “donut-shaped” complexes that enclose solvent molecules in their apertures. The solvent can then be removed to yield robust frameworks capable of absorbing a variety of gases (Figure 21).

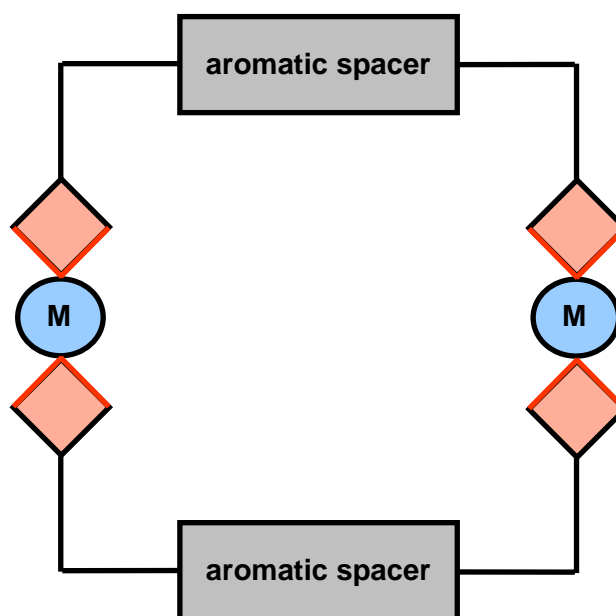


Figure 21. Basic outline of the “donut-shaped” metal-organic complex. The grey rectangles represent the variable aromatic spacer, the red diamonds represent the imidazole moieties with their coordinating nitrogen atoms simplified as red arrow heads. Metal ions are shown as blue ellipses.

The current study was designed to assess what would happen to the resulting coordination networks if the ligand is slightly modified. To this end a series of novel

ligands, based on a modification of the previous design principle, was prepared. In these ligands an extra thioether linkage has been inserted between the aromatic spacer and the imidazole moiety and, in so doing, the coordination mode of the two nitrogen atoms is changed. In the previous ligand design, one of the nitrogen atoms of the imidazole ring was covalently bound to a sp^3 carbon and the second nitrogen atom was available to coordinate to the metal ion. In the new ligand design, the imino nitrogen atom is available to coordinate to a metal ion while the amino nitrogen atom is protonated and thus capable of donating a hydrogen bond to an acceptor atom/group.

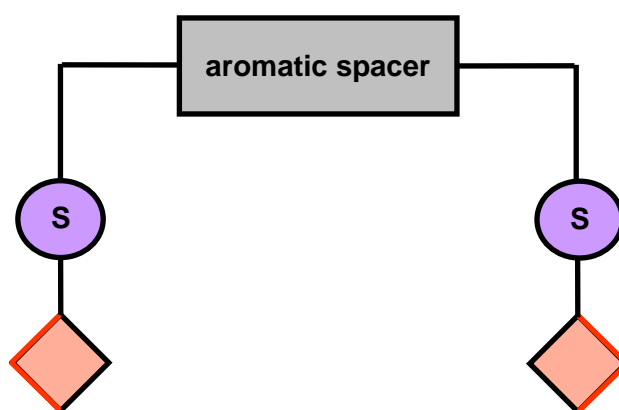


Figure 22. Basic design principle of the ligands that form the basis of the current study. The variable aromatic spacer is represented as a grey rectangle and the thioether linkages are shown as purple ellipses. The imidazole moieties are represented as red diamonds with their amine and imine nitrogens shown as black and red arrow heads, respectively.

In **Chapter 2** the synthesis and characterisation of the novel ligands is presented, as well as the description of the single crystal structures obtained for each of the free ligands. **Chapter 3** contains the single-crystal structural analyses of 27 coordination compounds obtained from the reaction of the ligands with a variety of metal salts. **Chapter 4** concerns itself with a novel coordination compound with gas sorption capabilities. The structural analysis of the compound was undertaken by SCD and reveals the formation of a cage-like hemicarcerand with individual cavities sufficiently large to accommodate guest molecules. Further aspects of this chapter include a preliminary investigation into the thermal and sorption properties of this novel hemicarcerand. **Chapter 5** presents a summary and concluding remarks on the work described in **Chapters 3** and **4**.

REFERENCES

1. J. M. Lehn, *Angew. Chem. Int. Ed. Engl.*, **1988**, 27, 89.
2. J. M. Lehn, *Supramolecular chemistry : concepts and perspectives : a personal account built upon the George Fisher Baker lectures in chemistry at Cornell University and the Lezione Lincee, Accademia nazionale dei Lincei, Roma*, VCH, Weinheim ; New York, **1995**.
3. J. W. Steed and J. L. Atwood, *Supramolecular Chemistry* John Wiley & Sons, Ltd, West Sussex, **2000**.
4. H. Davy, *Philos. Trans. R. Soc. London, Ser. A*, **1814**, 1, 62.
5. M. Faraday and H. Davy, *Philosophical Transactions of the Royal Society of London, On Fluid Chlorine*, **1823**, 113, 160.
6. P. Ehrlich, *Studies on Immunity*, Wiley ; New York, **1906**.
7. E. Fischer, *Ber. Deutsch. Chem. Gesl.*, **1894**, 27, 2985.
8. A. Werner, *Zeitschr. Anorg. Chem.* , **1893**, 3, 267.
9. K. L. Wolf, H. Frahm and H. Harms, *Z. Phys. Chem. Abt. B*, **1937**, 36, 237.
10. J. D. Dunitz, *Pure Appl. Chem.*, **1991**, 63, 177.
11. F. H. Allen, J. E. Davies, J. J. Galloy, O. Johnson, O. Kennard, C. F. Macrae, E. M. Mitchell, G. F. Mitchell, J. M. Smith and D. G. Watson, *J. Chem. Inf. Comput. Sci.*, **1991**, 31, 187.
12. D. Braga, *Chem. Commun.*, **2003**, 2751.
13. in *Comprehensive Supramolecular Chemistry*, eds. J. L. Atwood, D. Davies, D. D. MacNicol and F. Vögtle, Pergamon, Oxford, **1996**.
14. in *Encyclopedia of Supramolecular Chemistry*, eds. J. W. Atwood and J. W. Steed, Marcel Dekker, Inc., New York, **2004**.
15. M. C. Etter, *J. Am. Chem. Soc.*, **1987**, 109, 7786.
16. G. R. Desiraju, in *Comprehensive Supramolecular Chemistry*, eds. J. L. Atwood, D. Davies, D. D. MacNicol and F. Vögtle, Pergamon, Oxford, **1996**.
17. G. R. Desiraju, *Angew. Chem. Int. Ed. Engl.*, **1995**, 34, 2311.
18. R. Pepinsky, *Phys. Rev.*, **1955**, 100, 971.
19. G. M. J. Schmidt, *Appl. Chem.* , **1971**, 27, 647.
20. G. R. Desiraju, *Crystal Engineering, the Design of Organic Solids*, Elsevier, Amsterdam, **1989**.
21. G. R. Desiraju, *J. Mol. Struct.*, **2003**, 656, 5.

22. C. Janiak, *Dalton Trans.*, **2003**, 2781.
23. O. M. Yaghi, M. O'Keefe, N. W. Ockwig, H. K. Chae, M. Eddaoudi and J. Kim, *Nature*, **2003**, 423, 705.
24. M. Eddaoudi, D. B. Moler, H. Li, B. Chen, T. M. Reineke, M. O'Keefe and O. M. Yaghi, *Acc. Chem. Res.*, **2000**, 34, 319.
25. N. L. Rosi, M. Eddaoudi, J. Kim, M. O'Keefe and O. M. Yaghi, *Crystengcomm*, **2002**, 4, 401.
26. G. R. Desiraju and T. Steiner, *The Weak Hydrogen Bond in Structural Chemistry and Biology*, Oxford University Press, Oxford ; New York, **1999**.
27. D. Braga and F. Grepioni, in *Encyclopedia of Supramolecular Chemistry*, eds. J. W. Atwood and J. W. Steed, Marcel Dekker, Inc., New York, **2004**.
28. A. Werner, *Liebig's Annalen der Chemie*, **1902**, 322, 261.
29. A. Hantzsch, *Chem. Ber.*, **1910**, 43, 3049.
30. L. Pauling, *J. Am. Chem. Soc.*, **1939**, 57, 2680.
31. L. Pauling, *The Nature of the Chemical Bond.*, Cornell University Press, Ithaca, New York, **1939**.
32. T. Steiner, *Angew. Chem. Int. Ed*, **2002**, 41, 48.
33. G. C. Pimentel and A. L. McClellan, *The Hydrogen Bond*, Freeman, San Francisco, **1960**.
34. C. B. Aakeröy and K. R. Seddon, *Chem. Soc. Rev.*, **1993**, 22, 397.
35. G. A. Jeffrey and W. Saenger, *Hydrogen Bonding in Biological Structures*, Springer-Verlag, Berlin, **1991**.
36. G. R. Desiraju, *Acc. Chem. Res.*, **1991**, 24, 290.
37. S. L. Price, *Intermolecular Forces- From the Molecular Charge Distribution to the Molecular Packing.*, Wiley, Chichester, **1997**.
38. I. Dance, in *Encyclopedia of Supramolecular Chemistry*, eds. J. W. Atwood and J. W. Steed, Marcel Dekker, Inc., New York, **2004**.
39. G. R. Desiraju and A. Gavezzotti, *J. Chem. Soc., Chem. Commun.*, **1989**, 621.
40. C. A. Hunter and J. K. M. Sanders, *J. Am. Chem. Soc.*, **1990**, 112, 5525.
41. P. Pyykko, *Chem. Rev.*, **1997**, 97, 597.
42. A. N. Khlobystov, A. J. Blake, N. R. Champness, D. A. Lemenovskii, A. G. Majouga, N. V. Zyk and M. Schroder, *Coord. Chem. Rev.*, **2001**, 222, 155.
43. M. Mascal, J. L. Kerdelhue, A. J. Blake, P. A. Cooke, R. J. Mortimer and S. J. Teat, *Eur. J. Inorg. Chem.*, **2000**, 485.

44. S. Leininger, B. Olenyuk and P. J. Stang, *Chem. Rev.*, **2000**, 100, 853.
45. B. Moulton and M. J. Zaworotko, *Chem. Rev.*, **2001**, 101, 1629.
46. L. Carlucci, G. Ciani and D. M. Proserpio, in *Making Crystals by Design. Methods, Techniques and Applications*, eds. D. Braga and F. Grepioni, Wiley, New York, **2007**, pp. 58.
47. *The American Heritage® Science Dictionary*, Published by Houghton Mifflin. All rights reserved., **2002**.
48. C. Tien, *Adsorption Calculations and Modeling, Butterworth-Heinemann Series in Chemical Engineering.*, Butterworth-Heinemann, USA, **1994**.
49. K. S. W. Sing, D. H. Everett, R. A. W. Haul, L. Moscou, R. A. Pierotti, J. Rouguerol and T. Siemieniewska, *Pure Appl. Chem.*, **1985**, 57, 603.
50. D. M. Ruthven, *Principles of Adsorption and Adsorption Processes*, John Wiley & Sons, Inc. , USA, **1984**.
51. L. J. Barbour, *Chem. Commun.*, **2006**, 1163.
52. S. Kitagawa, R. Kitaura and S.-I. Noro, *Angew. Chem. Int. Ed*, **2004**, 43, 2334.
53. S. Kitagawa and K. Uemura, *Chem. Soc. Rev.*, **2005**, 34, 109.
54. S. Kitagawa, T. Nakamura and N. S.-I., *Chem. Commun.*, **2006**, 706.
55. J. L. Atwood, L. J. Barbour, A. Jerga and B. L. Schottel, *Science* **2002**, 298, 1000.
56. J. W. Steed, *Science*, **2002**, 976.
57. M. Albrecht, M. Lutz, A. L. Spek and G. van Koten, *Nature* **2000**, 406, 970.
58. A. A. Riddle, J. C. Bollinger and D. Lee, *Angew. Chem. Int. Ed*, **2005**, 44, 6689.
59. B. Sui, J. Fan, T. A. Okamura, W. Y. Sun and N. Ueyama, *Solid State Sciences*, **2005**, 7, 969.
60. C. Y. Su, Y. P. Cai, C. L. Chen, H. X. Zhang and B. S. Kang, *Journal of the Chemical Society Dalton Transactions*, **2001**, 359.
61. B. F. Hoskins, R. Robson and D. A. Slizys, *J. Am. Chem. Soc.*, **1997**, 119, 2952.
62. C. Y. Su, Y. P. Cai, C. L. Chen, M. D. Smith, W. Kaim and H. C. Z. Zoye, *J. Am. Chem. Soc.*, **2003**, 125, 8595.
63. C. Y. Su, Y. P. Cai, C. L. Chen, H. X. Zhang and B. S. Kang, *J. Chem. Soc., Dalton Trans*, **2001**, 359.

64. L. Dobrzanska, G. O. Lloyd, T. Jacobs, I. Rootman, C. L. Oliver, M. W. Bredenkamp and L. J. Barbour, *J. Mol. Struct.*, **2006**, 796, 107.
65. L. Dobrzańska, H. G. Raubenheimer and L. J. Barbour, *Chem. Commun.*, **2005**, 5050.
66. L. Dobrzanska, G. O. Lloyd and L. J. Barbour, *New J. Chem.*, **2007**, 31, 669.
67. L. Dobrzanska, D. J. Kleinhans and L. J. Barbour, *New J. Chem.*, **2008**, 32, 813.
68. L. Dobrzańska, G. O. Lloyd, C. Esterhuysen and L. J. Barbour, *Angew. Chem. Int. Ed.*, **2006**, 45, 5856.
69. L. Dobrzańska, G. O. Lloyd, H. G. Raubenheimer and L. J. Barbour, *J. Am. Chem. Soc.*, **2005**, 127, 13134.
70. L. Dobrzańska, G. O. Lloyd, H. G. Raubenheimer and L. J. Barbour, *J. Am. Chem. Soc.*, **2006**, 128, 698.
71. J. Atwood, L. J. Barbour, P. K. Thallapally and T. B. Wirsig, *Chem. Commun.*, **2005**, 51.

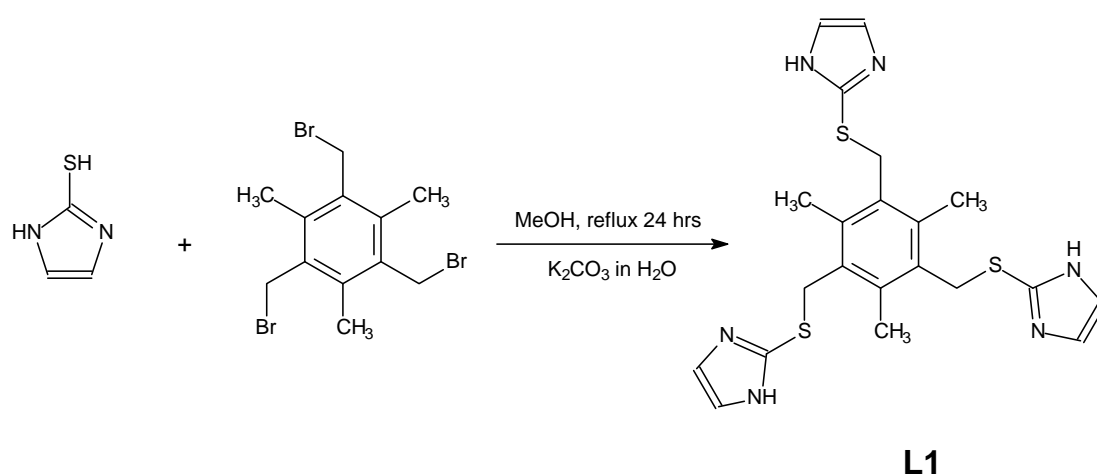
CHAPTER 2

Synthetic Methods and Experimental Techniques

This chapter presents the synthesis and characterisation of six novel ligands, as well as a description of the single-crystal structure obtained for each of the free ligands. Standard instruments and methods, as well as computer packages employed during the course of this study are also outlined.

2.1 SYNTHESIS AND CHARACTERISATION OF LIGANDS L1 – L2

2.1.1 Preparation of 1,3,5-tris(1-imidazolyl-2-thione)-2,4,6-trimethylbenzene (L1)



Scheme 1. Synthesis of **L1** by the S_N2 reaction of 2-mercaptoimidazole and 2,4,6-tris(bromomethyl)mesitylene.

2-Mercaptoimidazole (1.60 g, 16 mmol) was added to 2,4,6-tris(bromomethyl)mesitylene (0.91 g, 2.3 mmol) in 200 mL of MeOH. The resulting solution was refluxed for 24 hours. The solvent was then removed *in vacuo* to yield a yellow oil. K₂CO₃ (6.91 g, 50 mmol) in 100 mL of H₂O was added to the oil and the solution was stirred until the product precipitated. The white solid was then filtered,

washed with 100 mL of H₂O and left to air dry. Crystals suitable for single-crystal X-ray diffraction analysis were obtained by allowing a solution of **L1** in methanol, to crystallise by slow evaporation over a period of several days.

Yield: 91.5%. M.p.: 227-229°C (CH₃OH); IR (KBr): ν_{max} 3434 (N-H of Im), 2361, 1870, 1625 (Aromatic C=C), 1541, 1414 (CH₂ bend), 1223 (CH₂-S wag), 1099, 962, 768 cm⁻¹; ¹H-NMR (DMSO-D₆, 400 MHz): δ 2.32(9H, s, ArCH₃), 4.27(6H, s, SCH₂), 7.09 (6H, s, CN(H)CHCHN); ¹³C-NMR (DMSO-D₆, 75.5 MHz): δ 15.8, 34.9, 131.9, 136.3, 138.6; MS (ESI+): m/z 457 (69%, ([M+H]⁺)), 345 (40%, M⁺ -CH₂SIm), 199 (48%, M⁺ -[2(CH₃)+2(CH₂SIm)]), 115 (100%, M⁺ -3(CH₂SIm)).

Single Crystal Structure of L1

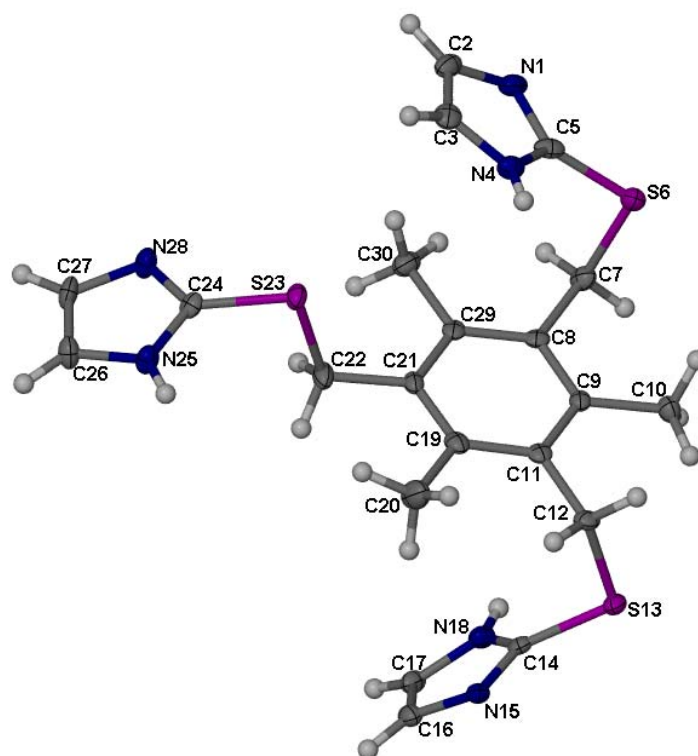


Figure 1. The molecular structure of **L1**, showing the crystallographic labelling scheme. Displacement ellipsoids are drawn at the 50% probability level and H atoms are shown as spheres of arbitrary radius.

L1 crystallises in the monoclinic space group $P2_1/n$, with one molecule in the ASU. Figure 1 displays a perspective view of the molecular structure of **L1**, together with the crystallographic labelling scheme used in the structural analysis.

The conformation of the ligand molecule can best be described as up-up-down (**UUD**) with respect to the orientation of the pendant arms relative to the aromatic spacer, *i.e.* one of the pendant groups is situated on one side of the central benzene ring plane, in contrast to the other two.

The dihedral angles between the least-square planes of the imidazole groups and the central benzene ring as listed in Table 1. These values show that, of the three imidazole rings, the atoms occupying the plane of the “down” imidazole ring is the most tilted with respect to the benzene ring. The torsion angles in Table 1 indicate the rotation of each imidazole group about the S-Csp³ bond. A torsion angle of 0° indicates eclipse of the imidazole group and the benzene ring, whilst a 180° torsion angle is indicative of the *anti* conformation *i.e.* where the two rings are as far apart as possible. Indeed, this is observed for one of the imidazole rings, as is reflected by a C24-S23-C22-C21 torsion angle of 177.7(4)°.

Adjacent ligand molecules interact *via* N-H⋯N hydrogen bonds to form 2D layers along [100] (see Table 2 for details of hydrogen bonding parameters). For the N18 and N25 donors the hydrogen bonding is unambiguous, but the assignment of the third donor is more problematic. The third hydrogen atom has only been shown at position H4 in Figure 1 for the sake of clarity, but it is disordered over two positions *i.e.* it is bonded to either N4 or N1. If it is attached to N4 in one molecule, the adjacent molecule will be protonated at the N1 site and an N4-H4⋯N1' hydrogen bond will exist. However, if it is bonded to N1, the adjacent molecule will be protonated at the N4 site and a N1-H1⋯N4' hydrogen bond will occur. Adjacent molecules within each layer are related to one another by a centre of inversion (Figure 2).

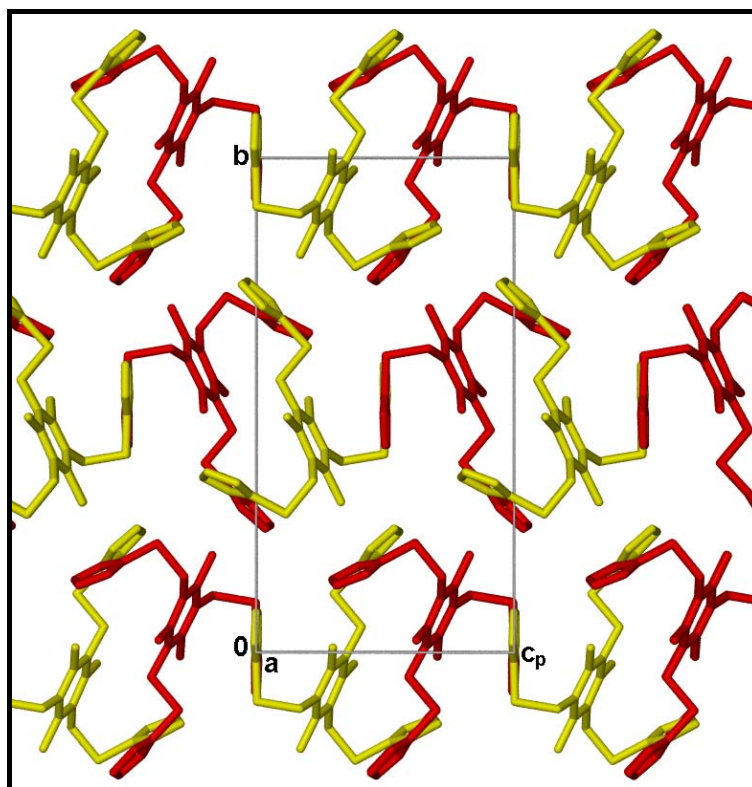


Figure 2. Packing arrangement of **L1** showing three distinct 2D layers, as viewed down [100]. Adjacent molecules within each layer are related by a centre of inversion and have been coloured red and yellow to distinguish them from one another.

Table 1. Selected angles for **L1** (°).

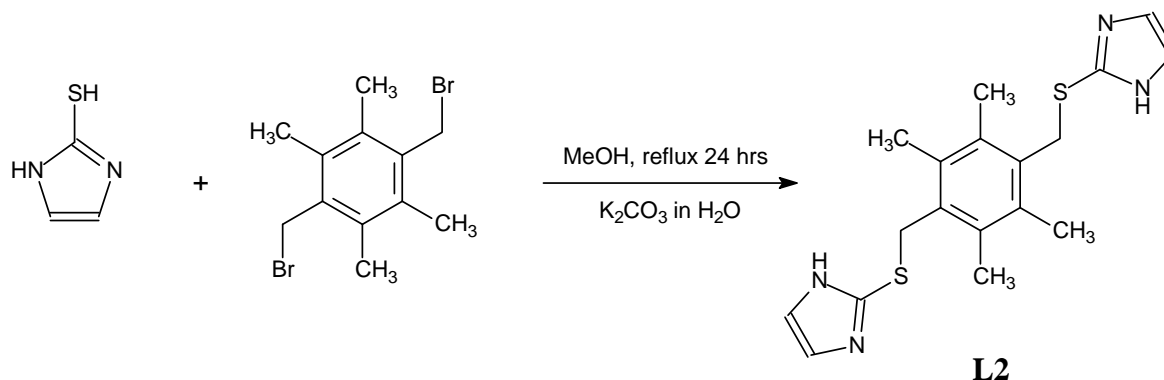
Selected torsion angles	
C5-S6-C7-C8	-66.1(4)
C14-S13-C12-C11	-67.5(4)
C24-S23-C22-C21	177.7(4)
Dihedral angle between the planes of the imidazole and benzene rings. Atoms constituting the imidazole group are given as reference.	
N1-C2-C3-N4-C5 (up)	26.2(1)
C14-N15-C16-C17-N18 (down)	48.2(2)
C24-N25-C26-C27-N28 (up)	21.3(2)

Table 2. Hydrogen-bond geometry for **L1** (Å, °).

D-H...A	D-H	H...A	D...A	D-H...A
N25-H25...N15 ⁱ	0.88	1.91	2.784(5)	172
N18-H18...N28 ⁱⁱ	0.88	1.93	2.811(5)	178
N4-H4...N1 ⁱⁱⁱ	0.88	1.87	2.743(8)	172
N1-H1...N4 ^{iv}	0.88	1.69	2.718(8)	177

Symmetry codes: (i) $-x+2, -y, -z+1$; (ii) $-x+1, -y, -z+1$; (iii) $-x+1, -y, -z$; (iv) $-x, -y, -z$

2.1.2 Preparation of 1,4-bis(1-imidazolyl-2-thione)-2,3,5,6-tetramethylbenzene (L2)



Scheme 2. Synthesis of **L2** by the S_N2 reaction of 2-mercaptimidazole and 4-bis(bromomethyl)-2,3,5,6-tetramethylbenzene.

2-Mercaptoimidazole (1.60 g, 16 mmol) was added to 1,4-bis(bromomethyl)-2,3,5,6-tetramethylbenzene (1.30 g, 4.0 mmol) in 200 mL of MeOH. The resulting solution was refluxed for 24 hours. The solvent was then removed under vacuum and K₂CO₃ (6.91 g, 50 mmol) in 100 mL of H₂O was added. The solution was stirred until the product precipitated. The white solid was then filtered, washed with 100 mL of H₂O and left to air dry. Crystals suitable for single-crystal X-ray diffraction analysis were obtained by allowing a solution of **L2** in methanol, to crystallise by slow evaporation over a period of several days.

Yield: 90.3% M.p.: 204-206°C (CH₃OH); IR (KBr): ν_{max} 3734 (N-H of Im), 3471, 2919, 2362, 1620 (Aromatic C=C), 1542, 1416 (CH₂ bend), 1261 (CH₂-S wag), 1104, 805 cm⁻¹; ¹H-NMR (DMSO-D₆, 400 MHz): δ 2.22 (12H, s, ArCH₃), 4.29 (4H, s, SCH₂), 7.09 (4H, s, CN(H)CHCHN); ¹³C-NMR (DMSO-D₆, 75.5 MHz): δ 15.9, 34.7, 132.3, 133.1, 138.5; MS (ESI⁺): m/z 359 (100%, ([M+H]⁺)), 199 (11%, M⁺ -[2(CH₃) + 2(CH₂SCH₃)]), 115 (2%, M⁺ -3(CH₂SIm)).

Single Crystal Structure of **L2**

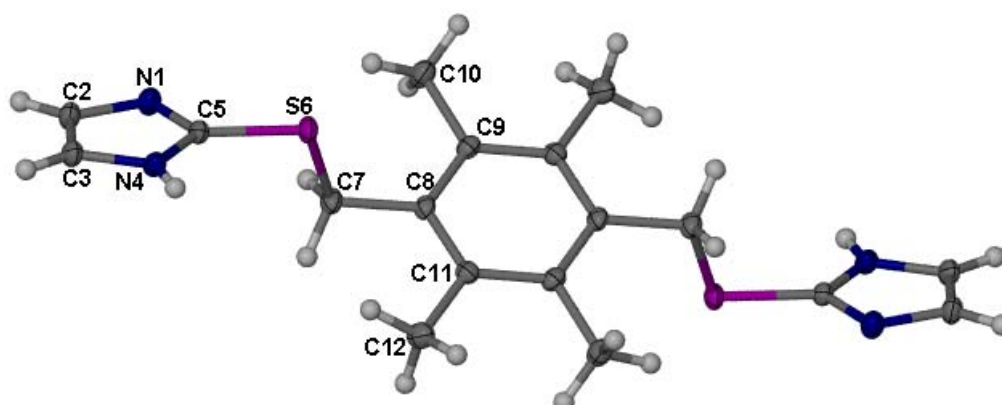


Figure 3. The molecular structure of **L2**, showing the crystallographic labelling scheme. The unlabeled atoms are related to the labeled atoms by a centre of inversion. Displacement ellipsoids are drawn at the 50% probability level and H atoms are shown as spheres of arbitrary radius.

L2 crystallises in the monoclinic space group $C2/c$. The ASU consists of half a molecule which is situated on an inversion centre. The two pendant groups are situated on opposite sides of the central benzene ring plane relative to each other. Figure 3 shows a perspective view of the crystal structure of **L2**, together with the crystallographic labelling scheme. The bond distance between S6 and C5 (1.752(2) Å) is significantly shorter than that observed for S6-C7 (1.836(2) Å). This is due to the conjugation between the S-atom and the imidazole ring. These values agree well with those previously reported.¹ The C5-S6-C7-C8 torsion angle of $-178.57(15)^\circ$ indicates that the rotation about the S6-C5 bond brings the imidazole group and the benzene ring into a near *anti* conformation, with a dihedral angle between the planes of the rings of $28.8(2)^\circ$. The molecules are linked to form an undulating 2D brick-wall network *via* intermolecular N-H \cdots N hydrogen bonding (N4 \cdots N1 = 2.839(3) Å), as is shown in Figure 4. These layers stack over one another such that atoms of the first layer are placed directly over the atoms of the third layer. No appreciable π - π interactions are apparent.

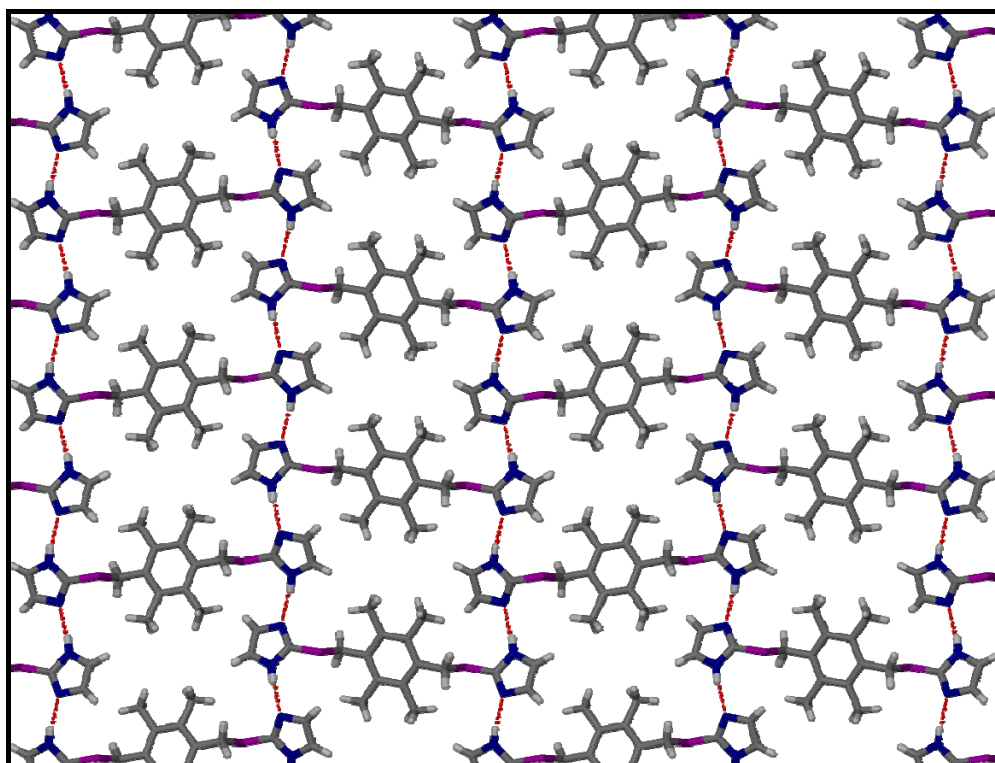
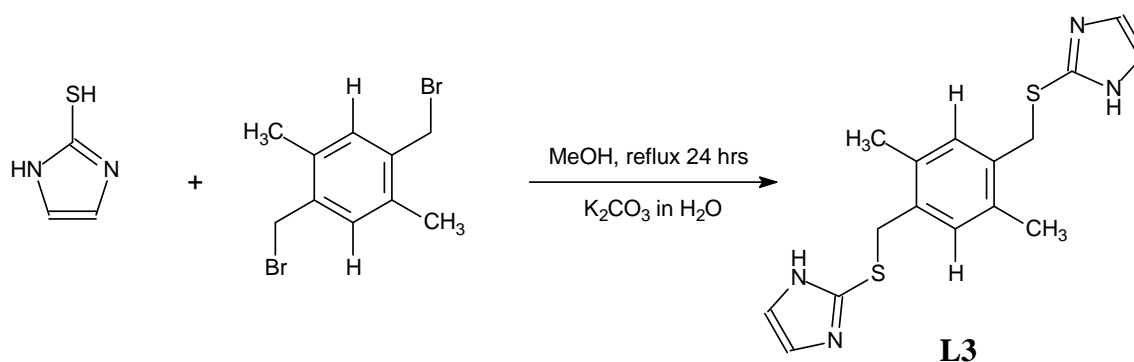


Figure 4. The 2D brick-wall network facilitated by intermolecular N-H...N hydrogen bonds, as viewed down [101]. Molecules are shown in the capped-stick representation and hydrogen bonds are represented as dashed lines.

2.1.3 Preparation of 1,4-bis(1-imidazolyl-2-thione)-2,5-dimethylbenzene (L3)



Scheme 3. Synthesis of **L3** by the S_N2 reaction of 2-mercaptoimidazole and 1,4-bis(bromomethyl)-2,5-dimethylbenzene.

2-Mercaptoimidazole (1.60 g, 16 mmol) was added to 1,4-bis(bromomethyl)-2,5-dimethylbenzene (1.30 g, 4.0 mmol) in 200 mL of MeOH. The resulting solution was refluxed for 24 hours. The solvent was then removed *in vacuo* and K_2CO_3 (6.91 g, 50 mmol) in 100 mL of H_2O was added. The solution was stirred until the product precipitated. The white solid was then filtered, washed with 100 mL of H_2O and left to air dry. Crystals suitable for single-crystal X-ray diffraction analysis were obtained by allowing a solution of **L3** in methanol to crystallise by slow evaporation over a period of several days.

Yield: 89.7% M.p.: 194-196°C (CH_3OH); IR (KBr): ν_{max} 3435 (N-H of Im), 2371, 1869, 1629 (Aromatic C=C), 1551, 1416 (CH_2 bend), 1326, 1219 (CH_2 -S wag), 1101, 965 cm^{-1} ; 1H -NMR (DMSO- D_6 , 400 MHz): δ 2.38(6H, s, Ar CH_3), 4.20(4H, s, SCH_2), 6.91(2H, s, ArH), 7.18(4H, s, CN(H)CHCHN); ^{13}C -NMR (DMSO- D_6 , 75.5 MHz): δ 17.9, 36.0, 123.3, 131.5, 133.7, 134.3, 138.2; MS (ESI+): m/z 331 (100%, ([M+H] $^+$)).

Single Crystal Structure of **L3**

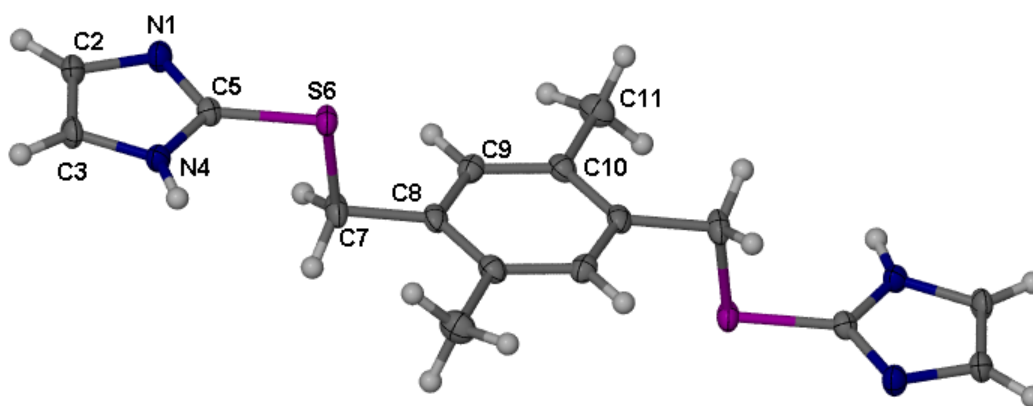


Figure 5. The molecular structure of **L3** showing the crystallographic labelling scheme. The unlabeled atoms are related to the labeled atoms by a centre of inversion. Displacement ellipsoids are drawn at the 50% probability level and H atoms are shown as spheres of arbitrary radius.

L3 crystallises in the monoclinic space group $P2_1/n$. The ASU consists of half a molecule which is situated on an inversion centre. The two pendant groups are situated on opposite sides of the central benzene ring plane relative to each other. Figure 5 displays a perspective view of the molecular structure of **L3**, together with

the labelling scheme. As was observed in the molecular structure of **L2**, the bond distance S6-C5 (1.752(3) Å) is significantly shorter than that observed for S6-C7 (1.841(4) Å). These values again agree well with those previously reported.¹ The packing of **L3** is similar to that of **L2** in that the molecules are linked into an undulating 2D brick-wall network *via* intermolecular N-H···N' hydrogen bonds (Figure 6). However, the observed hydrogen bond is shorter in the crystal structure of **L3** ($D\cdots A = 2.799(4)$ Å) than in **L2** ($D\cdots A = 2.839(3)$ Å). This can be attributed to the fact that a hydrogen atom is attached to C9 in **L3** and allows adjacent molecules to come into closer contact thereby shortening the hydrogen bond. As a consequence of the shorter hydrogen bond the rotation about the C5-S6 bond is also restricted, as reflected in the C5-S6-C7-C8 torsion angle of 175.1(3)°.

The layers are stacked on top of each other along [010] such that atoms of the first layer directly overlay the atoms in the third layer and, as with **L2**, no significant π - π interactions are observed. The dihedral angle between the least-squares planes defined by the benzene ring and the imidazole ring is 5.7(5) Å.

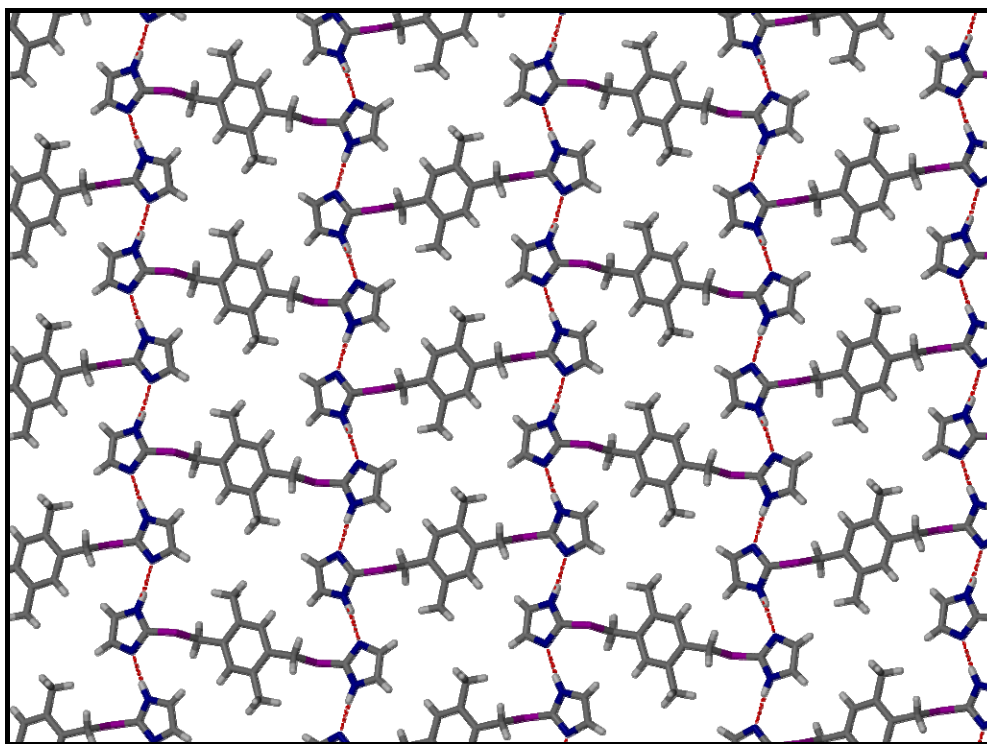
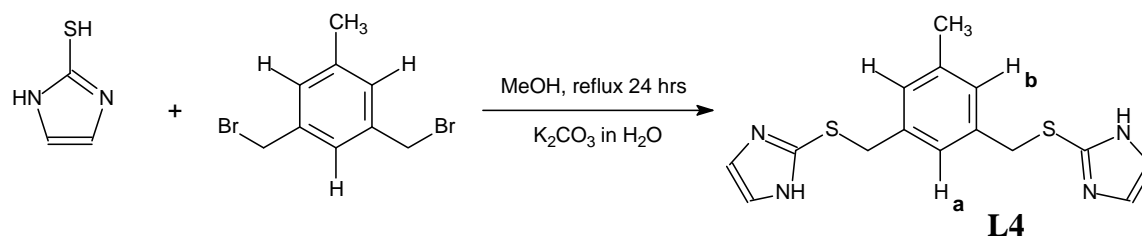


Figure 6. The 2D brick-wall network formed by intermolecular N-H···N' hydrogen bonds as viewed along [-101]. Molecules are shown in the capped-stick representation and hydrogen bonds are represented as dashed red lines.

2.1.4 Preparation of 3,5-bis(1-imidazolyl-2-thione)toluene (L4)

Scheme 4. Synthesis of **L4** by the S_N2 reaction of 2-mercaptoimidazole and, 3,5-bis(bromomethyl)toluene.

2-Mercaptoimidazole (2.88 g, 28 mmol) was added to 3,5-bis(bromomethyl)toluene (2.00 g, 7.0 mmol) in 200 mL of MeOH. The resulting solution was refluxed for 24 hours. The solvent was then removed *in vacuo* and K₂CO₃ (6.91 g, 50 mmol) in 100 mL of H₂O was added. The solution was stirred until the product precipitated. The white solid was then filtered, washed with 100 mL of H₂O and left to air dry. Crystals suitable for single-crystal X-ray diffraction analysis were obtained by allowing a solution of **L4** in methanol to crystallise by slow evaporation over a period of several days.

Yield: 94.5%. M.p.: 168-170°C; IR (film): ν_{max} 3434 (N-H of Im), 2363, 1858, 1605 (aromatic C=C), 1547, 1414 (CH₂ bend), 1232 (CH₂-S wag), 1096, 963, 746 cm⁻¹; ¹H-NMR (DMSO-D₆, 400 MHz): δ 2.18 (3H, s, ArCH₃), 4.14 (4H, s, CH₂S), 6.909 (2H, s, ArH_a), 6.94 (1H, s, ArH_b), 7.05 (4H, s, CN(H)CHCHN); ¹³C-NMR (DMSO-D₆, 75.5 MHz): δ 20.69, 37.6, 123.7, 126.1, 128.1, 137.5, 137.7, 138.3; MS (ESI⁺): m/z 317 (100%, [(M+H)⁺]), 218 (20%, M⁺ -SIm), 159 (87%).

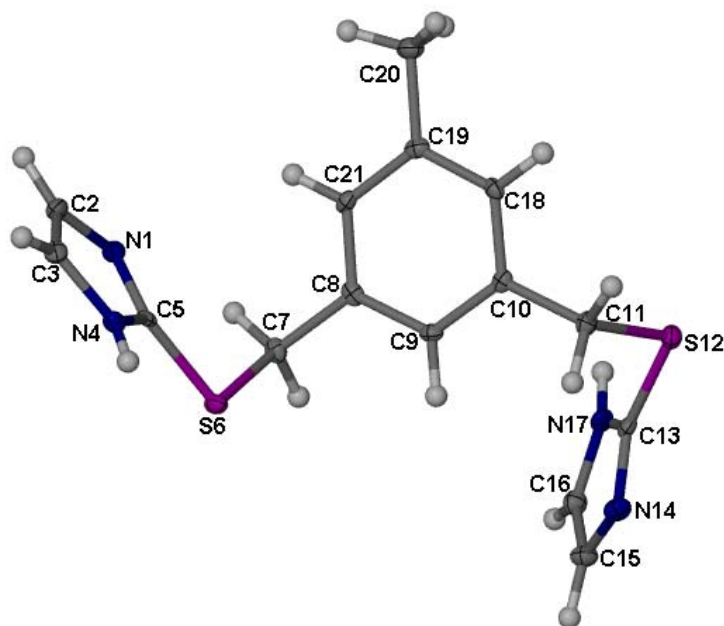
Single Crystal Structure of L4

Figure 7. The molecular structure of **L4** showing the crystallographic labelling scheme. Displacement ellipsoids are drawn at the 50% probability level and H atoms are shown as spheres of arbitrary radius.

L4 crystallises in the triclinic space group $P-1$, with one molecule in the asymmetric unit. Figure 7 displays a perspective view of the crystal structure of **L4**, together with the crystallographic labelling scheme used in the structural analysis. The two pendant groups are *meta* with respect to each other and are located on opposite sides of the plane of the central aromatic spacer. The molecules interact with one another *via* intermolecular N-H \cdots N' hydrogen bonding (details of the hydrogen bonding parameters can be found in Table 3), to form parallel ladders along [010]. The ladders are then connected in 2D *via* offset π - π interactions; the centroid-centroid distance between two nearest imidazole ring planes is 3.454 Å (Figure 8, left). This gives rise to two separate orientations of the molecules related by a centre of inversion (Figure 8, right). The two pendant arms are not symmetrically orientated with respect to the aromatic spacer as is reflected by the dihedral angles of 53.2(1)° and 88.8(9)° between the central benzene ring and the two imidazole rings.

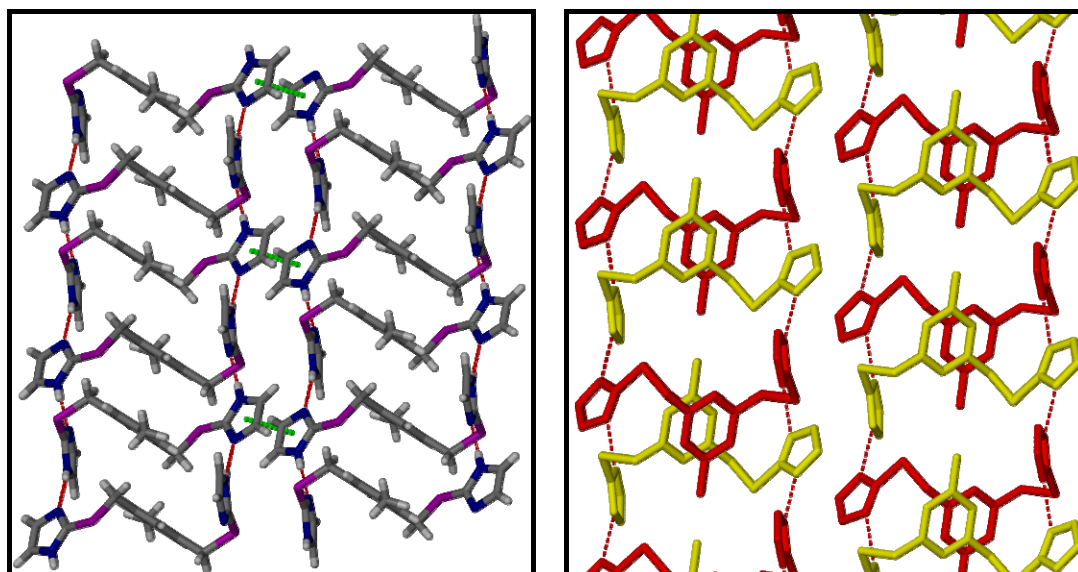


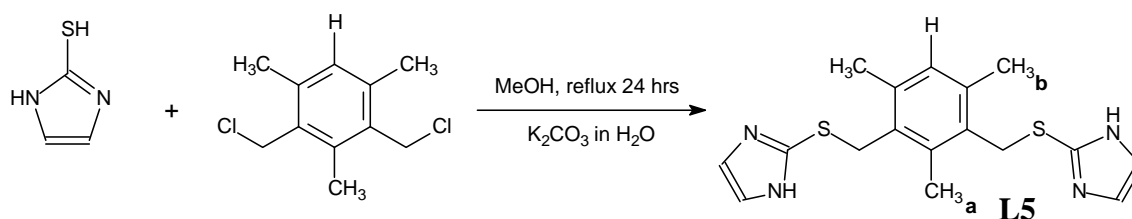
Figure 8. (Left) Capped-stick representation of the 1D ladders formed by intermolecular N-H...N' hydrogen bonds in **L4**, as viewed down [100]. The π - π interactions connecting adjacent ladders are represented as dashed green lines from the centroid of one imidazole ring to the centroid of an adjacent imidazole ring. (Right) Packing arrangement of **L4** as viewed down [010]. Each molecule shown in yellow is related to an adjacent molecule shown in red by a centre of inversion. Hydrogen atoms are omitted for clarity.

Table 3. Hydrogen-bond geometry for **L4** (Å, °).

D-H...A	D-H	H...A	D...A	D-H...A
N4-H4...N14 ⁱ	0.88	1.94	2.816(3)	173
N17-H17...N1 ⁱⁱ	088	1.96	2.792(3)	156

Symmetry codes: (i) $-x+1, -y+1, -z$; (ii) $-x, -y, -z$

2.1.5 Preparation of 1,3-bis(1-imidazolyl-2-thione)-2,4,6-trimethylbenzene (**L5**)



Scheme 5. Synthesis of **L5** by the SN2 reaction of 2-mercaptoimidazole and 2,4-bis(chloromethyl)-1,3,5-trimethylbenzene.

2-Mercaptoimidazole (2.0 g, 20 mmol) was added to 2,4-bis(chloromethyl)-1,3,5-trimethylbenzene (1.09 g, 5.0 mmol) in 200 mL of MeOH. The resulting solution was refluxed for 24 hours. The solvent was then removed under reduced pressure and yielded a yellow oil, to which K_2CO_3 (6.91 g, 50 mmol) in 100 mL of H_2O was added. The solution was stirred until the product precipitated. The white solid was then filtered, washed with 100 mL of H_2O and left to air dry. Crystals suitable for single-crystal X-ray diffraction analysis were obtained by slow diffusion of triethylamine into a solution of **L5** in acetonitrile.

Yield: 95.4%. M.p.: 166-169°C; IR (film): ν_{max} 3455 (N-H of Im), 2361, 1534, 1413 (CH_2 bend), 1328, 1221 (CH_2-S wag), 1097, 963, 758cm^{-1} ; $^1\text{H-NMR}$ (DMSO- D_6 , 400 MHz): δ 2.24 (6H, s, CH_{3b}), 2.30 (3H, s, CH_{3a}), 4.23 (4H, s, CH_2S), 6.86 (1H, s, ArH), 7.01 (4H, s, $CN(H)CHCHN$); $^{13}\text{C-NMR}$ (DMSO- D_6 , 75.5 MHz): δ 14.7, 19.2, 33.9, 129.8, 131.2, 135.9, 136.2, 138.3; MS (ESI+): m/z 345 (100%, $[(M+H)^+]$), 245 (15%, $M^+ -SIm$), 175 (18%).

Single Crystal Structure of **L5**

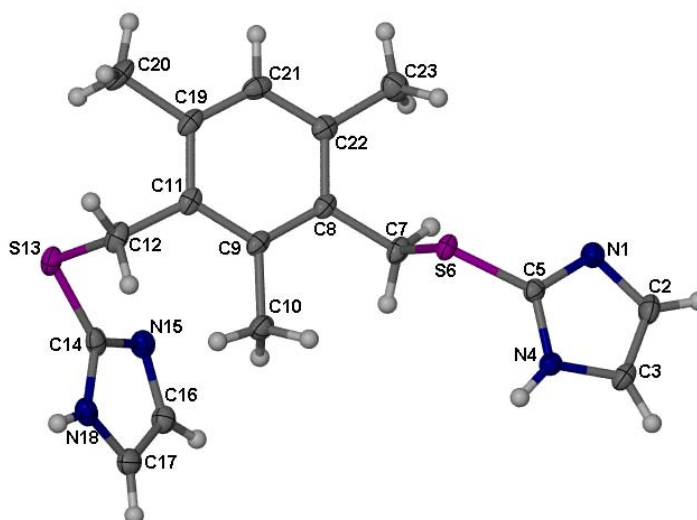


Figure 9. The molecular structure of **L5** showing the crystallographic labelling scheme. Displacement ellipsoids are drawn at the 50% probability level and H atoms are shown as spheres of arbitrary radius.

L5 crystallises in the monoclinic space group $P2_1/n$ with one molecule in the asymmetric unit. Figure 9 displays a perspective view of the crystal structure of **L5**, together with the crystallographic labelling scheme used in the structural analysis. The two pendant groups are *meta* with respect to each other and are located on opposite sides of the plane of the central aromatic spacer. In contrast to the 1D ladders formed by the packing of the *meta* substituted **L4**, the crystal structure of **L5** is comprised of undulating 2D brick-wall networks that are formed by intermolecular N-H...N' hydrogen bonds (Figure 10). Details of the hydrogen bonding parameters can be found in Table 4. The two-dimensional layers stack along [001] in an ...*ABAB*... fashion, as shown in Figure 11. No significant π - π interactions are observed.

The difference in the dimensionality of the two structures can be attributed to the orientations of the pendant arms with respect to the central benzene ring. This becomes more apparent upon closer examination of the dihedral angles between the benzene ring and the two imidazole rings for **L5** and **L4**.

In **L5**, the dihedral angle between the benzene ring plane and the atoms of the N1-C2-C3-N4-C5 imidazole group is $6.8(1)^\circ$. This is close to planarity (a 0° dihedral angle), and facilitates the formation of the 2D brick-like packing arrangement. The analogous dihedral angle in **L4** is $88.8(9)^\circ$, indicating an almost perpendicular orientation of the imidazole group with respect to the aromatic spacer, and results in ladder-like stacking.

Table 4. Hydrogen-bond geometry for **L5** (Å, °).

D-H...A	D-H	H...A	D...A	D-H...A
N4-H4...N15 ⁱ	0.88	1.94	2.817(2)	173
N18-H18...N1 ⁱⁱ	088	1.97	2.812(2)	160

Symmetry codes: (i) $x+1, y, z$; (ii) $-x+1/2, y-1/2, -z+1/2$

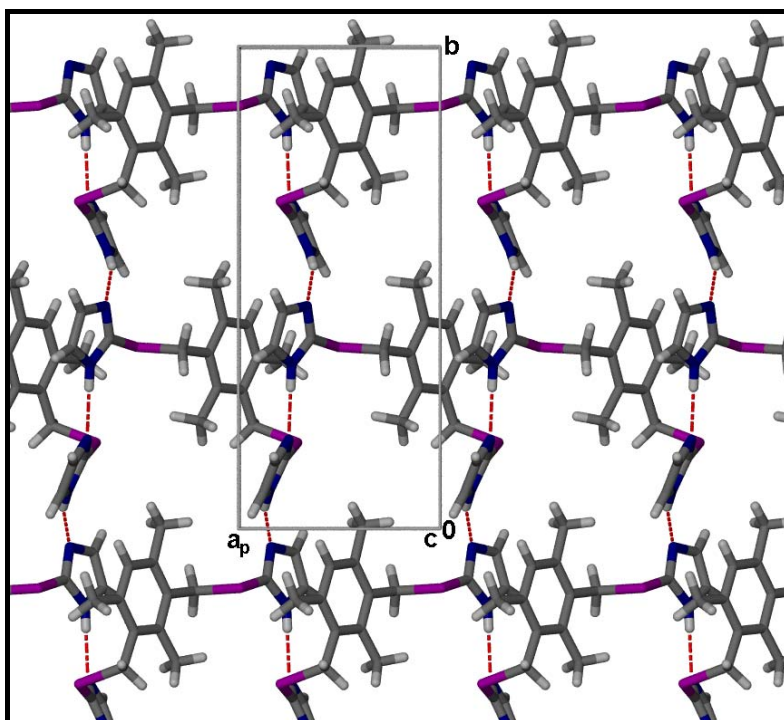


Figure 10. The 2D brick-wall network formed by N-H \cdots N' hydrogen bonds in **L5**, as viewed down [001]. All molecules are shown in the capped-stick representation and hydrogen bonds are shown as dashed red lines.

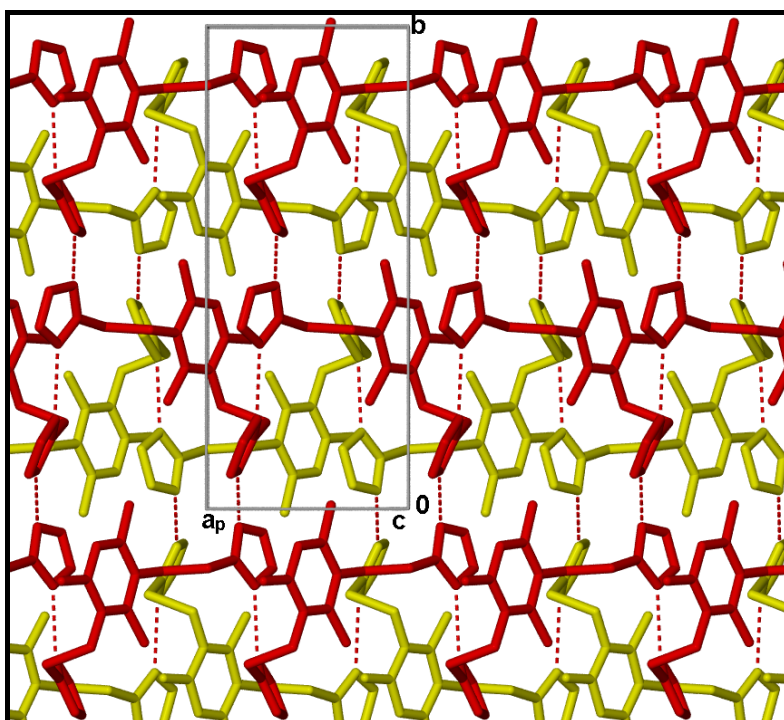
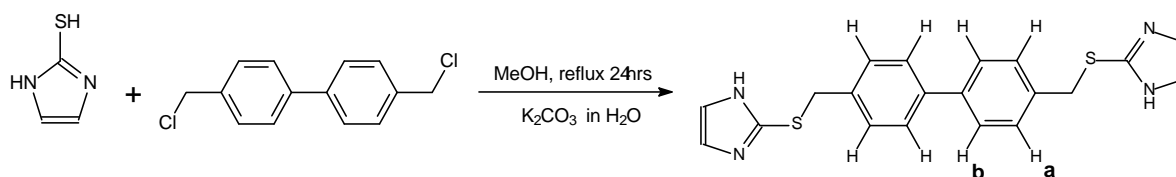


Figure 11. The ...*ABAB*... stacking arrangement observed in **L5** as viewed down [001]. Alternating layers are coloured red and yellow to distinguish them from one another. All molecules are shown in the capped-stick representation and hydrogen atoms have been omitted for clarity. The dashed red lines represent intermolecular N-H \cdots N' hydrogen bonding.

2.1.6 Preparation of 4,4'-bis(1-imidazolyl-2-thione)-1,1'-biphenyl (**L6**)

Scheme 6. Synthesis of **L6** by the S_N2 reaction of 2-mercaptoimidazole and 4,4'-bis(chloromethyl)-1,1'-biphenyl.

2-Mercaptoimidazole (1.60 g, 16 mmol) was added to 4,4'-bis(chloromethyl)-1,1'-biphenyl (1.34 g, 5.33 mmol) in 200 mL of MeOH. The resulting solution was refluxed for 24 hours. The solvent was then removed *in vacuo* and K_2CO_3 (6.91 g, 50 mmol) in 100 mL of H_2O was added to the cream solid. The solution was stirred until the product precipitated. The off-white solid was then filtered, washed with 100 mL of H_2O and left to air dry. Crystals suitable for single-crystal X-ray diffraction analysis were obtained by allowing a solution of **L6** in methanol to crystallise by slow evaporation over a period of several days.

Yield: 84.3%. M.p.: 182-184°C (CH_3OH); IR (film): ν_{max} 3434 (N-H of Im), 2916, 2754, 1670 (aromatic C=C), 1546, 1416 (CH_2 bend), 1098, 960, 748 cm^{-1} ; 1H -NMR (DMSO- D_6 , 300 MHz): δ 4.504 (4H, s, SCH_2), 7.344 (4H, d, $^3J = 8.345Hz$, ArH**b**), 7.414 (4H, s, NCHCHN), 7.5635 (4H, d, $^3J = 8.345 Hz$, ArH**a**); ^{13}C -NMR (DMSO- D_6 , 75.5 MHz): δ 37.438, 122.289, 126.575, 129.214, 136.4, 138.4, 138.6; MS (ESI+): m/z 379 (100%, ($[M+H]^+$));

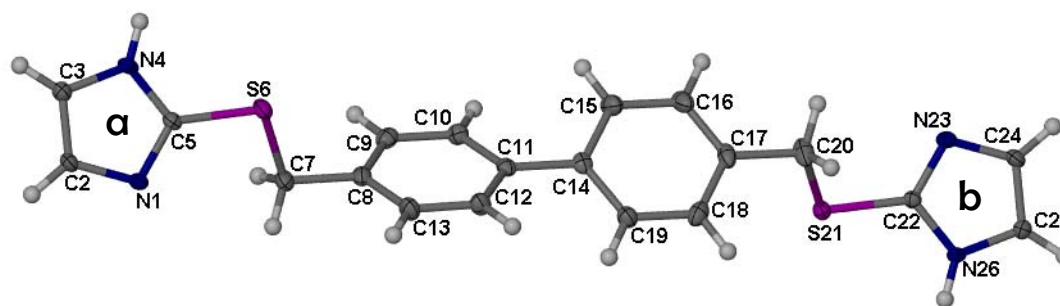
Single Crystal Structure of L6

Figure 12. The molecular structure of **L6** showing the crystallographic labelling scheme. The letters **a** and **b** have been chosen arbitrarily to distinguish the two imidazole rings from each other. Displacement ellipsoids are drawn at the 50% probability level and H atoms are shown as spheres of arbitrary radius.

L6 crystallises in the monoclinic space group $P2_1/n$. The ASU consists of one molecule and the pendant groups are located on opposite sides with respect to the plane of the biphenyl aromatic spacer. Figure 12 shows a perspective view of the crystal structure of **L6**, together with the crystallographic labelling scheme used in the structural analysis.

The two benzene rings are twisted with respect to each other[†] and the dihedral angle between the least-squares planes occupied by the 6 carbon atoms of each ring is $29.3(1)^\circ$. The dihedral angle between the planes of imidazole rings **a** and **b** with respect to their neighbouring benzene rings are $51.4(1)^\circ$ and $23.1(1)^\circ$ respectively.

Adjacent molecules are connected *via* N-H \cdots N' hydrogen bonds (see Table 5 for details of the hydrogen bonding parameters) to form 1D ladders running parallel to [001]. C-H \cdots π interactions (C2 \cdots centroid of imidazole ring **b** = 3.518 Å and C24 \cdots centroid of imidazole ring **a** = 3.654 Å) connect the 1D ladders into a characteristic herringbone motif (Figure 13).

[†] The structure was checked for missed symmetry, however, it was established that it is this twisting of the benzene rings with respect to each other that is the reason of the large ASU.

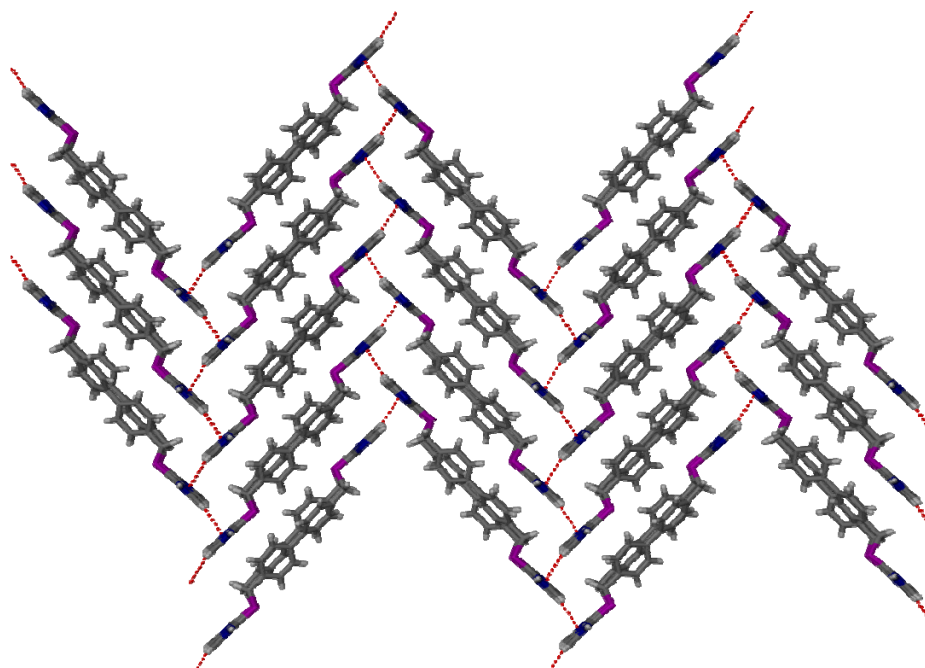


Figure 13. Packing arrangement of **L6** showing the characteristic herringbone motif formed by C-H... π interactions, as viewed down [100]. Molecules are shown in capped-stick representation and C-H... π interactions are shown as dashed red lines.

Table 5. Hydrogen-bond geometry for **L6** (Å, °).

D-H...A	D-H	H...A	D...A	D-H...A
N4-H4...N23 ⁱ	0.88	2.04	2.866(3)	157
N26-H26...N1 ⁱⁱ	088	2.02	2.867(3)	160

Symmetry codes: (i) $-x+2, -y+1, -z+1$; (ii) $-x+2, -y+1, -z+2$

2.2 EXPERIMENTAL TECHNIQUES

2.2.1 Single-Crystal X-Ray Diffraction Analysis (SCD)

In all cases suitable single crystals (*i.e.* those found by inspection to have good morphology and extinguished plane polarized light uniformly) were placed on the end of a mitegen mount using paratone oil. Intensity data were collected on a Bruker SMART Apex CCD single-crystal X-ray diffractometer² equipped with an Oxford Cryostream cooling system. The system was operated at 1.2 kW power (40 kV, 30 mA) using monochromated Mo-K α radiation ($\lambda = 0.71073 \text{ \AA}$). Data reduction was carried out by means of a standard procedure using the Bruker software package SAINT.³ Empirical corrections were performed where necessary using SADABS.^{4, 5} All crystal structures were solved using the SHELXS-97⁶ suite of programs, either by direct methods or a combination of Patterson and partial structure expansion. X-Seed⁷ was used as a graphical interface for SHELX. Structures were expanded by iterative examination of difference Fourier maps following least squares refinements of the earlier models. All ordered non-hydrogen atoms were refined anisotropically by means of full-matrix least squares calculations on F^2 using SHELXL-97 within the X-Seed environment. The hydrogen atoms were all placed in calculated positions using a riding model and assigned isotropic thermal parameters 1.2- 1.5 times U_{eq} of their parent atoms. According to the SHELX-97 manual:⁸ “It is difficult to locate hydrogen atoms accurately using X-ray data because of their low scattering power, and because the corresponding electron density is smeared out, asymmetrical, and is not centered at the position of the nucleus. In addition hydrogen atoms tend to have larger librational amplitudes than other atoms. For most purposes it is preferable to calculate the hydrogen positions according to well-established geometrical criteria and then to adopt a refinement procedure which ensures that a sensible geometry is retained.” We believe that the method used by SHELXL-97 to place hydrogen atoms in calculated positions is adequate for the purposes of this study – *i.e.* that a superior method is not immediately apparent.

2.2.2 X-Ray Powder Diffraction (XPRD)

Diffraction patterns of intensity vs. 2θ were recorded on a Bruker D8 ADVANCE with Bragg-Brentano geometry, using Cu- K_{α} radiation ($\lambda = 1.5418 \text{ \AA}$). Intensity data were collected from multiple 2θ scans by a dynamic scintillation (point type) detector. All samples were first pulverised and then spun during data collection at 15 rotations per minute to minimise preferred orientation contributions to intensity data. A step size of 0.02 degrees and a scan-speed of 2 sec per step were used during data collection. X-ray powder diffraction patterns were also calculated from single-crystal X-ray structures using Lazy Pulverix⁹ from within the X-Seed graphical interface.

2.2.3 Thermogravimetric Analysis (TGA)

A TA Instruments Q500 thermogravimetric analyser was used and sample sizes typically ranged from 5-15 mg. N_2 gas flowing at a rate of 50 ml/min was used to purge the furnace. Heating was effected from ambient temperature to 400-600 °C at a constant heating rate of either 2, 5 or 10 °C/min. The resulting thermograms were analysed using the TA Instruments Universal Analysis program.

2.2.4 Differential Scanning Calorimetry (DSC)

Differential Scanning Calorimetry is an analytical technique that measures the heat flow into or out of a sample, relative to a reference (most often an empty pan), as a function of time and temperature in a controlled atmosphere.¹⁰ This difference in temperature between the sample and the reference infers that a thermal event (generally a physical or chemical change in the material) has taken place.

DSC measurements were carried out using a TA Instruments Q100 differential scanning calorimeter on sample sizes of typically 3-10 mg. Samples were run under hermetic conditions which involved crimping the pan and lid tightly (two pin holes were made in each lid). Both the reference and the sample pans were prepared using the same method. N_2 gas, flowing at a rate of 50ml/min was used to purge the furnace. Heating was always effected from ambient temperature to 400 °C at a rate of

2 °C/min. The resulting thermograms were analysed using TA Instruments Universal Analysis program.

2.2.5 Gravimetric gas Sorption

Gravimetric sorption isotherms were measured using an Intelligent Gravimetric Analyser (IGA-002) supplied by Hiden Analytical (Ltd), Warrington, UK¹¹ at the Central Analytical Facility of the University of Stellenbosch. The system precisely measures mass change in a controlled temperature environment and allows sorption experiments to be studied up to pressures of 20 bar. The pressure is monitored using a pressure transducer with a range of 0-20 bar and buoyancy effects are corrected for automatically by the control software. Temperature control is maintained to an accuracy of +/- 0.05 °C using a Grant refrigerated re-circulating bath.

Each sample was initially placed under vacuum for 24 hours to ensure that all traces of solvent are removed and then exposed to gas. After collection of the sorption isotherms the results were saved as mmol of gas (or guest) per gram of host as a function of equilibrium pressure. This was then converted to mmol guest per mmol of host. All data collection on the IGA is controlled by Real-Time Processing computer software.¹²⁻¹⁸

2.2.6 Infrared Spectroscopy (IR)

IR spectra were obtained using the KBr pellet method. Spectra were recorded in the 4000-400cm⁻¹ region, using Nexus 670 FT-IR instrument (Thermo Nicolet Instruments, USA) with a Golden Gate ATR accessory.

2.2.7 Nuclear Magnetic Resonance Spectroscopy (NMR)

All samples were dissolved in deuterated dimethylsulphoxide (DMSO-D₆). ¹H-NMR and ¹³C-NMR was performed on Varian Unity INOVA (400 MHz) equipped with two channels, Z gradients, and the following probes: 5 mm 15N-31P dual broadband PFG 10 mm 15N-31P broadband, or a Varian VNMRS (300 MHz) NMR Spectrometer equipped with two channels and the following probes: 5 mm 15N-31P

dual broadband PFG 5mm 1H/19F/13C/31P four-nucleus 5mm 15N-31P broadband. All analyses were carried out at the Central Analytical Facility of the University of Stellenbosch.

2.2.8 Liquid Chromatography Electrospray Ionisation Mass Spectrometry (LC ESI-MS)

LC ESI-MS analysis was carried out on a Waters API Quattro Micro mass spectrometer with an electrospray ionization source. All samples were dissolved in methanol at a concentration of 5 μM and introduced into the ESI-MS at a flow rate of 50 L/h during analysis. A capillary voltage of 3.5 kV was applied, with a source temperature of 80 °C and a cone voltage of 15 V. The desolvation temperature was set at 400°C and the desolvation gas flow rate to 400 L/h. All data was acquired in the positive mode and scanning occurred through $m/z = 100\text{-}1000$ (where m/z is defined as the molecular mass to charge ratio). All analyses were carried out at the Central Analytical Facility of the University of Stellenbosch.

2.3 COMPUTER PROGRAMS

2.3.1 X-Seed^{7, 9, 19}

This crystallographic software tool provided a graphical user interface to several non-interactive utilities to aid the process of crystal structure solution, refinement, analysis and presentation of the resulting model. Some of these utilities and their primary functions are listed below:

SHELX-97⁶- this suite of programs was used for crystal structure solution and refinement. It is comprised of six computer programs (SHELXS, SHELXL, CIFTAB, SHELXA, SHELXPRO and SHELXWAT).

Lazy-Pulverix⁹- a program used for calculating theoretical X-ray and neutron diffraction powder patterns.

POV-Ray²⁰ – a ray-tracing program that was used to produce high quality molecular graphics images. A set of unique and complex commands is used to render

an image of a scene from the perspective of an imaginary camera. A scene is comprised of an object (or set of objects) and light sources. Labelling of atoms and unit cell axes was done using POV-Label.

MSROLL^{21, 22} – a program that was incorporated into X-Seed in order to calculate the volume of void spaces in a structure. MROLL was originally designed by Michael Connolly to map the solvent-accessible areas of proteins and nucleic acids for graphical display. Lee and Richards²³ define the solvent-accessible area as the surface area created by tracing the centre of a sphere with a known radius as it is rolled around the surface of interest. The original software calculated the *contact* surface of the spherical probe with a preset radius, but in order to calculate pore sizes efficiently the guest *accessible* surface must also be calculated. After MSROLL was incorporated into X-Seed it was appropriately modified to give the option of mapping either type of surface. The modification entails adding the specified probe radius to the van der Waals radii of each of the atoms involved, once this is done the probe radius is then given as zero and the accessible surface is the “contact” surface traced by the centre of the probe.

2.3.2 *CrystalExplorer*²⁴

CrystalExplorer is a program used to generate and display Hirshfeld surfaces, and is a valuable tool for the visualisation of intermolecular interactions. A Hirshfeld surface is a means of dividing space in a crystal into regions of electron density and the actual surface is defined by the portion of space where the *promolecule* electron density contributes more than the total *procrystal* electron density (the terms *promolecule* and *procrystal* refer to the spherical atoms of the molecule of interest and to the atoms of the whole crystal respectively).

For a molecule in a crystal, a molecular weight function, $w(r)$ is defined from Hirshfeld's stockholder partitioning concept,²⁵ by the following equation:

$$w(r) = \rho_{\text{promolecule}}(r) / \rho_{\text{procrystal}}(r)$$

$$= \frac{\sum_{\text{in molecule}} \rho_A(r)}{\sum_{\text{in crystal}} \rho_A(r)}$$

$\rho_{promolecule}(r)$ and $\rho_{procrystal}(r)$ denote the sums over the atoms belonging to the molecule and to the crystal respectively and $\rho_A(r)$ is a spherically-averaged atomic electron density centered on nucleus A. Furthermore, the distances d_e and d_i are defined within Crystal Explorer. d_e is the distance from a point on the surface to the nearest atom external to the surface and d_i the distance from that same point on the surface to the nearest atom on the inside of the surface. When these distances are mapped on the Hirshfeld surface, they create an aesthetically pleasing visualisation in three-dimensions of intermolecular close contacts in the crystal. These distances do not, however, take the relative size of the atoms into account. Thus a normalised contact distance d_{norm} ²⁶ (equation 2) has been defined to overcome this problem.

$$\mathbf{d}_{norm} = \frac{d_i - r_i^{vdW}}{r_i^{vdW}} + \frac{d_e - r_e^{vdW}}{r_e^{vdW}} \quad (2)$$

All surfaces presented in this work have been mapped using the d_{norm} function.

REFERENCES

1. Y. J. Xie, *Acta Crystallographica Section E-Structure Reports Online*, **2005**, 61, O3538.
2. *SAINTE Data Collection Software, Version 6.45*;Madison, WI,Bruker AXS Inc. **2003**.
3. *SMART Data Collection Software,Version 5.629*;Madison, WI,Bruker AXS Inc. **2003**.
4. *SADABS, Version 2.05*;Madison, WI,Bruker AXS Inc. **2002**.
5. R. H. Blessing, *Acta Crystallogr., Sect. A: Found. Crystallogr.*, **1995**, 51, 33.
6. G. M. Sheldrick, *Acta Crystallogr., Sect. A Found. Crystallogr.* , **2008**, 64, 112.
7. L. J. Barbour, *Journal of Supramolecular Chemistry*, **2001**, 1, 189.
8. G. M. Sheldrick, *Programs for crystal structure analysis*, University of Gottingen, Amsterdam, **1997**.
9. K. Yvon, W. Jeitshko and E. Parthe, *J. Appl. Crystallogr.*, **1997**, 10, 73.
10. M. A. White, in *Comprehensive Supramolecular Chemistry*, eds. J. E. Davies and J. A. Ripmeester, Pergamon, Oxford, **1996**, pp. 179.
11. M. J. Benham and D. K. Ross, *Z. Phys. Chem. (Muenchen, Ger.)*, **1989**, 163, 25.
12. A. J. Fletcher and K. M. Thomas, *Langmuir*, **1999**, 15, 6908.
13. A. J. Fletcher and K. M. Thomas, *Langmuir*, **2000**, 16, 6253.
14. N. J. Foley, K. M. Thomas, P. L. Forshaw, D. Stanton and P. R. Norman, *Langmuir*, **1997**, 13, 2083.
15. A. W. Harding, N. J. Foley, P. R. Norman, D. C. Francis and K. M. Thomas, *Langmuir*, **1998**, 14, 3858.
16. I. P. Okoye, M. J. Benham and K. M. Thomas, *Langmuir*, **1997**, 13, 4054.
17. C. R. Reid, I. P. O'Koye and K. M. Thomas, *Langmuir*, **1998**, 14, 2415.
18. C. R. Reid and K. M. Thomas, **1999**, 15, 3206.
19. J. Atwood and L. J. Barbour, *Crystal Growth & Design*, **2003**, 3, 3.
20. *POV-Ray™ for Windows, Version 3.6*;Williamstown, Australia,Persistence of Vision Raytracer Pty. Ltd., **2004**.
21. M. L. Connolly, *Science*, **1983**, 221, 709.

22. M. L. Connolly, *J. Mol. Graphics*, **1993**, 11, 139.
23. B. Lee and F. M. Richards, *J.Mol. Biol.*, **1971**, 55, 379.
24. *CrystalExplorer 1.6*; S. K. Wolff, D. J. Grimwood, J. J. McKinnon, D. Jayatilaka and M. A. Spackman, University of Western Australia, Perth, **2006**.
25. F. L. Hirshfeld, *Theor.Chim.Acta*, **1997**, 44, 129.
26. J. J. McKinnon, D. Jayatilaka and M. A. Spackman, *Chem. Commun.*, **2007**, 3814.

CHAPTER 3

Structural Analysis of a Variety of Transition Metal Complexes of Imidazole-Derived Ligands

3.1 INTRODUCTION

The control of architectures derived from the self-assembly of transition metal salts and organic bridging ligands remains an elusive aspect of crystal engineering.¹⁻³ Over the past several years much attention has been devoted to the elucidation of the factors that influence the process of crystallisation, with a view to developing a means of tailoring the structures of these materials towards specific functions. Indeed, transition-metal-based supermolecules have already been recognised for their potential use in optics,⁴⁻⁶ gas sorption⁷⁻¹³ and catalysis.¹⁴⁻¹⁶ In general, the factors that influence the process of crystallisation include the choice of organic ligand,¹⁷⁻¹⁹ the coordination geometry of the metal ion,^{20, 21} the inorganic counterions,²² the metal-to-ligand ratio^{23, 24} and the solvent system.²⁵

Crystal structure prediction is impeded by the plethora of weak, non-covalent interactions possible within a crystal. This can largely be attributed to the fact that they display poor directionality when compared to covalent interactions (this does not, however, diminish the crucial role that these interactions play in crystal packing). One of the advantages of incorporating metal ions to the construct coordination polymers lies in the metal-ligand coordinative bond. These coordinative bonds occur in the energy range 10-30 kcal/mol per interaction²⁶ and are thus weaker than conventional covalent bonds, but stronger than hydrogen bonds, (also displaying more directionality than the latter).² Another advantage is the relative predictability of the coordination geometry around a metal centre, which is an important feature in the construction of coordination polymers. If one can predict, or at least assess what the most likely coordination around the metal centre is going to be, this forms an important first step in the rational design of these materials. This relative predictability of the coordination geometry around the metal centre is especially accurate for the d-block elements,²¹ and it is thus no surprise that transition metals

have been used extensively as templating nodes for organic bridging ligands in the construction of coordination polymers.

To date, most structures have employed rigid ligands (mostly pyridyl and carboxylate functionalised ligands) in the formation of these systems owing to the relative ease of prediction of the resulting networks and the limited conformational changes that can occur. However, the interest in comparatively flexible organic bridging ligands is on the rise due to the conformational freedom that these ligands could lend to the discovery of unique frameworks, and thus add further understanding of the manner in which supramolecular structures assemble.¹⁹

Imidazole functionalised ligands represent another class of N-donor organic linkers that can be used in the construction of coordination networks. These ligands have been attracting increasing attention due to their high affinity for metals and their relative ease of functionalisation.¹⁶ Indeed, our group has shown that imidazole-based ligands have a rich coordination chemistry which has successfully been exploited to construct a range of coordination networks with interesting topologies and specific functions (see Chapter 1 for a summary of these results).^{9, 23, 25, 27-30} The main focus of our work, however, is in the synthesis of porous materials. All of the ligands utilised in these systems are based on a simple design strategy (Chapter 1).

As an extension to these previous studies, one novel tripodal ligand and five novel bipodal ligands have been synthesised based on a modification of the previously mentioned design principle.[†] The six ligands are 1,3,5-tris(1-imidazolyl-2-thione)-2,4,6-trimethylbenzene (**L1**), 1,4-bis(1-imidazolyl-2-thione)-2,3,5,6-tetramethylbenzene (**L2**), 1,4-bis(1-imidazolyl-2-thione)-2,5-dimethylbenzene (**L3**), 3,5-bis(1-imidazolyl-2-thione)toluene (**L4**), 1,3-bis(1-imidazolyl-2-thione)-2,4,6-trimethylbenzene (**L5**) and 4,4'-bis(1-imidazolyl-2-thione)-1,1'-biphenyl (**L6**) (Scheme 1). It has been found that the salient features of these ligands are:

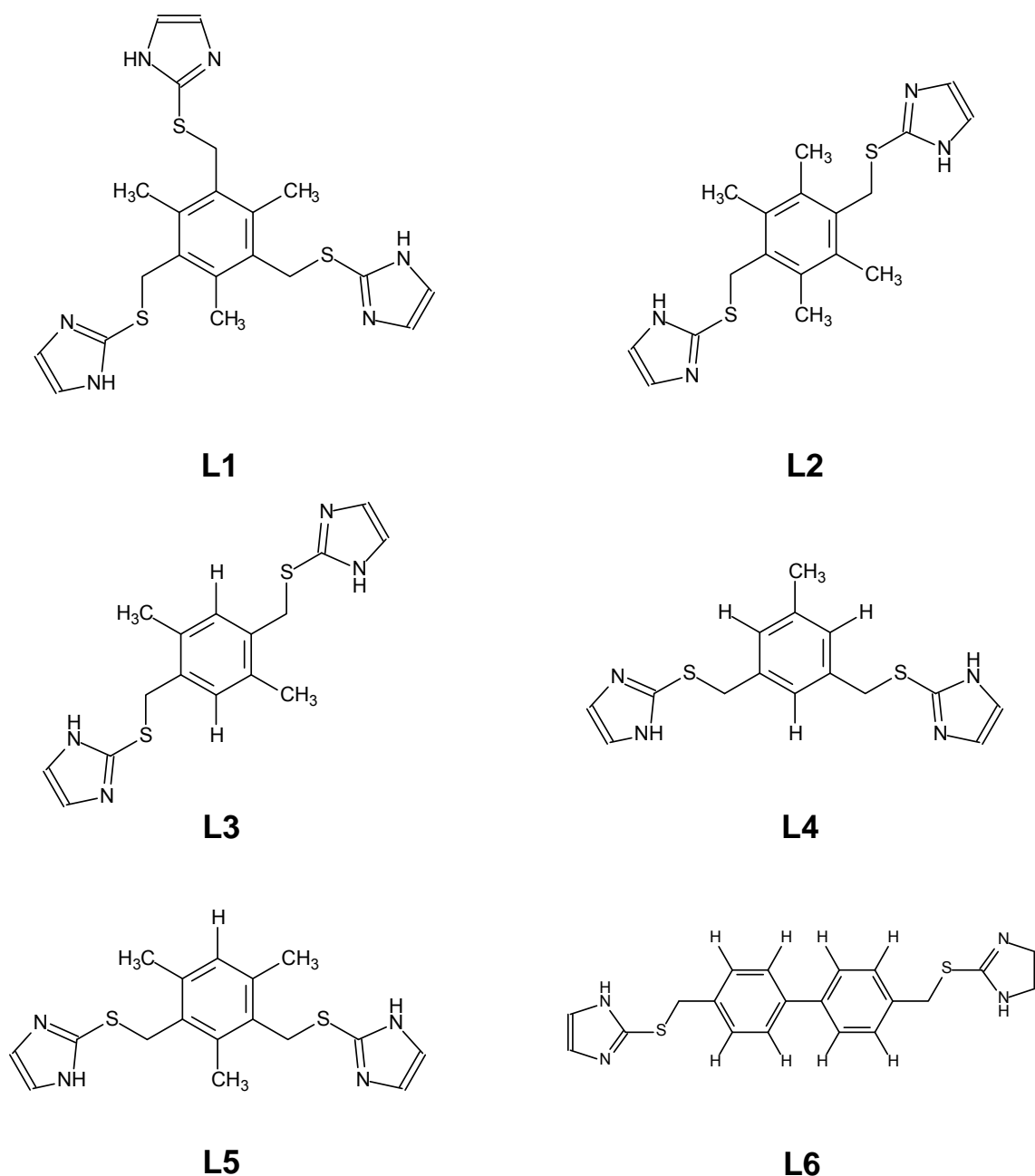
- 1) **L1** is tripodal and ligands **L2–L6** are bipodal,
- 2) Each imidazolyl moiety is linked to a central phenyl ring through a methylene group and a sulphur bridge,
- 3) Each imidazolyl hetero-aromatic ring contains one nitrogen atom with a lone electron pair (an imino nitrogen atom) and one protonated nitrogen atom (an amino nitrogen atom),

[†] For a complete description of this modification the reader is referred to Chapter 1, section 1.7.

Chapter 3- Structural Analysis of a Variety of Transition Metal Complexes Of Imidazole-Derived Ligands

4) Coordination to the metal cation predominantly occurs *via* the donation of the imidazolyl lone electron pair and occasionally *via* the donation of an electron lone pair, situated on the sulphur atoms,

5) The protons on the nitrogen atoms of the imidazolyl rings are available to donate hydrogen bonds to a myriad of hydrogen bond acceptors.



Scheme 1. (**L1**) 1,3,5-tris(1-imidazolyl-2-thione)-2,4,6-trimethylbenzene, (**L2**) 1,4-bis(1-imidazolyl-2-thione)-2,3,5,6-tetramethylbenzene, (**L3**) 1,4-bis(1-imidazolyl-2-thione)-2,5-dimethylbenzene, (**L4**) 3,5-bis(1-imidazolyl-2-thione)toluene, (**L5**) 1,3-bis(1-imidazolyl-2-thione)-2,4,6-trimethylbenzene, (**L6**) 4,4'-bis(1-imidazolyl-2-thione)-1,1'-biphenyl.

Chapter 3- Structural Analysis of a Variety of Transition Metal Complexes Of Imidazole-Derived Ligands

In each ligand the imidazolyl ring and aromatic core are rigid; however the joints between the arms and the core, *i.e.* the methylene group and sulphur bridge, allow the arms to rotate freely in solution. As a result of this flexibility the ligands are able to assume a variety of conformations in the solid state and it is therefore convenient in the discussion that follows to describe the overall conformation of each ligand with respect to the orientation of the pendant arms relative to the aromatic spacer. In this regard, the pendant groups can be directed either up (**U**) or down (**D**) with respect to the central aromatic ring.

Following this system the conformation of **L1** is either **UUU**, *i.e.* all three of the pendant arms are located on the same side of the central mesitylene plane, or **UUD**, *i.e.* one of the pendant groups is situated on one side of the central mesitylene plane in contrast to the other two (Figure 1). For the bipodal ligands, **L2–L6**, the conformation of the ligand molecule may be described as either **UU**, where the two imidazolyl rings are situated on the same side of the central aromatic core or **UD**, where the two rings are positioned on opposite sides of the core (Figure 2).

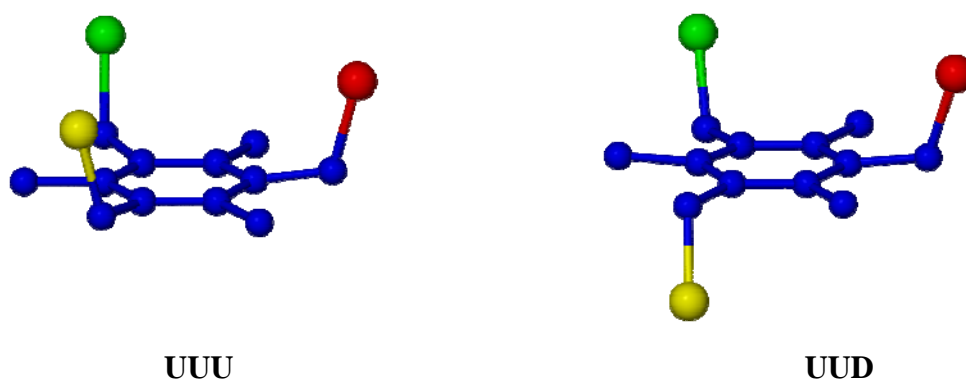


Figure 1. The two possible conformations of ligand **L1**.

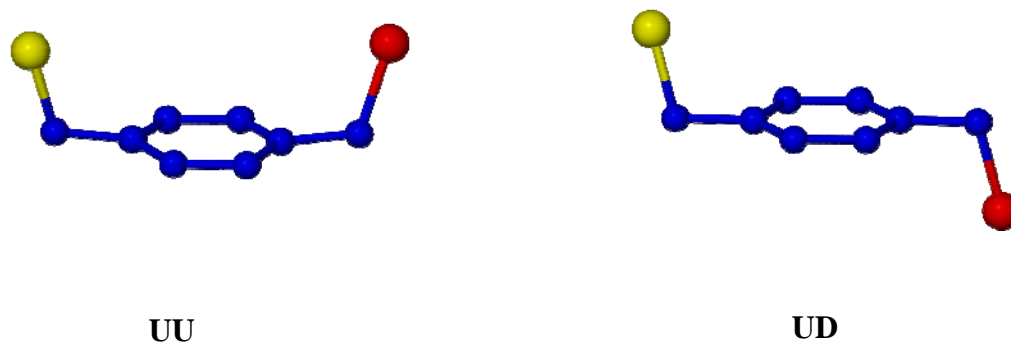


Figure 2. The two possible conformations of ligands **L2–L6**.

Preliminary investigations showed that the ligands are only soluble in a few common solvents (Table 1) and, accordingly, all crystals were grown by the method

Chapter 3- Structural Analysis of a Variety of Transition Metal Complexes Of Imidazole-Derived Ligands

of slow evaporation from acetonitrile or methanol in varying ligand-to-metal ratios at room temperature. Although the ligands are soluble in DMF and DMSO, these solvent systems did not yield any crystals suitable for SCD and are therefore not discussed further. The choice of metal salts used in the reactions included a variety of readily available transition metals (care was taken to include all of the metal salts that were shown to successfully complex to the imidazole-derived ligands previously synthesised in our group).

Table 1. Solubility of ligands **L1–L6** in a variety of common solvents.

Solvent	Soluble (✓) or Insoluble (×)
acetone	×
acetonitrile	✓
benzene	×
dichloromethane	×
diethyl ether	×
dimethyl sulphoxide	✓
dioxane	×
ethanol	×
ethyl acetate	×
methanol	✓
N,N-dimethyl formamide	✓
n-hexane	×
tetrahydrofuran	×
toluene	×
water	×

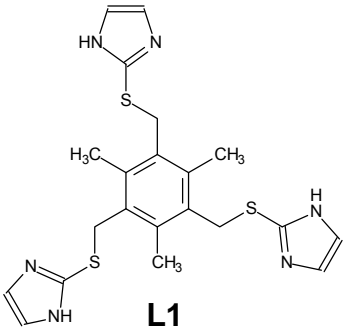
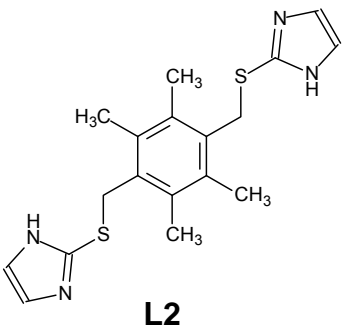
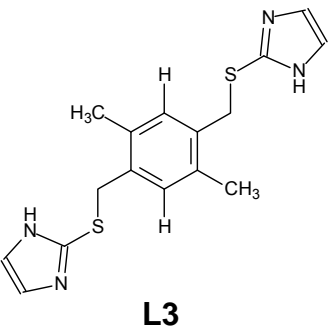
An outline of the reaction conditions used in each case is provided in Table 3, as well as a brief summary of the nature of the product obtained in each vial. A typical entry consists of three parts: the ratio of ligand-to-metal, the solvent used in the reaction and a description of the nature of the product obtained in each vial (see Table 2).

Table 2. A key to the description of the nature of the products obtained in the reaction vials.

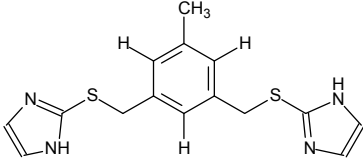
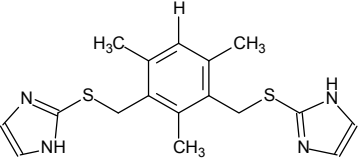
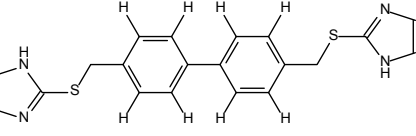
Symbol	Description
1-28	A single crystal structure was obtained for the metal-organic complex
a	only precipitate formed in the vial
b	only polycrystalline material formed in the vial
c	unit cell measured and found to match that of the free ligand
d	unit cell measured and found to match that of the metal salt
e	single crystals formed but were too small for SCD
-	no reaction was set-up

Chapter 3- Structural Analysis of a Variety of Transition Metal Complexes Of Imidazole-Derived Ligands

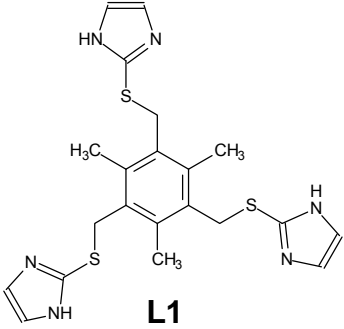
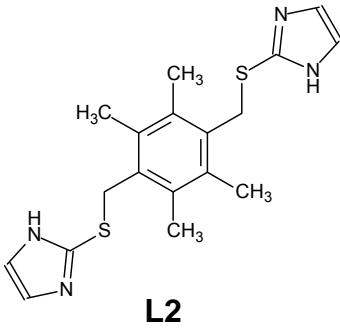
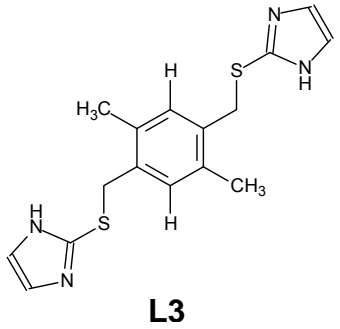
Table 3. Reaction conditions used in the preparation of metal-organic complexes with L1 – L6.

Metal Salt	 L1			 L2				 L3			
AgNO ₃	1:1 MeOH	3:1 MeOH	1:3 MeOH	1:1 MeOH	2:1 MeOH	4:1 MeOH	1:2 MeOH	1:1 MeOH	2:1 MeOH	4:1 MeOH	1:2 MeOH
	1	a	c	a	c	c	d	c	c	c	c
	1:1 MeCN	3:1 MeCN	1:3 MeCN	1:1 MeCN	2:1 MeCN	4:1 MeCN	1:2 MeCN	1:1 MeCN	2:1 MeCN	4:1 MeCN	1:2 MeCN
	e	c	a	3	a	a	4	a	a	a	6
AgBF ₄	1:1 MeOH	3:1 MeOH	1:3 MeOH	1:1 MeOH	2:1 MeOH	4:1 MeOH	1:2 MeOH	1:1 MeOH	2:1 MeOH	4:1 MeOH	1:2 MeOH
	e	a	a	a	a	a	a	a	a	c	e
	1:1 MeCN	3:1 MeCN	1:3 MeCN	1:1 MeCN	2:1 MeCN	4:1 MeCN	1:2 MeCN	1:1 MeCN	2:1 MeCN	4:1 MeCN	1:2 MeCN
	a	a	b	a	a	c	a	a	a	c	a
Ag(SO ₃ CF ₃)	1:1 MeOH	3:1 MeOH	1:3 MeOH	1:1 MeOH	2:1 MeOH	4:1 MeOH	1:2 MeOH	1:1 MeOH	2:1 MeOH	4:1 MeOH	1:2 MeOH
	a	c	a	a	c	a	a	a	a	a	b
	1:1 MeCN	3:1 MeCN	1:3 MeCN	1:1 MeCN	2:1 MeCN	4:1 MeCN	1:2 MeCN	1:1 MeCN	2:1 MeCN	4:1 MeCN	1:2 MeCN
	b	a	d	a	a	a	d	a	a	a	a
AgPF ₆	1:1 MeOH	3:1 MeOH	1:3 MeOH	1:1 MeOH	2:1 MeOH	4:1 MeOH	1:2 MeOH	1:1 MeOH	2:1 MeOH	4:1 MeOH	1:2 MeOH
	-	-	-	-	-	-	-	-	-	-	-
	1:1 MeCN	3:1 MeCN	1:3 MeCN	1:1 MeCN	2:1 MeCN	4:1 MeCN	1:2 MeCN	1:1 MeCN	2:1 MeCN	4:1 MeCN	1:2 MeCN
	-	-	-	-	-	-	-	-	-	-	-
AgSbF ₆	1:1 MeOH	3:1 MeOH	1:3 MeOH	1:1 MeOH	2:1 MeOH	4:1 MeOH	1:2 MeOH	1:1 MeOH	2:1 MeOH	4:1 MeOH	1:2 MeOH
	-	-	-	-	-	-	-	-	-	-	-
	1:1 MeCN	3:1 MeCN	1:3 MeCN	1:1 MeCN	2:1 MeCN	4:1 MeCN	1:2 MeCN	1:1 MeCN	2:1 MeCN	4:1 MeCN	1:2 MeCN
	-	-	-	-	-	-	-	-	-	-	-
Cd(NO ₃) ₂ ·4H ₂ O	1:1 MeOH	3:1 MeOH	1:3 MeOH	1:1 MeOH	2:1 MeOH	4:1 MeOH	1:2 MeOH	1:1 MeOH	2:1 MeOH	4:1 MeOH	1:2 MeOH
	2	a	2	a	b	c	a	a	a	a	a
	1:1 MeCN	3:1 MeCN	1:3 MeCN	1:1 MeCN	2:1 MeCN	4:1 MeCN	1:2 MeCN	1:1 MeCN	2:1 MeCN	4:1 MeCN	1:2 MeCN
	a	a	a	a	a	a	a	a	a	a	a
CdCl ₂ ·2.5H ₂ O	1:1 MeOH	3:1 MeOH	1:3 MeOH	1:1 MeOH	2:1 MeOH	4:1 MeOH	1:2 MeOH	1:1 MeOH	2:1 MeOH	4:1 MeOH	1:2 MeOH
	b	c	a	a	a	c	a	12	a	c	a
	1:1 MeCN	3:1 MeCN	1:3 MeCN	1:1 MeCN	2:1 MeCN	4:1 MeCN	1:2 MeCN	1:1 MeCN	2:1 MeCN	4:1 MeCN	1:2 MeCN
	a	a	a	a	a	a	a	a	a	a	a

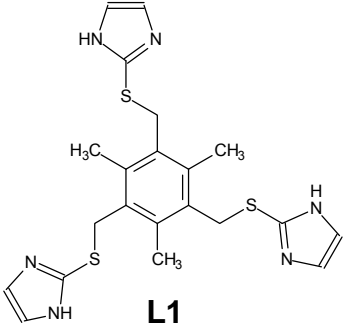
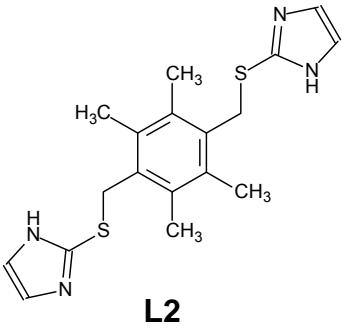
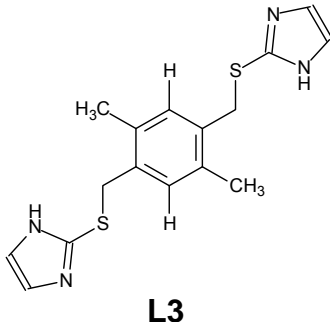
Chapter 3- Structural Analysis of a Variety of Transition Metal Complexes Of Imidazole-Derived Ligands

 <p style="text-align: center;">L4</p>	 <p style="text-align: center;">L5</p>	 <p style="text-align: center;">L6</p>
1:1 2:1 4:1 1:2 MeOH MeOH MeOH MeOH b c c a 1:1 2:1 4:1 1:2 MeCN MeCN MeCN MeCN a a c b	1:1 2:1 4:1 1:2 MeOH MeOH MeOH MeOH 16 a a 14 1:1 2:1 4:1 1:2 MeCN MeCN MeCN MeCN 15 a a 15	1:1 2:1 4:1 1:2 MeOH MeOH MeOH MeOH a c c a 1:1 2:1 4:1 1:2 MeCN MeCN MeCN MeCN a c c a
1:1 2:1 4:1 1:2 MeOH MeOH MeOH MeOH b c c a 1:1 2:1 4:1 1:2 MeCN MeCN MeCN MeCN c a c a	1:1 2:1 4:1 1:2 MeOH MeOH MeOH MeOH 20 a 20 a 1:1 2:1 4:1 1:2 MeCN MeCN MeCN MeCN a a a a	1:1 2:1 4:1 1:2 MeOH MeOH MeOH MeOH c a c d 1:1 2:1 4:1 1:2 MeCN MeCN MeCN MeCN e e c a
1:1 2:1 4:1 1:2 MeOH MeOH MeOH MeOH a b c a 1:1 2:1 4:1 1:2 MeCN MeCN MeCN MeCN a a a a	1:1 2:1 4:1 1:2 MeOH MeOH MeOH MeOH 17 a c e 1:1 2:1 4:1 1:2 MeCN MeCN MeCN MeCN a a c b	1:1 2:1 4:1 1:2 MeOH MeOH MeOH MeOH - - - - 1:1 2:1 4:1 1:2 MeCN MeCN MeCN MeCN - - - -
1:1 2:1 4:1 1:2 MeOH MeOH MeOH MeOH - - - - 1:1 2:1 4:1 1:2 MeCN MeCN MeCN MeCN - - - -	1:1 2:1 4:1 1:2 MeOH MeOH MeOH MeOH 19 e e b 1:1 2:1 4:1 1:2 MeCN MeCN MeCN MeCN a a a a	1:1 2:1 4:1 1:2 MeOH MeOH MeOH MeOH - - - - 1:1 2:1 4:1 1:2 MeCN MeCN MeCN MeCN - - - -
1:1 2:1 4:1 1:2 MeOH MeOH MeOH MeOH - - - - 1:1 2:1 4:1 1:2 MeCN MeCN MeCN MeCN - - - -	1:1 2:1 4:1 1:2 MeOH MeOH MeOH MeOH 18 a - a 1:1 2:1 4:1 1:2 MeCN MeCN MeCN MeCN - - - -	1:1 2:1 4:1 1:2 MeOH MeOH MeOH MeOH e e c d 1:1 2:1 4:1 1:2 MeCN MeCN MeCN MeCN a a a a
1:1 2:1 4:1 1:2 MeOH MeOH MeOH MeOH c c c b 1:1 2:1 4:1 1:2 MeCN MeCN MeCN MeCN a a a a	1:1 2:1 4:1 1:2 MeOH MeOH MeOH MeOH a b a d 1:1 2:1 4:1 1:2 MeCN MeCN MeCN MeCN a a a a	1:1 2:1 4:1 1:2 MeOH MeOH MeOH MeOH b a c a 1:1 2:1 4:1 1:2 MeCN MeCN MeCN MeCN a a a a
1:1 2:1 4:1 1:2 MeOH MeOH MeOH MeOH a a c c 1:1 2:1 4:1 1:2 MeCN MeCN MeCN MeCN a a a a	1:1 2:1 4:1 1:2 MeOH MeOH MeOH MeOH a b c b 1:1 2:1 4:1 1:2 MeCN MeCN MeCN MeCN a a a a	1:1 2:1 4:1 1:2 MeOH MeOH MeOH MeOH a a a a 1:1 2:1 4:1 1:2 MeCN MeCN MeCN MeCN a a a a

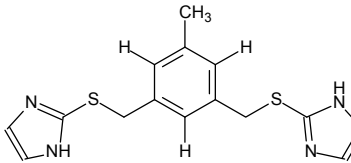
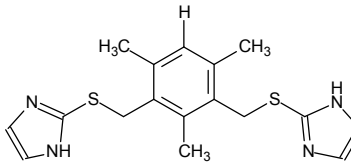
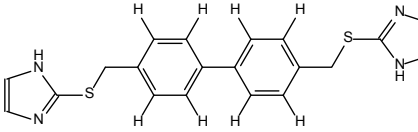
Chapter 3- Structural Analysis of a Variety of Transition Metal Complexes Of Imidazole-Derived Ligands

Metal Salt	 <p style="text-align: center;">L1</p>	 <p style="text-align: center;">L2</p>	 <p style="text-align: center;">L3</p>
CdI₂	1:1 MeOH a 3:1 MeOH a 1:3 MeOH e 1:1 MeCN a 3:1 MeCN a 1:3 MeCN a	1:1 MeOH 5 2:1 MeOH 5 4:1 MeOH a 1:2 MeOH 5 1:1 MeCN a 2:1 MeCN a 4:1 MeCN a 1:2 MeCN a	1:1 MeOH 7 2:1 MeOH a 4:1 MeOH 8 1:2 MeOH 9 1:1 MeCN a 2:1 MeCN b 4:1 MeCN c 1:2 MeCN a
CoCl₂·6H₂O	1:1 MeOH a 3:1 MeOH c 1:3 MeOH d 1:1 MeOH a 3:1 MeOH a 1:3 MeOH a	1:1 MeOH a 2:1 MeOH a 4:1 MeOH a 1:2 MeOH a 1:1 MeCN a 2:1 MeCN a 4:1 MeCN c 1:2 MeCN e	1:1 MeOH 11 2:1 MeOH a 4:1 MeOH a 1:2 MeOH d 1:1 MeCN a 2:1 MeCN b 4:1 MeCN a 1:2 MeCN a
Co(NO₃)₂·6H₂O	1:1 MeOH a 3:1 MeOH c 1:3 MeOH d 1:1 MeOH a 3:1 MeOH a 1:3 MeOH a	1:1 MeOH a 2:1 MeOH a 4:1 MeOH c 1:2 MeOH a 1:1 MeCN a 2:1 MeCN a 4:1 MeCN c 1:2 MeCN e	1:1 MeOH a 2:1 MeOH b 4:1 MeOH a 1:2 MeOH d 1:1 MeCN a 2:1 MeCN a 4:1 MeCN c 1:2 MeCN d
CuBr₂	1:1 MeOH a 3:1 MeOH c 1:3 MeOH a 1:1 MeCN a 3:1 MeCN a 1:3 MeCN a	1:1 MeOH c 2:1 MeOH b 4:1 MeOH a 1:2 MeOH c 1:1 MeCN a 2:1 MeCN b 4:1 MeCN a 1:2 MeCN a	1:1 MeOH d 2:1 MeOH b 4:1 MeOH a 1:2 MeOH d 1:1 MeCN a 2:1 MeCN c 4:1 MeCN c 1:2 MeCN d
CuCl₂·2H₂O	1:1 MeOH a 3:1 MeOH c 1:3 MeOH a 1:1 MeCN a 3:1 MeCN a 1:3 MeCN a	1:1 MeOH a 2:1 MeOH a 4:1 MeOH a 1:2 MeOH a 1:1 MeCN a 2:1 MeCN b 4:1 MeCN a 1:2 MeCN a	1:1 MeOH 10 2:1 MeOH a 4:1 MeOH b 1:2 MeOH a 1:1 MeCN a 2:1 MeCN b 4:1 MeCN a 1:2 MeCN a
Cu(NO₃)₂·3H₂O	1:1 MeOH a 3:1 MeOH c 1:3 MeOH a 1:1 MeCN a 3:1 MeCN a 1:3 MeCN a	1:1 MeOH a 2:1 MeOH b 4:1 MeOH b 1:2 MeOH a 1:1 MeCN a 2:1 MeCN b 4:1 MeCN a 1:2 MeCN e	1:1 MeOH a 2:1 MeOH b 4:1 MeOH a 1:2 MeOH a 1:1 MeCN b 2:1 MeCN b 4:1 MeCN c 1:2 MeCN d
ZnBr₂	1:1 MeOH a 3:1 MeOH a 1:3 MeOH a 1:1 MeCN a 3:1 MeCN a 1:3 MeCN a	1:1 MeOH a 2:1 MeOH b 4:1 MeOH c 1:2 MeOH a 1:1 MeCN a 2:1 MeCN a 4:1 MeCN a 1:2 MeCN a	1:1 MeOH 13 2:1 MeOH d 4:1 MeOH c 1:2 MeOH a 1:1 MeCN a 2:1 MeCN a 4:1 MeCN a 1:2 MeCN e

Chapter 3- Structural Analysis of a Variety of Transition Metal Complexes Of Imidazole-Derived Ligands

Metal Salt	 <p style="text-align: center;">L1</p>	 <p style="text-align: center;">L2</p>	 <p style="text-align: center;">L3</p>
ZnCl₂	1:1 MeOH a 3:1 MeOH a 1:3 MeOH a	1:1 MeOH a 2:1 MeOH a 4:1 MeOH a 1:2 MeOH a	1:1 MeOH e 2:1 MeOH a 4:1 MeOH c 1:2 MeOH e
	1:1 MeCN a 3:1 MeCN a 1:3 MeCN a	1:1 MeCN a 2:1 MeCN a 4:1 MeCN a 1:2 MeCN a	1:1 MeCN a 2:1 MeCN a 4:1 MeCN a 1:2 MeCN a
NiCl₂	1:1 MeOH c 3:1 MeOH c 1:3 MeOH b	1:1 MeOH a 2:1 MeOH a 4:1 MeOH a 1:2 MeOH a	1:1 MeOH a 2:1 MeOH a 4:1 MeOH a 1:2 MeOH c
	1:1 MeCN a 3:1 MeCN a 1:3 MeCN a	1:1 MeCN a 2:1 MeCN a 4:1 MeCN c 1:2 MeCN a	1:1 MeCN e 2:1 MeCN a 4:1 MeCN d 1:2 MeCN a
Ni(NO₃)₂·6H₂O	1:1 MeOH a 3:1 MeOH c 1:3 MeOH a	1:1 MeOH a 2:1 MeOH a 4:1 MeOH a 1:2 MeOH a	1:1 MeOH c 2:1 MeOH e 4:1 MeOH c 1:2 MeOH d
	1:1 MeCN a 3:1 MeCN a 1:3 MeCN a	1:1 MeCN e 2:1 MeCN a 4:1 MeCN d 1:2 MeCN a	1:1 MeCN e 2:1 MeCN a 4:1 MeCN c 1:2 MeCN d

Chapter 3- Structural Analysis of a Variety of Transition Metal Complexes Of Imidazole-Derived Ligands

 <p style="text-align: center;">L4</p>	 <p style="text-align: center;">L5</p>	 <p style="text-align: center;">L6</p>
<p>1:1 2:1 4:1 1:2 MeOH MeOH MeOH MeOH a b a a</p> <p>1:1 2:1 4:1 1:2 MeCN MeCN MeCN MeCN a a d a</p>	<p>1:1 2:1 4:1 1:2 MeOH MeOH MeOH MeOH b a a e</p> <p>1:1 2:1 4:1 1:2 MeCN MeCN MeCN MeCN a b d a</p>	<p>1:1 2:1 4:1 1:2 MeOH MeOH MeOH MeOH 26 e a 27</p> <p>1:1 2:1 4:1 1:2 MeCN MeCN MeCN MeCN a a a a</p>
<p>1:1 2:1 4:1 1:2 MeOH MeOH MeOH MeOH c c c c</p> <p>1:1 2:1 4:1 1:2 MeCN MeCN MeCN MeCN e a d a</p>	<p>1:1 2:1 4:1 1:2 MeOH MeOH MeOH MeOH a a a a</p> <p>1:1 2:1 4:1 1:2 MeCN MeCN MeCN MeCN a a d a</p>	<p>1:1 2:1 4:1 1:2 MeOH MeOH MeOH MeOH e a a e</p> <p>1:1 2:1 4:1 1:2 MeCN MeCN MeCN MeCN a a d e</p>
<p>1:1 2:1 4:1 1:2 MeOH MeOH MeOH MeOH c c c a</p> <p>1:1 2:1 4:1 1:2 MeCN MeCN MeCN MeCN e a c a</p>	<p>1:1 2:1 4:1 1:2 MeOH MeOH MeOH MeOH 28 a a 28</p> <p>1:1 2:1 4:1 1:2 MeCN MeCN MeCN MeCN b a d a</p>	<p>1:1 2:1 4:1 1:2 MeOH MeOH MeOH MeOH a e a d</p> <p>1:1 2:1 4:1 1:2 MeCN MeCN MeCN MeCN a a c d</p>

3.2 RESULTS AND DISCUSSIONS - STRUCTURE DETERMINATIONS FROM SINGLE-CRYSTAL X-RAY DIFFRACTION

The single crystal structures obtained from the reaction conditions outlined in Table 3 are described in this section. All of the structures have been grouped according to ligand and the crystallographic data of complexes **1-28** is available in the tables at the end of the chapter.

3.2.1 Single-crystal structures obtained with ligand L1

3.2.1.1 [AgL1]NO₃·CH₃OH (1)

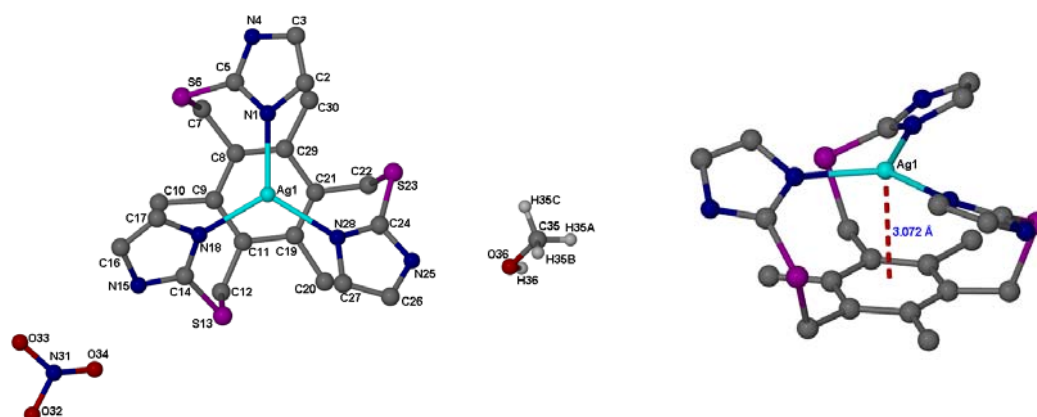


Figure 3. The ASU of **1** (left) and the Ag- π interactions within the Ag(L1)⁺ unit (right). The Ag- π interaction has been shown as a dashed red line, and both figures are shown in the ball-and-stick metaphor. Hydrogen atoms of the ligand have been omitted for clarity.

Crystals suitable for X-ray diffraction analysis were obtained by the reaction of AgNO₃ with **L1** (1:1 molar ratio) in MeOH, followed by slow evaporation of the solvent. The ASU consists of one Ag(L1)⁺ unit, one uncoordinated nitrate anion and one methanol molecule (Figure 3). In each discrete unit, **L1** is in the UUU conformation and all three of the imidazole rings are simultaneously coordinated to the Ag(I) ion. A distorted trigonal planar geometry occurs around the metal centre with an average Ag-N bond length of 2.243(1) Å and an average N-Ag-N angle of 119.8(5)°. As a result of this coordination mode, each discrete unit adopts a characteristic propeller-like conformation when viewed down the crystallographic three-fold axis which passes through the Ag ion and the centroid of the aromatic ring.

Chapter 3- Structural Analysis of a Variety of Transition Metal Complexes Of Imidazole-Derived Ligands

The canted imidazole groups (the dihedral angles are given in Table 4) form the blades of the propeller and the protonated nitrogen atoms of the imidazole groups are thus sterically accessible to participate in hydrogen bonding. This conformation has previously been observed in similar tripodal ligand complexes.^{31, 32}

Ag- π interactions* are present within the cationic units (the distance from the metal-ion to the centroid of the benzene ring = 3.072 Å, see Figure 3), and due to this interaction the metal centre is located 0.093(7) Å below the basal plane defined by the three coordinating nitrogen atoms.

One of the oxygen atoms of the nitrate anion is a bifurcated hydrogen bond acceptor and forms hydrogen bonds with both a protonated nitrogen of one imidazole group (N15...O34 = 2.705(2) Å) and the oxygen atom of the methanol molecule (O36...O34 = 2.733(2) Å). The latter, in turn, accepts a hydrogen bond (N25...O36 = 2.770(2) Å) from a protonated nitrogen of a neighbouring complex. By virtue of these hydrogen bonds and a 2_1 screw operation, adjacent units are connected into a 1D strand running parallel to [001] (Figure 4) (see Table 5 for details of all hydrogen bonding parameters).

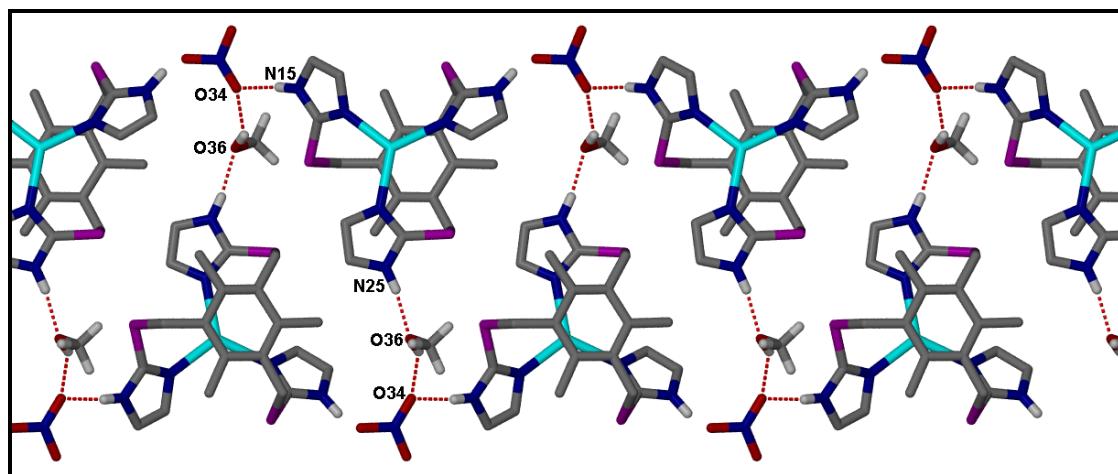


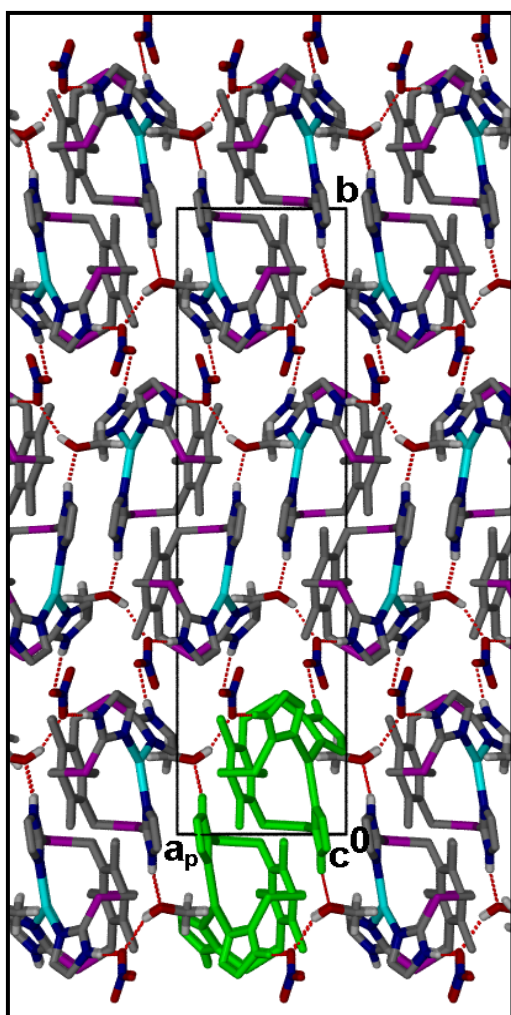
Figure 4. Capped-stick representation of the 1D strands formed in **1**. Hydrogen bonds are represented as dashed red lines and all hydrogen atoms not participating in hydrogen bonds have been omitted for clarity.

* In order for this to be considered a true Ag- π interaction the distance from the Ag ion to the centroid must fall within the reported range of 2.89-3.37 Å³¹ (see section 1.2.1.)

Chapter 3- Structural Analysis of a Variety of Transition Metal Complexes Of Imidazole-Derived Ligands

Table 4. Dihedral angle between the least squares plane of each respective imidazole ring and the benzene ring for **1**. Atoms constituting the imidazole group are given as reference.

Atoms constituting the imidazole ring	Dihedral angle (°)
N1-C2-C3-N4-C5	26.32(9)
N18-C17-C16-N15-C14	32.24(7)
N28-C27-C26-N25-C24	28.49(4)

**Figure 5.** Capped-stick representation of the 3D array formed by hydrogen bonding in **1** as viewed down [001]. A single 1D strand has been coloured green for clarity. Hydrogen atoms not involved in hydrogen bonding have been omitted for clarity.

Finally, the protonated nitrogen of the third imidazole group donates a hydrogen bond to another oxygen of the nitrate group ($N4 \cdots O32 = 2.981(3) \text{ \AA}$) to connect neighbouring strands into a 3D array consisting of layers of 1D strands stacked one on top of another in an *...ABAB...* fashion- *i.e.* the atoms of the first layer are placed directly over the atoms of the third layer (Figure 5).

Table 5. Hydrogen-bond geometry for **1** (Å, °).

D-H...A	D-H	H...A	D...A	D-H...A
N15-H14...O34	0.88	1.83	2.705(2)	172
N25-H25...O36	0.88	1.91	2.770(2)	166
O36-H36...O34 ⁱ	0.84	2.02	2.733(2)	142
N4-H4...O32 ⁱⁱ	0.88	2.13	2.981(3)	163

Symmetry codes: (i) $-x + 1, -y, z + 1/2$; (ii) $x - 1/2, -y + 1/2, z + 1$.

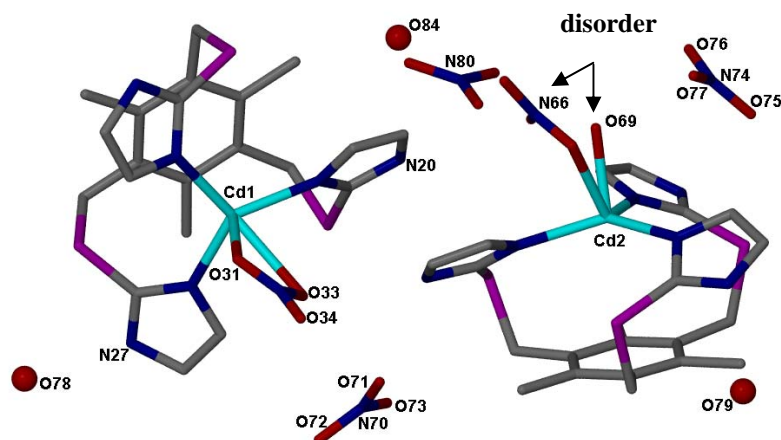
3.2.1.2 [CdL1(μ -NO₃)] [CdL1(H₂O)(NO₃)](NO₃)₃·2H₂O (**2**)

Figure 6. Capped-stick representation of the asymmetric unit of **2**. Hydrogen atoms have been omitted for clarity and water molecules are shown in the ball-and-stick metaphor.

Single crystals of **2** were obtained by slow evaporation of a methanolic solution of **L1** and Cd(NO₃)₂·4H₂O in either a 1:1 or 1:3 ligand-to-metal molar ratio. The structure of **2** consists of two crystallographically independent mononuclear complexes. In each complex the ligand **L1** is in the UUU conformation with each Cd ion in a distorted pseudo-tetrahedral coordination environment. In the first complex Cd1 is coordinated to one ligand **L1** and a bidentate nitrate ion. The three imidazole groups are oriented in a propeller-like arrangement about the metal centre with N-Cd-N coordinating angles ranging from 115.55(1)° - 123.54(1)° and an average Cd-N bond distance of 2.195(3) Å. The nitrate ion is not symmetrically bonded to the Cd ion and the Cd-O33 bond distance of 2.625(3) Å is significantly longer than the Cd-O31 bond distance of 2.406(3) Å (See Table 6 for all coordination geometric parameters). The distance from the Cd ion to the centroid of the benzene ring is 3.382 Å.

The coordination geometry around the second Cd ion is similar to that of Cd1 in that Cd2 is coordinated to one ligand **L1** with the three imidazole groups oriented in a propeller-like arrangement about the metal centre (see Table 6). However, the fourth coordination site of the tetrahedral environment about Cd2 differs from that of Cd1 and is an interesting case of disorder. X-ray structural analysis reveals that either a water molecule or a monodentate nitrate ion occupies the fourth position of the tetrahedron, and exists as a disordered pair with an uncoordinated nitrate ion or water molecule, *i.e.* if the nitrate ion is coordinated to Cd2, O84 is present in the ASU, but if

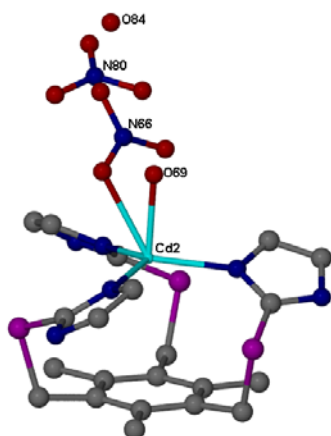


Figure 7. Ball-and-stick plot showing the molecular structure of the second mononuclear unit in **2**.

O69 is coordinated to the metal centre the nitrate ion bearing N80 at its centre is present in the ASU (refer to Figure 7).

In addition to the two mononuclear complexes mentioned above, the ASU also contains two more nitrate ions and two water molecules. These form hydrogen bonds with the ligated water molecules and nitrate ions to connect the 0D mononuclear units to one another (Table 7).

Finally, structurally analogous mononuclear units (*i.e.* those with the same coordination

environment about their Cd-centres) interact with one another by means of weak offset face-to-face (OFF) π - π interactions between benzene rings (centroid-to-centroid distances = 3.757 Å and 4.513 Å for the mononuclear units bearing the Cd1 and Cd2 centres respectively) (Figure 8).

Table 6. Coordination geometric parameters for **2** (Å, °).

2			
Cd1-N30	2.180(3)	Cd2-O69	2.146(5)
Cd1-N23	2.201(3)	Cd2-N57	2.187(3)
Cd1-N1	2.210(3)	Cd2-N35	2.198(3)
Cd1-O31	2.406(3)	Cd2-N64	2.210(3)
Cd1-O33	2.625(3)	Cd2-O65	2.446(5)
N30-Cd1-N23	123.54(10)	O69-Cd2-N57	94.22(16)
N23-Cd1-O31	108.43(10)	O69-Cd2-N35	97.30(16)
N30-Cd1-N1	117.66(10)	N57-Cd2-N35	115.22(11)
N1-Cd1-O31	78.81(9)	O69-Cd2-N64	98.18(15)
N23-Cd1-N1	115.55(10)	N57-Cd2-N64	116.78(11)
N30-Cd1-O33	84.79(10)	N57-Cd2-O65	124.90(15)
N30-Cd1-O31	98.97(10)	N35-Cd2-O65	87.72(13)
		N64-Cd2-O65	79.20(14)

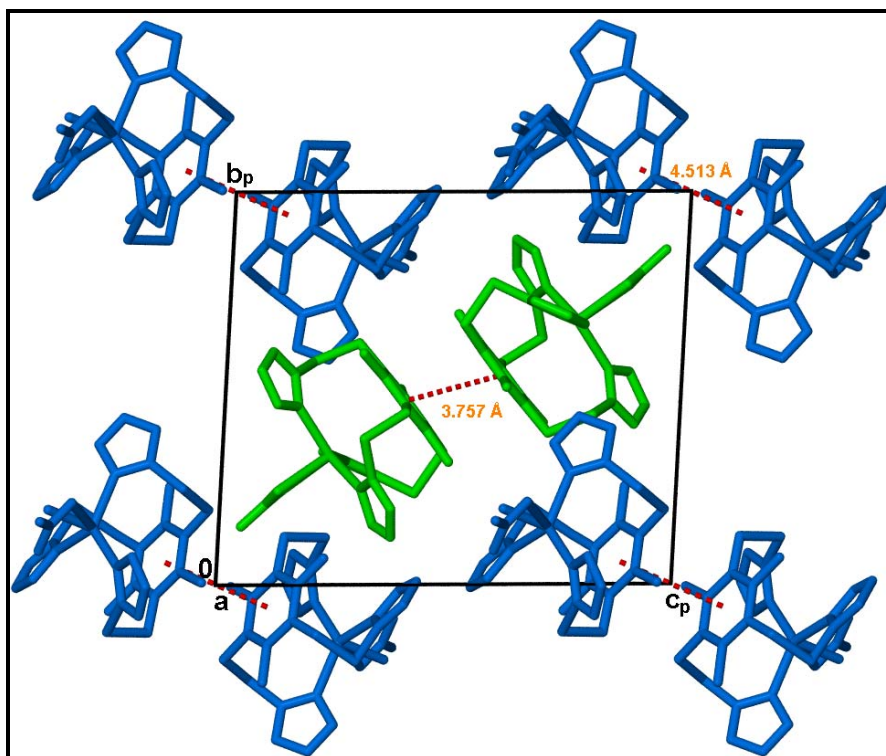


Figure 8. Packing arrangement of **2** as viewed down [100]. Hydrogen atoms and uncoordinated nitrate ions and water molecules have been omitted for clarity. Structurally analogous mononuclear units have been coloured green and blue to distinguish them from one another. π - π interactions are shown as dashed red lines.

Table 7. Hydrogen-bond geometry for **2** (Å, °).

D-H...A	D-H	H...A	D...A	D-H...A
N27-H27...O34	0.88	1.91	2.786(4)	173
N38-H38...O79	0.88	2.03	2.825(5)	150
N4-H4...O76 ⁱ	0.88	1.91	2.788(4)	179
N20-H20...O76 ⁱⁱ	0.88	1.93	2.799(4)	169
O78-H78A...O34 ⁱⁱⁱ	0.99	1.96	2.912(4)	161
O78-H78B...O71 ⁱⁱⁱ	0.99	1.87	2.857(5)	173
O79-H79A...O72 ^{iv}	1.00	1.84	2.744(5)	148
O79-H79B...O73 ^v	1.00	2.15	2.916(6)	132

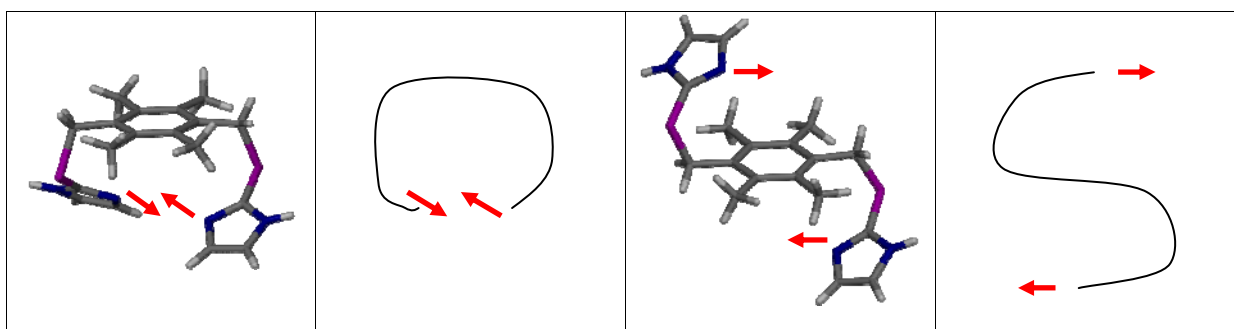
Symmetry codes: (i) $-x + 1, -y + 2, -z + 1$; (ii) $-x + 2, -y + 2, -z + 1$; (iii) $-x + 1, -y + 1, -z + 2$; (iv) $x + 1, y + 1, z$; (v) $-x + 2, -y + 2, -z + 2$.

Comparison of complexes 1 and 2

The crystal structures of both **1** and **2** feature a solid state ligand-to-metal ratio of 1:1. The ligand molecule assumes the UUU conformation in both structures with all three of the imidazole rings simultaneously coordinated to the metal centres in a propeller-like arrangement, leading to the formation of discrete mononuclear units connected to one another through a series of hydrogen bonds. The two structures are thus similar in many ways, but differ most significantly in the coordination geometry of the metal centres (distorted trigonal planar in **1** and tetrahedral in **2**), and by the absence of π - π stacking interactions in **1**.

3.2.2 Single-crystal structures obtained with ligand L2

Ligand L2 and AgNO₃



Scheme 2. A representation of the approximate C-shaped conformation of the ligand found in **3** where the coordinating nitrogen atoms are pointed in opposite directions, but towards each other (left) and the S-shaped conformation found in **4** where the coordinating nitrogen atoms are pointed in opposite directions, but away from each other (right). The red arrows indicate points where coordination bonds are formed.

Crystals suitable for single-crystal X-ray diffraction analysis of the metal complexes **3** and **4** were obtained by allowing solutions of **L2** and AgNO₃ in acetonitrile to crystallise by slow evaporation over a period of several days. Crystals of **3** were isolated from a vial in which the solution ratio of metal to ligand was 1:1 and **4** from a vial where the solution ratio was 1:2. The resulting structures were analysed in terms of their overall arrangement in the solid state as well as with respect to the energies of the specific conformations of the ligands within each complex. In order to further

clarify the results of the computational study, a Hirshfeld surface³³ was generated as a means of visualising the intermolecular contacts for each individual complex.

3.2.2.1 [AgL2]NO₃ (3)

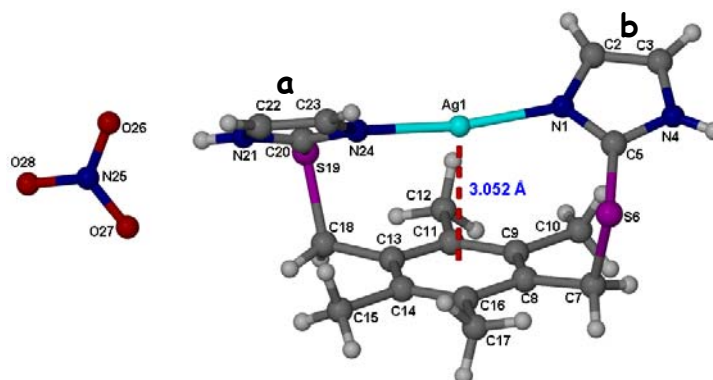


Figure 9. Ball-and-stick plot showing the ASU of **3**. The Ag- π interaction is indicated by the dashed red line.

The ASU of **3** consists of a single cationic unit and an uncoordinated nitrate counterion (Figure 9). The conformation of **L2** within the cationic unit is approximately C-shaped, *i.e.* the ligand assumes the **UU** conformation with the coordinating nitrogen atoms of the imidazole groups pointing towards each other (Scheme 2). This conformation facilitates the formation of discrete units in which the Ag ion is linearly coordinated by two imidazole nitrogens from the same ligand. The N-Ag-N angle of $170.01(5)^\circ$ and the distance from the Ag ion to the centroid of the benzene ring of 3.0562 \AA indicates the presence of Ag- π interactions within the complex. The protonated imidazole nitrogen atoms and nitrate ions form hydrogen bonds that link the discrete units together into a 1D strand that runs parallel to [001] (Figure 10).

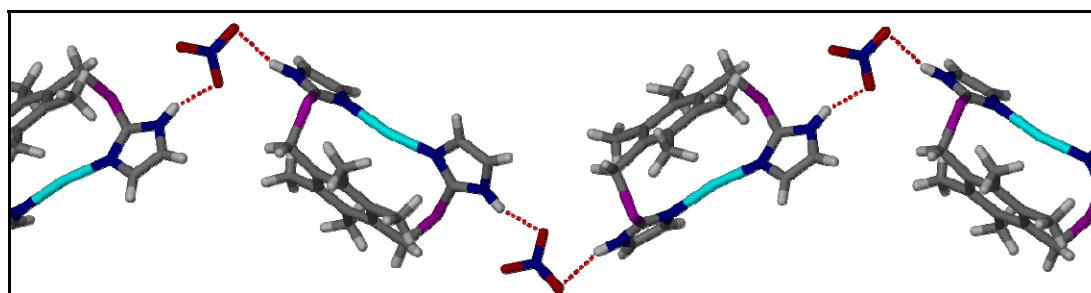


Figure 10. Capped-stick representation of the 1D strands formed by the N-H...O hydrogen bonding in **3**, as viewed along [001]. Hydrogen bonds are indicated by dotted red lines.

Weaker C10-H10B...O28 hydrogen bonds and π - π stacking interactions between the benzene ring and imidazole ring **a** (Figure 9) (centroid-centroid distance = 3.672 Å) connect neighbouring strands together to form a 2D layer running parallel to (100) (Figure 11). The final 3D assembly is stabilised by C2-H2...O27 hydrogen bonds which connect adjacent layers (see Table 8 for details of all hydrogen bonding parameters).

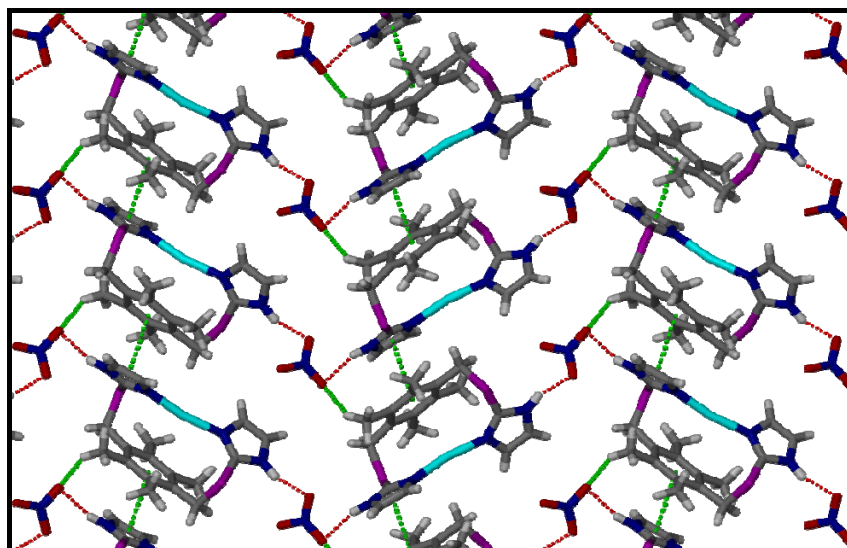


Figure 11. Capped-stick representation of the 2D layers formed in **3** as a result of hydrogen bonding and π - π stacking, as viewed along (100). N-H...O hydrogen bonds are indicated by dashed red lines, C-H...O hydrogen bond and π - π stacking interactions are shown as dashed green lines.

3.2.2.2 ([AgL2]NO₃)_n (**4**)

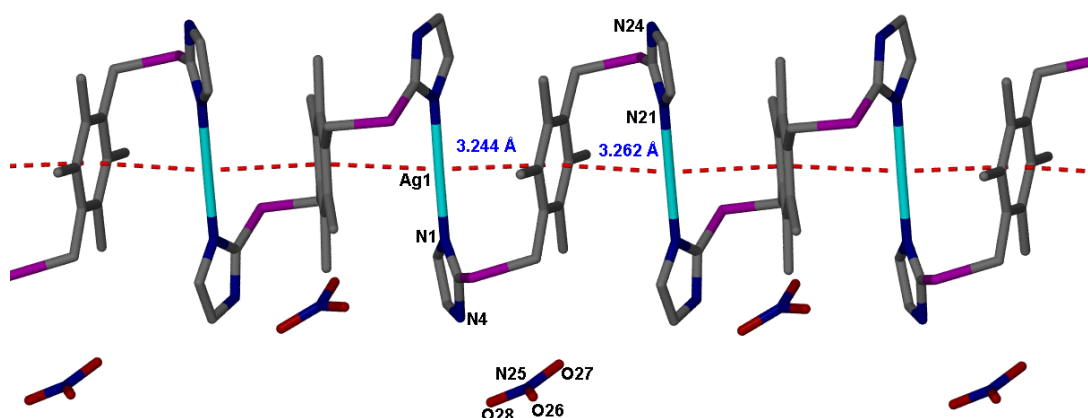


Figure 12. Capped-stick representation of the 1D strand formed in **4**. Ag- π interactions are shown as dashed red lines and hydrogen atoms have been omitted for clarity.

Chapter 3- Structural Analysis of a Variety of Transition Metal Complexes Of Imidazole-Derived Ligands

In **4** the Ag(I) ions are linearly coordinated by two imidazolate-nitrogens from separate ligands, with a corresponding N-Ag-N angle of 178.73(9)°. An infinite 1D polymeric strand running parallel to [001] is thus formed, in which metal centres are connected to one other by means of a single ligand **L2** (Figure 12). The conformation of the bridging ligand is approximately S-shaped, *i.e.* the ligand assumes the **UD** conformation with the coordinating nitrogen atoms of the imidazole groups pointed away from each other (Scheme 2) such that each Ag ion is in close proximity to two benzene rings. The distances from the Ag⁺ ion to the centroids of these rings are 3.244 Å, and 3.264 Å, and fall within the distance range reported for Ag- π interactions (Figure 12).³⁴ However, the expected deviation from linearity in the N-Ag-N angle associated with this type of interaction is not apparent, which could be an indication that the silver ion is experiencing an almost equal, simultaneous attraction to both π systems.

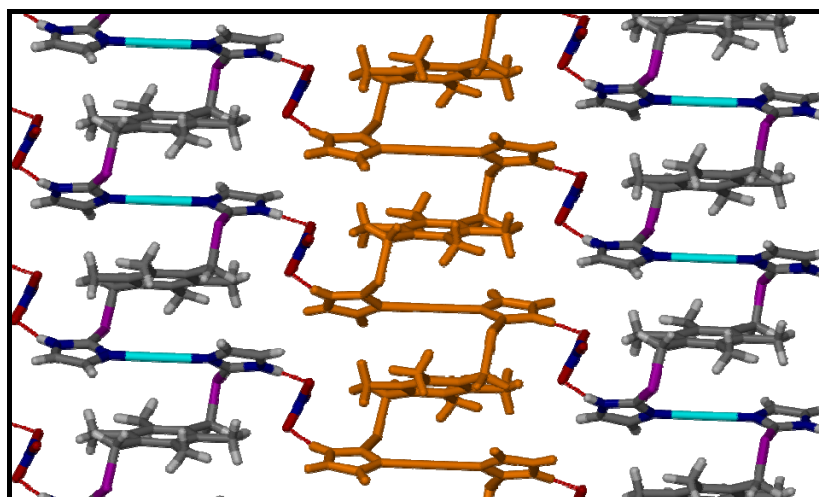
The non-coordinated nitrate counter-ions present in the crystal form N-H \cdots O hydrogen bonds with the protonated nitrogens of the imidazole groups (Table 8). Adjacent 1D strands are connected to another by virtue of these hydrogen bonds to form 2D layers parallel to (010) (Figure 13). Finally, the third oxygen atom of the nitrate group (the one not participating in N-H \cdots O hydrogen bonding) protrudes into a neighbouring layer and forms a ‘quasi’ Ag-O bond³⁵ (Ag \cdots O distance = 2.709(2) Å) and connects the 2D layers into a 3D array such that atoms of alternating layers are placed directly over one another (Figure 14).

Chapter 3- Structural Analysis of a Variety of Transition Metal Complexes Of Imidazole-Derived Ligands

Table 8. Selected bond distances (Å) and angles (°) for complexes **3** and **4**.

Complex 3				
Ag1- N1			2.078(2)	
Ag1- N24			2.069(2)	
N1-Ag1-N24			170.0(5)	
Hydrogen-bond geometry for 3 (Å, °).				
D-H...A	D-H	H...A	D...A	D-H...A
N21-H21...O26	0.88	1.89	2.73(2)	160
N4-H4...O28 ⁱ	0.88	2.18	3.04(2)	163
C10-H10B...O28 ⁱⁱ	0.98	2.52	3.36(2)	144
Complex 4				
Ag1- N1			2.109(3)	
Ag1- N21			2.105(2)	
N1-Ag1-N21 ⁱ			178.73(9)	
Hydrogen-bond geometry for 4 (Å, °).				
D-H...A	D-H	H...A	D...A	D-H...A
N4-H4...O28	0.88	1.95	2.807(3)	165
N24-H24...O27 ⁱⁱ	0.88	1.87	2.745(3)	171

Symmetry codes: **3** (i) $-x, -y + \frac{3}{2}, z - \frac{1}{2}$; (ii) $-\frac{1}{2} - x, 2-y, z - \frac{1}{2}$; **4** (i) $x, \frac{1}{2} - y, \frac{1}{2} + z$; (ii) $x-1, -y + \frac{1}{2}, z - \frac{1}{2}$.

**Figure 13.** Capped-stick representation of the 2D layers formed parallel to (010) in **4**. Hydrogen bonds are indicated by dashed red lines, and a single 1D strand has been coloured orange for clarity.

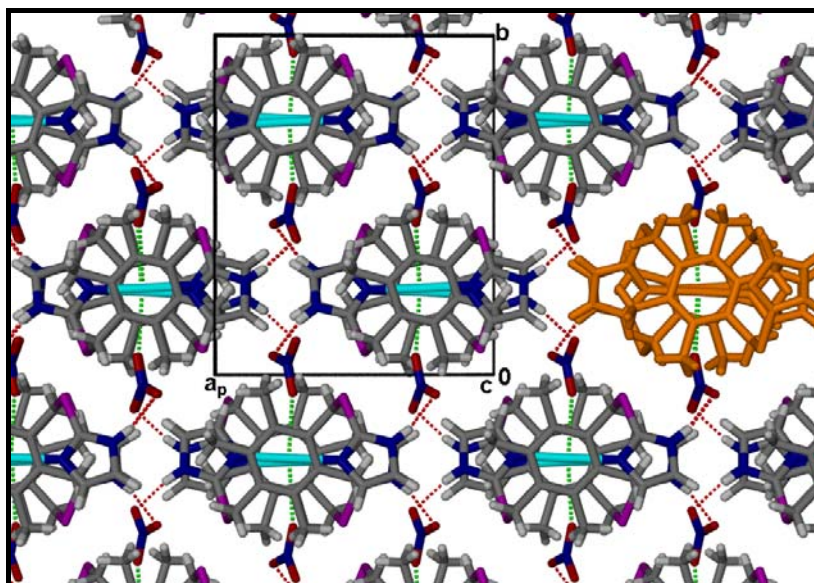


Figure 14. View down [001] of the 3D array formed in **4**. N-H...O hydrogen bonds are drawn as dotted red lines and 'quasi' Ag-O bonds are drawn as dotted green lines. A single strand has again been coloured orange in order to follow the orientation of the 1D strand from the 2D layers to the 3D array.

Comparison of **3** and **4**

Although complexes **3** and **4** have the same structural formula, *i.e.* $\text{AgL2}(\text{NO}_3)$, their crystal structures are markedly distinct. The most obvious difference between the two structures is the conformation of the ligand, which leads to different arrangements of the constituents in the solid state. In **4** an infinite 1D chain is formed with the ligand in the **UD** conformation (approximately S-shaped), whereas in **3**, **L2** is in the **UU** conformation (approximately C-shaped) and discrete mononuclear units are formed. This raises the question of which conformation is more stable and to this end an investigation into the relative energies of the ligands in the crystal structures of **3** and **4** was carried out.

The following calculations* were executed at the B3LYP³⁶/6-311G(d) level of theory³⁷:

1. The energies of the ligands in the conformations found in the crystal structures were determined. However, since the H-atom positions in crystal structures are notoriously incorrect (as H-atoms are usually placed in calculated positions),

* Calculations were conducted by Dr C. Esterhuysen using a parallel version of the program package Gaussian 03³⁴ at the Department of Chemistry and Polymer Science at the University of Stellenbosch.

Chapter 3- Structural Analysis of a Variety of Transition Metal Complexes Of Imidazole-Derived Ligands

the H-atom positions were optimised prior to the single-point calculation (also at the B3LYP/6-311G(d) level of theory).

2. The conformations of the individual ligands in gas phase (*i.e.* without any external influences such as metal complex formation or other intermolecular interactions) were optimised.
3. A single molecule of the complex found in **3** was optimised at the B3LYP/LANL2DZ/6-311G(d) level [Ag is calculated using the LANL2DZ³⁸,³⁹ basis set and the rest of the atoms with 6-311G(d)], again in gas phase thus excluding intermolecular interactions, whereafter the energy of the ligand only in this optimised geometry was determined. A similar calculation was performed for **4**, but using a "molecule" where two identical ligands are coordinated to a single Ag metal atom, and again optimised using the B3LYP/LANL2DZ/6-311G(d) level of theory.

Table 9. Results of the energy calculations for the different conformations of **L2**. All entries are recorded as energy values relative to that found for **L2** in crystal structure of complex **3**.

Crystal structure	Conformation of ligand	Relative energy ^{##} (kcal/mol)	Calculation	Colour of the molecule in Figures 15 and 16
3	Crystal structure [#]	0	1	CPK
	Optimised	-25.6	2	pink
	Complex optimised	-17.9	3	green
4	Crystal structure [#]	-12.3	1	CPK
	Optimised	-23.4	2	pink
	Complex optimised	-15.5	3	green

[#] H-atom positions optimised

^{##} Relative to the energy of the conformation of **3** in the crystal structure

The results in Table 9 show that the conformation of the ligand in the crystal structure of **4** is lower in energy than the conformation of the ligand in **3**. Furthermore, when the conformations of the individual ligands are allowed to optimize in the absence of any external forces, both systems show a substantial drop in energy and a change in conformation (shown as pink molecules in Figure 15 and Figure 16).

Chapter 3- Structural Analysis of a Variety of Transition Metal Complexes Of Imidazole-Derived Ligands

This indicates that, upon complexation, both ligands become strained within their respective crystal structures. However, the large stabilisation energies still found for the ligand (particularly in **3**) show that there are also influences from intermolecular interactions that cannot be ignored.

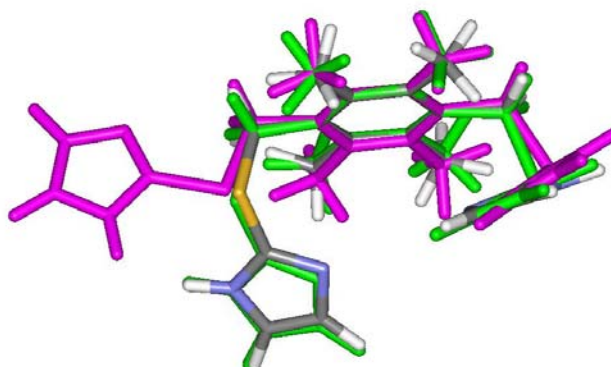


Figure 15. Comparison of the experimental and calculated conformations of the ligand in **3**; conformations shown are of the ligand optimised alone (pink) and in the complex (green). The CPK molecule shows the ligand as it is in the crystal structure.



Figure 16. Comparison of the experimental and calculated conformation of the ligand in **4**; conformations shown are of the ligand optimised alone (pink) and in the complex (green). The CPK molecule shows the ligand as it is in the crystal structure.

The impact of this large difference in energy would be most noticeable in the gas phase conformation of the free ligand, *i.e.* it is expected that the optimised conformations shown in pink in Figure 15 will dominate over the conformations found in both the crystal structures and the optimised structures based on the **3** crystal structure. A mixture of conformations of the free ligand in the gas phase is thus expected, constituting: 97.5% of optimised **3** and 2.5% of optimised **4**. A similar

Chapter 3- Structural Analysis of a Variety of Transition Metal Complexes Of Imidazole-Derived Ligands

situation is expected in terms of the conformations of the ligands in the complexes in the gas phase *i.e.* 98.0% of optimised **3** and 2.0% of optimised **4**.

However, the conformations of the ligands in the crystal structures should be 100% that of the **4** conformation, as the energy of the **4** structure is much lower than the energy of the **3** structure. The fact that **3** exists implies that intermolecular interactions play a key role in stabilising the strained conformations in the crystal structure.

A convenient way to view these intermolecular interactions is by mapping a Hirshfeld surface³³ onto a molecule of the complex, using the program *CrystalExplorer*⁴⁰. The Hirshfeld surface is loosely defined as the portion of space where the promolecule electron density contributes more than half of the total procrystal electron density, and as such provides a smooth surface onto which certain scalar properties, for example contact distances, can be mapped. Together with the colour mapping implemented in *CrystalExplorer*, this is an effective method for analysing and visualising intermolecular contacts in a crystal.

In the figures below, Hirshfeld surfaces were generated for a single molecule each of both **3** and **4**. A normalised contact distance d_{norm}^* was mapped onto the Hirshfeld surface in order to obtain a graphical representation of the intermolecular contacts in each crystal structure. Red areas represent intermolecular contacts shorter than the van der Waals separations for two given atoms and, as can be seen from Figure 17 and Figure 18, these areas are far more abundant in **3** than in **4**. Indeed, aside from the intense red areas caused by the covalent connections of the propagating 1D chain, the only significant short intermolecular contacts viewed on the surface are as a result of hydrogen bonding to the nitrate counter-ion.

In summary, the relative energies of the ligands in the crystal structures of **3** and **4**, two complexes with the same structural formula, were investigated. The calculated results revealed that the S-shaped conformation of the ligand in **4** is lower in energy than the C-shaped conformation in **3**. However, both systems are strained, as indicated by the drop in energy upon optimisation of the structures in gas phase calculations.

The results show that in the absence of any external forces, the conformations in the free ligand and for the ligand in the complex, should be a mixture of conformations dominated by that of optimised **3**, but the conformations of the ligands

* See section 2.3.3 for a more complete description of the Hirshfeld surface and a definition of a promolecule and the normalised contact distance see section 2.3.3.

Chapter 3- Structural Analysis of a Variety of Transition Metal Complexes Of Imidazole-Derived Ligands

in the crystal structures should be exclusively the conformation of **4**. Since this is not what is observed in the crystal structures, it can be concluded that intermolecular interactions play an important role in stabilising strained conformations in the crystal structure and this also supports the notion that a crystal structure should be considered as a supramolecular entity³ and that the existing structure and conformations observed therein occur as a result of a summation of many different contributions. The Hirshfeld surface implemented in *CrystalExplorer* is an invaluable tool for visualising these stabilising intermolecular interactions.

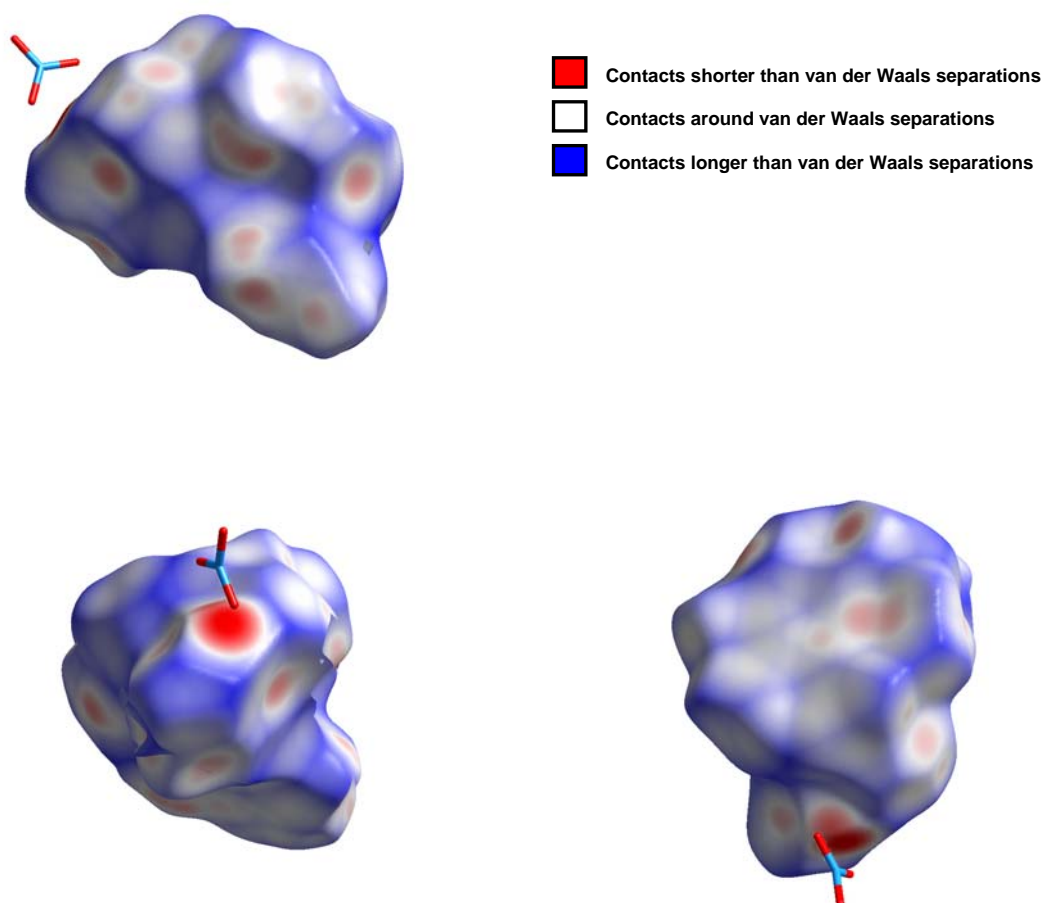


Figure 17. Hirshfeld surfaces generated for a single complex of **3** viewed in three orientations, *i.e.* down the *a*-axis (top left), down the *b*-axis (bottom left) and down the *c*-axis (bottom right).

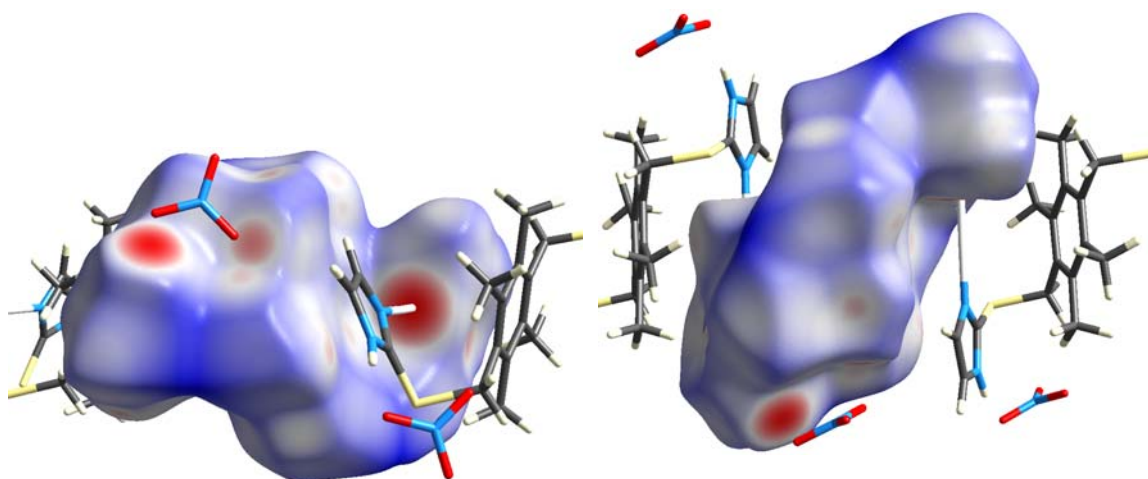
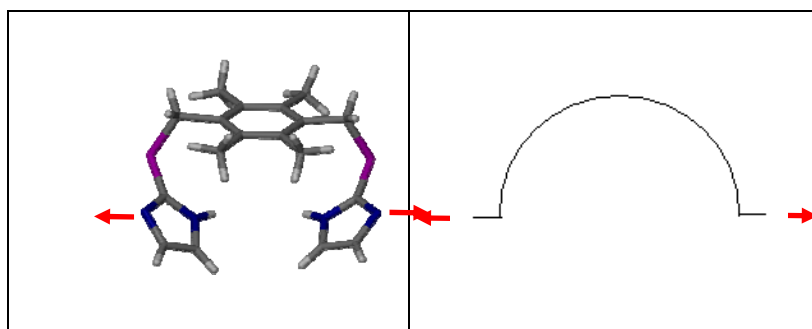


Figure 18. Hirshfeld surfaces generated for a single complex of **4** viewed in two orientations, *i.e.* down the *a*-axis (left) and down the *b*-axis (right). The propagating chain has been shown where intense regions of red on the surface are due to covalent bonds.

3.2.2.3 [CdL₂I₂]_n (**5**)



Scheme 3. In **5** the ligand assumes the UU conformation with the coordinating nitrogen atoms of the imidazole groups pointing in opposite directions (red arrows).

Single crystals of **5** were obtained by slow evaporation of a methanolic solution of **L2** and CdI₂ in a 1:1, 2:1 or 1:2 ligand-to-metal molar ratio. The ASU of **5** consists of one ligand **L2**, a Cd cation and two iodide anions. The ligand molecules are in the UU conformation with the two coordinating nitrogen atoms of the imidazole groups pointed in opposite directions (Scheme 3). Each Cd ion is in a tetrahedral coordination environment and coordinates to two iodine atoms and two nitrogen atoms from distinct ligands. The metal centres are thus connected to one another by means of a single ligand **L2**, to form a 1D strand running parallel to [10-1]. The 1D strands are connected into a

Chapter 3- Structural Analysis of a Variety of Transition Metal Complexes Of Imidazole-Derived Ligands

3D array *via* the simultaneous donation of two hydrogen bonds from the protonated nitrogens of the imidazole moieties to one of the coordinated iodine atoms (I1) (Table 10). The iodine atom therefore acts as a bifurcated hydrogen bond acceptor in this regard; the second coordinated iodine atom (I2) does not participate in any hydrogen bonding.

The manner in which the 1D strands are connected requires further clarification and it is convenient in the description that follows to view each 1D strand as consisting of two distinct ASU equivalents, which alternate along the strand (Figure 19). These distinct units are related to one another by a glide operation parallel to the axis of propagation, and have arbitrarily been assigned the labels **ASUE1** and **ASUE2**.

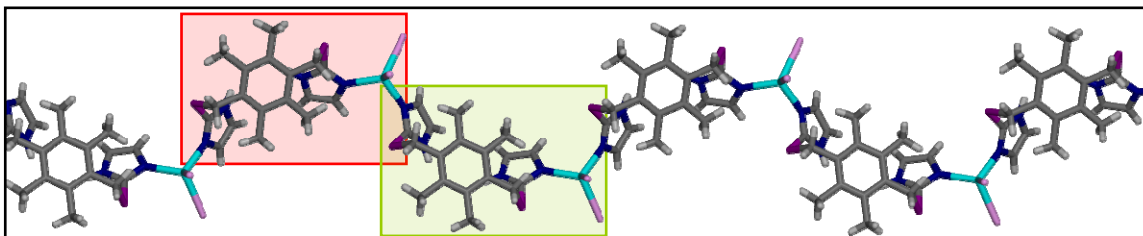


Figure 19. Capped-stick representation of the 1D strand formed in **5**, as viewed perpendicular to [10-1]. The distinct ASU equivalents which alternate along the growing strand have been enclosed in opaque red (**ASUE1**) and green (**ASUE2**) boxes, respectively.

The protonated nitrogens of the imidazole moieties of **ASUE1** donate two hydrogen bonds to I1 of **ASUE1** in an adjacent 1D strand, thereby linking the strands into a 2D rectangular grid in the (111) plane (Figure 20). The 2D grids are connected in 3D *via* analogous hydrogen bonding between the imidazole groups of **ASUE2** in one layer and the I1 atoms of **ASUE2** in an adjacent layer (Figure 21).

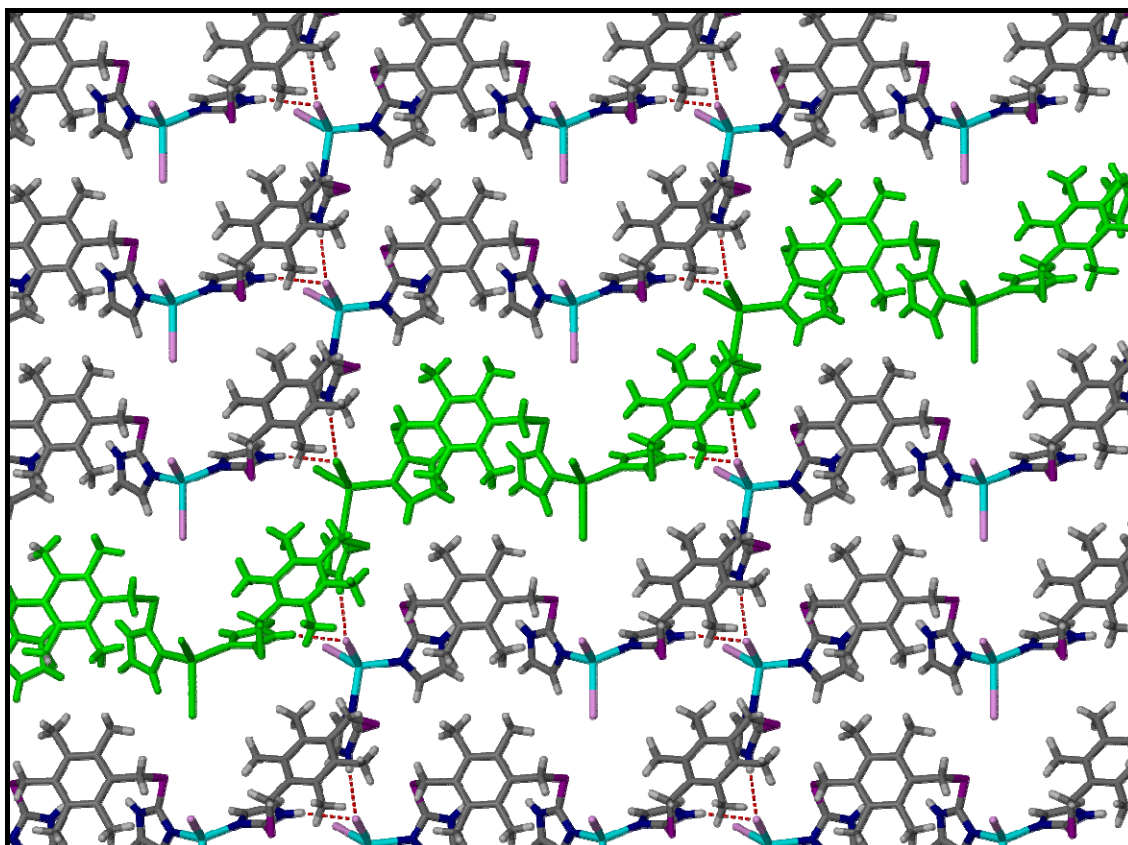


Figure 20. The 2D rectangular grids formed by the hydrogen bonding interactions between ASUE1 units in adjacent 1D strands, as viewed perpendicular to the (111) plane. A single 1D strand has been coloured green for clarity. All hydrogen bonds are shown as dashed red lines.

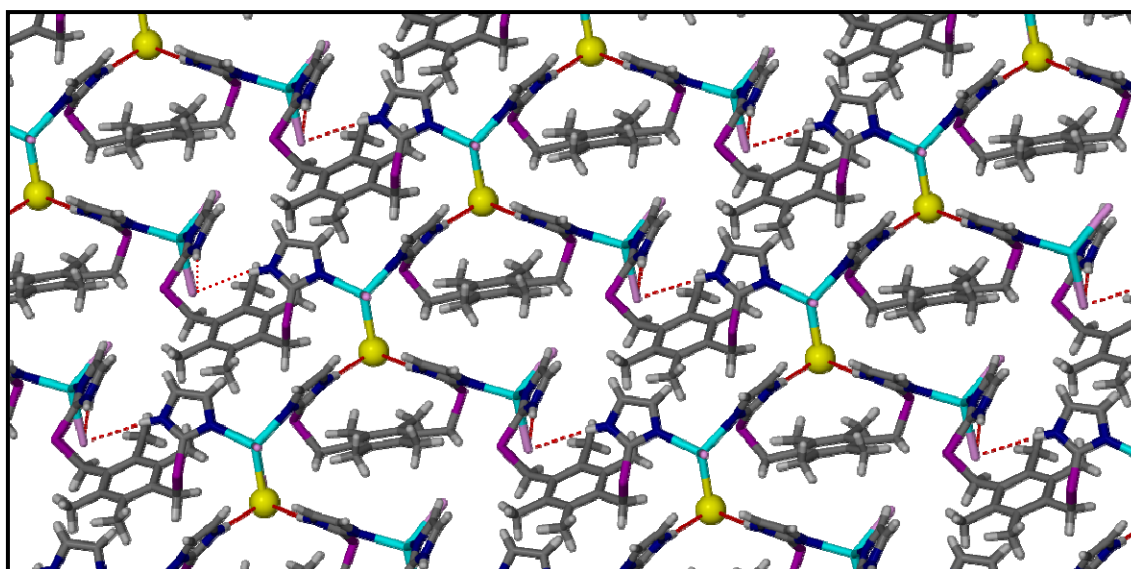


Figure 21. Stacking of the 2D layers formed in **5** via hydrogen bonding interactions between ASUE2 units, as viewed down [-110]. The I1 atoms of the ASUE2 are shown as enlarged yellow spheres for clarity. All hydrogen bonds are shown as dashed red lines.

Table 10. Hydrogen-bond geometry for **5** (Å, °).

D-H...A	D-H	H...A	D...A	D-H...A
N6-H6...I1 ⁱ	0.88	2.85	3.714(4)	167
N23-H23...I1 ⁱ	0.88	2.94	3.819(4)	177

Symmetry codes: (i) $x+1, -y+1, z+1/2$.Comparison of the crystal structures obtained for **L2**

The conformation of **L2** in **5** is similar to that of the ligand in **3** in that both ligands adopt the **UU** conformation, but differs in the orientation of the coordinating nitrogen atoms. In complex **3** the coordinating nitrogen atoms of each ligand molecule are pointed towards each other (Scheme 2), and coordinate to the metal ion such that the preferred linear coordination geometry³⁴ about the Ag ion is satisfied. In complex **5** the coordinating nitrogen atoms are pointed away from each other (Scheme 3) which facilitates the coordination of the ligand to the Cd ion such that the preferred tetrahedral coordination geometry around the Cd centre²⁰ is maintained. Even in complex **4** where the conformation of the ligand is different to both **3** and **5**, *i.e.* the **UD** conformation, the preferred linear geometry of the Ag ion is preserved. These examples testify to the ability of this flexible ligand to conform to the required geometry of the metal ions whilst demonstrating a variety of conformations in the solid state.

It would be interesting to compare the results of a gas-phase energy calculation of the conformation of the free ligand in **5** to the energies for the gas-phase calculations of the free ligand in both **3** and **4**. This forms part of future studies.

3.2.3 Single-crystal structures obtained from ligand L3

3.2.3.1 $[\text{Ag}_4(\text{L}2)_2(\text{H}_2\text{O})_2(\text{NO}_3)_2]2n\text{NO}_3 \cdot 2n\text{H}_2\text{O} \cdot n\text{CH}_3\text{CN}$ (**6**)

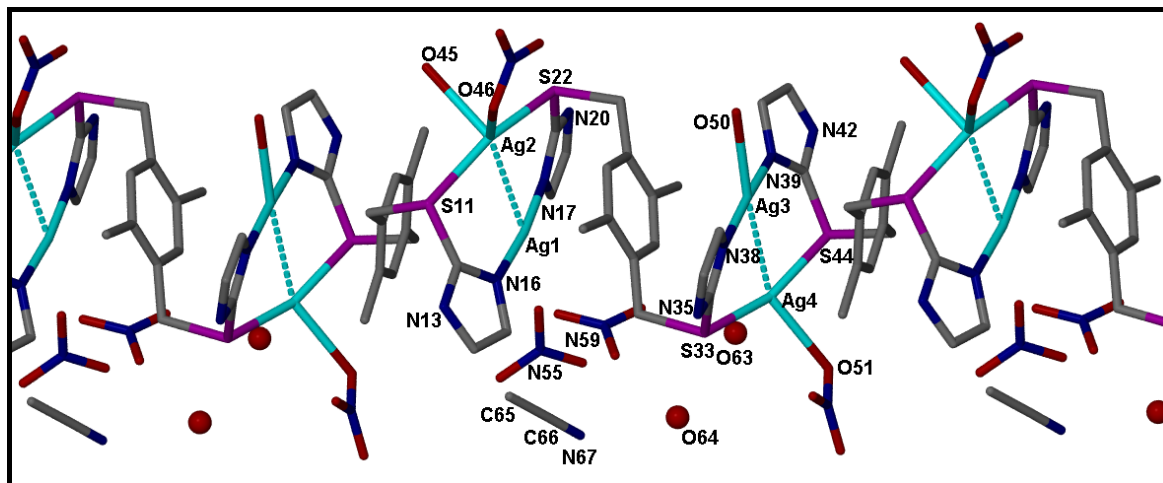


Figure 22. Capped-stick representation of the 1D strand formed in **6**, as viewed perpendicular to [100]. The Ag-Ag interactions are shown as dashed blue lines. Water molecules are shown as spheres and hydrogen atoms have been omitted for clarity.

The ASU of **6** consists of two ligands **L3**, four silver cations, four nitrate anions, two water molecules and one acetonitrile molecule. Both ligands are approximately S-shaped, *i.e.* they both assume the **UD** conformation with their coordinating nitrogen atoms pointing in opposite directions. Each silver ion is in close contact with one other silver ion such that two distinct ligand-supported argentophilic interactions⁴¹ are observed within the structure. The first of these interactions occurs between Ag1 and Ag2 with an Ag...Ag separation of 2.966(2) Å; the second argentophilic interaction between Ag3 and Ag4 is slightly weaker and occurs at an intermetallic distance of 3.046(3) Å. All four of the silver ions are in unique coordination environments; Ag1 is coordinated to two imidazole groups from two distinct **L3** ligands (Ag1–N16 = 2.100(4) Å and Ag1–N17 = 2.104(4) Å) and is in a linear coordination environment. Ag2 is in a pseudo-square pyramidal coordination environment, where the vertices of the square consist of two sulphur atoms (Ag2–S11 = 2.5417(1) Å and Ag2–S22 = 2.5202(1) Å) situated *trans* with respect to one another, a water molecule (Ag2–O45 = 2.423(4) Å) and the fourth coordination site is occupied by the argentophilic interaction with Ag1. The apex of the pyramid consists of a monodentate nitrate ion (Ag2–O46 = 2.461(4) Å). Ag3 is in a pseudo-square planar coordination environment with two imidazole nitrogen atoms from distinct ligands situated *trans* with respect to each other (Ag3–N38 =

Chapter 3- Structural Analysis of a Variety of Transition Metal Complexes Of Imidazole-Derived Ligands

2.107(4) Å and Ag3–N39 = 2.107(4) Å). The remaining two coordination sites are occupied by a coordinated water molecule (Ag3–O50 = 2.596(4) Å) and the argentophilic interaction with Ag4. The fourth silver ion, Ag4, is similarly in a pseudo-square planar coordination environment and coordinates to two sp³ sulphur atoms located *trans* with respect to each other (Ag4–S33 = 2.5365(1) Å and Ag4–S44 = 2.5578(1) Å). The remaining sites are occupied by a monodentate nitrate ion (Ag4–O51 = 2.543(5) Å) and the argentophilic interaction with Ag3.

Complex **6** forms 1D strands propagating along [100] (Figure 22). An intricate network of hydrogen bonds serves to connect adjacent strands into a 3D array (Figure 23) (Table 11). Within this packing arrangement four distinct 1D strands are related to the ASU by three symmetry operations (as seen in Figure 24).

Table 11. Hydrogen-bond geometry for **6** (Å, °).

D-H...A	D-H	H...A	D...A	D-H...A
N35-H35...O64	0.88	1.87	2.739(6)	171
O63-H63B...O61	1.00	1.81	2.796(6)	169
O64-H64B...O58	1.00	2.21	3.053(7)	141
C65-H65B...O45 ⁱ	0.98	2.44	3.409(9)	170
N13-H13...O46 ⁱ	0.88	1.97	2.820(6)	163
N20-H20...O58 ⁱⁱ	0.88	1.95	2.829(6)	175
N42-H42...O63 ⁱⁱⁱ	0.88	1.90	2.776(6)	170
O63-H63A...O49 ^{iv}	1.00	1.88	2.863(5)	169
C36-H36...O54 ^v	0.95	2.52	3.227(7)	131
O64-H64A...O51 ^v	1.00	1.96	2.946(7)	167

Symmetry codes: (i) $-x-1, -y, -z$; (ii) $x, -y + \frac{1}{2}, -z$; (iii) $-x, -y+1, -z$; (iv) $x, -y+1, -z$; (v) $-x, y - \frac{1}{2}, -z - \frac{1}{2}$.

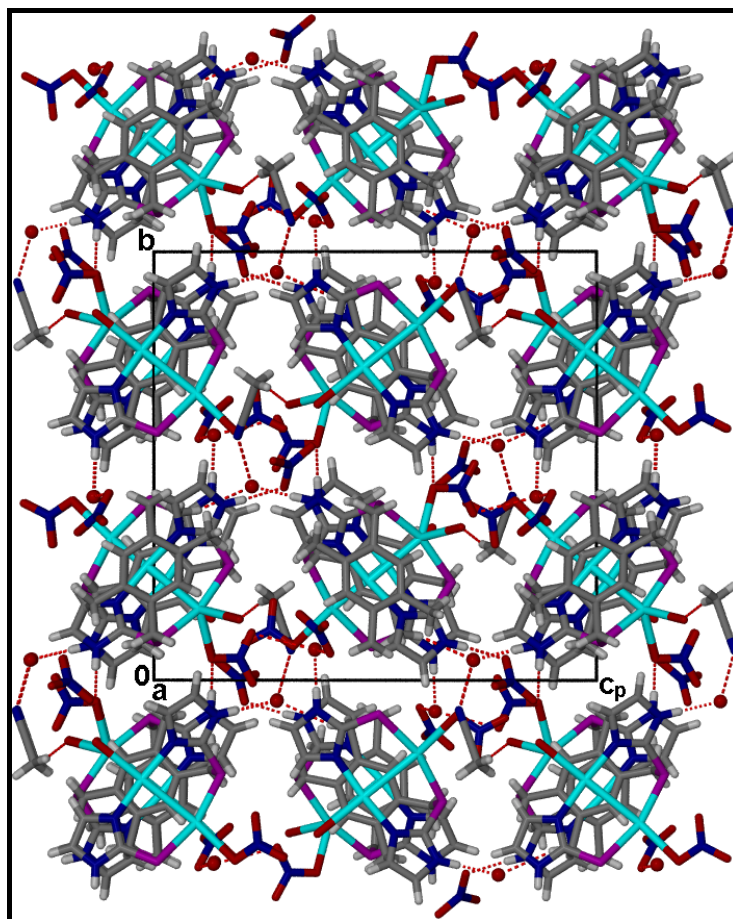


Figure 23. Capped-stick representation of the 3D array formed by hydrogen bonding in **6**, as viewed down [100]. Water molecules are shown as spheres.

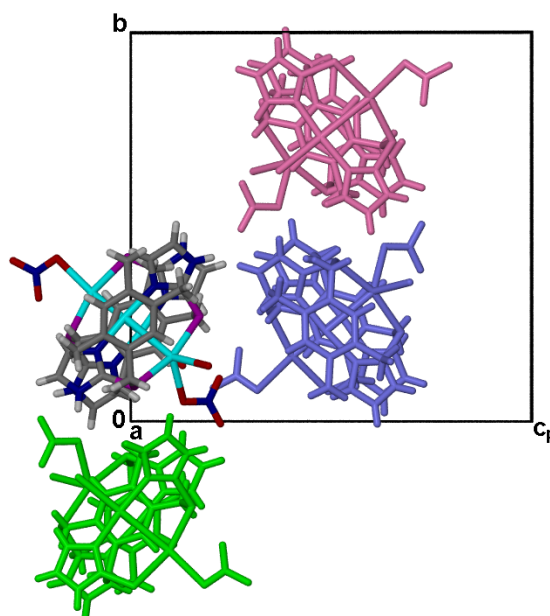


Figure 24. The four distinct 1D strands in **6**. The coloured strands can each be related to the ASU (shown in CPK colours) by a symmetry operation. The pink strand is related to the ASU by a 2_1 screw operation, the blue strand is related to the ASU by a glide plane and the green strand is related to the ASU by an inversion centre.

Ligand L3 and CdI₂

Single crystals of **7**, **8** and **9** were grown by slow evaporation of a methanolic solution of **L3** and CdI₂ in a 1:1, 4:1 and 1:2 ligand-to-metal ratio, respectively. XRPD analysis of the bulk solid material in the vials from which the single crystals of **7** and **8** were isolated, revealed that the minority phase in each vial was that of **7** and **8** and the majority solid phase was unreacted ligand. However, the 1:2 solution ratio yielded a pure phase of complex **9**.

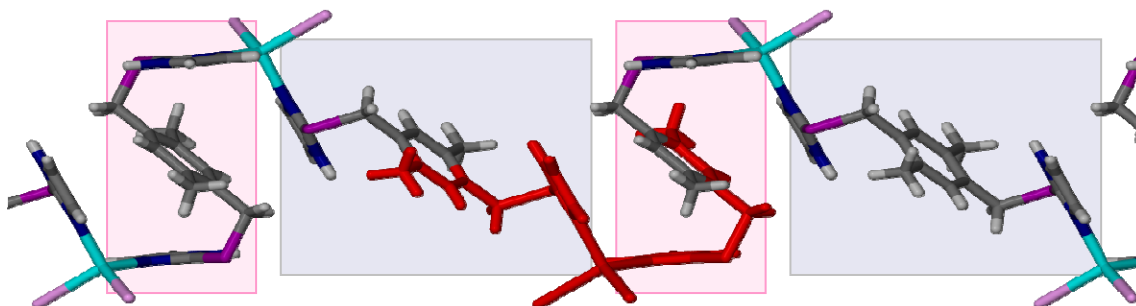
3.2.3.2 [CdL3I₂]_n (**7**)

Figure 25. Capped-stick representation of the 1D strands formed in **7**, as viewed along [100]. The ASU has been coloured red, and opaque pink and grey boxes have been used to highlight the orientations of the two unique ligands within the 1D strand.

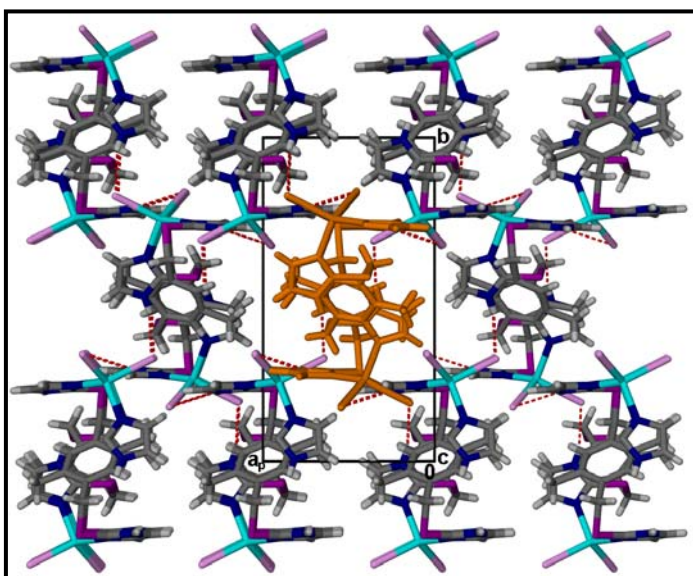
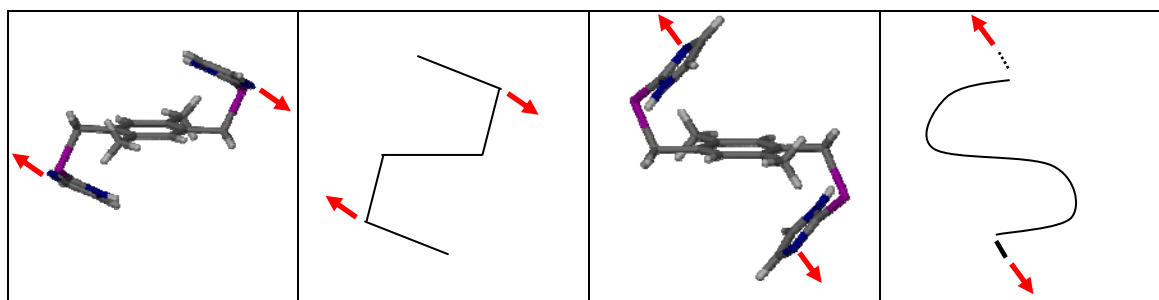


Figure 26. Packing arrangement of **7** as viewed down [001]. Molecules are shown in the capped-stick metaphor and hydrogen bonds are shown as dashed red lines. A single 1D strand has been coloured orange for clarity.

Complex **7** forms an infinite 1D strand running parallel to [001] (Figure 25). The ASU (highlighted in red in Figure 25) consists of two unique half molecules of **L3**, each situated about an inversion centre. The second half of each **L3** molecule is generated by the symmetry operations, $1-x, 1-y, -z$ (for the ligand in the first opaque grey box) and $1-x, 1-y, 1-z$ (for

Chapter 3- Structural Analysis of a Variety of Transition Metal Complexes Of Imidazole-Derived Ligands



Scheme 4. A representation of the two distinct conformations of **L3** in **7**; both feature the ligand in the **UD** conformation, but differ in the orientation of the coordinating nitrogen atoms. The conformation on the left corresponds to the ligand enclosed in the opaque grey box in Figure 25, and the conformation on the right corresponds to the ligand enclosed in the opaque yellow box in Figure 25. The red arrows indicate points where coordination bonds are formed.

the ligand in the second opaque pink box). The dihedral angle between the planes defined by the atoms of the imidazole groups and the benzene rings are $28.2(3)^\circ$ and $48.4(2)^\circ$ for the grey and yellow boxed ligands respectively. As can be seen in Figure 25 the ligand **L3** assumes two distinctive conformations in connecting adjacent Cd ions. Both ligands are in the **UD** conformation, but differ in the orientations of their coordinating nitrogen atoms (Scheme 4).

In addition to the two nitrogens from the distinct ligand **L3** molecules, each Cd ion is coordinated by two iodine atoms, thereby completing a distorted tetrahedral coordination environment around the metal centres, with coordinating angles ranging from $101.24(1)^\circ$ - $119.62(1)^\circ$ (Table 12). Each protonated imidazole nitrogen is hydrogen bonded to one of the coordinated iodine atoms on an adjacent strand (see Table 12 for details of hydrogen bonding parameters), and by virtue of these hydrogen bonds the 1D strand are connected into a 3D array (Figure 26).

Table 12. Selected geometric parameters for **7** (\AA , $^\circ$).

Complex 7				
Cd1-I1	2.711(4)	N11-Cd1-I1	107.68(1)	
Cd1-N11	2.235(4)	N12-Cd1-I1	101.24(1)	
Cd1-N12	2.204(4)	N12-Cd1-N11	113.94(1)	
Cd1-I2	2.693(4)	N11-Cd1-I2	102.17(1)	
		N12-Cd1-I2	119.62(1)	
		I2-Cd1-I1	112.02(2)	
Hydrogen-bond geometry for 7 (\AA , $^\circ$).				
D-H...A	D-H	H...A	D...A	D-H...A
N8-H8...I2 ⁱ	0.86	2.69	3.528(5)	166
N15-H15...I1 ⁱⁱ	0.86	2.83	3.482(4)	134

Symmetry codes: (i) $-x + \frac{1}{2}, y + \frac{1}{2}, -z + \frac{1}{2}$; (ii) $x + \frac{1}{2}, -y + \frac{1}{2}, z + \frac{1}{2}$.

3.2.3.3 [CdL3I₂]_n (**8**)

The complex **8** forms a 1D strand in a fashion similar to **7**; each metal centre is connected to an adjacent metal centre by means of a single bridging ligand, but differs from **7** in that there is no inversion symmetry in the ligand. The coordination environment around each Cd ion is also tetrahedral and the range of coordination angles is 97.4(3)°-122.9(3)°. The dihedral angles between the planes of the imidazole and benzene rings are 36.6(4)° and 42.3(4)° respectively, and the ligand **L3** assumes the **UD**, S-shaped conformation.

The coordinated I1 ion acts as a bifurcated hydrogen bond acceptor as it is simultaneously hydrogen bonded to two protonated imidazole nitrogens; one of these coordinated imidazole nitrogen atoms can be found within the same 1D chain (N19...I1 = 3.475 Å) and the second imidazole nitrogen is from an adjacent 1D strand (N4...I1 = 3.452 Å). It is this latter hydrogen bond which serves to connect adjacent 1D strands into a 2D layer (Figure 27, top). The 2D layers stack in an ...*ABAB*... fashion, *i.e.* atoms in the first layer are placed over atoms in the third layer (Figure 27, bottom). Finally, I2 is not involved in any hydrogen bonding interactions and points into the space between two 2D layers.

Table 13. Selected geometric parameters for **8** (Å, °).

Complex 8				
Cd1-I1	2.714(1)	N1-Cd-I1	97.4(3)	
Cd1-N1	2.209(1)	N22 ⁱ -Cd1-I1	99.2(3)	
Cd1-N22 ⁱ	2.219(1)	N1-Cd1-N22 ⁱ	106.4(4)	
Cd1-I2	2.686(1)	N1-Cd1-I2	116.3(3)	
		N22 ⁱ -Cd1-I2	122.9(3)	
		I2-Cd1-I1	110.8(4)	
Hydrogen-bond geometry for 8 (Å, °).				
D-H...A	D-H	H...A	D...A	D-H...A
N4-H4...I1 ⁱⁱ	0.88	2.58	3.452(1)	169
N19-H19...I1 ⁱⁱⁱ	0.88	2.73	3.476(1)	144

Symmetry codes: (i) $-x+1, y + \frac{1}{2}, -z + \frac{3}{2}$; (ii) $-x, y - \frac{1}{2}, -z + \frac{3}{2}$; (iii) $x, y-1, z$.

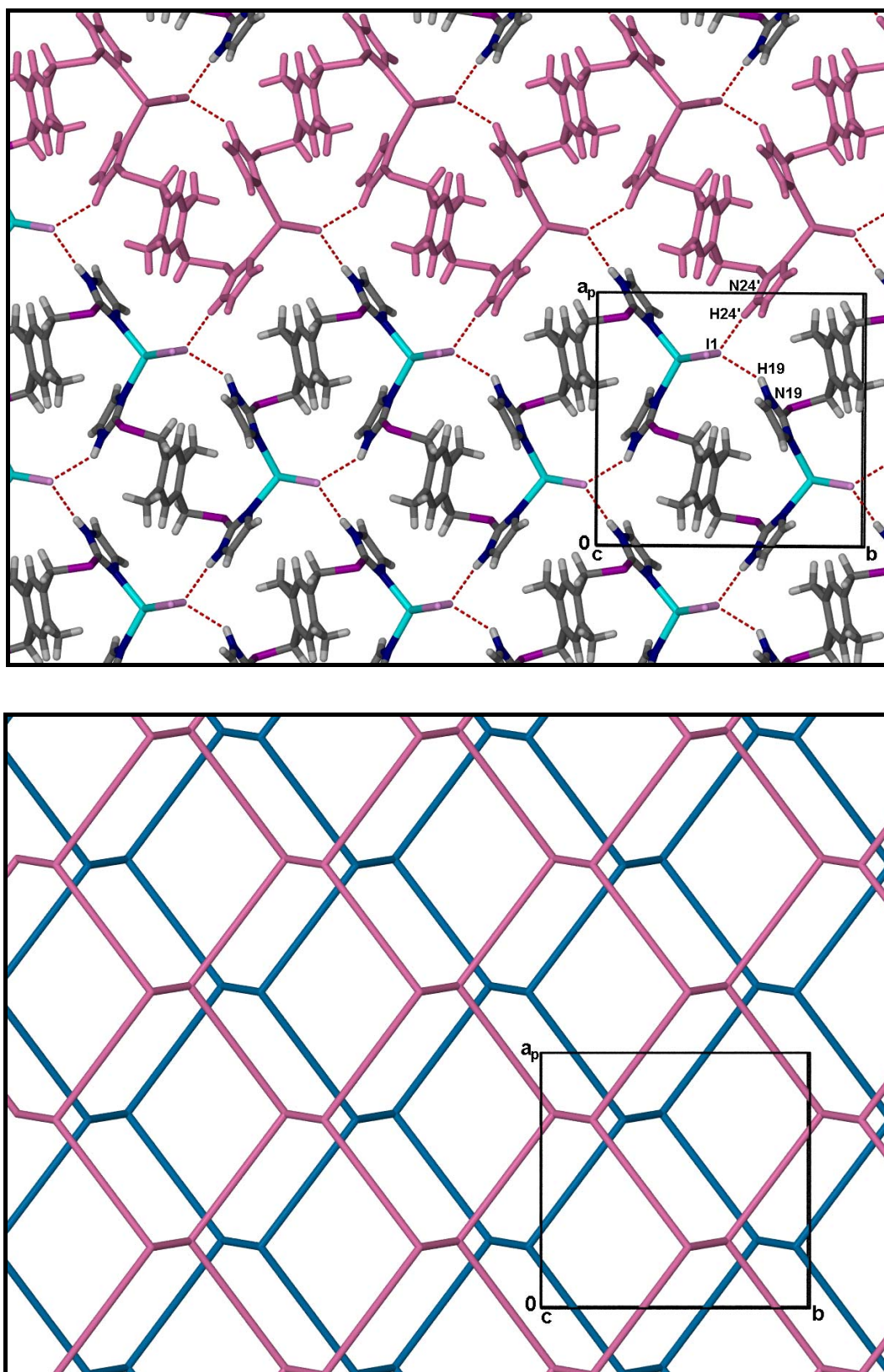


Figure 27. Capped-stick representation of the 2D layers formed in **8**. A single 1D chain has been coloured pink for clarity, and hydrogen bonds are shown as dashed red lines (top). A schematic projection of the 2D layers showing the ...*ABAB*... stacking arrangement (bottom). Both the top and bottom figures are viewed down [001].

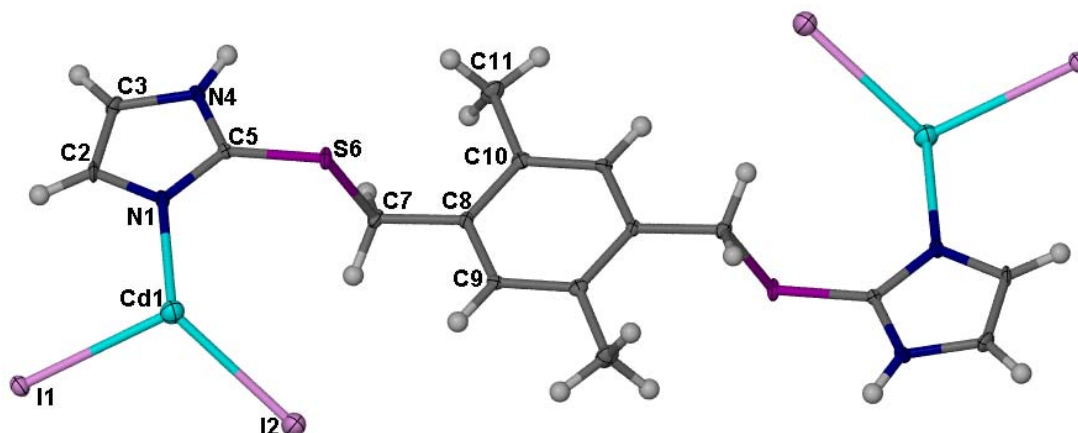
3.2.3.4 [Cd₂L3I₄]_n (9)

Figure 28. Atomic displacement (50% probability) plots showing the molecular structure of **9**. Unlabelled atoms are related to the labelled atoms by a centre of inversion.

The ASU of **9** consists of one half of an **L3** ligand, one metal ion and two coordinated iodine ions (Figure 28). The ligand is in the **UD** conformation and the plane defined by the atoms of the imidazole group is approximately parallel to the plane of the benzene ring, as indicated by the dihedral angle of 2.75° between the two planes.

Each cadmium ion is in a tetrahedral coordination environment and coordinates to a single imidazole nitrogen, a terminal iodine ion and two bridging iodine ions. The structure of **9** consists of infinite 1D ladders propagating parallel to [100], where the ligand molecules form the rungs of the ladder (Figure 29). The Cd...Cd ion separation between adjacent ladders is 6.722 Å.

Table 14. Selected geometric parameters for **9** (Å, °).

Complex 9				
Cd1-I1	2.805(8)	N1-Cd-I2	122.86(2)	
Cd1-N1	2.224(6)	N1-Cd1-I1 ⁱ	103.55(2)	
Cd1-I2	2.700(9)	I2-Cd1-I1 ⁱ	113.22(2)	
Cd-I1 ⁱ	2.763(9)	N1-Cd1-I1	99.51(2)	
		I2 -Cd1-I1	109.20(3)	
		I1 ⁱ -Cd-I1	106.79(3)	
Hydrogen-bond geometry for 9 (Å, °).				
D-H...A	D-H	H...A	D...A	D-H...A
N4-H4...I2 ⁱⁱ	0.88	2.73	3.602(6)	173

Symmetry codes: (i) $x-1, y, z$; (ii) $-x, y - \frac{1}{2}, -z + \frac{3}{2}$.

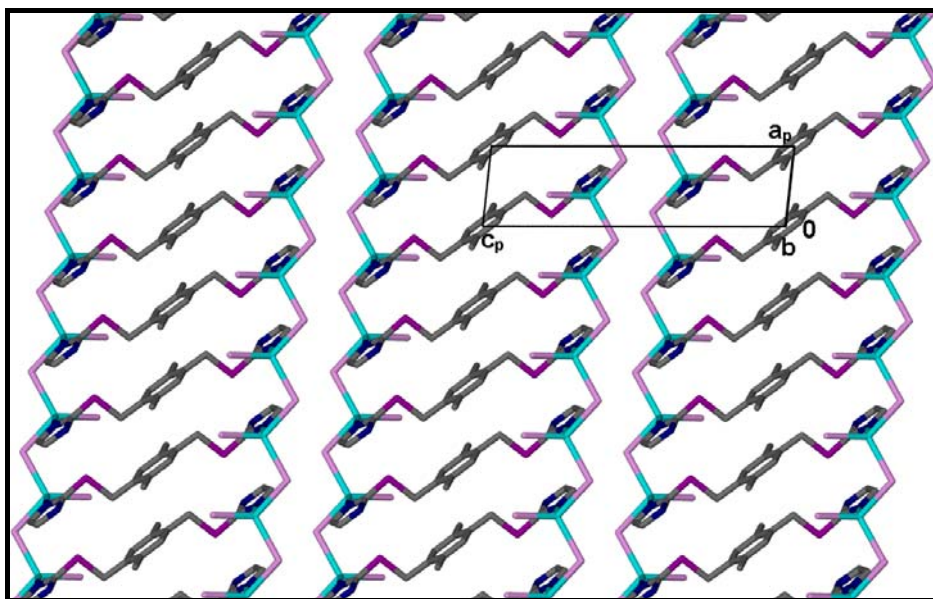


Figure 29. Capped-stick representation of the infinite 1D ladders formed in **9**, as viewed down [010]. Hydrogen atoms have been omitted for clarity.

The terminal iodine ion hydrogen bonds to the protonated imidazole nitrogen ($N \cdots I = 3.602(6) \text{ \AA}$), and by virtue of these hydrogen bonds each 1D ladder is connected to the ladder below and that above (relative to [0 1 0]) to form a 2D layer (Figure 30).

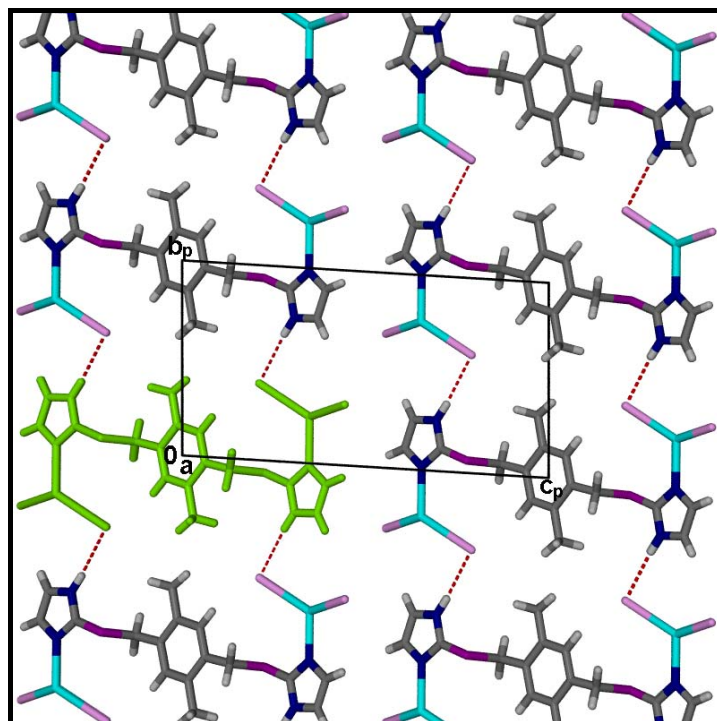


Figure 30. Packing arrangement of **9** to form 2D layers, viewed down [100]. N-H \cdots I hydrogen bonds are shown as dashed red lines and a single ladder has been coloured green for clarity.

Comparison of **7**, **8** and **9**

Complexes **7** and **8** were grown from solutions in which the ligand-to-metal ratios were 1:1 and 4:1, yielding 1D polymeric strands featuring a ligand-to-metal ratio of 1:1. Single crystals of complex **9** were grown from a solution ratio of 1:2 and formed 1D ladders in which the solution ligand-to-metal ratio was reflected in the solid state. In all three of the complexes the ligand molecules were found to adopt the **UU** conformation.

A comparison of the structural formula of **7** and **8** (*i.e.* $[\text{Cd}_2\text{L3I}_2]_\infty$) reveals that the two structures are polymorphs of one another. Polymorphism can loosely be described as a phenomenon in which molecules of a substance pack in at least two different crystalline arrangements in the solid state.⁴² It is generally agreed in the field of solid state chemistry that polymorphs can have different hydrogen bonding patterns, but not different covalent connectivity.²³ By this definition the structures obtained for **7** and **8** can be considered to be polymorphs, but more specifically they are conformational polymorphs of each other. This form of polymorphism occurs when a molecule can assume different conformations due to internal degrees of freedom (typically torsional degrees of freedom) and occurs most readily in systems containing flexible ligands.^{43,44} The 1D polymeric strands formed in **7** and **8** are similar in covalent connectivity but differ in the conformation of the ligands which connect adjacent Cd centres. This subtle change in ligand conformation changes the packing arrangement in the two crystal structures such that the 1D strands are connected into a 3D array in **7**, and a 2D layer in **8**.

L3 and halogenated transition metal salts (excluding CdI_2)

To assess by SCD analysis whether the coordination geometry around the metal centre would conform to the predicted geometry, the single crystal structures obtained from the complexation of **L3** with four halogenated divalent transition metals were analysed. Crystals suitable for X-ray diffraction were obtained by the reaction of **L3** with four halogenated divalent transition metals, namely $\text{CuCl}_2 \cdot \text{H}_2\text{O}$, $\text{CoCl}_2 \cdot 6\text{H}_2\text{O}$, $\text{CdCl}_2 \cdot 2.5\text{H}_2\text{O}$ and ZnBr_2 in 1:1 ligand-to-metal molar ratios in MeOH, followed by slow evaporation of the solvent. The results of this study are described below.

Table 15. Unit cell parameters for **10-13**.

	10	11	12	13
Metal salt	CuCl ₂ ·H ₂ O	CoCl ₂ ·6H ₂ O	CdCl ₂ ·2.5H ₂ O	ZnBr ₂
Ratio (ligand: metal)	1:1	1:1	1:1	1:1
Crystal System	monoclinic	monoclinic	monoclinic	monoclinic
Space Group	<i>P2₁/c</i>	<i>P2₁/n</i>	<i>P2₁/n</i>	<i>P2₁/n</i>
<i>a</i> (Å)	18.209(2)	8.1525(7)	8.3283(6)	8.3455(9)
<i>b</i> (Å)	7.7498(9)	15.9946(1)	16.2405(1)	16.1009(2)
<i>c</i> (Å)	15.2000(2)	14.9612(1)	15.0879(1)	15.0243(2)
α (°)	90	90	90	90
β (°)	92.185(2)	94.314(2)	93.3260(1)	94.409(2)
γ (°)	90	90	90	90
<i>V</i> (Å ³)	2143.4(4)	1945.4(3)	2037.3(3)	2012.8(4)
<i>Z</i>	4	4	4	4

3.2.3.5 [CuL3Cl₂]_n·nCH₃OH (**10**)

The asymmetric unit of **10** consists of one metal ion, two coordinated chloride counter-ions, two half ligand molecules and one methanol molecule. In the crystal structure, two unique one-dimensional strands are formed. The first strand runs parallel to [1-10]. The second strand runs parallel to [110], this is shown in Figure 31 (left) as the blue and orange strands respectively, and is represented schematically in Figure 31 (right).

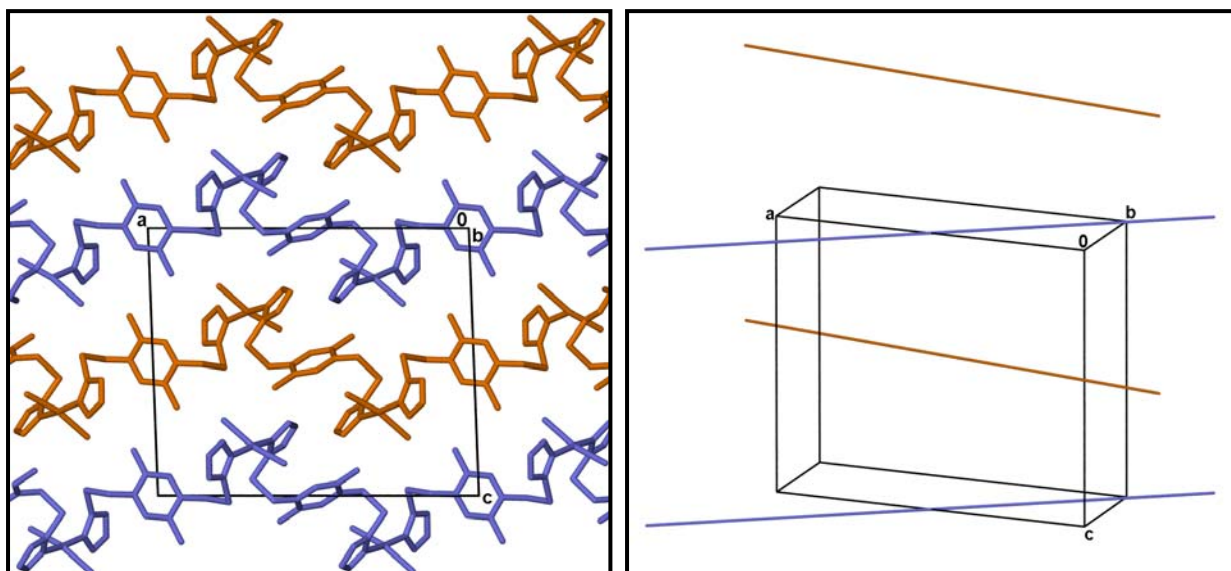


Figure 31. The 1D strands formed in **10**; the two unique orientations of the strands are coloured orange and blue to distinguish them from each other (left). A schematic representation of the 1D strands showing their orientations with respect to the unit cell (right).

Each metal centre is linked to an adjacent metal centre by means of a single bridging ligand in the **UD** conformation. The Cu^{2+} ions are in a square planar coordination environment and coordinate to two imidazole groups that are located *trans* to one another ($\text{Cu1} - \text{N11} = 1.957(4) \text{ \AA}$ and $\text{Cu2} - \text{N12} = 1.947(4) \text{ \AA}$) and two *trans*-coordinated Cl anions ($\text{Cu1} - \text{Cl1} = 2.3325(1) \text{ \AA}$ and $\text{Cu2} - \text{Cl2} = 2.2923(1) \text{ \AA}$).

The protonated nitrogens of the imidazole groups, the chloride anions and the methanol molecules serve to link the strands into a three dimensional array *via* a series of cooperative hydrogen bonds; strands of different colours are linked *via* the donation of an imidazole hydrogen to the oxygen of the methanol molecule ($\text{N15} \cdots \text{O23} = 2.731(6) \text{ \AA}$), which in turn donates a hydrogen bond to one of the ligated chloride ions ($\text{O23} \cdots \text{Cl1} = 3.179(5) \text{ \AA}$). Finally, the second protonated imidazole nitrogen and a ligated chloride anion form a hydrogen bond in the direction of the *b*-axis, connecting adjacent strands of the same colour ($\text{N8} \cdots \text{Cl2} = 3.193(4) \text{ \AA}$) (Figure 32) (see Table 11 for details of hydrogen bonding parameters).

Table 16. Hydrogen-bond geometry for **10** (\AA , $^\circ$).

D-H...A	D-H	H...A	D...A	D-H...A
N8-H8...Cl2 ⁱ	0.88	2.32	3.193(4)	173
O23-H23...Cl1 ⁱⁱ	0.84	2.35	3.179(5)	172
N15-H15...O23	0.88	1.87	2.731(6)	164

Symmetry codes: (i) $x, y-1, z$; (ii) $x, -y + \frac{3}{2}, z - \frac{1}{2}$.

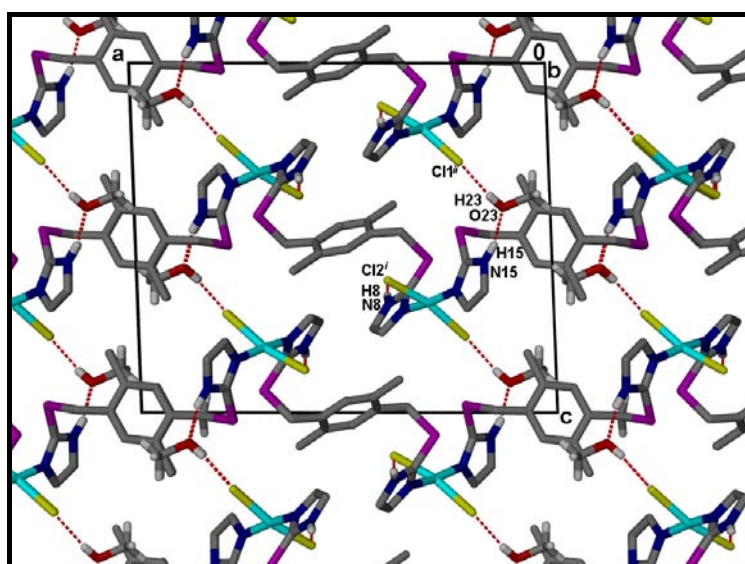


Figure 32. Capped-stick representation showing the packing arrangement of **10** as viewed down [010]. Hydrogen atoms of the ligand molecules not participating in hydrogen bonding have been omitted for clarity. Symmetry transformations used to generate equivalent positions are the same as those listed in Table 16.

3.2.3.6 [CoL3Cl₂]_n (11)

The ASU of **11** consists of one metal ion, two coordinated chloride anions and two half ligand molecules. The complex forms an infinite 1D chain running parallel to [001]. Each cobalt ion is coordinated by two chloride counter-ions (Co1–Cl1 = 2.2889(7) Å and Co1–Cl2 = 2.2742(7) Å) and two imidazole groups (Co1–N11 = 2.0193(2) Å and Co1–N12 = 2.0020(2) Å) to form a tetrahedral coordination environment around the metal centre. The ligand assumes two conformations in connecting successive Co ions; these conformations are identical to those found in complex **7**. Both are in the **UD** conformation and correspond to those conformations detailed in Scheme 4 (this had previously been observed in complex **7**). The protonated imidazole nitrogens donate hydrogen bonds to the ligated chloride ions in adjacent strands, thereby linking the strands in 3D. (Figure 33, see Table 17 for details of hydrogen bonding parameters).

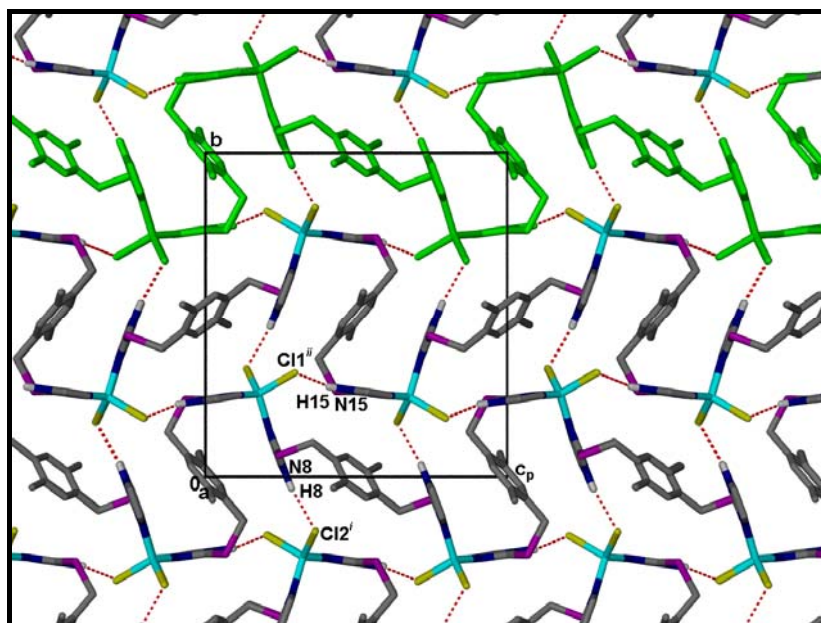


Figure 33. Packing arrangement of **11** as viewed down [100]. Hydrogen bonds are shown as dashed red lines and hydrogen atoms not participating in hydrogen bonding have been omitted for clarity. A single 1D strand has been coloured green for clarity.

Table 17. Hydrogen-bond geometry for **11** (Å, °).

D-H...A	D-H	H...A	D...A	D-H...A
N8-H8...Cl2 ⁱ	0.88	2.41	3.268(2)	165
N15-H15...Cl1 ⁱⁱ	0.88	2.38	3.189(2)	153

Symmetry codes: (i) $-x + \frac{1}{2}, y - \frac{1}{2}, -z + \frac{1}{2}$; (ii) $x - \frac{1}{2}, -y + \frac{1}{2}, z - \frac{1}{2}$.

3.2.3.7 [CdL3Cl₂]_n (12) and [ZnL3Br₂]_n (13)

The molecular structures of **12** and **13** are similar to that of **11**. In fact, the unit cell parameters and space groups are similar enough that all three may be regarded as isostructural (in a non-rigorous sense, refer to Table 15). The coordination geometry around the Cd²⁺ and Zn²⁺ metal centres are unambiguously tetrahedral. All unique bond distances and angles for the isostructural complexes **11–13** are given in Table 18.

Table 18. Selected bond distances (Å) and angles (°) for complexes **11–13**.

Complex 11			
Co1—N12	2.002(2)	Co1—Cl2	2.2742(7)
Co1—N11	2.019(2)	Co1—Cl1	2.2889(7)
N12—Co1—N11	113.25(8)	N12—Co1—Cl1	103.29(7)
N12—Co1—Cl2	116.44(7)	N11—Co1—Cl1	110.37(7)
N11—Co1—Cl2	106.66(7)	Cl2—Co1—Cl1	106.57(2)
Complex 12			
Cd1—N12	2.197(4)	Cd1—Cl2	2.470(9)
Cd1—N11	2.210(4)	Cd1—Cl1	2.505(9)
N12—Cd1—N11	114.72 (14)	N12—Cd1—Cl1	101.15 (12)
N12—Cd1—Cl2	121.16 (11)	N11—Cd1—Cl1	107.80 (11)
N11—Cd1—Cl2	103.53 (11)	Cl2—Cd1—Cl1	107.81 (3)
Complex 13			
Zn1—N12	1.993 (4)	Zn1—Br2	2.3766 (8)
Zn1—N11	2.019 (4)	Zn1—Br1	2.4167 (8)
N12—Zn1—N11	112.68 (17)	N12—Zn1—Br1	103.82 (12)
N12—Zn1—Br2	116.72 (12)	N11—Zn1—Br1	108.62 (12)
N11—Zn1—Br2	106.47 (12)	Br2—Zn1—Br1	108.24 (3)

Discussion on the coordination geometry of metal centres in complexes **10**, **11**, **12** and **13**

In a contribution by Rulíšek *et al.*²⁰ an investigation into the preferred coordination geometry of selected divalent transition metal ions, including Co²⁺, Cd²⁺, Zn²⁺ and Cu²⁺, was made. Using the Protein Data Bank (PDB)⁴⁵ and the Cambridge Structural

Database (CSD)⁴⁶ as sources of experimental data, a comprehensive analysis of transition metal complexes, adhering to a specific set of criteria, yielded the following results:

- Co^{2+} prefers an octahedral arrangement
- Cu^{2+} prefers to bind in a square planar mode
- Zn^{2+} is found almost exclusively in a tetrahedral coordination environment
- Cd^{2+} displays equal preference for octahedral and tetrahedral coordination.

In the current study it was found that in all four of the complexes obtained, the divalent, d-block metal was coordinated by two halogen counterions and two imidazole nitrogens from separate ligands to form 1D polymeric chains. Three of the four complexes are isostructural, namely the Co^{2+} , Cd^{2+} and Zn^{2+} complexes and show tetrahedral coordination around the metal centres, while the coordination geometry around Cu^{2+} was square planar. These results all agree well with those obtained by Rulišek *et al*, barring of course that of Co^{2+} . In order to rationalise this it is pertinent to consider the nature of a tetrahedral environment. Tetrahedral coordination is favoured by steric requirements, *i.e.* the presence of large ligands (e.g. Cl^-) and small metal ions which do not strongly favour other structures by virtue of the LFSE, of which Co^{2+} , a d^7 metal, is a prime example. Thus, when one considers the nature of the ligating species (*i.e.* chloride ions, bulky imidazole groups) and the requirements of tetrahedral complexes, the tetrahedral coordination of **11** is unsurprising.

3.2.4 Single-crystal structures obtained with ligand L4

No metal-organic complexes containing **L4** could be elucidated by SCD. For all vials where single crystals occurred, a unit cell determination revealed the formation of single crystals of the free ligand only.

3.2.5 Single-crystal structures obtained from ligand L5

3.2.5.1 [Ag₃(L5)₂(NO₃)₂](NO₃)·3H₂O (14)

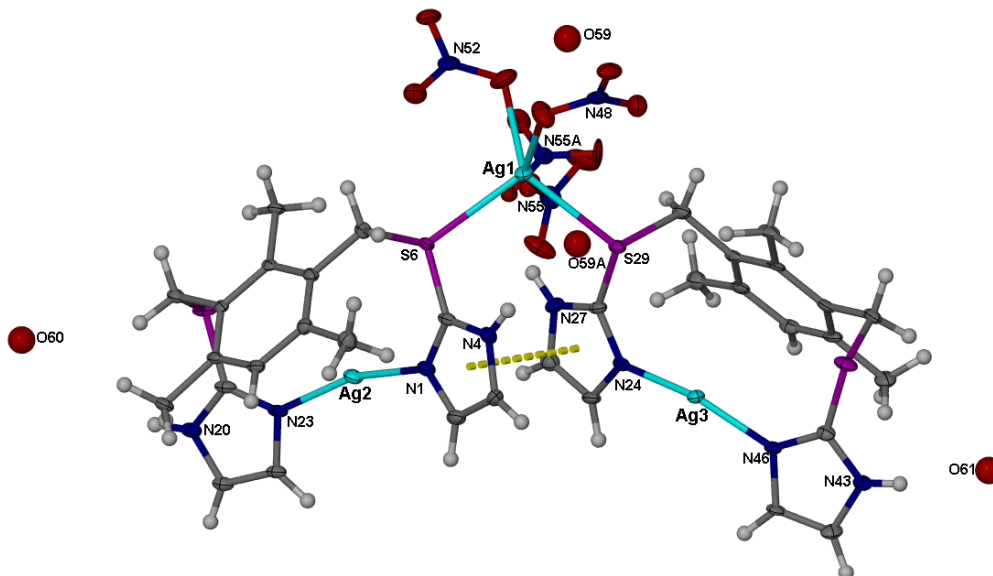


Figure 34. The ASU of **14**. Displacement ellipsoids are drawn at the 50% probability level; hydrogen and water molecules are represented as spheres. The intramolecular π - π interaction is shown as a dashed yellow line.

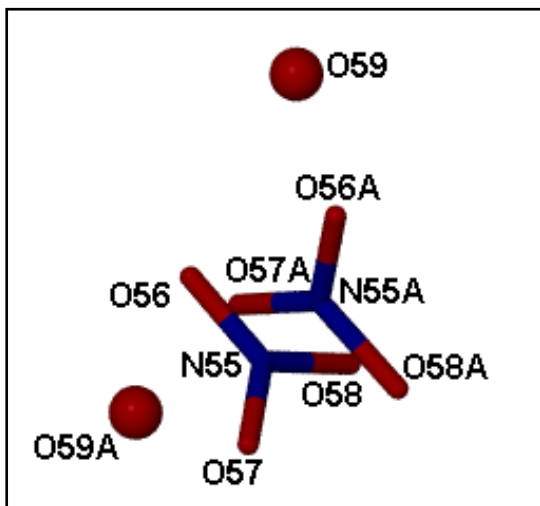


Figure 35. The two disordered nitrate ion and water molecule pairs. Atoms labelled with the letter A constitute one pair, and the remaining atoms constitute the second pair.

Single crystals of **14** were obtained by slow evaporation of a methanolic solution of **L5** and AgNO₃ in a 1:2 ligand-to-metal molar ratio. The ASU of **14** consists of two independent ligands **L5**, three silver cations, three nitrate anions and three water molecules. Two of the silver ions, namely Ag2 and Ag3, are linearly coordinated by two separate **L5** ligands, effectively creating two mononuclear units that are bridged by the third silver ion, Ag1, to form a trinuclear complex (Figure 34). The bridging Ag1 ion is in a tetrahedral coordination environment and coordinates to two monodentate nitrate ions and two sulphur atoms from distinct **L5**

ligands, thereby creating the bridge between the two mononuclear units. This arrangement is further stabilised by the intramolecular π - π interaction between the two imidazole rings attached to the coordinated sulphur atoms (centroid-to-centroid distance = 3.907 Å). The third nitrate anion is disordered over two positions. Each of the disordered nitrate ions is coupled to a water molecule and the two molecules exist as disordered pairs, *i.e.* if the nitrate ion bearing N55 at its centre is present, O59 will also be present in its vicinity. However, if O59A is present, the nitrate ion bearing N55A at its centre will be present (Figure 35).

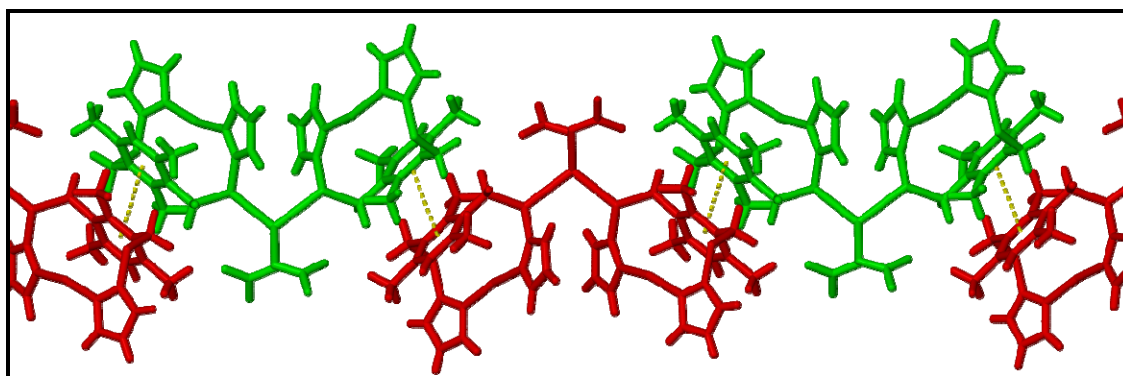


Figure 36. Capped-stick representation of the 1D strands formed in **14**. Green trinuclear units are related to the red units by a centre of inversion and π - π interactions between phenyl rings are shown as dashed yellow lines.

By virtue of weak π - π interactions between phenyl rings (centroid-to-centroid distances of 3.935 Å and 3.907 Å apply) and inversion symmetry, adjacent discrete trinuclear units interact with one another to form a 1D polymeric strand running parallel to [-111] (Figure 36). N4 and N43 both donate a hydrogen bond to one of the free-standing water molecules in the lattice, thus linking the 1D strands into a corrugated 2D layer, viewed perpendicular to [100] (see Table 19 for details of hydrogen bonding parameters, Figure 37).

Table 19. Hydrogen-bond geometry for **14** (Å, °).

D-H...A	D-H	H...A	D...A	D-H...A
N4-H4...O61 ⁱ	0.88	2.01	2.798(5)	148
N43-H43...O61	0.88	1.96	2.781(5)	154

Symmetry codes: (i) $-x, -y+2, -z$.

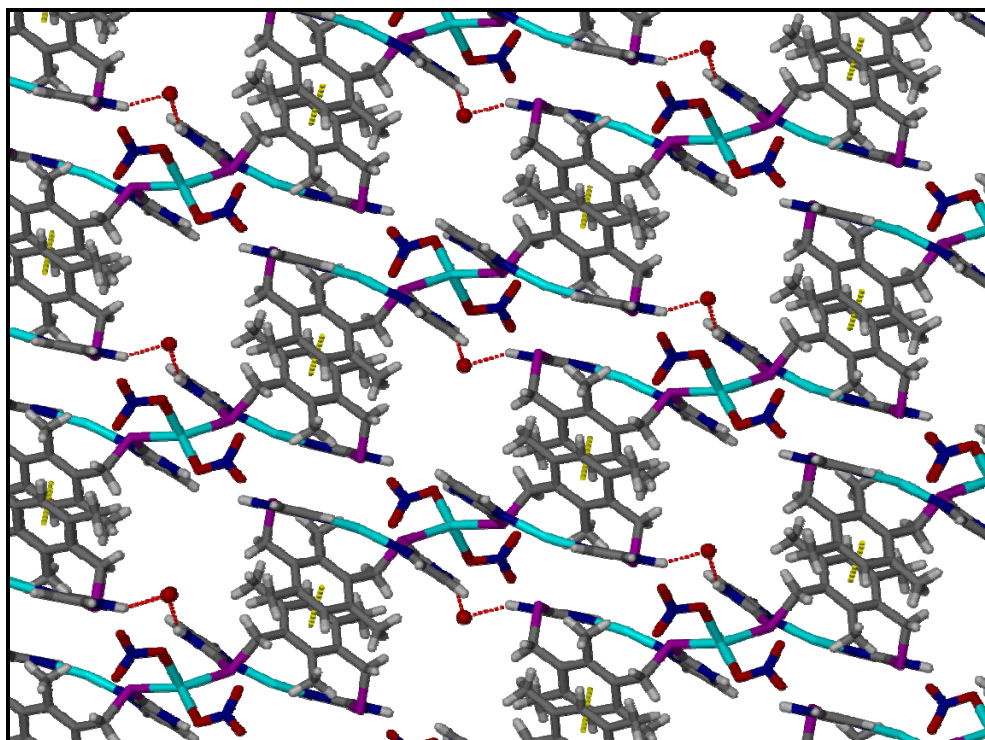


Figure 37. Packing arrangement of **14** to form 2D layers viewed perpendicular to [100]. Oxygen atoms of the water molecules are shown as spheres; all other atoms are represented using the capped-stick metaphor. Disordered nitrate ions and water molecules are omitted for clarity.

3.2.5.2 [Ag₂(L5)₂](NO₃)₂ (**15**)

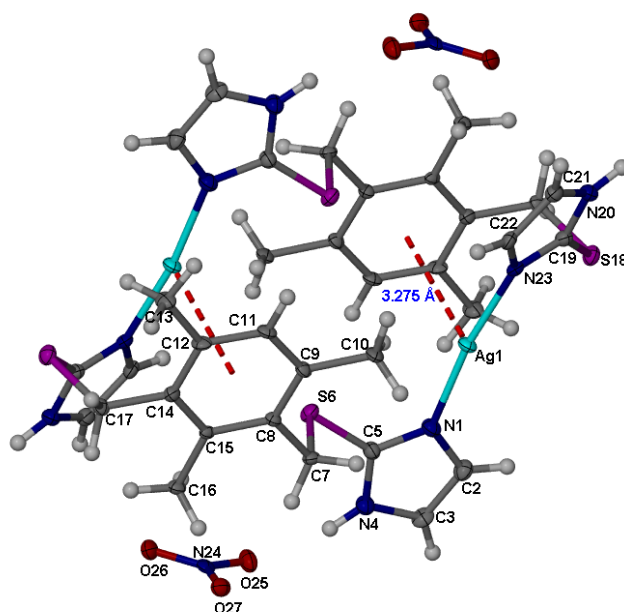


Figure 38. Atomic displacement plot (50% probability) of the molecular structure of **15**. In the [Ag₂(L5)₂]⁺ unit, the unlabelled atoms are related to the labelled atoms by a centre of inversion and the Ag- π interaction is indicated by a dashed red line.

Crystals of **15** were obtained by the reaction of **L5** with AgNO₃, in either a 1:1 or a 1:2 ligand-to-metal ratio in MeCN, followed by slow evaporation of the solvent. The ASU consists of one ligand **L5**, a silver cation and a nitrate anion. Each silver ion is linearly coordinated to two ligands, and each ligand is coordinated to two imidazole groups *via* the unprotonated nitrogen atoms of the imidazole groups to form discrete cationic dinuclear metallocyclic complexes with the formula [Ag₂(**L5**)₂]⁺ (Figure 38). Adjacent [Ag₂(**L5**)₂]⁺ units are connected by means of hydrogen bonding where the protons of the imidazole groups act as H-bond donors to the oxygen atoms of the nitrate groups to form 1D strands running parallel to [011] (Figure 39, Table 20). The distance from the Ag centre to the centroid of the benzene ring (3.275 Å) and the N-Ag-N angle of 172.18(2)° indicates the presence of Ag-π interactions within the dinuclear complexes.

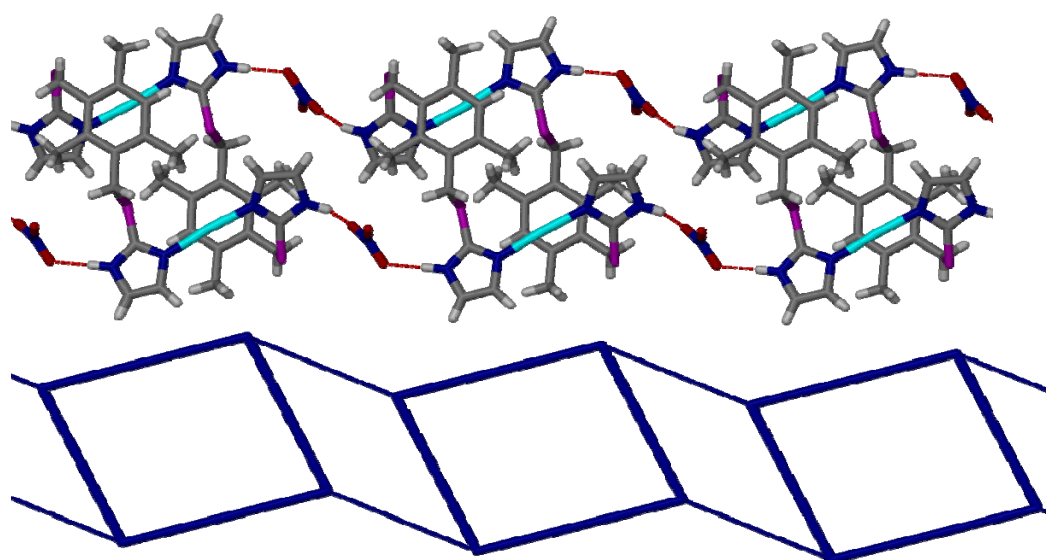


Figure 39. Capped-stick representation of the 1D strands formed in **15** (top). A simplification of the 1D strands; thick lines represent the [Ag₂(**L5**)₂]⁺ units and the thin lines the hydrogen bonded links (bottom).

Table 20. Hydrogen-bond geometry for **15** (Å, °).

D-H...A	D-H	H...A	D...A	D-H...A
N4-H4...O25	0.88	1.91	2.767(5)	163
N20-H20...O27 ⁱ	0.88	1.91	2.782(5)	170

Symmetry codes: (i) $x, y+1, z+1$.

L5 and various Ag(I) salts in a 1:1 ratio in MeOH

As previously mentioned there are many factors that influence the process of crystallisation and hence the resulting solid-state structure. It is important to study these various structure-directing factors as an initial step towards driving the process of crystallisation in the direction of a specific structure.

Using the flexible *meta*-substituted **L5** and Ag(I), an investigation was made into the diversity of structures obtainable when complex formation is influenced by only one parameter *i.e.* the choice of counter-ion. A series of crystal structures was obtained by allowing solutions of equimolar amounts of **L5** and various Ag(I) salts in MeOH to crystallise by slow evaporation over a period of several days to yield crystals suitable for single-crystal X-ray diffraction analysis. All complexes formed 0D mononuclear or dinuclear structures with the Ag(I) ion linearly coordinated by two imidazole groups from, the same ligand (in the mononuclear cases) and separate ligands (in the dinuclear cases). The mononuclear structures will be described first (**16** and **17**), followed by the dinuclear structures (**18-20**).

Table 21. Unit cell parameters and selected information for complexes **16-20**.

	16	17	18	19	20
Complex	[Ag L5](NO ₃)	[Ag L5][Ag L5] (SO ₃ CF ₃) ₂ · MeOH	[Ag ₂ (L5) ₂] (SbF ₆) ₂	[Ag ₂ (L5) ₂] (PF ₆) ₂	[Ag ₂ (L5) ₂] (BF ₄) ₂
Description	mononuclear	mononuclear	dinuclear	dinuclear	dinuclear
Crystal System	triclinic	monoclinic	triclinic	triclinic	monoclinic
Space Group	<i>P</i> -1	<i>P</i> 2 ₁ / <i>n</i>	<i>P</i> -1	<i>P</i> -1	<i>P</i> 2 ₁ / <i>n</i>
<i>a</i> (Å)	9.109(6)	12.706(8)	8.455(4)	8.333(2)	8.455(9)
<i>b</i> (Å)	11.388(8)	26.257(2)	11.422(6)	11.738(3)	22.370(3)
<i>c</i> (Å)	11.857(8)	13.626(8)	12.623(6)	12.299(4)	11.503(1)
α (°)	107.081(1)	90	98.397(8)	98.048(6)	90
β (°)	107.138(1)	91.161(1)	91.039(8)	93.683(7)	93.702(2)
γ (°)	105.031(1)	90	92.767(8)	93.417(7)	90
<i>V</i> (Å ³)	1039.9(1)	4545.0(5)	1204.2(1)	1185.8(6)	2171.3(4)

Mononuclear structures

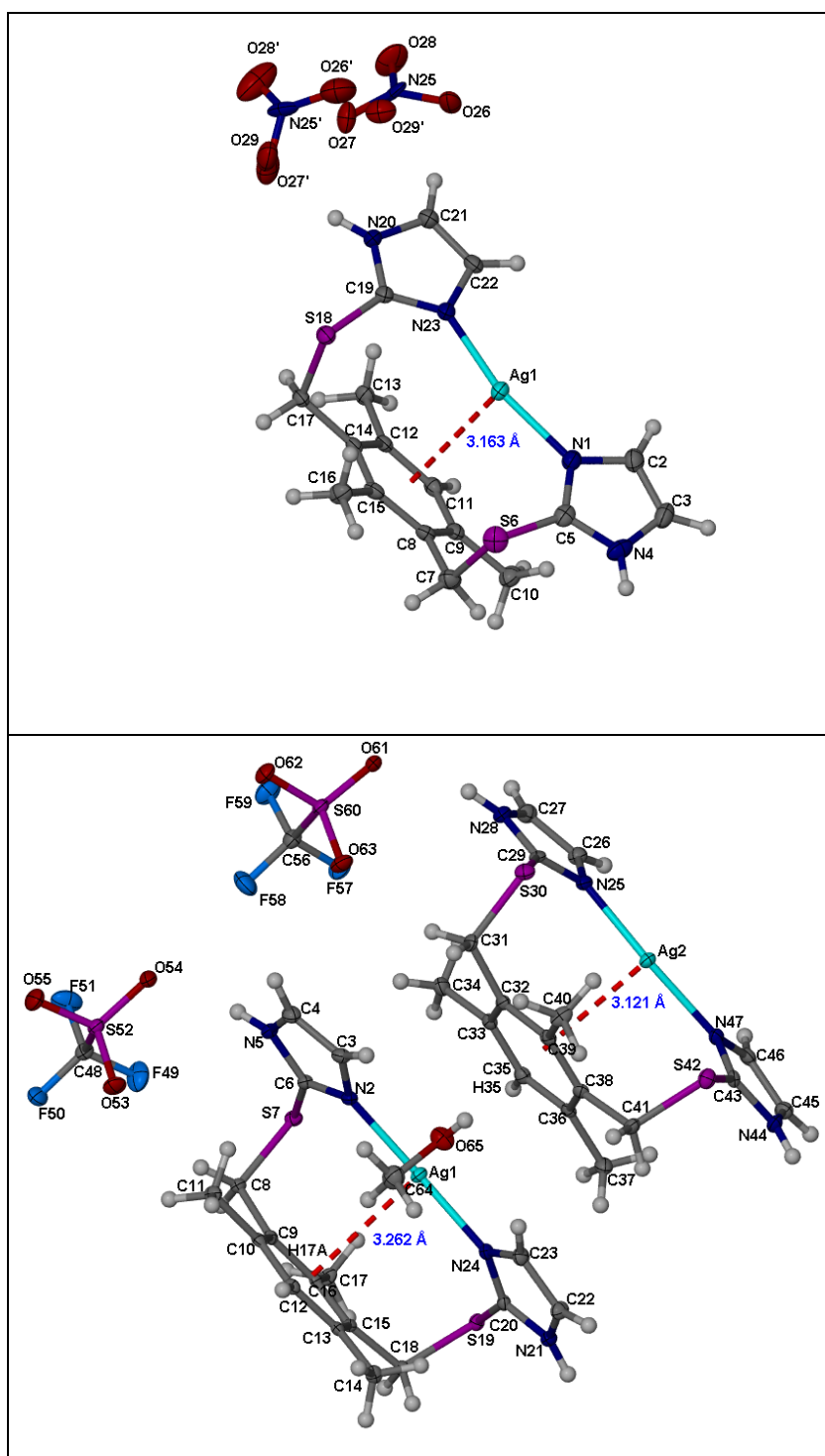


Figure 40. Atomic displacement (50% probability) plots showing the ASUs of **16** (top) and **17** (bottom). Hydrogen atoms are shown as spheres of arbitrary radius and Ag- π interactions are shown as dashed red lines.

3.2.5.3 [AgL5](NO₃) (16)

As seen in Figure 40 (top) the ASU of **16** comprises a single cationic unit, as well as a nitrate anion and a water molecule each disordered over two positions. Each Ag ion is linearly coordinated to two N-atoms from separate imidazole groups of the same ligand to form a 0D mononuclear cationic unit. The ligand molecule is approximately C-shaped *i.e.* it assumes the UU conformation with the two coordinating nitrogen atoms pointed towards each other. The N-Ag-N angle of 165.90(1)° deviates from linearity owing to the presence of Ag- π interactions (Ag-centroid distance = 3.163 Å).

Adjacent cationic units are connected to one another to form columns running parallel to [010] by means of alternating OFF π - π interactions between, two benzene rings and two imidazole rings, with centroid-to-centroid separations of 3.894 Å and 3.935 Å, respectively (Figure 41). The Ag ions of adjacent mononuclear units within a column are separated by a distance of 3.542 Å, which is too long to be considered an argentophilic interaction.³² The nitrate and water groups exist in disordered pairs (a 'pair' constitutes one nitrate anion and one water molecule) and sit in channels between the columns and are hydrogen bonded to the protonated nitrogens of the imidazole groups (see ESI for details of hydrogen bonding parameters).

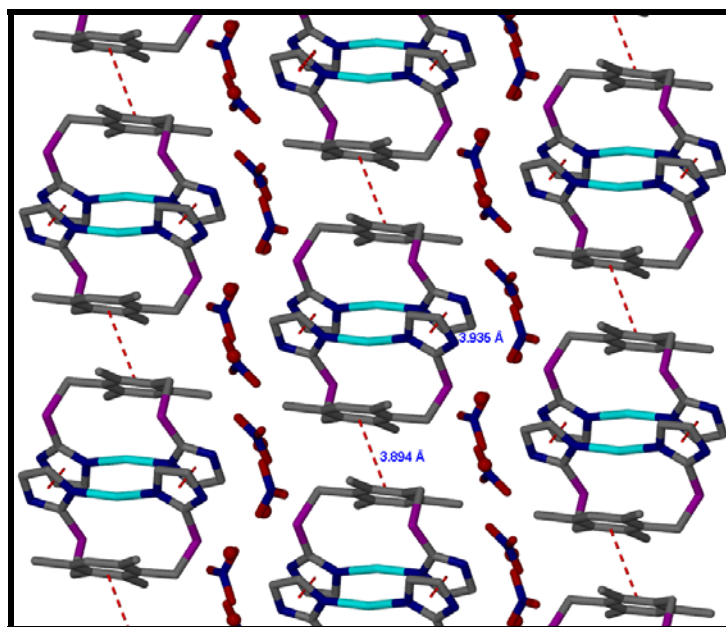


Figure 41. Capped-stick representation of the columns formed in **16** by π - π stacking interactions (shown as dashed red lines) between benzene and imidazole rings respectively, as viewed down [100]. The nitrate ions and water molecules are situated in channels between the columns. All hydrogen atoms have been omitted for clarity and oxygen atoms of the water molecules have been shown as spheres.

3.2.5.4 [AgL5]₂(SO₃CF₃)₂·CH₃OH (17)

In contrast to **16**, the ASU of **17** contains two cationic units, two charge balancing triflate counter-ions as well as a single methanol molecule (Figure 40). The coordination environment around the metal centre in each cationic unit is similar to that found in **16**, with analogous Ag- π interactions. In the first cationic unit the distance from Ag1 to the centroid of the benzene ring = 3.262 Å, with a corresponding N2-Ag1-N24 angle of 170.99(9)°. The distance from Ag2 to the centroid of its benzene ring is shorter at 3.121 Å. One would expect a greater deviation from linearity in the coordination environment around Ag in this second cationic unit as the Ag- π interaction is stronger; indeed, the N25-Ag2-N24 angle is 163.66(9)°. The cationic units stack along [100] with the benzene rings of one unit facing the Ag ion of an adjacent unit. One of the oxygen atoms of each triflate anion is in van der Waals contact with a fluorine atom of the neighbouring triflate anion (O54...F58 = 2.840(1) Å and O61...F40 = 2.877(3) Å) and these weak interactions, together with the hydrogen bonding of pillared cationic units to neighbouring triflate ions, results in the formation of a 2D square grid parallel to (010) [see Figure 42 (left) and the first four entries in Table 22]. The schematic projection in Figure 42 (right) shows that adjacent grids are offset in one direction by about 25%, *i.e.* atoms of the first layer are placed over the atoms of the fifth layer.

The methanol molecules serve a dual function as both a bifurcated hydrogen bond acceptor and donor, and these hydrogen bonds bind the 2D layers to one another (Figure 43, and see the last four entries in Table 22). The most notable difference in the crystal packing of the two mononuclear structures is the absence of intermolecular π - π stacking interactions in **17**. The cationic units are, however, correctly oriented towards intermolecular Ag- π interactions with neighbouring benzene rings, but these distances of 3.414 Å and 3.715 Å fall just out of the reported range of distances for such interactions (2.89-3.37 Å; distance from Ag(I) to the centroid of the benzene ring), and will therefore not be considered further.³⁴

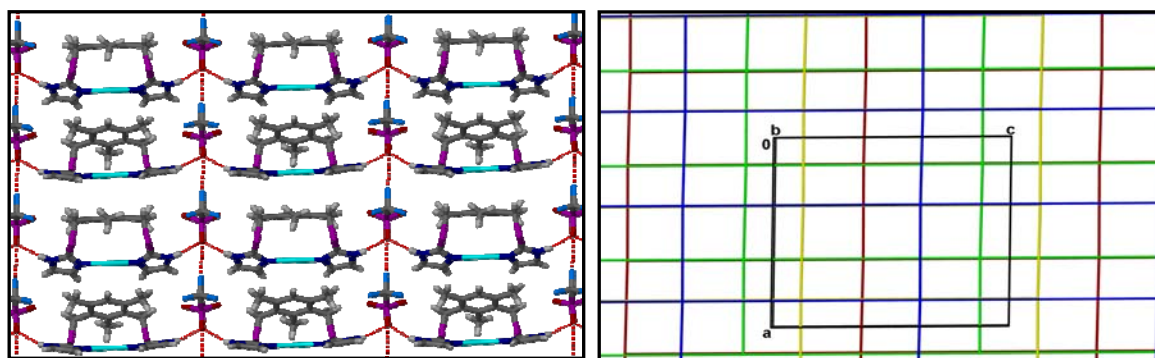


Figure 42. Capped-stick representation of the 2D square grid formed in **17** (left). A simplification of the ...*ABCD*... stacking of the 2D grids (right). Both are viewed down [010].

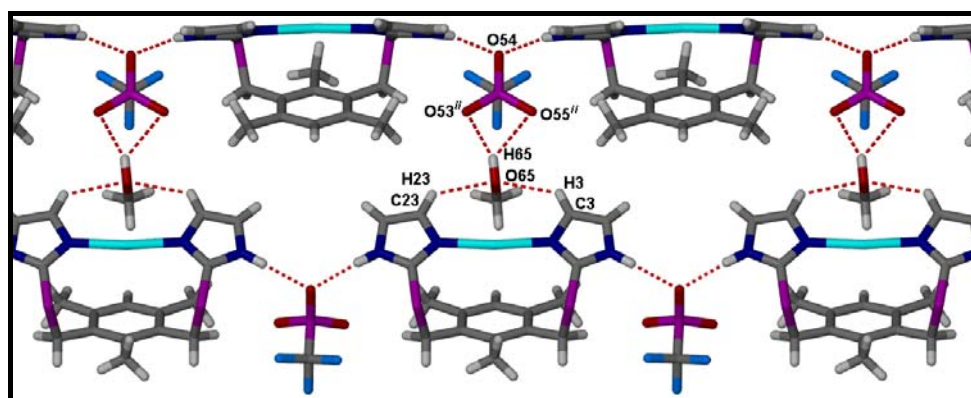


Figure 43. Capped-stick representation of the hydrogen bond motif responsible for connecting adjacent 2D layers. Hydrogen bonds have been shown as dashed red lines.

Table 22. Hydrogen-bond geometry for **17** (Å, °).

D-H...A	D-H	H...A	D...A	D-H...A
N5-H5...O54	0.88	2.04	2.892(3)	163
N21-H21...O54 ⁱ	0.88	2.02	2.880(3)	166
N28-H28...O61	0.88	2.04	2.872(2)	157
N44-H44...O61 ⁱ	0.88	2.04	2.847(3)	152
C3-H3...O65	0.95	2.51	3.217(4)	131
C23-H23...O65	0.95	2.45	3.179(4)	133
O65-H65...O53 ⁱⁱ	0.84	2.32	3.071(3)	150
O65-H65...O55 ⁱⁱ	0.84	2.58	3.219(3)	134

Symmetry codes: (i) $x, y, z-1$; (ii) $x - \frac{1}{2}, -y + \frac{1}{2}, z - \frac{1}{2}$.

Dinuclear structures

3.2.5.5 [Ag₂(L5)₂](SbF₆)₂ (**18**)

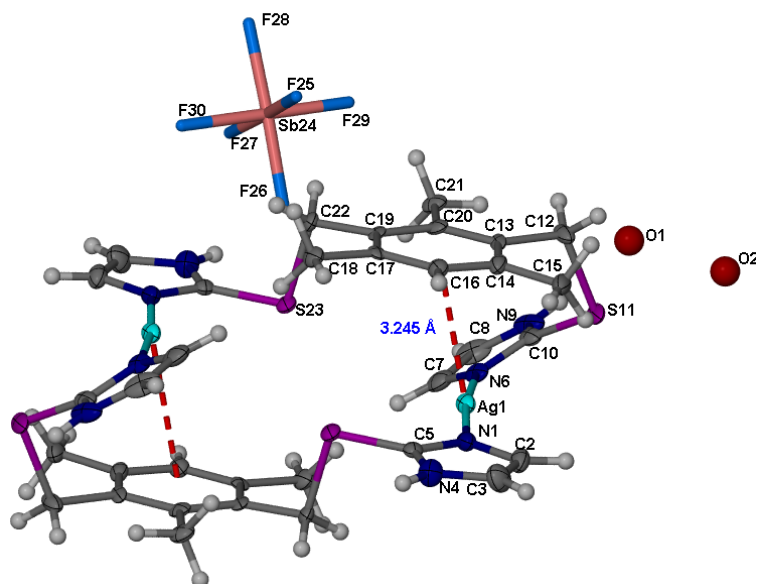


Figure 44. Atomic displacement (50% probability) plots showing the molecular structure of **18**. Water molecules are shown as spheres and, owing to disorder, the counter-ion is shown in the capped-stick representation. Ag- π interactions are shown as dashed red lines from the centroid of the benzene rings to the Ag ions. In the [Ag₂(L5)₂]²⁺ unit, the unlabelled atoms by a centre of inversion.

The ASU of **18** consists of one silver ion, one ligand **L5**, one hexafluoroantimonate ion, one water molecule at full occupancy (O1) and one water molecule at half occupancy (O2) (Figure 44). Each ligand is coordinated to two silver ions at its opposite ends and, in turn, each silver ion is coordinated to two ligands **L5** to form a 0D dinuclear metallocycle. The coordination environment about each silver ion is linear, but owing to the presence of Ag- π interactions within each dinuclear unit (distance from Ag to the centroid of the benzene ring = 3.245 Å), the N-Ag-N angle shows a deviation from linearity (\angle N-Ag-N = 172.5(3)^o). The ligand assumes the **UU** conformation with the coordinating nitrogens of the imidazole groups pointing in the same direction. The two pendant arms are not symmetrically oriented about the central aromatic core. This is reflected most obviously in the dihedral angles between the planes of each respective imidazole ring and the central benzene ring plane of 35.3(4)^o (for the imidazole ring containing N1) and 1.5(6)^o (for the imidazole ring containing N6).

The $[\text{Ag}_2(\mathbf{L5})_2]^{2+}$ units stack along [001] to form columns, which are connected to one another by hydrogen bonds to form a 2D layer (Figure 45). Owing to the partial occupancy of the second water molecule, it is not possible to unambiguously assign a bridging hydrogen bonding motif. However, from the numerous possibilities that may exist, one possible hydrogen bonding motif is suggested in Figure 46 for the instance where the second water molecule is indeed present in the ASU. These hydrogen bonds have been divided in terms of *permanent* hydrogen bonds *i.e.* those that exist whether O2 is there or not, which are represented by dashed yellow lines, and *possible* hydrogen bonds, *i.e.* those that may only exist when O2 is present, which are represented as dashed red lines. Three sets of *permanent* hydrogen bonds exist, two of which involve the protonated nitrogens of the imidazole groups acting as hydrogen bond donors to F26 of the counter-ion ($\text{N4}\cdots\text{F26} = 2.887(2) \text{ \AA}$) and O1 ($\text{N9}\cdots\text{O1} = 2.794(3) \text{ \AA}$), respectively. The latter in turn donates a hydrogen bond to F28 of the counter-ion ($\text{O1}\cdots\text{F28} = 2.823(3) \text{ \AA}$) to complete the list of *permanent* hydrogen bonds.

Possible hydrogen bonds include the partially occupied water molecule acting as both a hydrogen bond donor and a hydrogen bond acceptor. In the former case O2 is hydrogen bonded to F29 ($\text{O2}\cdots\text{F29} = 2.661(4) \text{ \AA}$) and a second partially occupied water molecule ($\text{O2}\cdots\text{O2} = 3.275(3) \text{ \AA}$), in the latter case O2 is hydrogen bonded to the fully occupied water molecule ($\text{O1}\cdots\text{O2} = 2.620(3) \text{ \AA}$). Figure 46 is essentially an enlargement of the hydrogen bonding pattern of **18**, and its placement in the overall packing arrangement in Figure 45 has been indicated by a green rectangle.

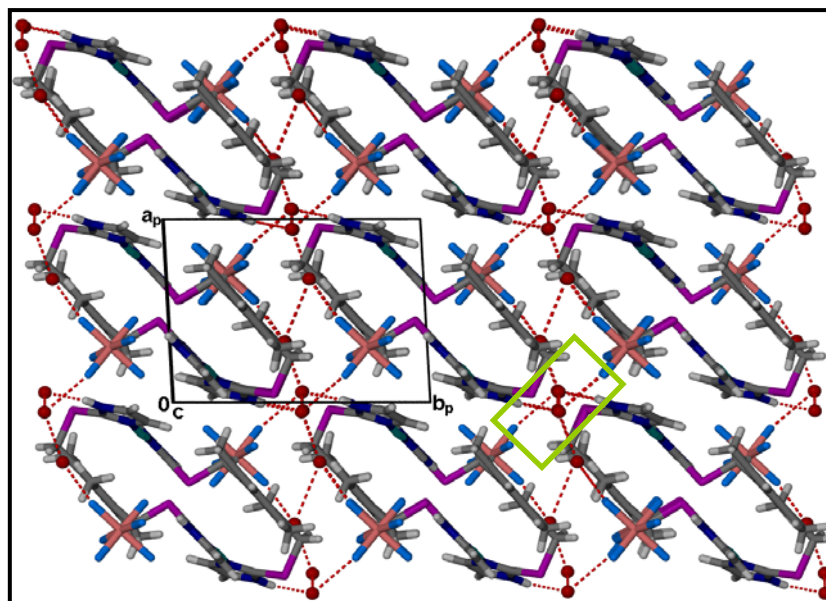


Figure 45. Capped-stick representation of the packing arrangement of **18** as viewed down [001]. Hydrogen bonds are shown as dashed red lines and oxygen atoms have been shown as spheres. The green rectangle highlights the hydrogen bonding motif that is expanded in the Figure 46 below.

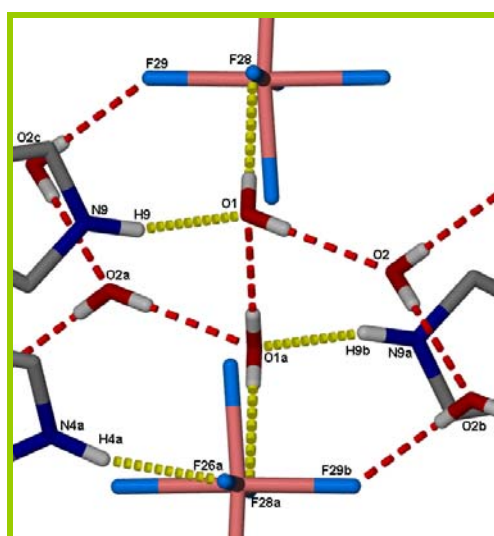


Figure 46. The hydrogen-bonding motif present in complex **18** involving partially occupied (O2) and fully occupied (O1) water molecules, fluoride ions and imidazole nitrogens. All molecules are shown in capped-stick representation. *Permanent* and *possible* hydrogen bonds are shown as dashed yellow and red lines, respectively. Hydrogen atoms not participating in hydrogen bonds have been omitted for clarity. The lower-case letters a, b and c have been used to denote atoms within the same set of hydrogen bonds.

3.2.5.6 [Ag₂(L5)₂](PF₆)₂ (**19**)

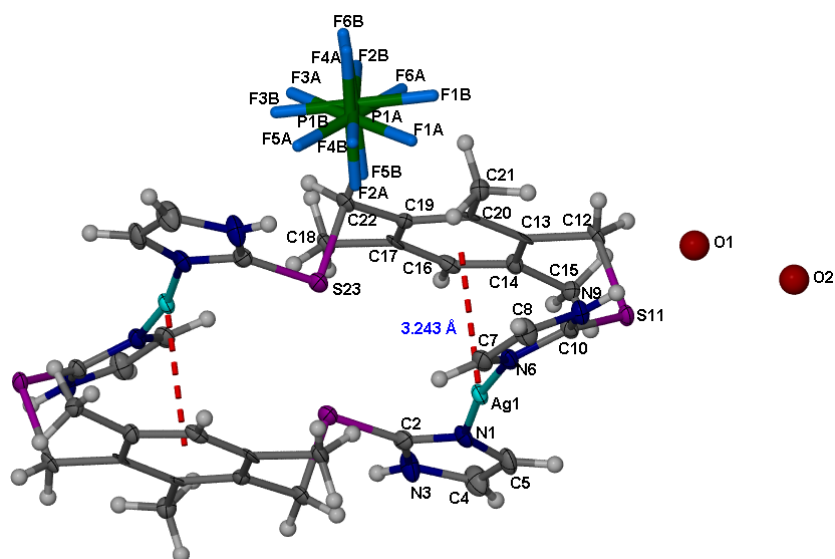


Figure 47. Atomic displacement (50% probability) plot showing the molecular structure of **19**. Water molecules are shown spheres and, owing to disorder, the counter-ion is shown in the capped-stick representation. Ag- π interactions have been shown as dashed red lines from the centroid of the benzene rings to the Ag ion. In the [Ag₂(L5)₂]²⁺ unit, the unlabelled atoms are related to the labelled atoms by a centre of inversion.

The ASU of **19** consists of one silver ion, one ligand **L5**, one hexafluorophosphate ion, one water molecule of full occupancy (O1) and one water molecule of half occupancy (O2) and, as such, is remarkably similar to **18**. However, there is a slight difference in that the PF₆⁻ counter-ion is disordered over two positions in **19** while the SbF₆⁻ ion of **18** is ordered.

Aside from the disorder of the counter-ion, the molecular structures of **18** and **19** are similar (Table 23) and, indeed, upon closer examination of the unit cell parameters and space group of the two structures (Table 21) it can be concluded that **18** and **19** can be considered to be isostructural (in a non-rigorous sense). Accordingly the packing arrangement of **19** is sufficiently similar to that of **18** and requires no further discussion.

Table 23. Selected geometric parameters for complexes **18** and **19** (Å, °).

Complex 18			
Ag1—N6	2.077(7)	C10—S11	1.736(10)
Ag1—N1	2.081(7)	S11—C12	1.841(9)
N6—Ag1—N1	172.5(3)	C10—S11—C12—C13	58.5(8)
N6—C10—S11—C12	-87.4(8)	C19—C22—S23—C5 ⁱ	170.9(5)
Complex 19			
Ag1—N1	2.087(7)	C10—S11	1.744(8)
Ag1—N6	2.109(7)	S11—C12	1.839(8)
N1—Ag1—N6	171.6(3)	C10—S11—C12—C13	61.4(7)
N6—C10—S11—C12	-86.8(8)	C19—C22—S23—C2 ⁱⁱ	170.7(6)

Symmetry codes: (i) $-x+1, -y, -z+2$; (ii) $-x+1, -y+1, -z+1$.

3.2.5.7 [Ag₂(L5)₂](BF₄)₂ (**20**)

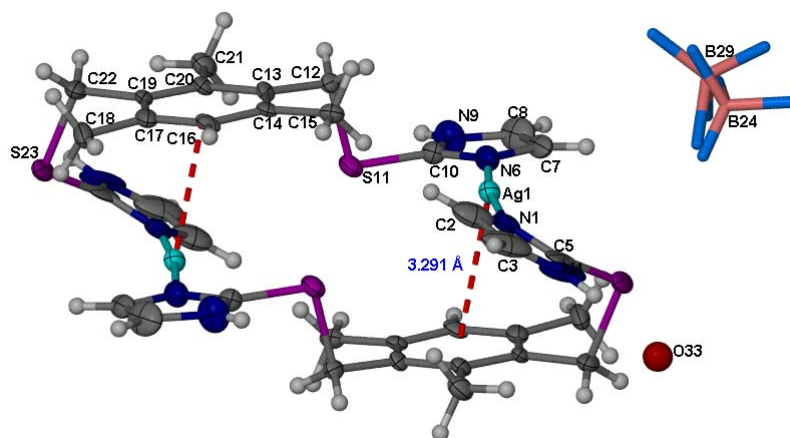


Figure 48. Atomic displacement (50% probability) plot showing the molecular structure of **20**. The water molecule is shown as a sphere and, owing to disorder, the counter-ion is shown in the capped-stick representation. Ag- π interactions have been shown as dashed red lines from the centroid of the benzene rings to the Ag ion. In the [Ag₂(L5)₂]²⁺ unit, the unlabelled atoms are related to the labelled atoms by a centre of inversion.

Complex **20** is the final dinuclear complex in this series of crystal structures. The ASU consists of one ligand **L5**, one water molecule and a tetrafluoroborate counter-ion disordered equally over two positions. Complex **20** forms [Ag₂(L5)₂]²⁺ metallocycles in a manner similar to those of the previous two structures. Each metal centre is

coordinated to two separate ligands **L5**, and is in a linear coordination environment. The N-Ag-N angle of $172.0(2)^\circ$ and the distance from the Ag ion to the centroid of the benzene ring of 3.291 \AA indicates the presence of Ag- π interactions within each cationic unit. The $[\text{Ag}_2(\text{L5})_2]^{2+}$ units stack parallel to $[-101]$ to form 1D chains. The water molecule acts as a bifurcated hydrogen bond acceptor to the protonated nitrogens of imidazole groups on separate $[\text{Ag}_2(\text{L5})_2]^{2+}$ units and, by virtue of these hydrogen bonds and a 2_1 screw operation, adjacent 1D channels are connected to one another to form 2D layers when viewed down $[101]$ (Figure 49).

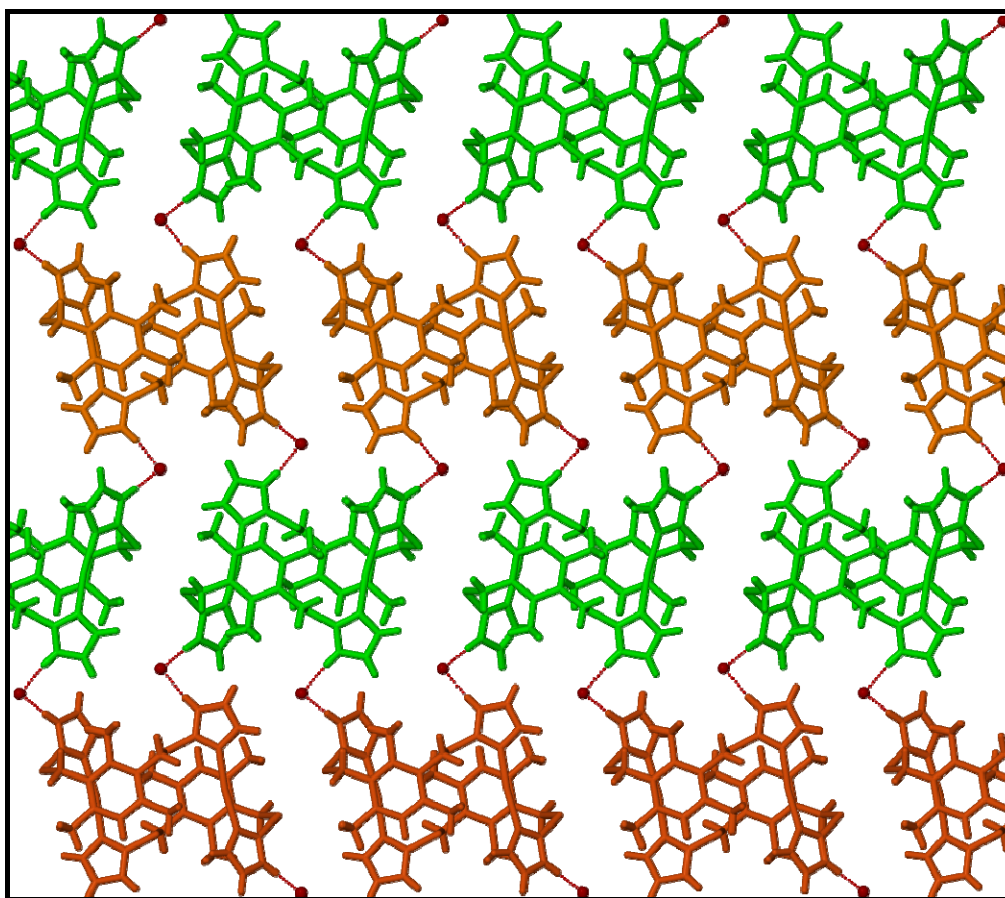


Figure 49. Capped-stick representation of the 2D layers form by N-H \cdots O hydrogen bonds in **20**, as viewed down $[101]$. Oxygen atoms are shown as spheres, and hydrogen bonds have been shown as dashed red lines, BF_4^- ions have been omitted for clarity. Adjacent columns have been coloured orange and green respectively, and are related to one another by a 2_1 screw operation.

Finally, the 2D layers are connected in 3D by O-H \cdots F hydrogen bonds. Owing to the disorder of the BF_4^- ion it is futile to assign specific hydrogen bonding parameters to this hydrogen bonding motif. However, for illustrative purposes it is convenient to present the scenario where only a single BF_4^- counter-ion exists in the crystal lattice

(Figure 50). In reality the two connecting O-H...F hydrogen bonds would entail the water molecule donating two hydrogen bonds to an averaged position for two acceptor fluoride ions.

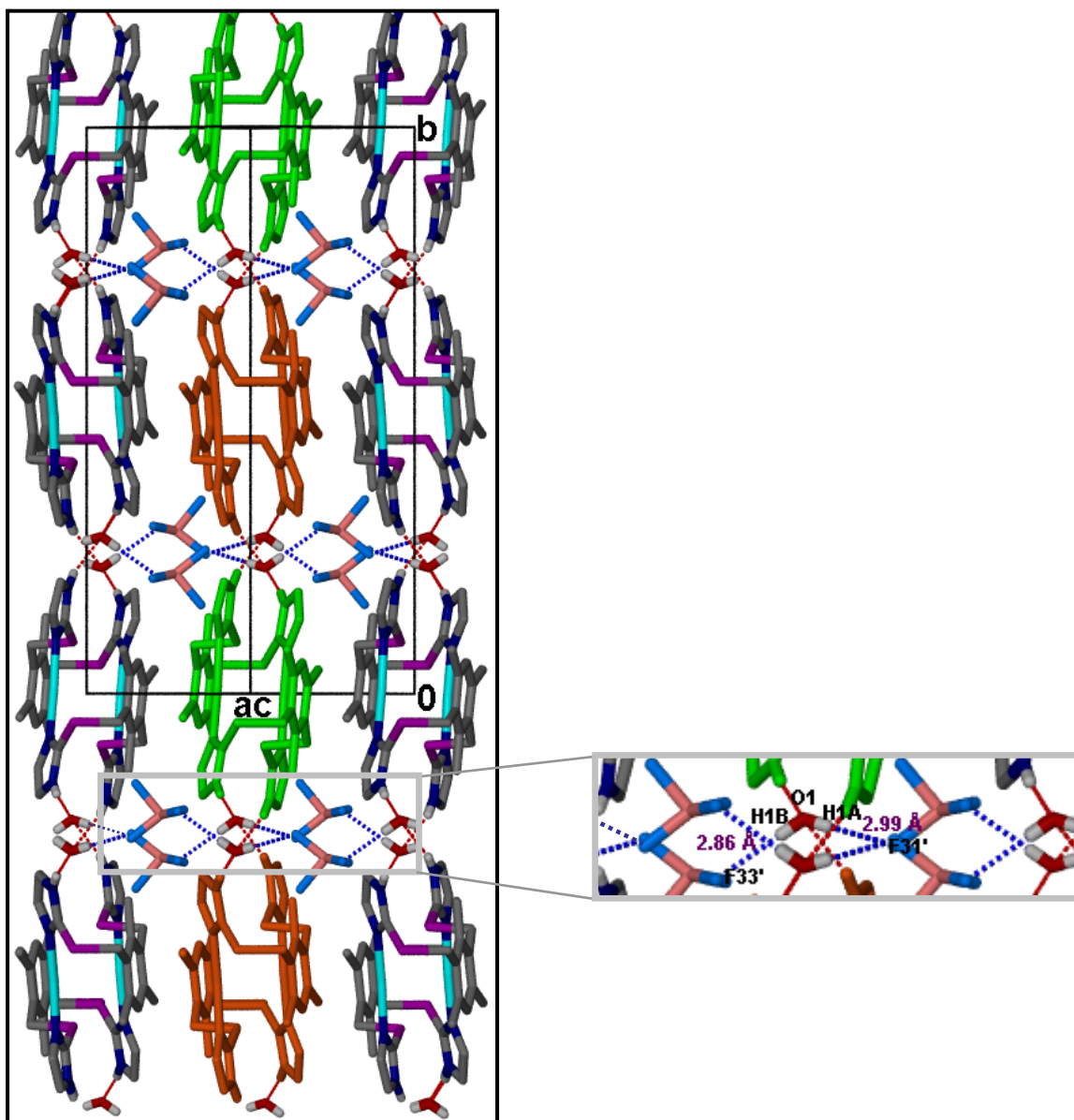


Figure 50. The molecular packing of the 2D hydrogen-bonded layers *via* O-H...F hydrogen bonds, as viewed down [-101]. One section of the hydrogen bonding motif has been enlarged on the right to show hydrogen bonding distances (O...F). Hydrogen bonds are shown as dashed blue (O-H...F) and red (N-H...O) lines. H-atoms not participating in hydrogen bonding have been omitted for clarity.

Effect of the counter-ion on the resulting crystal structure

In the above series, all crystals were grown under identical conditions: the ligand-to-metal solution ratio was 1:1; all reactants were dissolved in MeOH and the method of

crystal growth was slow evaporation of the solvent; only the nature of the counter-ion was varied. Unfortunately not all vials yielded sufficient product for XRPD analysis and thus only the phase compositions of the crystals deposited in vials containing **17** and **20**, have been verified using XRPD and confirmed to be pure (see ESI). SCD analysis, however, revealed that all structures formed are 0D, mononuclear or dinuclear structures with the Ag ions in a linear coordination environment. The counter-ions do not coordinate to the metal centre in any of the crystal structures and thus do not interfere with the ligand coordination or distort the linear geometry of the Ag cations.

It is interesting to note that although the counter-ions do not coordinate to the metal centres, the structures (**16** and **17**) containing counter-ions that are generally considered to be “coordinating counter-ions” *i.e.* NO_3^- and SO_3CF_3^- form discrete mononuclear cationic units which stacked on top of one another to form 1D columns with the anions situated in channels between the columns. While the structures (**18**, **19** and **20**) containing counter-ions that are generally considered to be “non-coordinating counter-ions”, namely SbF_6^- , PF_6^- and BF_4^- uniformly formed dinuclear cationic units. The major difference in these structures is that the hydrogen bonding network in **20** connects the dinuclear cationic units in 3D, whereas a 2D network is formed in **18** and **19**.

It is not obvious why the latter class of counter-ions would form dinuclear structures and the former class mononuclear structures. It is unlikely that the reason for these structural differences is due to the size of the counter-ion as the molecular volumes of NO_3^- and BF_4^- are comparable ($V_m[\text{NO}_3^-] = 34 \text{ \AA}^3$ and $V_m[\text{BF}_4^-] = 38 \text{ \AA}^3$).³⁴ Perhaps the most likely explanation lies in the nature of the atoms comprising the counter-ions and the overall geometry of the counter-ion. For the mononuclear structures the chief hydrogen bond acceptors are the oxygen atoms of the trigonal planar nitrate ion and the staggered triflate ions, respectively, while fluorine atoms of the octahedral hexafluorophosphate and hexafluoroantimonate, and the tetrahedral tetrafluoroborate ions participate in hydrogen bonding for the dinuclear structures. It is evident that the geometry of the counter-ion must also play an important role as the two structures (**18** and **19**) containing counter-ions with a central atom bonded to six fluorine atoms in an octahedral geometry, yield almost identical structures in the solid state.

Ligand L5 and CdI₂

Single crystals of **21**, **22** and **24** were obtained by the reaction of **L5** with CdI₂ (in ligand-to-metal molar ratios of 1:1, 2:1 and 1:2 respectively) in MeOH, followed by slow evaporation of the solvent. Single crystals of **23** were obtained from a solution of **L5** and CdI₂ in MeCN in either a 1:1 or 2:1 solution molar ratio, followed by slow evaporation of the solvent. A description of these structures follows.

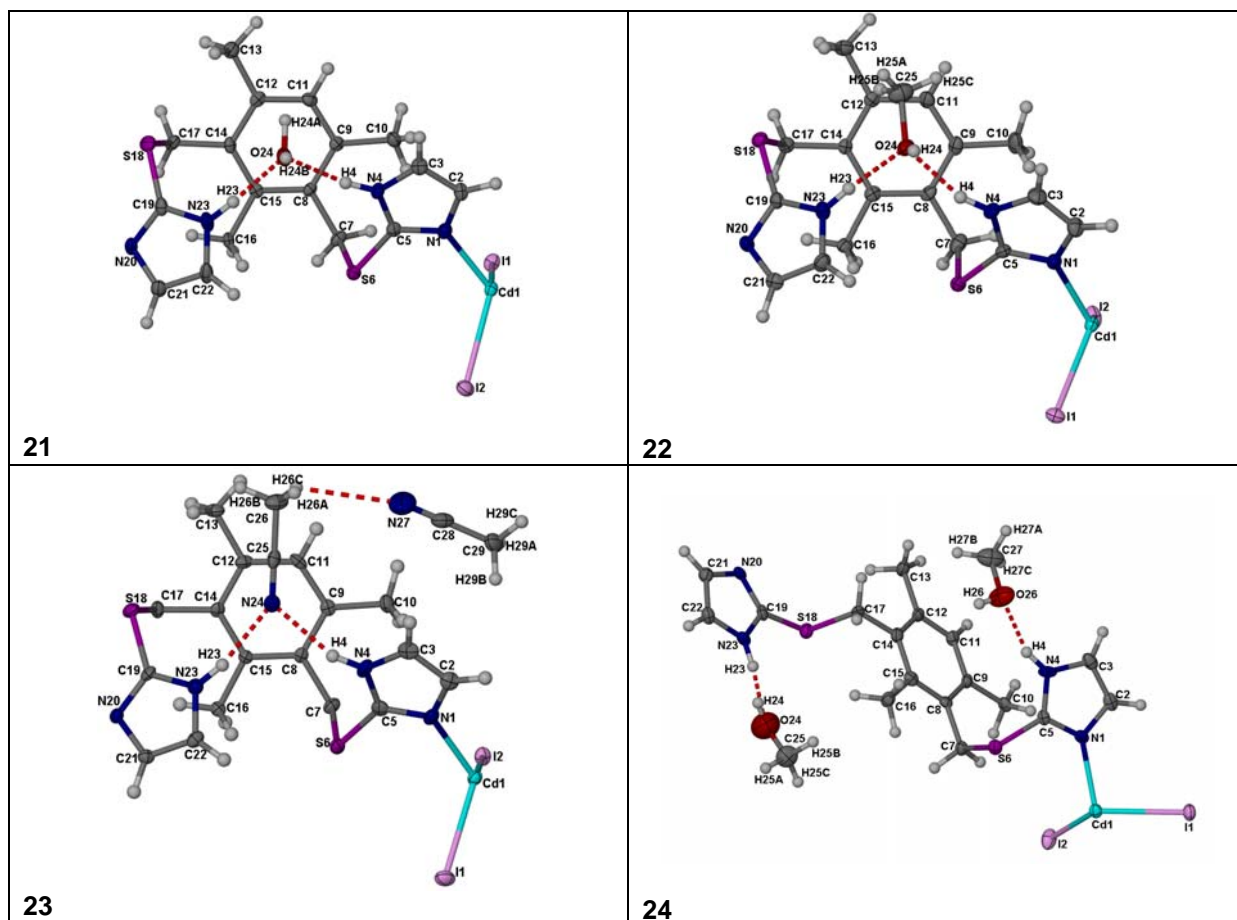


Figure 51. Atomic displacement (50% probability plots) showing the ASUs of **21**, **22**, **23** and **24**.

Hydrogen atoms are shown as spheres of arbitrary radius and hydrogen bonds are shown as dashed red lines.

3.2.5.8 [CdL5I₂]_n·nH₂O (21**)**

Complex **21** forms a 1D strand propagating along [010]. Adjacent Cd-ions are connected by means of a single ligand molecule in the UU conformation with the coordinating nitrogen atoms of the imiazole groups pointed away from one another. The dihedral angles between the planes of the two imidazole rings and the benzene ring are

28.5(1)° and 30.3(2)°, respectively. Each metal centre is coordinated to two iodine atoms and two nitrogen atoms from distinct ligand molecules and is in a distorted tetrahedral coordination environment (coordinating angles range from 101.38(9)°-116.74(2)°). In addition to the constituents that form part of the 1D chain, the ASU also contains one water molecule. The two uncoordinated nitrogens of the imidazole groups within the same ligand molecule simultaneously donate two hydrogen bonds to this water molecule to stabilise the overall UU conformation of the ligand (Figure 51 and Table 24).

Neighbouring 1D strands are connected into a distorted 2D honeycomb arrangement by the donation of two hydrogen bonds from the water molecule to the coordinated iodine atoms (Figure 53, top). The honeycomb layer is connected to another layer by means of OFF π - π interactions between neighbouring benzene rings (centroid-centroid distance = 3.569 Å) to essentially form a bilayer arrangement (Figure 53). As a result, the honeycomb layers stack on top of one another such that the atoms of the first layer are placed over the atoms of the third layer when viewed down [100] (Figure 52, bottom).

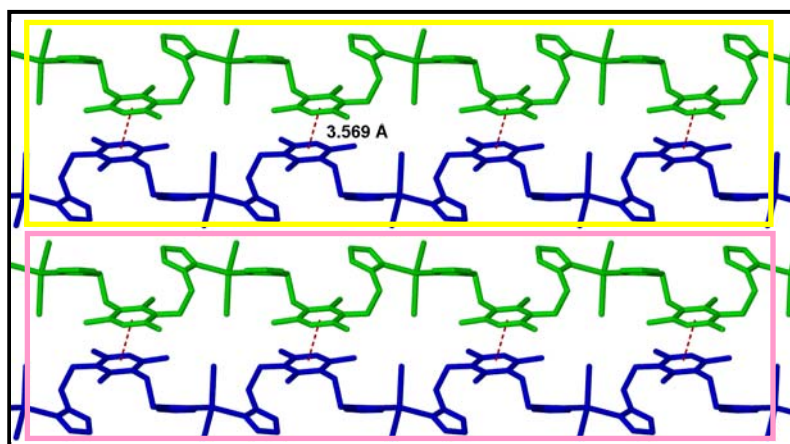


Figure 52. Packing arrangement of **21** to form bilayers as viewed down [101]. Molecules are shown in the capped-stick metaphor and OFF π - π stacking interactions are shown as dashed red lines. Two distinct bilayers have been enclosed in yellow and pink opaque rectangles and solvent molecule have been omitted for clarity.

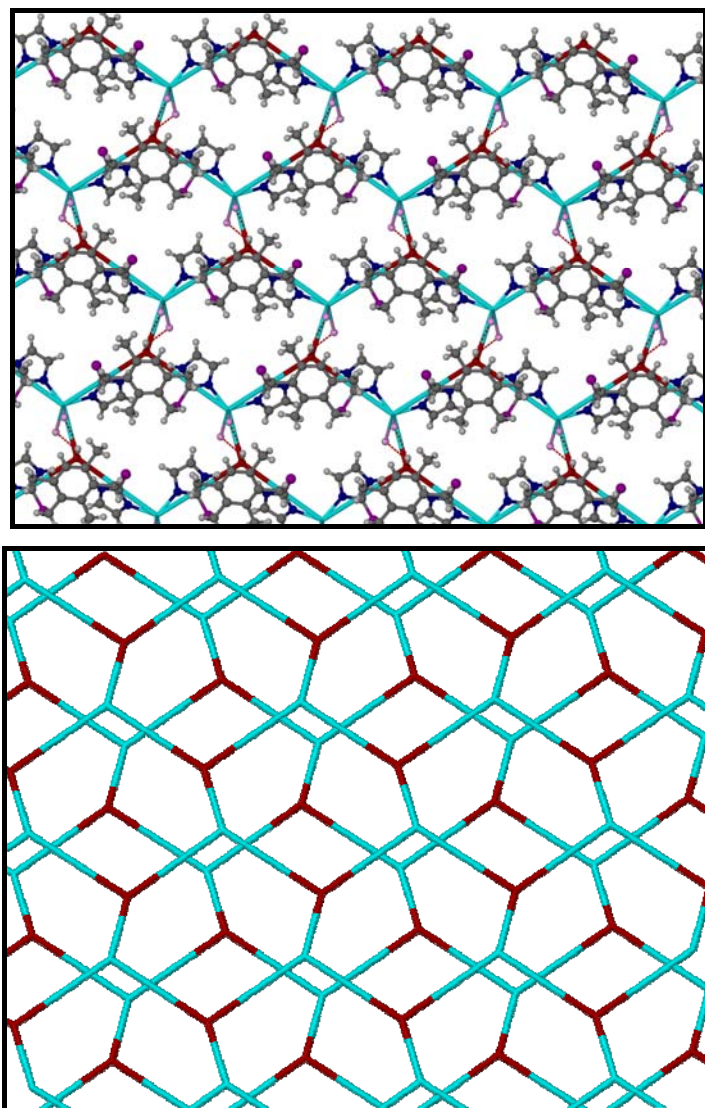


Figure 53. Distorted 2D honeycomb layer formed by hydrogen bonding in **21**. Molecules are shown in the ball-and-stick metaphor (top). A simplification of the 2D honeycomb layers showing the ...*ABAB*... stacking arrangement (bottom). Both are shown as viewed down [100].

3.2.5.9 [CdL5I₂]_n·nCH₃OH (**22**)

The ASU of **22** is similar to that of **21** in constituents as well as the relative arrangement of the atoms within the ASU (Figure 51). However, a methanol molecule replaces the water molecule, and assumes the role of bifurcated hydrogen bond acceptor to the nitrogen donors of the imidazole groups, thereby stabilising the **UU** conformation of the ligand. The dihedral angle between the planes of the two imidazole rings and the benzene ring are 31.8(3)° and 37.6(2)° respectively. The unique angles that complete the distorted tetrahedral environment around the Cd metal centre range from 98.44(1)°-120.63(9)° and successive metal centres are linked to one another *via* a individual

ligand molecules to form a 1D polymeric chain running parallel to [010]. The methanol molecule donates a hydrogen bond to one of the ligated iodide ions connecting adjacent 1D chains into bilayers (see Table 24 for hydrogen bonding parameters, Figure 54). Figure 55 shows the final 2D assembly in which the bilayers are connected to one another by π - π stacking interactions between adjacent benzene rings (centroid-centroid distance = 4.112 Å).

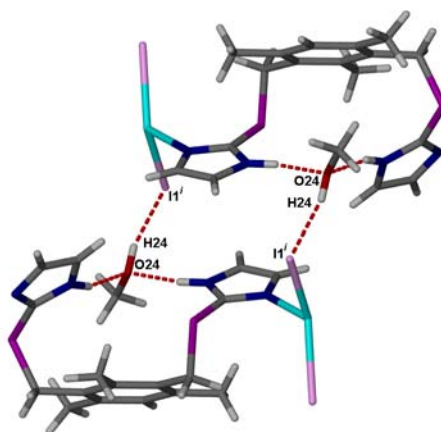


Figure 54. Capped-stick representation of all the hydrogen bonds formed in **22**. Atoms of the top molecule are related to the atoms of the bottom molecule by the symmetry operation $\frac{3}{2} - x, \frac{1}{2} - y, 1 - z$. Hydrogen bonds are shown as dashed red lines.

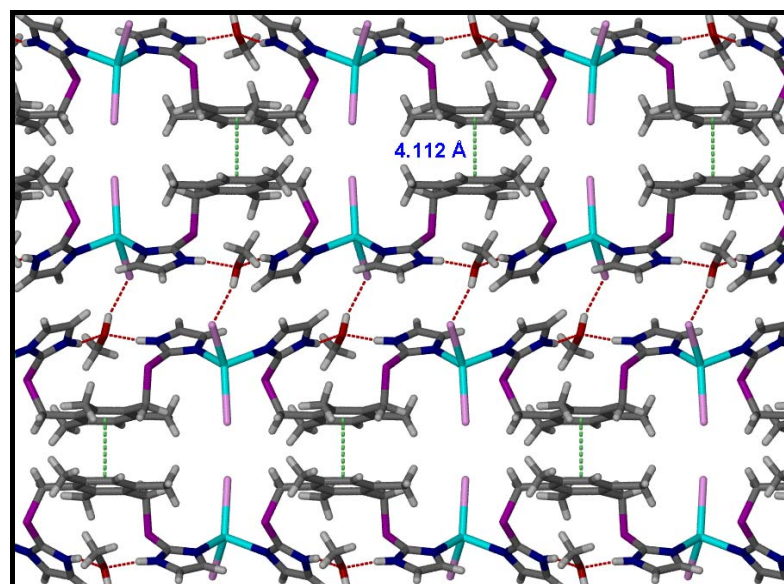


Figure 55. Packing arrangement of the 2D layers formed in **22** as viewed down [010]. Molecules are shown in the capped-stick metaphor; hydrogen bonds and π - π stacking interactions are shown as dashed red and green lines, respectively.

3.2.5.10 $[\text{CdL5I}_2]_n \cdot 2n\text{CH}_3\text{CN}$ (**23**)

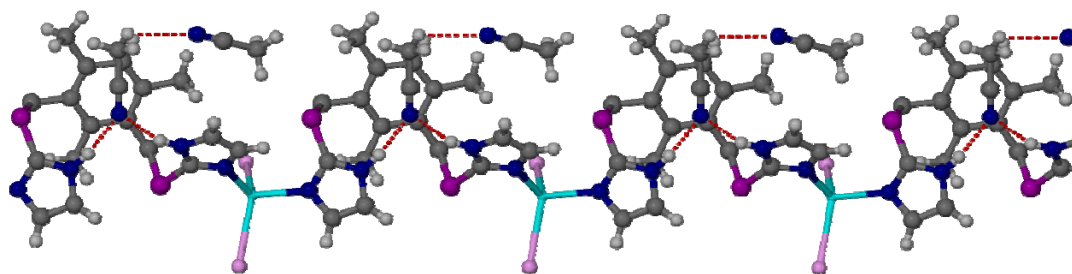


Figure 56. Ball-and-stick plot showing the 1D strand formed in **23**, as viewed down [100]. Hydrogen bonds are shown as dashed red lines.

Complex **23** is the last complex in this series to feature **L5** in the **UU** conformation. The ASU is similar to that of the previous two structures, barring the fact that it contains two solvent molecules of acetonitrile (Figure 51). One solvent molecule acts as a bifurcated hydrogen bond acceptor to the protonated nitrogen donors of the imidazole groups while simultaneously donating a hydrogen bond ($\text{C}\cdots\text{N} = 3.374(1) \text{ \AA}$) to the second acetonitrile molecule (Table 24). Complex **23** forms 1D strands, in a fashion similar to those of **21** and **22**, running parallel to [010] (Figure 56).

All neighbouring strands interact with one another by means of weak OFF π - π interactions between phenyl (centroid-to-centroid distance = 3.818 \AA) and imidazole rings (centroid-to-centroid distances of 3.538 \AA and 3.794 \AA) to form a 2D sheet running parallel to (100) (Figure 57).

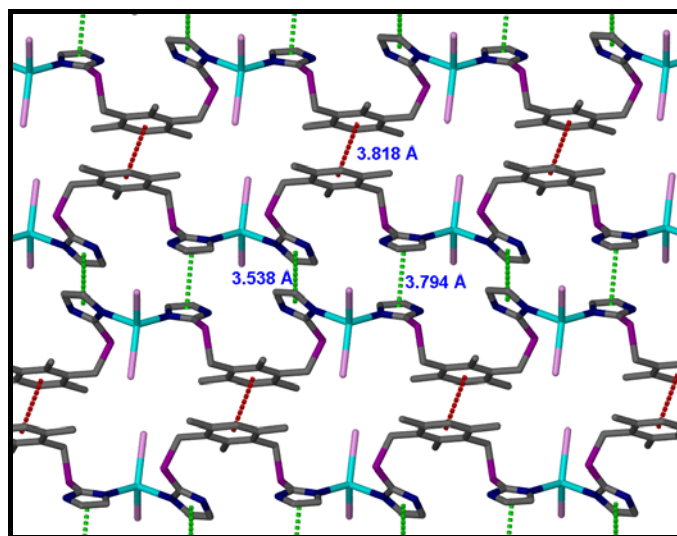


Figure 57. Capped-stick representation of the 2D layers formed in **23** as viewed along [100]. Hydrogen atoms and solvent molecules have been omitted for clarity and π - π stacking interactions have been shown as dashed red and green lines between phenyl and imidazole rings, respectively.

3.2.5.11 [CdL5I₂]_n·2nCH₃OH (24)

The ASU of **24** consists of one ligand **L5**, two iodine atoms and two methanol molecules (Figure 51). The Cd ion is coordinated by two iodine counter-ions and two imidazole nitrogens (from separate **L5** molecules), resulting in distorted tetrahedral coordination geometry around the metal ion (coordinating angles range from 101.49(14)°- 120.29(3)°). The metal centres are connected to one another *via* a single ligand **L5** to form a 1D zigzag polymeric strand running parallel to [101]. Each ligand assumes the **UD** conformation with the coordinating nitrogen atoms of the imidazole groups pointed in opposite directions. The dihedral angles between the planes of the imidazole and benzene rings are 37.9(3)° (for the ring containing N1) and 5.2(5)° (for the ring containing N20).

Each methanol molecule accepts a hydrogen bond from an uncoordinated nitrogen atom of an imidazole ring. One of these methanol molecules then donates a hydrogen bond (O...I2 = 3.450(6) Å) to one of the coordinated iodine molecules and, through this series of cooperative hydrogen bonds, adjacent 1D strands are linked into a 2D brick wall network in the (100) plane (see Table 24 for details of hydrogen bonding parameters). Each layer is then connected to one other layer through OFF π - π interactions between neighbouring imidazole rings (centroid-centroid distance = 3.569 Å). Figure 58 shows the progressive formation of these bilayers.

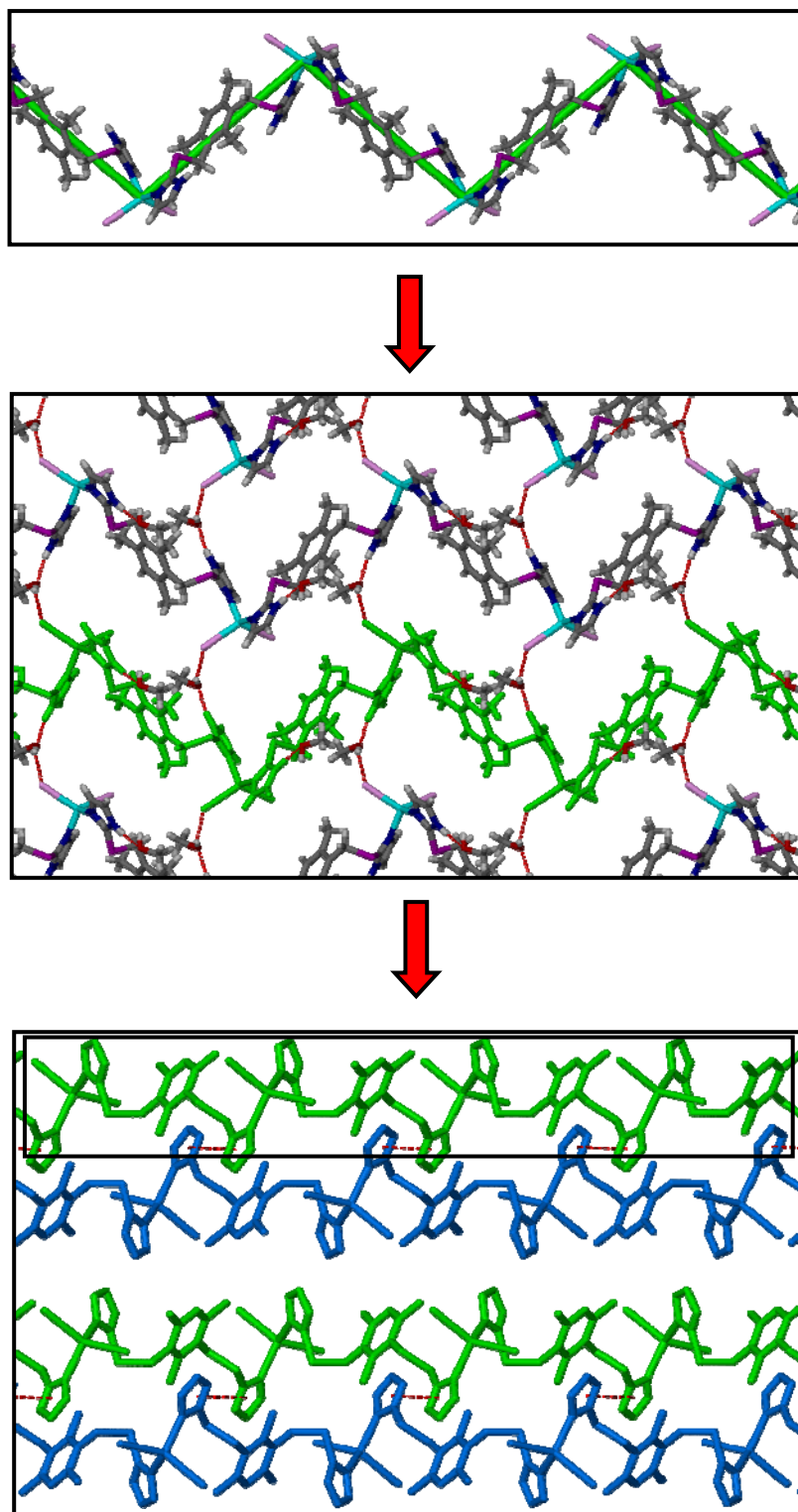


Figure 58. (Top) A single 1D strand of **24** running parallel to [101]; thick green lines are shown to emphasise the zigzag character of the strand. (Middle) A view perpendicular to (100) of the 2D brick wall network formed by hydrogen bonding; one 1D strand has been highlighted in green. (Bottom) The bilayers as viewed down [010]. π - π interactions have been drawn as dashed red lines from the centroid of one imidazole ring to the other, and the black rectangle encloses a single 2D layer as a point of reference. Hydrogen atoms and solvent molecules have been omitted for clarity. All molecules have been shown in the capped-stick metaphor.

Table 24. Hydrogen-bond geometry for complexes **21-24** (Å, °).

Complex 21				
D-H...A	D-H	H...A	D...A	D-H...A
N4-H4...O24	0.88	1.97	2.811(5)	161
N23-H23...O24	0.88	1.89	2.768(5)	173
O24-H24A...I1 ⁱ	0.99	2.63	3.508(3)	148
O24-H24B...I2 ⁱ	0.99	2.74	3.589(4)	145
Complex 22				
D-H...A	D-H	H...A	D...A	D-H...A
N4-H4...O24	0.88	2.00	2.836(5)	159
N23-H23...O24	0.88	1.96	2.812(5)	163
O24-H24A...I1 ⁱⁱ	0.84	2.67	3.436(3)	152
Complex 23				
D-H...A	D-H	H...A	D...A	D-H...A
N4-H4...N24	0.88	2.06	2.902(6)	160
N23-H23...N24	0.88	2.04	2.909(6)	168
C26-H26C...N27	0.98	2.74	3.374(1)	123
Complex 24				
D-H...A	D-H	H...A	D...A	D-H...A
N4-H4...O26	0.88	1.88	2.713(9)	158
N23-H23...O24	0.88	1.86	2.739(1)	173
O26-H26...I2 ⁱⁱⁱ	0.84	2.70	3.450(6)	150

Symmetry codes: (i) $x, -y + \frac{3}{2}, z - \frac{1}{2}$; (ii) $-x + \frac{3}{2}, -y + \frac{1}{2}, -z + 1$; (iii) $x, y + 1, z$.

Comparison of **21**, **22**, **23** and **24**

Four crystal structures were obtained from the reaction of **L5** and CdI₂ in either MeOH or MeCN. Even though the solution ligand-to-metal ratio was varied, a 1:1 ligand-to-metal ratio occurs in all of the solid-state structures. In all cases, a 1D polymeric strand is formed in which the Cd ion is tetrahedrally coordinated to two iodide ions and two nitrogen atoms from separate **L5** molecules. Each crystal structure also contains solvent molecules which participated in hydrogen bonding within the lattice. When the structures contain H₂O or MeOH as the solvent molecules (**21**, **22** and **24**), 1D strands are linked to adjacent strands by virtue of strong hydrogen bonds; weak π - π interactions served this purpose when the crystal structure contained MeCN (**23**).

The ligand adopts the UU conformation in complexes **21**, **22** and **23**. In all three of these structures the protonated nitrogen atoms of the imidazole rings donated hydrogen

bonds to the solvent molecules, and in this role of bifurcated hydrogen bond acceptor, the solvent molecule stabilises the **UU** conformation. This conformation also facilitates the formation of π - π stacking interactions between phenyl rings of adjacent 1D strands in **22** and **23**, and adjacent 2D layers in **21**.

In contrast to the three previously discussed structures, the two solvent molecules in **24** are not involved in bifurcated hydrogen bonding. Instead, each methanol molecule is hydrogen bonded to one uncoordinated nitrogen atom of an imidazole group. The ligand adopts the **UD** conformation, and the benzene rings are not able to form π - π stacking interactions. The imidazole rings are, however, oriented correctly for this type of interaction.

3.2.6 Single-crystal structures obtained from ligand L6

3.2.6.1 $[\text{CuL6Br}_2]_n$ (**25**)

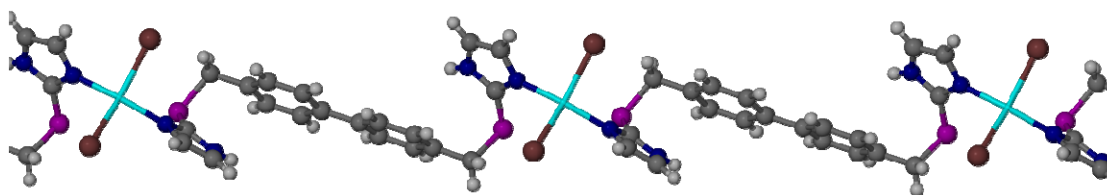


Figure 59. Ball-and-stick plot showing the 1D strands formed in **25**, as viewed perpendicular to $[101]$.

Crystals of **25** were obtained by the reaction of **L6** and CuBr_2 in a 1:1 ligand-to-metal molar ratio in MeOH, followed by slow evaporation of the solvent. The ASU of **25** consists of one half of a ligand **L6**, one half of a copper ion and one bromide ion. The copper ions are in a tetrahedrally distorted square planar coordination environment, and coordinate to two symmetry-related imidazole groups ($\text{Cu-N} = 1.954(5)$ Å) located *trans* with respect to each other, and two symmetry related bromide ions ($\text{Cu-Br} = 2.4221(7)$ Å) (see Table 25). The Cu ions are linked to one another by means of a single bridging ligand **L6**, in the **UD** conformation, to form a 1D polymeric strand running parallel to $[101]$. The uncoordinated nitrogen of the imidazole group in one strand donates a hydrogen bond to the ligated bromide ion in a neighbouring strand, and *via* this hydrogen bond neighbouring strands are connected to one another to form a 2D layer along (001) ($\text{N4}\cdots\text{Br1} = 3.508(5)$ Å). This arrangement is further stabilised by the

OFF π - π interactions between phenyl rings (centroid-to-centroid distance = 3.907 Å) and imidazole rings (centroid-to-centroid distance = 3.452 Å).

Table 25. Coordination geometric parameters for **25** (Å, °).

Complex 25			
Br1—Cu1	2.4221(7)	Cu1—N1	1.954(5)
Cu1—N1 ^{<i>i</i>}	1.954(5)	Cu1—Br1 ^{<i>i</i>}	2.4221(7)
N1 ^{<i>i</i>} —Cu1—N1	164.2(3)	N1 ^{<i>i</i>} —Cu1—Br1	92.26(15)
N1 ^{<i>i</i>} —Cu1—Br1 ^{<i>i</i>}	92.30(14)	N1—Cu1—Br1	92.30(14)
N1—Cu1—Br1 ^{<i>i</i>}	92.26(15)	Br1 ^{<i>i</i>} —Cu1—Br1	146.26(6)

Symmetry code: (*i*) $-x+1, y, z+1/2$.

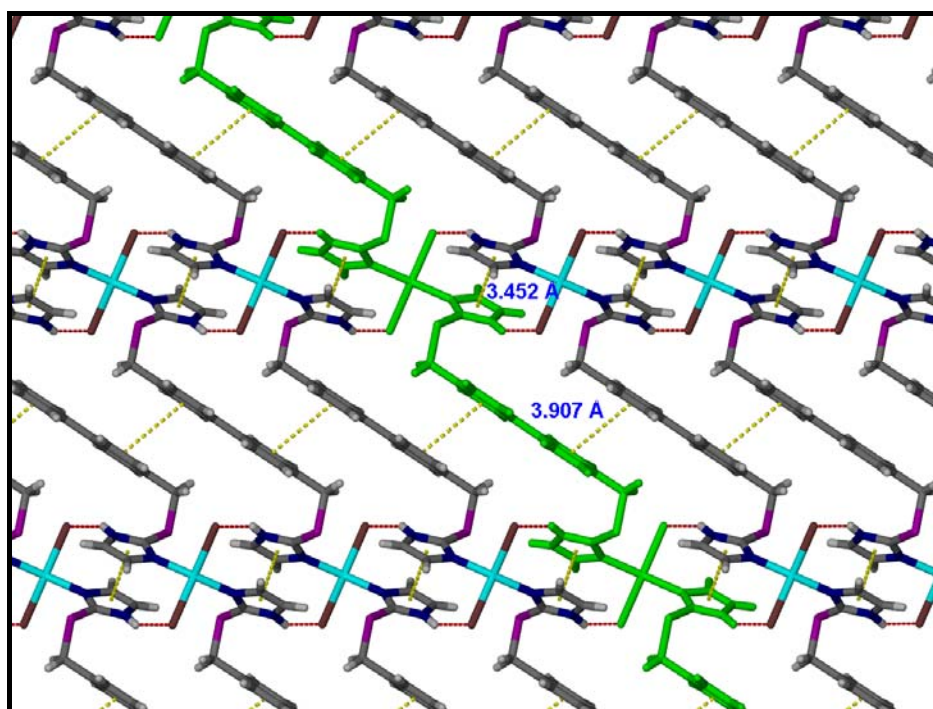


Figure 60. Capped-stick representation of the 2D layers formed in **25** as viewed along [010]. Hydrogen bonds have been shown as dashed red lines and π - π stacking interactions have been shown as dashed yellow lines between the centroids of respective rings.

3.2.6.2 [ZnL6Cl₃]·CH₃OH (26)

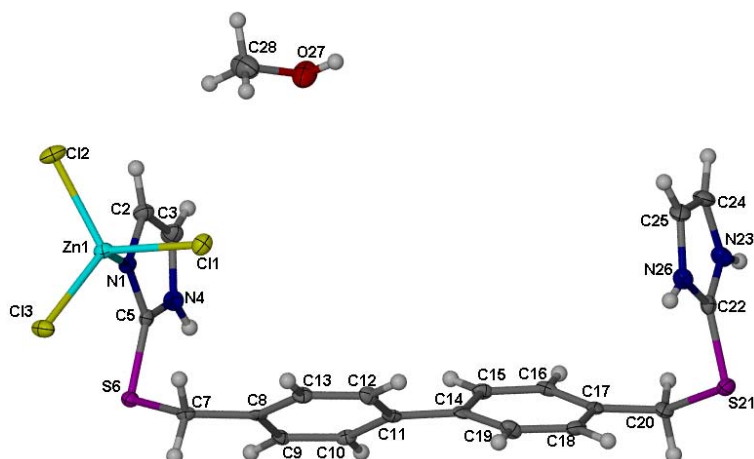


Figure 61. Atomic displacement (50% probability) plot showing the ASU of complex **26**. Hydrogen atoms are shown as spheres of arbitrary radius.

Single crystals of **26** were obtained by slow evaporation of a methanolic solution of **L6** and ZnCl₂ in a 1:1 molar ratio. The ASU of **26** consists of one protonated ligand **L6**, a zinc ion, three chloride ions and a methanol molecule. The two imidazole moieties of the ligand point upwards such that the ligand assumes an approximate U-shape, and the two benzene rings are twisted 40.61(9)° with respect to each another (Figure 61). At one end of the ligand the imidazole group is coordinated to a zinc ion, which is in a tetrahedral coordination environment; the remaining three coordination sites are occupied by chloride ions. The second imidazole group, situated at the opposite end of the ligand, is protonated at both nitrogen sites to balance the overall charge of the complex.

The discrete U-shaped complexes are connected *via* the donation of a hydrogen bond from N4 of one unit to Cl3 of an adjacent unit, to form a 1D chain running parallel to [100] (Figure 62). The nitrogens of the second imidazole ring (*i.e.* N23 and N26) and the methanol molecules cooperate in the formation of hydrogen bonds that link the 1D chains to one another to form 2D corrugated layers (see Table 26). As shown in Figure 63, within each layer adjacent 1D chains are related to one another by means of a glide operation parallel to [101], and as a result of this operation and the aforementioned hydrogen bonding the chains interdigitate. This arrangement is further stabilised by the OFF π - π interaction between imidazole rings of adjacent chains (centroid-to-centroid

distance = 3.935 Å). The 2D layers are related to one another by a crystallographic 2_1 screw axis.

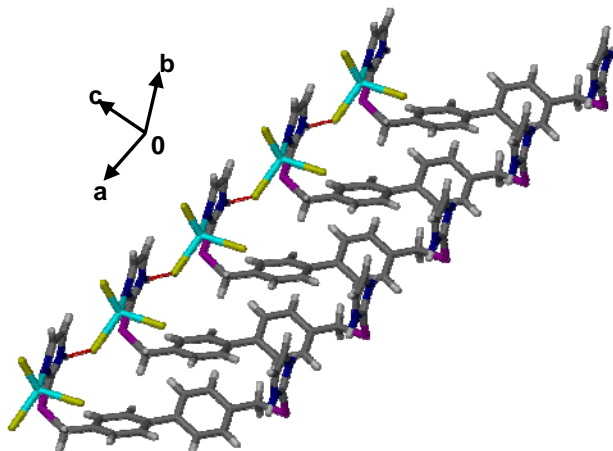


Figure 62. Capped-stick representation of a 1D chain formed in **26**. Hydrogen bonds have been shown as dashed red lines.

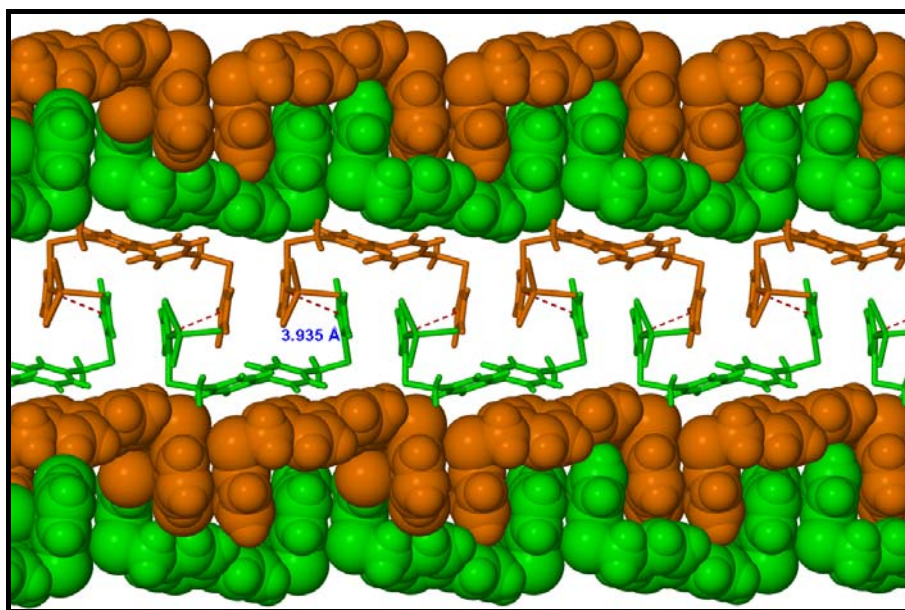


Figure 63. A set of three 2D layers viewed down [100]. Each orange strand is related to an adjacent green strand (and vice versa) within the same layer by a glide operation parallel to [101]. MeOH molecules have been omitted for clarity and π - π interactions have been shown as dashed red lines.

Table 26. Hydrogen-bond geometry for **26** (Å, °).

D-H...A	D-H	H...A	D...A	D-H...A
N4-H4...Cl3 ⁱ	0.88	2.47	3.308(4)	158.2
N23-H23...Cl1 ⁱⁱ	0.88	2.36	3.144(4)	148.2
N26-H26...O27 ⁱⁱⁱ	0.88	1.80	2.669(5)	167.0
O27-H27...Cl3 ^{iv}	0.84	2.34	3.148(4)	160.9

Symmetry codes: (i) $x-1, y, z$; (ii) $-x + \frac{3}{2}, -y + \frac{3}{2}, z - \frac{3}{2}$; (iii) $x - \frac{3}{2}, -y + \frac{3}{2}, z - \frac{3}{2}$; (iv) $x - \frac{1}{2}, -y + \frac{3}{2}, z - \frac{1}{2}$.

3.2.6.3 [ZnL6Cl₂]_n·nCH₃OH (27)

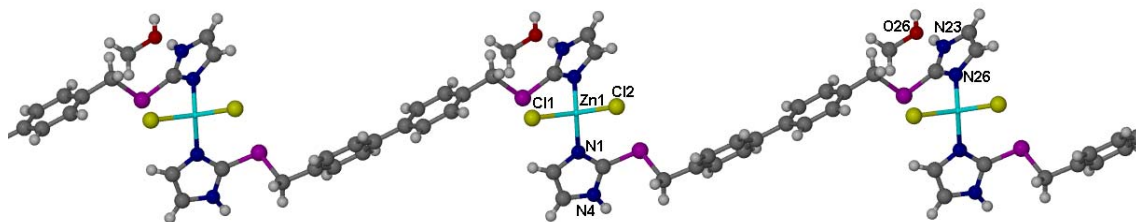


Figure 64. Ball-and-stick plot of the 1D strand formed in **27**, as viewed down [110].

Crystals of **27** were grown by slow evaporation of a methanolic solution of **L6** and ZnCl₂ in a 1:2 ligand-to-metal molar ratio. The ASU of **27** consists of one ligand **L6**, a Zn cation, two chloride anions and a MeOH molecule. Each metal centre is linked to an adjacent centre by means of one ligand **L6** (in the **UD** conformation) to form an infinite 1D strand running parallel to [101] (Figure 64). In each ligand molecule the two benzene rings are twisted 30.6(4)° with respect to each other. Each copper ion is in a tetrahedral coordination environment and coordinates to two distinct **L6** ligands, and two chloride ions, with coordinating angles ranging from 104.6(2)°-113.9(2)°. One of the protonated nitrogens from one of the imidazole rings is hydrogen bonded to the methanol molecule (N23···O26 = 3.745(1) Å), which in turn donates a hydrogen bond to a coordinated chloride ion (O26···Cl2 = 3.138(9) Å); the second chloride ion is hydrogen bonded to the other protonated nitrogen of the second imidazole ring (N4···Cl1 = 3.106(9) Å). By virtue of these hydrogen bonds the 1D strands are linked into an infinite 3D network which forms canted square channels along [100] (Figure 65-top). These channels are sufficiently large to accommodate a second 3D network where the vertices of one net fill the voids of the second net, thus creating a doubly interpenetrated structure sustained by both coordinative and hydrogen bonding. This has been represented in Figure 65, and the two interpenetrated networks have been coloured orange and blue.

Table 27. Hydrogen-bond geometry for **27** (Å, °).

D-H···A	D-H	H···A	D···A	D-H···A
N4-H4···Cl1 ⁱ	0.88	2.31	3.106(9)	151.0
N23-H23···O26 ⁱⁱ	0.88	1.87	2.745(1)	171.1
O26-H26···Cl2 ⁱⁱⁱ	0.84	2.31	3.138(9)	168.0

Symmetry codes: (i) $x+1, y, z$; (ii) $x+1, y, z+1$; (iii) $x, y+1, z$.

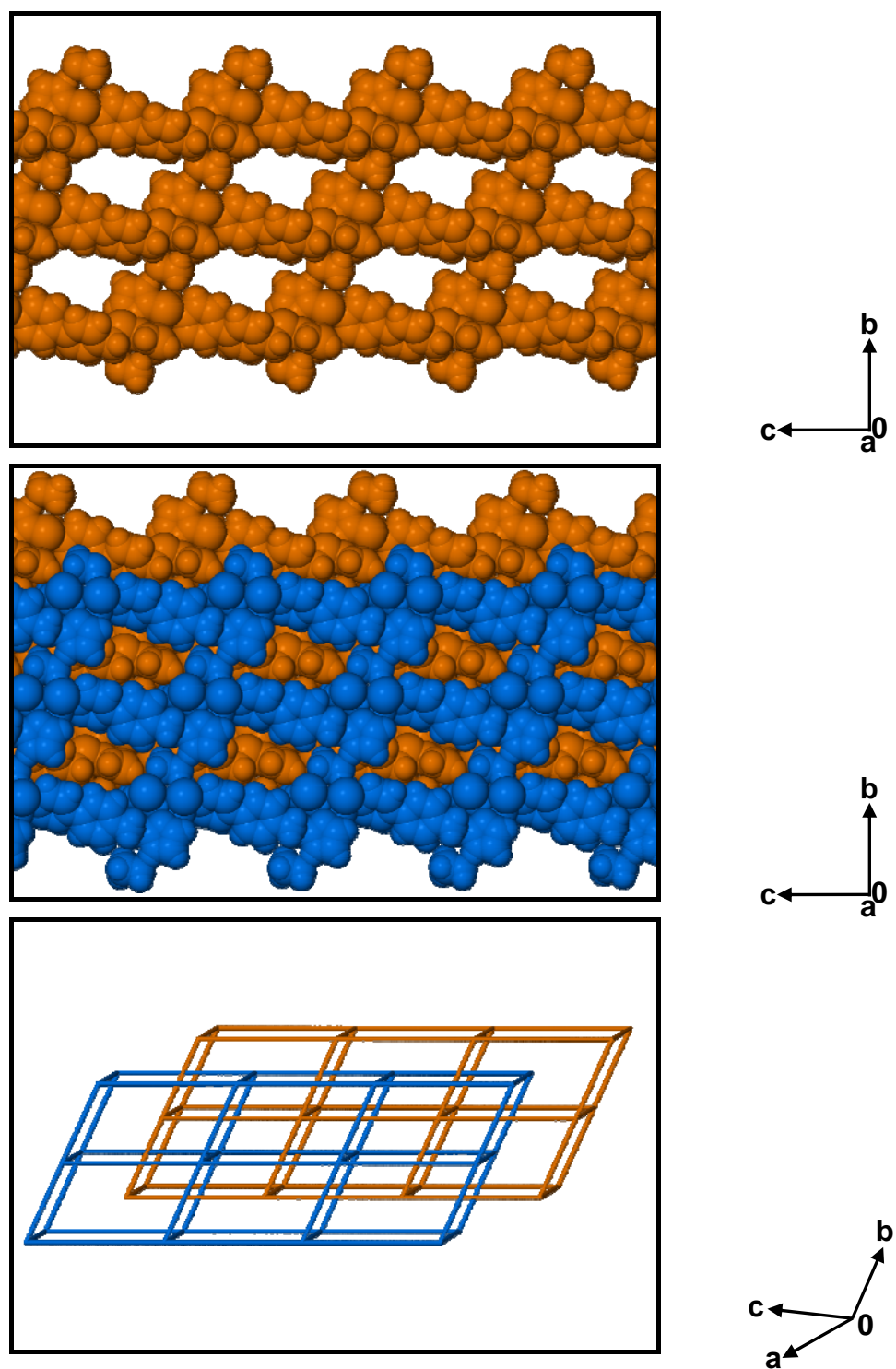


Figure 65. (Top) Space-filled projection showing the canted square channels formed by hydrogen bonding in **27**, as viewed down [100]. (Middle) Space-filled projection of the doubly interpenetrated network; the vertices of the blue net fill the voids of the orange net, as viewed down [100]. (Bottom) A simplification of the interpenetrated nets.

Comparison of the structures obtained from ligand **L6**

Three structures single crystal structures were elucidated from the reaction of **L6** with a variety of metal salts. In complex **26** the ligand adopts the **UU** conformation, and discrete U-shaped units are formed which stack to create 1D chains. The MeOH solvent molecules play an integral role in connecting the 1D chains into 2D layers.

In contrast to **26**, both **25** and **27** form 1D polymeric strands with the ligand in the **UD** conformation. In **25** the 1D strands are linked into a 2D layer *via* the donation of a hydrogen bond from a protonated nitrogen of the imidazole group to a ligated bromide ion. In **27** the presence of solvent molecules in the crystal structure serve to link the 1D strands into a 3D network with canted square channels. These channels were sufficiently large to accommodate a second 3D network, thus forming a doubly interpenetrated structure. As seen in Figure 65, the only way that the orange net could be separated from the blue net would be to break either a coordinative or a hydrogen bond and, as such, this structure conforms to the classic description of interpenetrating nets propounded by Wells,⁴⁷ these are nets that “cannot be separated without breaking links”. The topic of interpenetrating nets is an interesting one, and although it is not the case in this particular example, it has been shown that this phenomenon does not necessarily preclude the formation of porous materials.^{48,49}

3.3 GENERAL CONCLUSIONS

The successful synthesis of six novel ligands that have reacted with a selection of transition metals to form coordination complexes with interesting architectures and topologies has been presented here. With regard to the aims of the present study, the desired structural arrangement would have had two molecules of the ligand, each in a U-shaped conformation, with both ligands complexed to two metals cations to form a discrete closed-ring structure with voids sufficiently large enough to absorb gases. Although we were unable to obtain any structures with this preferred topology, we have been able to analyse, by means of SCD, a total of 27 novel coordination complexes: two coordination complexes containing **L1**, three containing **L2**, eight containing **L3**, eleven containing **L5** and three containing **L6**. It is unclear why **L4** did not form any coordination complexes. Since single crystals of the free ligand were the only crystals attainable in any of the vials containing **L4**, perhaps the simplest explanation is that these represent the most stable form of this ligand at room temperature.

Coordination bonds formed from the association of metal cations with **L1-L6** chiefly result from the donation of the lone electron pair of the imidazole groups to the metal cation, and in two cases (complexes **6** and **14**) from the donation of a lone pair situated on a sulphur atom, to form positively charged cationic complexes. Accordingly, charge-balancing counter-ions are present in the crystal lattice, either coordinated to the metal centre (as is the case with all of the compounds containing halogenated counter-ions) or uncoordinated, to participate in weaker interactions such as hydrogen bonding.

The protonated nitrogen atoms of the imidazole groups donate hydrogen bonds in every crystal structure to either a counter-ion or a solvent molecule. These interactions, together with π - π stacking interactions lead to an increase in structural dimensionality and interesting topologies. Other secondary, non-covalent interactions that feature exclusively in the crystal structures containing Ag cations are metal- π and metal-metal interactions. Of the eleven structures obtained with silver, only one structure (complex **6**) featured metal-metal interactions, but with the exception of complex **17**, all contained Ag- π interactions.

In general, the reaction of CdI₂ with ligands **L2**, **L3** and **L5** leads to the formation of extended 1D polymeric systems. Seven of the eight structures obtained with CdI₂ form 1D polymeric strands in which the Cd centres are linked to one another *via* a single bridging ligand. The remaining structure forms infinite 1D ladders where the

ligand molecules represent the rungs of the ladder. This is in stark contrast to the discrete complexes generally formed by the reaction of the ligands with silver. Nine of the eleven structures obtained with silver form 0D mononuclear, dinuclear or trinuclear complexes and only two form 1D polymeric strands. Our results also show that the dimensionality of the complexes obtained by the reaction of Ag-salts and **L5** are not dramatically affected by a change in counter-ion.

We have also shown that, owing to the flexible nature of the ligands they are able to assume a variety of conformations in the solid state. These conformations differ not only in the positions of the imidazole rings with respect to the central aromatic spacer, but also in the orientations of the coordinating nitrogen atoms. Our results show that the ligands are able to adopt different conformations according to the geometric needs of different metal ions; however, no clear pattern has emerged that might allow us to predict the conformation, given the identity of the metal ion, counter-ions and solvent system. It was calculated that the different conformations for **L2** in complexes **3** and **4** have different energies and that intermolecular interactions play an important role in stabilising strained conformations within the crystal structure. The Hirshfeld surface implemented in *CrystalExplorer* was shown to be an invaluable tool for visualising these stabilising intermolecular interactions.

Finally, with regard to the initial aims of this study *i.e.* the synthesis of porous materials based on the “donut-shaped” metal-organic host design, we speculate that ligands **L1-L6** may be too flexible to facilitate the formation of the anticipated ring structure. We suggest then that modifying the existing ligands slightly by removing the methyl linkage between the sulphur bridge and the aromatic core would lead to a more rigid ligand that might enhance its ability to complex metals in the desired manner.

REFERENCES

1. B. Moulton and M. J. Zaworotko, *Chem. Rev.*, **2001**, 101, 1629.
2. C. Janiak, *Dalton Trans.*, **2003**, 2781.
3. G. R. Desiraju, *J. Mol. Struct.*, **1996**, 374, 191.
4. P. J. Langley and J. Hulliger, *Chem. Soc. Rev.*, **1999**, 28, 279.
5. G. R. Desiraju, *Crystal Engineering, the Design of Organic Solids*, Elsevier, Amsterdam, **1989**.
6. A. S. Batsanov, J. C. Collings, R. M. Ward, A. E. Goeta, L. Porres, A. Beeby, J. A. K. Howard, J. W. Steed and T. B. Marder, *Crystengcomm*, **2006**, 8, 622.
7. H. Li, M. Eddaoudi, M. O'Keefe and O. M. Yaghi, *Nature*, **1999**, 402, 276.
8. S. Norro, S. Kitagawa, M. Kondo and K. Seki, *Angew. Chem. Int. Ed*, **2000**, 39, 2081.
9. L. Dobrzańska, G. O. Lloyd, H. G. Raubenheimer and L. J. Barbour, *J. Am. Chem. Soc.*, **2006**, 128, 698.
10. P. Sozzani, S. Bracco, A. Comotti, L. Ferretti and R. Simonutti, *Angewandte Chemie-International Edition*, **2005**, 44, 1816.
11. J. Atwood, L. J. Barbour, P. K. Thallapally and T. B. Wirsig, *Chem. Commun.*, **2005**, 51.
12. J. L. Atwood, L. J. Barbour and A. Jerga, *Angew. Chem. Int. Ed*, **2004**, 43, 2948.
13. P. K. Thallapally, G. O. Lloyd, T. B. Wirsig, M. W. Bredenkamp, J. L. Atwood and L. J. Barbour, *Chem. Commun.*, **2005**, 5272.
14. L. R. MacGillivray, J. L. Reid and J. A. Ripmeester, *J. Am. Chem. Soc.*, **2000**, 122, 7817.
15. K. Tanaka and F. Toda, *Chem. Rev.*, **2000**, 100, 1025.
16. B. Sui, J. Fan, T. A. Okamura, W. Y. Sun and N. Ueyama, *Solid State Sciences*, **2005**, 7, 969.
17. I. Kuzu, I. Krummenacher, J. Meyer, F. Armbruster and F. Breher, *Dalton Transactions*, **2008**, 5836.
18. W. Y. Sun, J. Fan, T. Okamura, J. Xie, K. B. Yu and N. Ueyama, *Chemistry-a European Journal*, **2001**, 7, 2557.
19. G. C. Xu, Y. J. Ding, T. A. Okamura, Y. Q. Huang, G. X. Liu, W. Y. Sun and N. Ueyama, *Crystengcomm*, **2008**, 10, 1052.
20. L. Rulisek and J. Vondrasek, *J. Inorg. Biochem.*, **1998**, 71, 115.

21. C. L. Cahill, D. T. de Lill and M. Frisch, *Crystengcomm*, **2007**, 9, 15.
22. J. S. Fleming, K. L. V. Mann, C. A. Carraz, E. Psillakis, J. C. Jeffery, J. A. McCleverty and M. D. Ward, *Angew. Chem. Int. Ed*, **1998**, 37, 1279.
23. L. Dobrzanska, D. J. Kleinhaus and L. J. Barbour, *New J. Chem.*, **2008**, 32, 813.
24. J. Fan, H. F. Zhu, T. A. Okamura, W. Y. Sun, W. X. Tang and N. Ueyama, *Inorg. Chem.*, **2003**, 42, 158.
25. L. Dobrzanska, G. O. Lloyd and L. J. Barbour, *New J. Chem.*, **2007**, 31, 669.
26. S. Leininger, B. Olenyuk and P. J. Stang, *Chem. Rev.*, **2000**, 100, 853.
27. L. Dobrzanska, G. O. Lloyd, T. Jacobs, I. Rootman, C. L. Oliver, M. W. Bredenkamp and L. J. Barbour, *J. Mol. Struct.*, **2006**, 796, 107.
28. L. Dobrzańska, H. G. Raubenheimer and L. J. Barbour, *Chem. Commun.*, **2005**, 5050.
29. G. O. Lloyd, J. Alen, M. W. Bredenkamp, E. J. C. de Vries, C. Esterhuysen and L. J. Barbour, *Angew. Chem. Int. Ed*, **2006**, 45, 5354.
30. L. Dobrzańska, G. O. Lloyd, H. G. Raubenheimer and L. J. Barbour, *J. Am. Chem. Soc.*, **2005**, 127, 13134.
31. C. Fan, C. B. Ma, C. N. Chen, F. Chen and Q. T. Liu, *Inorg. Chem. Commun.*, **2003**, 6, 491.
32. W. Y. Sun, J. Xie, T. Okamura, C. Huang and N. Ueyama, *Chem. Commun.*, **2000**, 1429.
33. M. A. Spackman and P. G. Byrom, *Chem. Phys. Lett.*, **1997**, 215.
34. A. N. Khlobystov, A. J. Blake, N. R. Champness, D. A. Lemenovskii, A. G. Majouga, N. V. Zyk and M. Schroder, *Coord. Chem. Rev.*, **2001**, 222, 155.
35. L. Dobrzanska and G. O. Lloyd, *Acta Crystallographica Section E-Structure Reports Online*, **2006**, 62, M1638.
36. P. J. Stephens, F. J. Devlin, C. F. Chabalowski and M. J. Frisch, *J. Phys. Chem.*, **1994**, 98, 11623.
37. *Gaussian 03, Revision B.05*; M. J. T. Frisch, G. W.; Schlegel, H. B.; Scuseria, G. E.; Robb, M. A.; Cheeseman, J. R.; Montgomery, Jr., J. A.; Vreven, T.; Kudin, K. N.; Burant, J. C.; Millam, J. M.; Iyengar, S. S.; Tomasi, J.; Barone, V.; Mennucci, B.; Cossi, M.; Scalmani, G.; Rega, N.; Petersson, G. A.; Nakatsuji, H.; Hada, M.; Ehara, M.; Toyota, K.; Fukuda, R.; Hasegawa, J.; Ishida, M.; Nakajima, T.; Honda, Y.; Kitao, O.; Nakai, H.; Klene, M.; Li, X.; Knox, J. E.; Hratchian, H. P.; Cross, J. B.; Bakken, V.; Adamo, C.; Jaramillo, J.; Gomperts,

- R.; Stratmann, R. E.; Yazyev, O.; Austin, A. J.; Cammi, R.; Pomelli, C.; Ochterski, J. W.; Ayala, P. Y.; Morokuma, K.; Voth, G. A.; Salvador, P.; Dannenberg, J. J.; Zakrzewski, V. G.; Dapprich, S.; Daniels, A. D.; Strain, M. C.; Farkas, O.; Malick, D. K.; Rabuck, A. D.; Raghavachari, K.; Foresman, J. B.; Ortiz, J. V.; Cui, Q.; Baboul, A. G.; Clifford, S.; Cioslowski, J.; Stefanov, B. B.; Liu, G.; Liashenko, A.; Piskorz, P.; Komaromi, I.; Martin, R. L.; Fox, D. J.; Keith, T.; Al-Laham, M. A.; Peng, C. Y.; Nanayakkara, A.; Challacombe, M.; Gill, P. M. W.; Johnson, B.; Chen, W.; Wong, M. W.; Gonzalez, C, Pittsburgh PA, Gaussian, Inc **2003**.
38. J. T. H. Dunning and P. J. Hay, *Modern Theoretical Chemistry*, Plenum, New York, **1994**.
39. D. G. Hay, H. Jaeger and G. W. West, *J. Phys. Chem.*, **1985**, 89, 1070.
40. *CrystalExplorer 1.6*; S. K. Wolff, D. J. Grimwood, J. J. McKinnon, D. Jayatilaka and M. A. Spackman, University of Western Australia, Perth, **2006**.
41. M. A. Omary, T. R. Webb, Z. Assefa, G. G. Shankle and H. H. Patterson, *Inorg. Chem.*, **1998**, 1380.
42. W. C. McCrone, in *Polymorphism in Physics and Chemistry of the Organic Solid State*, eds. D. Fox, M. M. Labes and A. Weissburg, Interscience, New York, **1965**, p. 726.
43. J. Bernstein, *Polymorphism in Molecular Crystals*, Oxford University Press, Oxford, Great Britan, **2002**.
44. J. Bernstein, in *Conformational Polymorphism in Organic Solid State Chemistry*, ed. G. R. Desiraju, Elsevier, London, **1987**, p. 471.
45. Protein Data Bank, <http://pdb.pdb.bnl.gov>.
46. F. H. Allen, J. E. Davies, J. J. Galloy, O. Johnson, O. Kennard, C. F. Macrae, E. M. Mitchell, G. F. Mitchell, J. M. Smith and D. G. Watson, *J. Chem. Inf. Comput. Sci.*, **1991**, 31, 187.
47. A. F. Wells, *Three-Dimensional Nets and Polyhedra*, Wiley, New York, **1977**.
48. T. M. Reineke, M. Eddaoudi, D. Moler, M. O'Keeffe and O. M. Yaghi, *J. Am. Chem. Soc.*, **2000**, 122, 4843.
49. M. Kondo, M. Shimamura, S. Noro, S. Minakoshi, A. Asami, K. Seki and S. Kitagawa, *Chem. Mater.*, **2000**, 12, 1288.

CHAPTER 4

Preliminary Investigation of the Gas Sorption Properties of a Novel Hemicarcerand

This chapter describes a preliminary investigation of the structural, thermal and sorption properties of a novel coordination compound formed by the reaction of 1,3-bis(1-imidazolyl-2-thione)-2,4,6-trimethylbenzene (**L5**) and $\text{Ni}(\text{NO}_3)_2 \cdot 6\text{H}_2\text{O}$. The author concedes at the outset that the structure reported in this section is not of high quality, despite all reasonable attempts made to improve it. It would, however, be unfortunate to ignore the interesting data at hand and the notion that this result provides a firm foundation for further studies. A single-crystal X-ray diffraction study of the complex reveals the formation of a cage-like hemicarcerand in which four **L5** molecules are coordinated at their extremities to two Ni^{2+} ions. This forms a discrete 0D dinuclear complex with individual cavities large enough to accommodate guest molecules. Indeed, preliminary gas sorption studies suggest that this compound is *transiently* porous and capable of absorbing H_2 and, to a lesser extent, CO_2 . Although the topology of the complex does not adhere completely to our initial design principle, our aim to develop novel porous coordination compounds has been realised in this structure.

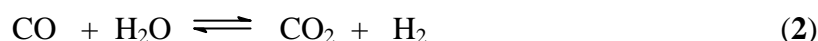
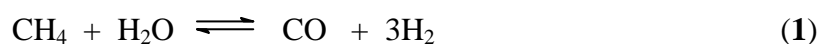
4.1 INTRODUCTION

The current surge in research attempts aimed at alternative fuel sources can be attributed to the dwindling fossil fuel reserves and the increasingly unacceptable levels of pollutants and greenhouse gases associated with this primary source of energy.¹ Of the several proposed alternative energy technologies, particular attention is being paid to the exploitation of hydrogen gas as an alternate energy carrier due to its high energy-density by weight.^{2,3} However, in order for hydrogen to be implemented as a viable energy source, several obstacles need to be overcome, one of which is hydrogen storage. Storing hydrogen at high pressures is dangerous and it has been shown that liquefied hydrogen has a lower energy-density by volume than

conventional fuels such as gasoline.² Several methods have been developed in an attempt to solve this problem. One such method involves storing hydrogen as a chemical hydride and then decomposing the storage material to yield hydrogen gas as required.⁴ Unfortunately, the high pressures and temperatures needed for hydride formation and subsequent hydrogen release, as well as the kinetic barrier that has to be overcome from the hydriding and dehydriding process, renders this method impractical. Another approach entails absorbing molecular hydrogen into a porous crystalline storage material. This method offers an advantage over the hydride method in that the hydrogen does not need to dissociate and recombine when utilised.

The study of porous crystalline materials has, until recently, been exclusively concerned with zeolites.⁵ However, in the last decade this field has grown to include organic compounds⁶⁻¹⁰ and coordination polymers.¹¹⁻¹⁵ Although metal-organic frameworks (MOFs)^{11,16} and selected organic host compounds¹⁰ have already been studied extensively for their hydrogen sorption capabilities, the target of 6.0 weight percentage (wt%) storage of H₂ (as set out by the U.S. Department of Energy¹⁷) has yet to be met. This necessitates further studies into novel porous crystalline materials.

Currently the commercial procedure for the production of hydrogen involves a two-step reaction *i.e.* steam reforming of natural gas and the water-gas shift reaction (see reactions **1** and **2** respectively).¹⁰



The final step involves purification of H₂ by the removal of impurities that largely constitute CO₂. Thus an absorbent which shows selectivity between CO₂ and H₂ would be essential in this purification process; hence our interest in both the H₂ as well as the CO₂ sorption properties of our materials.

The macromolecular host capsule described in this chapter can broadly be classified as a carcerand and, more specifically, as a hemicarcerand. The term carceplex was first introduced by the Nobel Laureate Donald J. Cram in 1983¹⁸ to describe the permanent incarceration of molecules *via* the synthesis of a closed-surface spherical molecule. He subsequently reported the first example of a carceplex in 1985¹⁹ that was only fully characterised in 1989.²⁰ A formal definition of a carceplex has been offered by J.C. Sherman as "... a closed surface compound that

permanently entraps guest molecules or ions within its shell, such that guest escape can only occur by rupture of covalent bonds."²¹ Hemicarceplexes differ from carceplexes in that the portals of the shell have the ability to allow guest egression to occur without significant disruption to the host framework *i.e.* guest molecules may enter and exit the capsule without breaking any covalent bonds.²² A characteristic of this type of complex is that it must be kinetically stable in order to allow characterisation at normal temperatures. They differ from clathrates (hosts with extramolecular cavities) in that empty hemicarceplexes retain their molecular structure and clathrates tend to decompose upon removal of the guest. The distinction between the terms hemicarcerand and a hemicarceplex is that the former refers to the capsule in the absence of any guests and the latter is used to describe the hemicarcerand-guest complex.

The design principle whereby two hemispheres of a hemicarcerand are separated by four equally spaced linking units along the longitudinal axis of the shell has led to a variety of different hosts and host-guest complexes.²³ However, the literature is beset with examples of purely organic hemicarceplexes and there is very little precedent for metal-containing complexes of this kind.

Carceplexes and hemicarceplexes provide a unique perspective by which to examine non-covalent interactions. Since their inception these systems have been studied in the field of crystal engineering for the valuable insight that they offer to the process of templation and for their ability to entrap reactive intermediates. Closely related to carcerands and hemicarcerands are catenanes,²⁴ rotaxanes²⁵ and fullerenes,²⁶ but as these compounds are beyond the scope of this study they will not be discussed further. For more information regarding carceplexes and hemicarceplexes, the reader is referred to the review by Jasat and Sherman.²³

4.2 SINGLE CRYSTAL STRUCTURE OF [Ni₂(L5)₄](NO₃)₄·H₂O (28)

Crystals suitable for X-ray diffraction analysis of **28** were obtained by the reaction of Ni(NO₃)₂·6H₂O with **L5** (1:1 molar ratio) in MeOH, followed by slow evaporation of the solvent. Single-crystal structural analysis of **28** revealed a dinuclear, macrotricyclic complex in which two Ni²⁺ ions are linked by four bridging ligands to form a cationic molecular cage [Ni₂L5₄]⁴⁺. This arrangement adheres to the topological requirements of a tetragonal prism, *i.e.* two 4-connecting nodes linked

together by four node-to-node connections²⁷ and this topology has been encountered in previous M_2L_4 cage structures²⁸⁻³¹ (Figure 1).

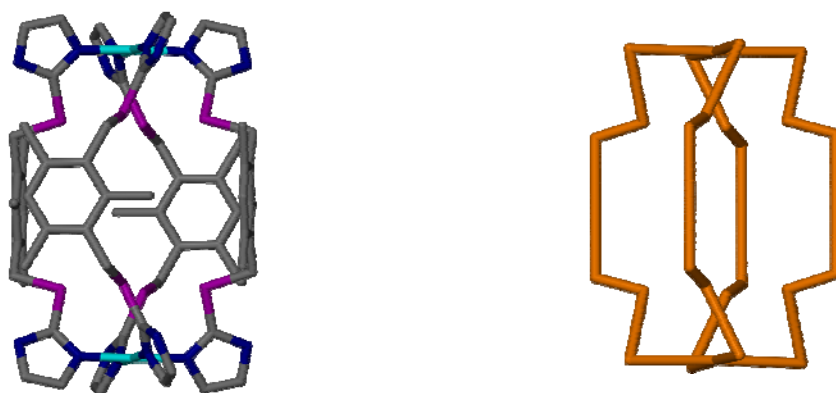


Figure 1. Capped-stick representation of the cage-like hemicarcerand formed in **28** (left). The cage adheres to the topological requirements of a tetragonal prism (right).

The compound crystallises in the tetragonal space group $I4/m$, and the ASU consists of one quarter of the $[Ni_2L_5_4]^{4+}$ cage. Within the complex the coordination environment about each Ni^{2+} ion is square planar and each metal centre is coordinated to four N atoms from four independent **L5** ligands. The high symmetry of the system necessitates that all four of the Ni-N bonds are identical and all of the metal-centred angles approach the ideal values of 90° and 180° (Table 1). Each ligand assumes the **UU** conformation and the planes of the imidazole rings are all approximately orthogonal to the planes of the linking mesitylene groups.

The dimensions of the $[Ni_2L_5_4]^{4+}$ cage are defined by the Ni...Ni separation of 11.039 Å and the distance between the centroids of the parallel mesitylene rings of 9.268 Å. The guest-accessible space within each cage was determined using the program MSROLL^{32,33} and was calculated to be *ca.* 62 Å³ using a probe radius of 1.55 Å (Figure 2). It is due to the presence of this cavity that the entire cage-like complex may be viewed as a hemicarcerand, in the absence of a guest, and a hemicarceplex when a guest molecule is present. External to the cage there is an uncoordinated water molecule. This water molecule is disordered equally over two positions with a total site occupancy of 0.5 (*i.e.* the SOF of each water molecule is 0.25). Each disordered molecule is situated on either side of the $\frac{4}{m}$ special position, $(0,0, \frac{1}{2})$, along [001] at

the apex of a *pseudo* square-based pyramid and is 2.549(1) Å from the metal centre.* The occupancy of the water molecules is somewhat perplexing as the total site occupancy for the disordered pair should amount to 0.25 in order to maintain a 0.5:1 (water:Ni²⁺) stoichiometric relationship with the Ni²⁺ centres (*i.e.* 0.125 each) as is required by the space available between two consecutive discrete units (the intramolecular Ni...Ni separation is 6.003(1) Å); this merits further investigation.

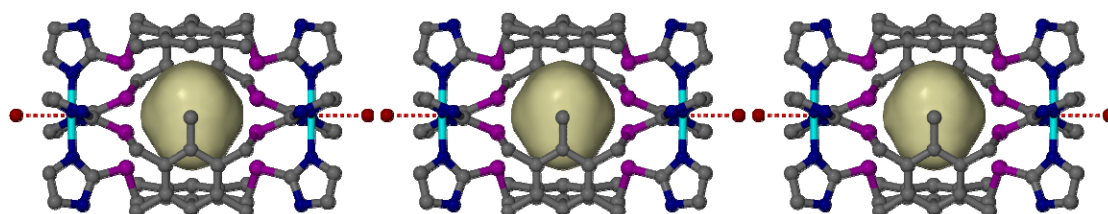


Figure 2. Ball-and-stick representation of a 1D column formed in **28**, as viewed down [100]. The guest accessible space within each cage (as determined by MSROLL) has been represented as a semi-transparent yellow surface. Hydrogen atoms have been omitted for clarity, oxygen atoms are shown as red spheres and Ni...O interactions are shown as dashed red lines.

Adjacent [Ni₂L₅]⁴⁺ cages form a 1D column with their Ni...Ni axes parallel to [001]. Each column is surrounded by four identical columns that are offset from one another along [001] by half a structural unit (Figure 3, left). As a result of this alternating stacking arrangement, small channels are formed between the 1D columns (Figure 3, right), which are thought to contain the NO₃⁻ counter-ions, *vide infra*.

The overall charge of the cationic cage is +4, requiring four charge balancing NO₃⁻ counter-ions. Dispersed residual electron density peaks were located only in the channels between the 1D columns and not within the cavities of the [Ni₂L₅]⁴⁺ cages. Although symmetry-imposed disorder precluded modelling this electron density as NO₃⁻ it is not unreasonable to ascribe the electron density in the channels to these counter-ions. Using a probe radius of 1.55 Å, it was determined using MSROLL that each anion-filled channel is comprised of discrete cavities of *ca.* 115 Å³, arranged

* The average distance reported for a Ni-O bond is 2.079(4) Å.³⁴ Therefore the Ni-O separation of 2.549(1) Å observed in **28** is too long to be considered a coordination bond. This long separation is likely due to steric hinderance from the imidazole groups.

head-to-head in a continuous fashion along [001]. A single channel has been shown in Figure 4.

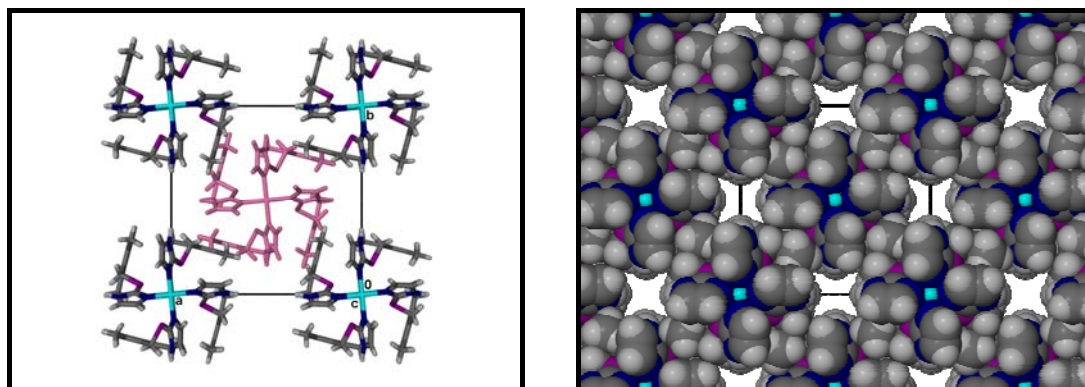


Figure 3. Capped-stick representation of the columns formed in **28**. Each column is surrounded by four identical columns, offset from one another by half a structural unit. A single column has been coloured pink for clarity (left). Spaced-filled projection of the packing arrangement in **28**, to show the channels formed between the 1D columns (right). Both are viewed down [001].

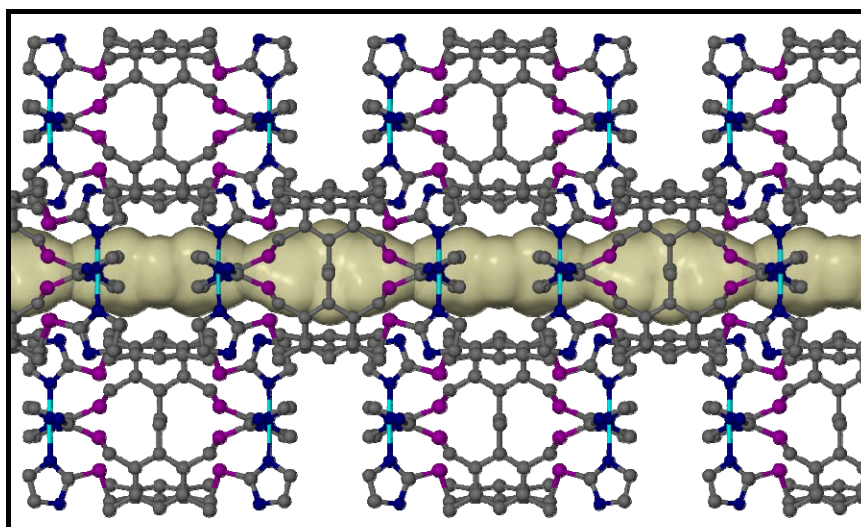


Figure 4. Packing arrangement of **28** showing a single channel formed by the stacking of the 1D columns, as viewed down [100]. The discrete cavities of *ca.* 115 Å³, as determined by MSROLL (*r* = 1.55 Å), arranged head-to-head within each channel have been represented as a yellow surface. The [Ni₂L₅]⁴⁺ molecular cages have been shown in the ball-and-stick metaphor.

Table 1. Coordination geometric parameters for **28** (Å, °).

Interatomic Separations (Å)			
Ni1—N13 ⁱ	1.972(9)	Ni1—N13 ⁱⁱ	1.972(9)
Ni1—N13	1.972(9)	Ni1—N13 ⁱⁱⁱ	1.972(9)
Interatomic Angles (°)			
N13 ⁱ —Ni1—N13	89.971(1)	N13 ⁱ —Ni1—N13	89.971(1)
N13 ⁱ —Ni1—N13 ⁱⁱ	89.971(1)	N13 ⁱ —Ni1—N13 ⁱⁱ	89.971(1)
N13—Ni1—N13 ⁱⁱ	177.4(5)	N13—Ni1—N13 ⁱⁱ	177.4(5)

Symmetry codes: (i) $y, -x, z$; (ii) $-x, -y, z$; (iii) $-y, x, z$

4.3 THERMAL ANALYSIS OF **28**

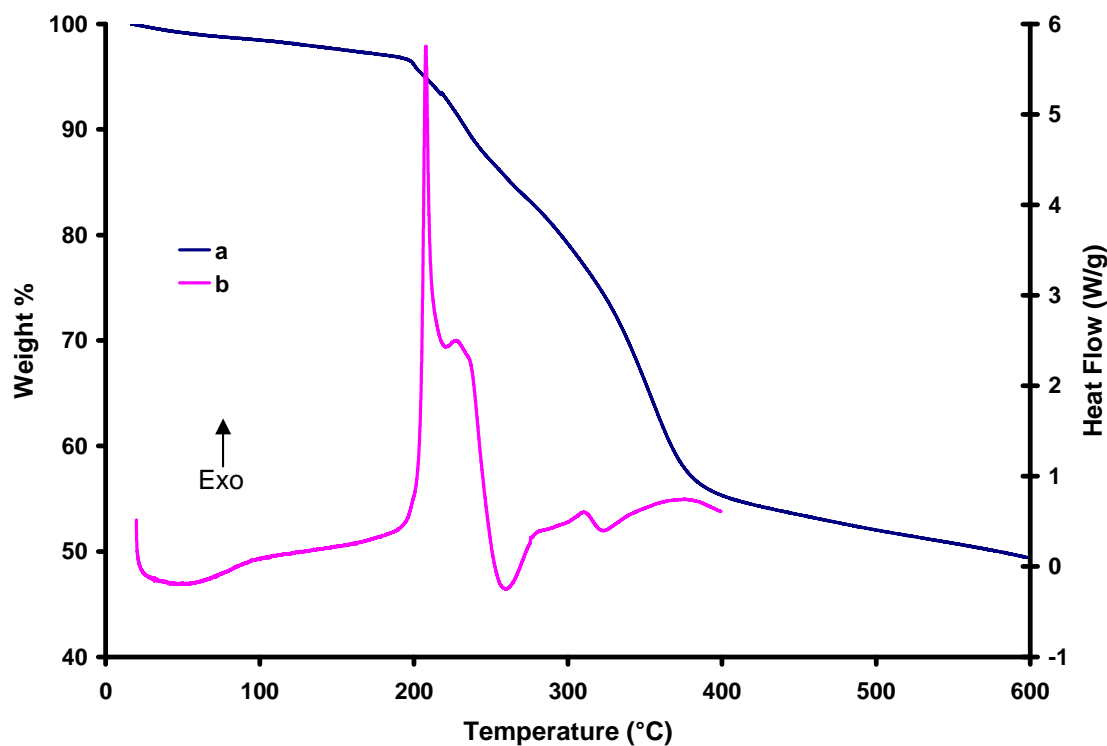


Figure 5. (a) Thermogravimetric analysis of **28** showing mass loss starting at room temperature. (b) Differential scanning calorimetry, indicating a sharp exothermic peak at *ca.* 200 °C.

In order to study the thermal behaviour of compound **28**, a powdered sample was subjected to thermogravimetric analysis and differential scanning calorimetry. The sample was heated at a constant rate of 2 °C/min from room temperature to 600 °C and 400 °C for the TGA and DSC analyses, respectively. The thermogram in Figure 5a indicates that mass loss already occurs at ambient temperatures. A theoretical

mass loss of 2.03 % is expected for one molecule of water per $[\text{Ni}_2\text{L5}_4]^{4+}$ cage, but a higher value of 3.64 % was obtained thermogravimetrically. This can be attributed to one of two reasons; either more than one unique water molecule is present in the crystal lattice that we have not been able to locate crystallographically, or the sample is hygroscopic and the mass loss can be attributed to both the water molecule present in the crystal lattice and aggregated atmospheric water on the surface of the sample. Crystals of **28** removed from the mother liquor and exposed to atmospheric conditions have a tendency to remain slightly wet, even after a period of several weeks, suggesting that the latter explanation is plausible. Further analysis of the thermogram reveals that the coordination complex is stable until *ca.* 200 °C at which point it begins decomposing. Differential scanning calorimetry reveals a single exotherm that coincides with the mass loss due to water and the subsequent decomposition of the compound.

4.4 PRELIMINARY GAS SORPTION STUDIES

In order to investigate the ability of **28** to behave as a conventionally porous functional material, a sample was prepared for gas sorption analysis (on the gram scale) based on the reaction conditions used to produce single crystals of the complex (Chapter 3, Table 3). The phase purity of the bulk crystalline material was verified using XRPD, which is consistent with the pattern simulated from the single-crystal XRD structure (Figure 6). The peaks in the diffractogram obtained experimentally are slightly shifted to the left in comparison to the simulated powder pattern due to the fact that the latter is generated from a crystal structure obtained at 100K and the experimental diffractogram is recorded at room temperature.

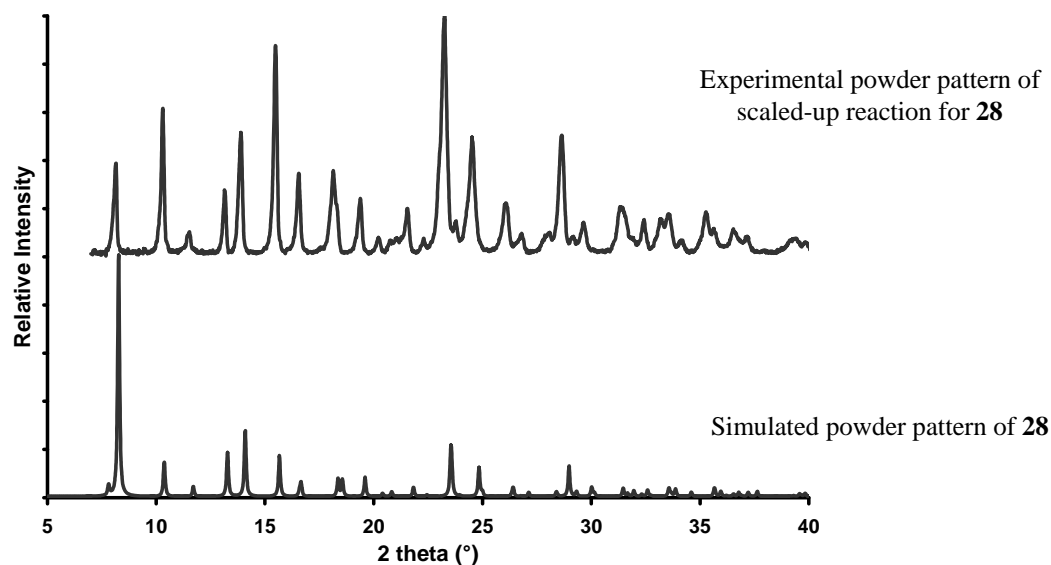


Figure 6. A comparison of the simulated and experimental powder patterns of **28**.

A 115 mg powdered sample of the complex was placed under vacuum for 24 hours to remove solvent, and then exposed first to CO₂ and then to H₂. Sorption isotherms were recorded gravimetrically at 0.1, 0.8, 1.5, 4, 7, 12, 18 and 20 bar for H₂ and CO₂ at 25 °C, and an additional isotherm was recorded at -40 °C for H₂, in order to investigate the influence of temperature on the resulting absorption process.

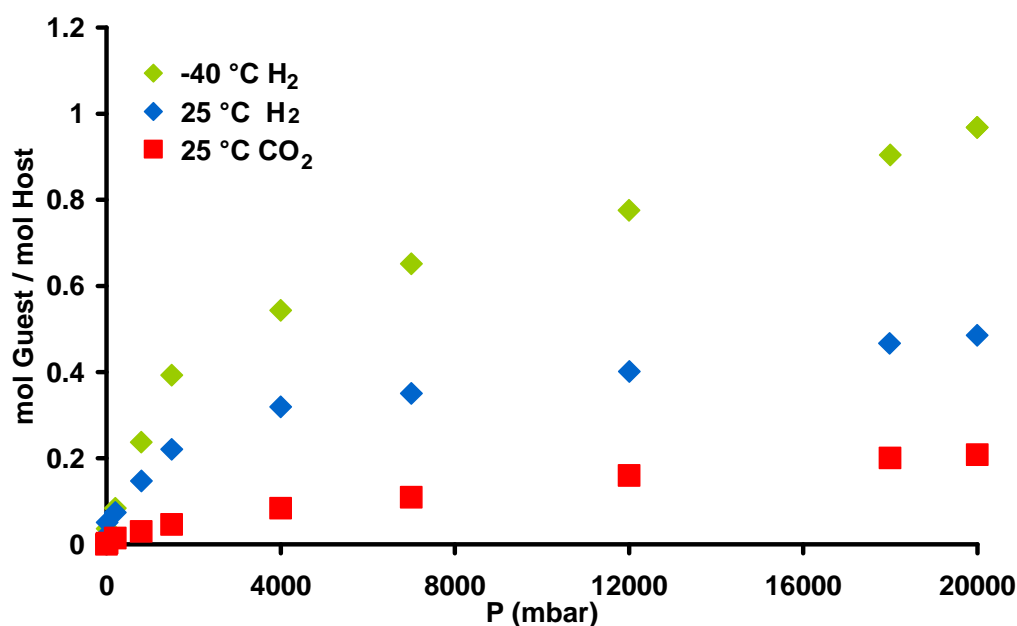


Figure 7. Gas sorption data for **28**; H₂ is absorbed in higher molar quantities than CO₂ at room temperature and as the temperature decreases the sample absorbs more H₂.

The three Type I isotherms shown in Figure 7 indicate that **28** is indeed permeable to H₂ and CO₂, and that the former is absorbed in much larger molar quantities. The isotherm recorded at -40 °C indicates that the sample exhibits increased uptake of H₂ with a decrease in temperature, which compares favourably to previously reported trends of this kind.^{35, 36} It is thought that this behaviour is due to the thermal motion of the host atoms; as the temperature increases the thermal motion of the host atoms increases, leading to steric obstruction of guest transport that encumbers not only the quantity of guest uptake but also the rate of guest uptake. These results are in stark contrast to what is observed in solution, where an increase in temperature generally facilitates the interaction of reactant molecules and promotes the formation of the final reaction product.

Closer inspection of the static model of the cage reveals that there are no atomic-scale pores that would facilitate the diffusion of gas into the cavity. This implies that the cage should be impermeable to even the smallest of gases. Since we have shown that the sample readily absorbs H₂, and to a lesser extent CO₂, it is thought that a dynamic cooperativity must exist between the host hemicarcerand and the guest molecules to create temporary openings through which the gas molecules may pass and enter the voids to form a hemicarceplex. Indeed, recent reports in the literature cite a few examples of materials known to exhibit this phenomenon, most of which constitute molecular organic crystalline materials such as calixarenes.^{10, 37-39} The compound is therefore not porous in the conventional sense as there are no continuous channels that can be mapped through the crystal, and it is therefore classed as *transiently* porous (see Section 1.4). This process may also account for the fact that **28** absorbs H₂ in larger molar quantities than CO₂, since a larger opening would have to be available for the CO₂ molecule to enter the cavity. Further evidence that implies this process may well be occurring is the length of time taken for an equilibrium mass to be attained for each pressure point of the isotherm. At each pressure, waiting 3 hours proved to be insufficient to reach equilibrium. Once this time was increased to 6 hours, the sample still absorbed gas at the end of this period, *albeit* at a much slower rate than initially. We presume that this extended equilibration time can be attributed to the cooperative movement that the host molecules must undergo in order to allow the gas molecules to enter the cavity.

4.5 CONCLUSIONS AND FUTURE STUDIES

In this chapter we have also shown that, whilst the ligands described in this study are not amenable to forming porous materials by the previous design principle *i.e.* the “donut-shaped” dinuclear metallocyclic topology outlined in section 3.1 this does not preclude them from forming porous materials entirely. To this end we have described the synthesis of a novel coordination compound that is generated from the reaction of Ni(NO₃).6H₂O and the ditopic imidazole-derived ligand **L5**. Single-crystal analysis revealed the formation of dinuclear cage-like hemicarcerands with cavities of *ca.* 62 Å³ that stack to form 1D columns. The packing diagram of the compound shows that open channels are formed by the arrangement of the 1D columns within the crystal lattice.

Although the single-crystal analysis provided sufficient information to prompt further investigation into the thermal and sorption behaviour of the compound, it was not possible to unambiguously characterise **28** by this method. Firstly the SOF of the uncoordinated water molecule assigned in the model is inconclusive. Our model assigns a water molecule to a SOF of 0.25, which implies that there is one water molecule for every Ni²⁺ ion. If this is indeed true, then two water molecules would be present at the same time in the interstice of the 1D column. This is not possible as the space between each discrete unit (intermolecular Ni...Ni distance = 6.003(2) Å) in the 1D column does not permit two water molecules.

Secondly, the nitrate counter-ions could not be modelled crystallographically due to symmetry-imposed disorder; however, once the atomic parameters of the hemicarcerand had been resolved, a significant level of residual electron density was located in the channels between the 1D columns and not in the cavities of the hemicarcerand itself. Thus it was concluded that the anions resided in these channels. The ambiguity in the assignment of the SOF of the water molecules and residual electron density is unacceptable if further studies are to be conducted by single crystal diffraction methods. Attempts to re-synthesise the compound using another anion are currently under way; if this proves unsuccessful an alternative would be to try exchanging the nitrate counter-ion for one with a higher symmetry, such as Cl⁻.

Three isotherms were recorded that show that **28** absorbs H₂ and CO₂ at room temperature and H₂ at -40 °C, despite the absence of conventional pores. The sorption studies also indicate that H₂ is absorbed in a higher molar quantity than CO₂ and

increased uptake of H₂ is observed as the temperature is decreased. It was rationalised that in order for the complex to absorb gases the host molecules must move in a concerted way to create temporary openings to allow guest egression to occur. The compound is therefore regarded as *transiently* porous. Future work is aimed at exposing the compound to a mixture of CO₂ and H₂. The rationale for this study is to determine if **28** selectively absorbs H₂ over CO₂ in the mixture. Such a property could be exploited for the purification of gases.

A systematic study of the increase in electron density as gas pressure is increased should also be undertaken. Equipment for studies of this nature has been developed in our group⁴⁰ and allows the collection of single-crystal intensity data on a conventional diffractometer whilst exposing the crystal to a constant and controlled gas pressure. Results obtained from this experiment would provide valuable insight into the structural changes that occur during the process of gas uptake by the host and would lead to a greater understanding of the processes that occur at the molecular level.

Finally, thermogravimetric analysis and differential scanning calorimetry showed that the sample is stable to *ca* 200 °C, after which decomposition occurs. The initial mass loss observed at ambient temperatures in the TGA is slightly ambiguous and is attributed to both surface and crystalline water.

Although the initial aim of the study was not met *i.e.* to generate novel porous materials based on the “donut-shaped” dinuclear metallocyclic topology outlined in section 3.1, the serendipitous discovery of **28** has led to a partial fulfilment of this goal in that a new transiently porous material was synthesised. The results outlined in this chapter are preliminary and provide a good indication of how to direct further studies.

To echo the words of Atwood *et al*¹⁰ “...*the classical riddle of how the ship gets into the bottle remains, at least for now, a subject for speculation.*”

REFERENCES

1. N. Armaroli and V. Balzani, *Angew. Chem. Int. Ed*, **2007**, 46, 52.
2. T. Burchell and M. Rogers, *SAE Technol. Pap. Ser.*, **2000**, 2205.
3. www.eere.energy.gov/hydrogenandfuelcells.
4. A. W. McClaine, R. W. Breault, C. Larsen, R. Konduri, J. Rolfe, F. Becker and G. Miskolczy, *Proceedings of the 2000 U.S. DOE Hydrogen Program Review*, **2000**.
5. D. W. Breck, *Zeolite Molecular Sieves*, Wiley and Sons, New York, **1974**.
6. M. R. Caira and L. R. Nassimbeni, in *Comprehensive Supramolecular Chemistry*, eds. J. Atwood, D. Davies, D. D. MacNicol and F. Vögtle, Elsevier Science, Oxford, **1996**.
7. L. R. Nassimbeni, *Acc. Chem. Res.*, **2003**, 36, 631.
8. J. L. Atwood, L. J. Barbour and A. Jerga, *Science*, **2002**, 296, 2367.
9. L. J. Barbour, *Chem. Commun.*, **2006**, 1163.
10. J. L. Atwood, L. J. Barbour and A. Jerga, *Angew. Chem. Int. Ed*, **2004**, 43, 2948.
11. O. M. Yaghi, M. O'Keefe, N. W. Ockwig, H. K. Chae, M. Eddaoudi and J. Kim, *Nature*, **2003**, 423, 705.
12. G. Ferey, *Chem. Mater.*, **2001**, 13, 3084.
13. G. Ferey, C. Mellot-Dzaznieks, C. Serre, F. Millange, J. Dutour, S. Surble and I. Margiolaki, *Science*, **2005**, 309, 2040.
14. X. B. Zhao, B. Xiao, A. J. Fletcjer, K. M. Thomas, D. Bradshaw and M. J. Rosseinsky, *Science*, **2004**, 304, 1012.
15. T. K. Maji, G. Mostafa, R. Matsuda and S. Kitagawa, *J. Am. Chem. Soc.*, **2005**, 127, 17152.
16. M. Eddaoudi, D. B. Moler, H. Li, B. Chen, T. M. Reineke, M. O'Keefe and O. M. Yaghi, *Acc. Chem. Res.*, **2000**, 34, 319.
17. *Hydrogen, Fuel Cells & Infrastructure Technologies Program: Multi-Year Research, Development and Demonstration Plan*, **2005**, U.S. Department of Energy, <http://www.eere.energy.gov/hydrogenandfuelcells/mypp/>.
18. D. J. Cram, *Science*, **1983**, 219, 1177.
19. D. J. Cram, S. Karabach, Y. H. Kim, L. Baczynskyj and G. W. Kalleymeyn, *J. Am. Chem. Soc.*, **1985**, 107, 2572.

20. J. C. Sherman and D. J. Cram, *J. Am. Chem. Soc.*, **1989**, 111, 4527.
21. J. C. Sherman, *Tetrahedron*, **1995**, 51.
22. M. E. Tanner, C. B. Knobler and D. J. Cram, *J. Am. Chem. Soc.*, **2000**, 112, 1659.
23. A. Jasat and J. C. Sherman, *Chem. Rev.*, **1999**, 99, 931.
24. D. B. Amabilino, P. R. Ashton, A. S. Reder, N. Spenser and J. F. Stoddart, *Angew. Chem. Int. Ed. Engl.*, **1994**, 33, 433.
25. R. A. Bissell, E. Cordova, A. E. Kaifer and J. F. Stoddart, *Nature*, **1994**, 369, 133.
26. R. Taylor and D. R. M. Walton, *Nature*, **1993**, 363, 685.
27. S. Leininger, B. Olenyuk and P. J. Stang, *Chem. Rev.*, **2000**, 100, 853.
28. D. K. Chand, K. Biradha and M. Fujita, *Chem. Commun.*, **2001**, 1652.
29. L. J. Barbour, G. William Orr and J. L. Atwood, *Nature*, **1998**, 393, 671.
30. T. D. Owens, F. J. Hollander, A. G. Oliver and J. A. Ellman, *J. Am. Chem. Soc.*, **2001**, 123, 1539.
31. D. A. McMorran and P. J. Steel, *Angew. Chem. Int. Ed.*, **1998**, 37, 3295.
32. M. L. Connolly, *Science*, **1983**, 221, 709.
33. M. L. Connolly, *J. Mol. Graphics*, **1993**, 11, 139.
34. F. H. Allen, O. Kennard and D. G. Watson, *J. Chem. Soc. Perkin Trans II*, **1987**, S1.
35. O. M. Yaghi, M. O'Keefe, R. Banerjee, A. Phan, B. Wang, C. B. Knobler and H. Furukawa, *Science*, **2008**, 319, 939.
36. J. L. C. Roswell and O. M. Yaghi, *Angew. Chem. Int. Ed.*, **2005**, 44, 4670.
37. J. Atwood, L. J. Barbour, P. K. Thallapally and T. B. Wirsig, *Chem. Commun.*, **2005**, 51.
38. J. Atwood, L. J. Barbour, A. Jerga and B. L. Schottel, *Science* **2002**, 298, 1000.
39. J. A. Riddle, J. C. Bollinger and D. Lee, *Angew. Chem. Int. Ed.*, **2005**, 44, 6689.
40. T. Jacobs, *Self-Assembly of New Porous Materials*, in Department of Chemistry & Polymer Science, **2009**, University of Stellenbosch, Stellenbosch.

CHAPTER 5

Summary and Concluding Remarks

The field of supramolecular chemistry is currently faced with a glut of experimental data accumulation. Advances in computing power and diffraction tools that allow rapid single-crystal X-ray diffraction experiments and ease of structure solution of even the most complex of systems have led to the discovery of countless new supramolecular compounds. It has been argued that the development of this branch of chemistry will be greatly aided by a classification of the experimental data, which will eventually lead to correlations between supramolecular interactions and structural characteristics.¹ Once this relationship is fully understood we will be able to harness this information to design and synthesise crystalline materials with desired solid state properties, and the epithet of crystal engineering, *i.e. making crystals by design*, will be realised.

Crystal engineering encompasses both the design and synthesis of crystalline materials from judiciously chosen building blocks that are assembled by means of supramolecular interactions; and therefore lies at the intersection of supramolecular chemistry and solid-state chemistry.² Although this field has its roots in organic chemistry, it has expanded to include metal-organic and coordination chemistry, thereby increasing the number of non-covalent interactions that need to be considered in crystal packing beyond those of just hydrogen bonding and π - π stacking interactions. Crystal engineering endeavours concerning coordination compounds are based on the basic design principle in which bidentate or polydentate ligands serve as the organic linkers between metal nodes to form coordination networks.³ The resulting structures can be classified as discrete, 0D coordination compounds or infinite 1D, 2D or 3D periodic nets.

Although the choice of ligand is essentially limitless, imidazole functionalised ligands represent a class of N-donor organic linkers that are being utilised more frequently in the synthesis of coordination networks owing to their high affinity for metals and their ease of functionalisation.⁴ Our group has shown that these ligands

can be successfully exploited to construct a range of coordination networks with interesting topologies and specific functions; these results have been summarised in **Chapter 1**. Our group has also devoted considerable attention to the development of porous crystalline materials. All of the ligands utilised in these systems are based on the simple design strategy in which two imidazole moieties are separated by a variable aromatic spacer. The nitrogen atoms then coordinate to metals to form 0D “donut-shaped” metallocycles that entrap solvent molecules in their apertures. The solvent molecules are then removed to yield a porous lattice capable of absorbing a variety of gases.

In this study we modified the previous ligand design by inserting extra thioether linkages between the aromatic spacer and the imidazole moieties. By varying the aromatic spacer, we prepared one novel tripodal ligand and five novel bidpodal ligands, namely 1,3,5-tris(1-imidazolyl-2-thione)-2,4,6-trimethylbenzene (**L1**), 1,4-bis(1-imidazolyl-2-thione)-2,3,5,6-tetramethylbenzene (**L2**), 1,4-bis(1-imidazolyl-2-thione)-2,5-dimethylbenzene (**L3**), 3,5-bis(1-imidazolyl-2-thione)toluene (**L4**), 1,3-bis(1-imidazolyl-2-thione)-2,4,6-trimethylbenzene (**L5**) and 4,4'-bis(1-imidazolyl-2-thione)-1,1'-biphenyl (**L6**). The common feature of these ligands is that the aromatic core and imidazole rings are rigid. However, the joints between the two *i.e.* the methylene group and sulphur bridge allow the imidazole rings to rotate freely in solution, endowing the ligands with conformational flexibility.

The synthesis and characterisation of these ligands was described in **Chapter 2**. All of the ligands were characterised by standard methods *i.e.* NMR, ESI-MS and IR as well as by SCD. All six of the single crystal structures of the free ligands featured the N-H \cdots N homosynthon. In the structures of **L1**, **L2**, **L3** and **L5** molecules are connected *via* the N-H \cdots N synthon to form 2D layers and in the structures of **L4** and **L6**, the analogous synthon connects molecules into 1D ladders. No appreciable π - π interactions are observed for the 2D structures, whereas the 1D ladders formed by **L4** and **L6** facilitate the formation of π - π stacking in the former and C-H \cdots π interactions in the latter.

Chapter 3 describes the self-assembly of novel coordination complexes from a variety of metal ions and the ligands **L1-L6**. The rationale behind this was to investigate the effect of the added flexibility of the ligand on the resulting coordination networks and to determine if we could synthesise new porous materials based on the “donut-shaped” metallocycle template. All coordination complexes were

studied by single-crystal X-ray diffraction methods owing to the unique information this analytical tool can provide regarding intermolecular interactions in the solid state. A total of 27 complexes were analysed; two coordination complexes were obtained containing **L1**, three containing **L2**, eight containing **L3**, eleven containing **L5** and three containing **L6**. No complexes were obtained with **L4** and it was suggested that since only crystals of the free ligand were isolated from reaction vials containing **L4**, this phase represents the most stable form of this ligand at room temperature.

The conformational freedom associated with the flexible nature of these ligands is advantageous as it can be employed in the construction of unique frameworks that add further understanding of the manner in which supramolecular structures assemble. This property also enables the ligand to conform to the symmetry of the metal centres, as demonstrated by the structures obtained with **L3** and halogenated salts *i.e.* **10**, **11**, **12** and **13**. This is important in the field of crystal engineering; if one can predict or at the very least assess what the most likely coordination geometry around the metal centre is going to be, this marks the first step forward in the process of crystal design.

The flexibility of these ligands can also be viewed as a disadvantage as it is impossible to predict the conformation of the ligand in the resulting crystal structure. Complexes **3** and **4** both contain **L2** and AgNO₃ in a 1:1 ratio, yet the conformation of the ligand is vastly different in the two crystal structures, as is evidenced by the formation of a 0D structure in the former and an infinite 1D structure in the latter. This is also seen in complexes **7** and **8** in which **L3** and CdI₂ are present in a 1:1 ratio. Although both form 1D polymeric strands in a similar fashion, a subtle difference in the conformation of the ligand results in remarkably different packing arrangements of the 1D strands. These cases where two different structures can arise from a single metal/ligand combination that has all components in the same stoichiometry, is somewhat disconcerting with regard to crystal structure design.⁵ The conformational flexibility is also disadvantageous in a systematic study where one wants to limit the contribution of as many factors as possible in order to ascertain the influence of one specific factor on structure formation. This problem may be negated somewhat in the utilisation of rigid ligands in which the symmetry of the coordination sites prescribes only one possible outcome for the self-assembly process.

Our results also show that the different conformations for **L2** in complexes **3** and **4** have different energies and that the intermolecular interactions, visualised as

Hirshfeld surfaces implemented by *CrystalExplorer*, play an important role in stabilising strained conformations in the crystal structure.

A few general observations can be made regarding the 27 structures reported in this section. In all of the crystal structures coordination bonds are formed from the donation of a lone electron pair of the imidazole group to the metal cation to form positively charged complexes. In two cases *i.e.* complexes **6** and **14**, additional coordination bonds are formed from the donation of a lone pair situated on a sulphur atom to a silver cation.

The charge balancing counter-ions present in the crystal lattice participate in hydrogen bonding. It is of interest that all of the structures obtained with halogenated counter-ions form 1D polymeric strands with the halogen coordinated to the metal centre, whereas nine of the eleven structures obtained with silver form 0D complexes and the counter ion remains, for the most part, uncoordinated. In fact, only structures **2**, **6** and **14** feature nitrate counter ion coordination. Secondary, non-covalent interactions serve to increase the dimensionality of all of the crystal structures. These include hydrogen bonds, π - π stacking interactions and, in the structures containing Ag cations, Ag- π and argentophilic interactions. The amino nitrogen atoms of the imidazole groups are involved in hydrogen bonding in every structure.

Although this series of coordination complexes did not yield a porous framework with the desired topology, single crystal studies have provided valuable information regarding the intermolecular interactions of the resulting coordination complexes. We speculate that the ligands **L1-L6** may be too flexible to facilitate the formation of the anticipated ring structure. We also suggested that removing the methyl linkage between the sulphur bridge and the aromatic core would lead to the formation of a more rigid ligand that might enhance its ability to complex to metals in the desired manner.

Future studies aimed at investigating intermolecular interactions of coordination networks with this series of ligands should be extended to include lanthanide- and actinide-based coordination polymers. Owing to the higher coordination numbers recorded for lanthanides (typically 8-12) over d-block metals,⁶ it is anticipated that the incorporation of these f-block elements into coordination networks with ligands **L1-L6** might lead to interesting topologies. Furthermore, heterometallic coordination polymers constructed from d-/f- metal pairings may also provide the opportunity to study materials with unique structural features that might otherwise be unattainable.

It would also be interesting to introduce a second, more rigid ligand (e.g. 4,4'-bipyridine) into the construction of co-ligand supramolecular architectures with **L1-L6**. Although the understanding of the combined effect of mixed ligand systems on the resulting structure is far from complete, a study of this kind would present an interesting long-term challenge.

As an extension to the computational studies outlined in section 3.2.2.2 the gas-phase energy of the conformation of **L2** in complex **5** should be calculated. This energy should then be compared to the energies of the ligand in complexes **3** and **4** to provide greater insight into the relative energies of the three different conformations of **L2** observed experimentally.

In **Chapter 4** a novel hemicarcerand, formed from the reaction of **L5** and $\text{Ni}(\text{NO}_3)_2 \cdot 6\text{H}_2\text{O}$, is described. The SCD analysis in conjunction with results obtained using MSROLL ($r = 1.55 \text{ \AA}$) reveals the formation of a cage-like complex with individual cavities of *ca.* 62 \AA^3 . Preliminary gas sorption analyses are included in this section and show that the compound is *transiently* porous and capable of absorbing H_2 and CO_2 . TGA and DSC analyses reveal that this compound is stable to *ca.* $200 \text{ }^\circ\text{C}$ after which decomposition occurs. In view of the fact that the results reported in this section are preliminary, a detailed account of future studies has already been provided at the end of the chapter. These include (1) exposing the sample to a mixture of CO_2 and H_2 in order to determine if the compound selectively absorbs H_2 over CO_2 , and (2) undertaking a systematic study of the increase in electron density as gas pressure is increased, using specialised equipment developed in our group.

The results in this section bare testament to the fact that the role of serendipity cannot be underestimated in the quest for new materials. Although we were not able to generate porous materials based on our design strategy, we did generate a novel porous material by a different method *i.e.* the M_2L_4 tetragonal prism of complex **28**. A cursory examination of the literature shows that trigonal (either M_2L_3 or M_3L_2 systems) and tetragonal (M_2L_4) prisms have the potential to be exploited in the formation of porous materials; in these systems ligand flexibility is a prerequisite.⁷

Finally, despite our continuing efforts, the lack of true predictability in the arrangement of molecules in the solid state remains an elusive aspect of crystal engineering. The interdisciplinary field of supramolecular chemistry is laying the foundations of research that will eventually bear fruit in the production of crystalline materials with desired solid state properties. It is, however, evident that in order for

this to become a reality the crystal engineer needs to master the mysteries of both solution chemistry and solid state chemistry.⁸

REFERENCES

1. A. N. Khlobystov, A. J. Blake, N. R. Champness, D. A. Lemenovskii, A. G. Majouga, N. V. Zyk and M. Schroder, *Coord. Chem. Rev.*, **2001**, 222, 155.
2. D. Braga, F. Grepioni and G. R. Desiraju, *Chem. Rev.*, **1998**, 98, 1375.
3. R. Robson, *J.Chem.Soc., Dalton Trans.*, **2000**, 3735.
4. B. Sui, J. Fan, T. A. Okamura, W. Y. Sun and N. Ueyama, *Solid State Sciences*, **2005**, 7, 969.
5. J. S. Fleming, K. L. V. Mann, C. A. Carraz, E. Psillakis, J. C. Jeffery, J. A. McCleverty and M. D. Ward, *Angew. Chem. Int. Ed*, **1998**, 37, 1279.
6. C. L. Cahill, D. T. de Lill and M. Frisch, *Crystengcomm*, **2007**, 9, 15.
7. C. Y. Su, Y. P. Cai, C. L. Chen, H. X. Zhang and B. S. Kang, *J. Chem. Soc., Dalton Trans*, **2001**, 359.
8. D. Braga, *J.Chem.Soc., Dalton Trans.*, **2000**, 3705.

APPENDICES

The supplementary CD attached contains:

- NMR spectra for **L1-L6** (including 2D NMR spectra)
- LC ESI-MS spectra for **L1-L6**
- IR spectra for **L1-L6**
- .res files for **L1- L6** and complexes **1-28** that can be used to visualise the structures
- .CIF files for **L1-L6** and complexes **1-28**
- Publications
- Poster presentations

Table S1. Crystallographic data for ligands **L1-L6**.

	L1	L2	L3	L4	L5	L6
Crystal system	monoclinic	monoclinic	monoclinic	triclinic	monoclinic	monoclinic
Space group	<i>P2₁/n</i>	<i>C2/c</i>	<i>P2₁/n</i>	<i>P-1</i>	<i>P2₁/n</i>	<i>P2₁/n</i>
<i>a</i> (Å)	9.6035(2)	15.003(4)	6.185(3)	8.0985(1)	7.4475(5)	7.5519(1)
<i>b</i> (Å)	21.035(2)	9.491(3)	9.517(5)	8.3829(2)	17.7401(1)	25.211(4)
<i>c</i> (Å)	11.1672(2)	12.989(4)	13.764(7)	12.317(2)	12.8528(9)	10.1373(1)
α (°)	90	90	90	98.920(3)	90	90
β (°)	101.578(3)	112.238(4)	95.400(8)	104.451(3)	96.7710(10)	111.059(2)
γ (°)	90	90	90	106.124(3)	90	90
<i>V</i> (Å ³)	2210.3(6)	1712.0(8)	806.6(7)	754.9(2)	1686.3(2)	1801.1(5)
<i>Z</i>	2	4	2	2	4	4
<i>D_c</i> (g/cm ³)	1.372	1.391	1.361	1.392	1.357	1.396
<i>R</i> _{int}	0.1169	0.0299	0.0718	0.0464	0.0360	0.0438
<i>R</i> 1 [<i>F</i> ² > 2σ(<i>F</i> ²)]	0.0789	0.0494	0.0666	0.0620	0.0486	0.0600
<i>wR</i> 2 (all data)	0.1460	0.1201	0.1419	0.1251	0.1139	0.1312
Goodness of fit	1.089	1.045	1.017	1.129	1.125	1.037
Largest difference peak (eÅ ⁻³)	0.49	0.51	0.74	0.40	0.56	0.57

Table S2. Crystallographic data for complexes **1-28**.

	1	2	3	4	5
Empirical formula	C ₂₂ H ₂₈ AgN ₇ O ₄ S ₃	C ₄₂ H ₅₂ Cd ₂ N ₁₆ O ₁₅ S ₆	C ₁₈ H ₂₂ AgN ₅ O ₃ S ₂	C ₁₈ H ₂₂ AgN ₅ O ₃ S ₂	C ₁₈ H ₂₂ CdI ₂ N ₄ S ₂
Crystal system	orthorhombic	triclinic	monoclinic	monoclinic	monoclinic
Space group	<i>Pna</i> 2 ₁	<i>P</i> -1	<i>P</i> 2 ₁ / <i>n</i>	<i>P</i> 2 ₁ / <i>c</i>	<i>Cc</i>
<i>a</i> (Å)	7.1984(2)	11.5196(1)	3.6451(1)	12.1043(1)	9.9456(7)
<i>b</i> (Å)	29.665(8)	14.3880(2)	11.8122(1)	13.6934(1)	14.5604(1)
<i>c</i> (Å)	12.754(4)	16.7930(2)	13.8752(1)	12.9909(1)	16.5650(1)
α (°)	90	86.131(2)	90	90	90
β (°)	90	81.308(2)	113.977(1)	111.634(1)	103.040(1)
γ (°)	90	85.746(2)	90	90	90
<i>V</i> (Å ³)	2723.4(1)	2739.3(5)	2043.4(3)	2001.6(3)	2336.9(3)
<i>Z</i>	4	2	4	4	4
<i>D</i> _c (g/cm ³)	1.606	1.744	1.718	1.753	2.060
<i>R</i> _{int}	0.0981	0.0317	0.0327	0.0357	0.0217
<i>R</i> 1 [<i>F</i> ² > 2σ(<i>F</i> ²)]	0.939	0.0442	0.0347	0.0396	0.0281
<i>wR</i> 2 (all data)	0.2001	0.0999	0.0763	0.0910	0.0683
Goodness of fit	1.042	11.046	1.060	1.110	1.073
Largest difference peak (eÅ ⁻³)	1.90	1.52	0.69	1.59	1.58

	6	7	8	9	10	11
Empirical formula	C ₃₄ H ₄₁ Ag ₄ N ₁₃ O ₁₆ S ₄	C ₁₆ H ₁₈ CdI ₂ N ₄ S ₂	C ₁₆ H ₁₈ CdI ₂ N ₄ S ₂	C ₈ H ₉ CdI ₂ N ₂ S	C ₁₇ H ₂₂ Cl ₂ CuN ₄ OS ₂	C ₁₆ H ₁₈ Cl ₂ CoN ₄ S ₂
Crystal system	monoclinic	monoclinic	monoclinic	triclinic	monoclinic	monoclinic
Space group	<i>P2₁/c</i>	<i>P2₁/n</i>	<i>P2₁/n</i>	<i>P-1</i>	<i>P2₁/c</i>	<i>P2₁/n</i>
<i>a</i> (Å)	13.2537(1)	8.7672(5)	11.6827(1)	4.4702(3)	18.209(2)	8.1525(7)
<i>b</i> (Å)	18.7107(1)	16.4823(1)	12.2711(2)	8.8595(6)	7.7498(9)	15.9946(2)
<i>c</i> (Å)	20.2387(2)	15.3572(9)	14.8596(2)	16.4492(1)	15.2000(2)	14.9612(1)
α (°)	90	90	90	92.4170(1)	90	90
β (°)	107.105(1)	95.097(1)	92.792(2)	95.3910(1)	92.185(2)	94.314(2)
γ (°)	90	90	90	100.9270(1)	90	90
<i>V</i> (Å ³)	4796.9(6)	2210.4(2)	2127.7(4)	635.61(8)	2143.4(4)	1945.4(3)
<i>Z</i>	4	4	4	2	4	4
<i>D_c</i> (g/cm ³)	2.004	2.093	2.175	2.777	1.540	1.572
<i>R</i> _{int}	0.0526	0.0242	0.0311	0.0182	0.0524	0.0273
<i>R</i> 1 [<i>F</i> ² > 2σ(<i>F</i> ²)]	0.0537	0.0348	0.0698	0.0458	0.0644	0.0386
<i>wR</i> 2 (all data)	0.1061	0.0998	0.1874	0.1232	0.1462	0.1036
Goodness of fit	1.077	1.046	1.059	1.107	1.031	1.057
Largest difference peak (eÅ ⁻³)	1.33	1.79	3.32	3.31	1.47	1.02

	12	13	14	15	16	17
Empirical formula	C ₁₆ H ₁₈ Br ₂ N ₄ S ₂ Zn	C ₁₆ H ₁₈ CdCl ₂ N ₄ S ₂	C ₃₄ H ₄₁ Ag ₄ N ₁₃ O ₁₆ S ₄	C ₁₇ H ₂₀ AgN ₅ O ₃ S ₂	C ₁₇ H ₂₀ AgN ₅ O ₄ S ₂	C ₃₇ H ₄₄ Ag ₂ F ₆ N ₈ O ₇ S ₆
Crystal system	monoclinic	monoclinic	monoclinic	triclinic	triclinic	monoclinic
Space group	<i>P2₁/n</i>	<i>P2₁/n</i>	<i>P2₁/c</i>	<i>P</i> -1	<i>P</i> -1	<i>P2₁/n</i>
<i>a</i> (Å)	8.3455(9)	8.3283(6)	13.2537	9.3735(2)	9.1098(6)	12.7059(8)
<i>b</i> (Å)	16.1009(2)	16.2405(1)	18.7107	9.9500(2)	11.3881(8)	26.2566(2)
<i>c</i> (Å)	15.0243(2)	15.0879(1)	20.2387	10.6469(2)	11.8573(8)	13.6264(8)
α (°)	90	90	90	96.113(3)	107.0810(1)	90
β (°)	94.409(2)	93.3260(1)	107.1050	91.356(3)	107.1380(1)	91.1610(1)
γ (°)	90	90	90	99.640(3)	105.0310(1)	90
<i>V</i> (Å ³)	2012.8(4)	2037.3(3)	4796.9(6)	972.5(3)	1040.0(1)	4545.0(5)
<i>Z</i>	4	4	4	2	2	4
<i>D_c</i> (g/cm ³)	1.834	1.675	2.004	1.757	1.694	1.805
<i>R</i> _{int}	0.0625	0.0270	0.0526	0.0272	0.0220	0.0366
<i>R</i> 1 [<i>F</i> ² > 2σ(<i>F</i> ²)]	0.0540	0.0533	0.0537	0.0541	0.0341	0.0405
<i>wR</i> 2 (all data)	0.0937	0.1656	0.1061	0.1221	0.0842	0.0876
Goodness of fit	1.010	1.031	1.077	1.058	1.178	1.033
Largest difference peak (eÅ ⁻³)	0.92	0.71	1.49	1.10	0.87	1.01

	18	19	20	21	22	23
Empirical formula	C ₂₀ H ₂₂ AgF ₆ N ₄ O _{1.5} S ₂ Sb	C ₁₇ H ₂₀ AgF ₆ N ₄ O _{1.5} PS ₂	C ₁₇ H ₂₂ AgBF ₄ N ₄ OS ₂	C ₁₇ H ₂₂ CdI ₂ N ₄ O S ₂	C ₁₈ H ₂₄ CdI ₂ N ₄ OS ₂	C ₂₁ H ₂₂ CdI ₂ N ₆ S ₂
Crystal system	triclinic	triclinic	monoclinic	monoclinic	monoclinic	triclinic
Space group	<i>P</i> -1	<i>P</i> -1	<i>P</i> 2 ₁ / <i>n</i>	<i>P</i> 2 ₁ / <i>n</i>	<i>C</i> 2/ <i>c</i>	<i>P</i> -1
<i>a</i> (Å)	8.455(4)	8.333(2)	8.455(9)	13.470(3)	31.625(3)	9.648(9)
<i>b</i> (Å)	11.422(6)	11.738(3)	22.370(3)	11.610(3)	11.051(1)	11.218(1)
<i>c</i> (Å)	12.623(6)	12.299(4)	11.504(1)	15.371(3)	16.343(2)	14.162(1)
α (°)	98.397(8)	98.048(6)	90	90	90	112.023(1)
β (°)	91.039(8)	93.683(7)	93.702(2)	99.904	119.084(1)	91.681(2)
γ (°)	92.767(8)	93.417(7)	90	90	90	101.926(2)
<i>V</i> (Å ³)	1204.2(1)	1185.8(6)	2171.3(4)	2367.9(9)	4992.0(8)	1380.7(2)
<i>Z</i>	2	2	4	4	8	2
<i>D</i> _c (g/cm ³)	2.047	1.740	1.704	2.044	1.977	1.897
<i>R</i> _{int}	0.0330	0.0839	0.0681	0.0349	0.0339	0.0425
<i>R</i> 1 [<i>F</i> ² > 2σ(<i>F</i> ²)]	0.0759	0.0853	0.0829	0.0378	0.0396	0.0479
<i>wR</i> 2 (all data)	0.1819	0.1995	0.1600	0.0828	0.0885	0.1165
Goodness of fit	1.108	1.098	1.143	1.074	1.060	1.080
Largest difference peak (eÅ ⁻³)	2.63	2.24	2.12	1.31	1.99	2.13

	24	25	26	27	28
Empirical formula	C ₁₉ H ₂₈ CdI ₂ N ₄ O ₂ S ₂	C ₂₀ H ₁₈ Br ₂ CuN ₄ S ₂	C ₂₁ H ₂₃ Cl ₃ N ₄ OS ₂ Zn	C ₂₁ H ₂₂ Cl ₂ N ₄ OS ₂ Zn	C ₃₄ H ₄₀ N ₈ NiOS ₄
Crystal system	monoclinic	monoclinic	monoclinic	triclinic	tetragonal
Space group	<i>C2/c</i>	<i>C2/c</i>	<i>P2₁/n</i>	<i>P-1</i>	<i>I4/m</i>
<i>a</i> (Å)	32.585(4)	13.099(1)	8.484(8)	8.328(2)	15.103(1)
<i>b</i> (Å)	10.298(1)	12.874(1)	21.121(2)	10.366(3)	15.103(1)
<i>c</i> (Å)	19.944(3)	13.011(1)	13.752(1)	15.322(4)	17.045(3)
α (°)	90	90	90	109.488(4)	90
β (°)	125.829(2)	103.012	97.953	97.815(4)	90
γ (°)	90	90	90	99.617(5)	90
<i>V</i> (Å ³)	5426.1(1)	2137.8(4)	2440.7(4)	1202.9(6)	3888.3(7)
<i>Z</i>	8	4	4	2	4
<i>D_c</i> (g/cm ³)	1.897	1.870	1.587	1.510	1.305
<i>R</i> _{int}	0.0525	0.0683	0.0583	0.0468	0.1596
<i>R</i> ₁ [<i>F</i> ² > 2σ(<i>F</i> ²)]	0.0594	0.0706	0.0663	0.1101	0.1530
<i>wR</i> ₂ (all data)	0.1143	0.1546	0.1269	0.2773	0.3617
Goodness of fit	1.064	1.168	1.125	1.190	1.175
Largest difference peak (eÅ ⁻³)	2.46	1.78	0.85	2.73	2.28

